



**HAL**  
open science

# Lysosomal defects in Duchenne muscular dystrophy : advancing combined therapeutic approaches

Abbass Jaber

► **To cite this version:**

Abbass Jaber. Lysosomal defects in Duchenne muscular dystrophy : advancing combined therapeutic approaches. Biochemistry, Molecular Biology. Université Paris-Saclay, 2024. English. NNT : 2024UPASL055 . tel-04769725

**HAL Id: tel-04769725**

**<https://theses.hal.science/tel-04769725v1>**

Submitted on 6 Nov 2024

**HAL** is a multi-disciplinary open access archive for the deposit and dissemination of scientific research documents, whether they are published or not. The documents may come from teaching and research institutions in France or abroad, or from public or private research centers.

L'archive ouverte pluridisciplinaire **HAL**, est destinée au dépôt et à la diffusion de documents scientifiques de niveau recherche, publiés ou non, émanant des établissements d'enseignement et de recherche français ou étrangers, des laboratoires publics ou privés.

Lysosomal Defects in Duchenne Muscular  
Dystrophy: Advancing Combined Therapeutic  
Approaches

*Anomalies lysosomales dans la myopathie de Duchenne : vers des  
approches thérapeutiques combinées*

**Thèse de doctorat de l'université Paris-Saclay**

École doctorale n°577, Structure et Dynamique des Systèmes Vivants (SDSV)  
Spécialité de doctorat : Sciences de la vie et de la santé  
Graduate School : Sciences de la vie et santé. Référent : Université d'Evry Val d'Essonne.

Thèse préparée dans Integrare research unit UMR\_S95 (Université Paris-Saclay, Univ  
Evry, Inserm, Généthon),  
Sous la direction de **David ISRAELI**, chargé de recherche, HDR

**Thèse soutenue à Paris-Saclay, le 23 septembre 2024, par**

**Abbass JABER**

**Composition du Jury**

Membres du jury avec voix délibérative

**Olivier BIONDI**

Professeur des Universités  
Université d'Evry Paris-Saclay

Président

**Kristl CLAEYS**

Professeur des Universités,  
Praticien hospitalier - Université de  
Leuven, Belgique

Rapporteuse & Examinatrice

**Karim HNIA**

Chargé de recherche,  
Université Paul Sabatier, Toulouse

Rapporteur & Examineur

**Caroline LE GUINER**

Chargée de recherche,  
Nantes Université

Examinatrice



*"The good thing about science is that it's true whether or not you believe in it."*

– Neil deGrasse Tyson

## PREAMBLE

The work presented in this thesis was carried out in the 'Progressive Muscular Dystrophies' laboratory led by Dr. Isabelle Richard at Genethon. Genethon is one of the three laboratories of AFM-Téléthon, an association of activists, patients, and relatives concerned with rare genetic diseases, particularly neuromuscular diseases. Founded in 1990, Genethon was one of the first laboratories to study the human genome. After identifying the genes responsible for genetic diseases in the 1990s, Genethon's research shifted towards the preclinical and clinical development of gene therapy drugs, with a particular focus on neuromuscular diseases.

Today, Genethon's research and development department houses an Inserm unit (UMR\_S951 - INTEGRARE), where academic research, including the work of this thesis, is conducted. Our team is dedicated to studying and developing innovative treatments for muscular dystrophies, a heterogeneous group of over 30 inherited diseases, the most well-known and prevalent being Duchenne muscular dystrophy (DMD).

DMD is a rare, debilitating genetic disease that primarily affects boys from an early age, causing progressive muscle degeneration, severe muscle weakness, and loss of motor function. The disease is caused by mutations in the *DMD* gene, which encodes the essential muscle protein dystrophin. Symptoms of DMD typically manifest early in childhood and have a profound impact on the quality of life of patients and their families. Current medical and therapeutic interventions aim to alleviate symptoms and improve patients' quality of life, but curative treatments remain elusive. One of the most promising approaches is microdystrophin gene therapy, which aims to restore the expression of a shortened yet functional form of dystrophin.

The project of this thesis focuses on two major areas: the first is investigating the incompletely understood pathological mechanisms of DMD, particularly disruptions in cholesterol metabolism and the endolysosomal system in muscle. The second is developing new combined therapeutic approaches, integrating gene therapy with treatments targeting the deregulations in cholesterol metabolism and the endolysosomal system.

# ACKNOWLEDGMENTS

Albert Einstein once said, "The more I learn, the more I realize how much I don't know." I believe this sentiment sums up perfectly the essence of a PhD and a scientific career. As I reach the end of my PhD journey, I find myself having learned so much, yet with an even greater awareness of how much there is still to discover. This realization has been shaped by the many incredible people around me, to whom I dedicate this thesis. I offer my deepest gratitude to all who made this journey both enlightening and exciting

First and foremost, I wish to express my deepest thanks to my thesis director and mentor, Dr. David Israeli. Working with you over the past three years has been an incredible experience. Your passion for science and curiosity have been a constant source of inspiration. I admire your courage to pursue unconventional topics and push the boundaries of knowledge. Our discussions were always enlightening, and with your vast knowledge, I never needed PubMed! I like to believe we made a great team, and I am grateful for your mentorship and for treating me as a colleague throughout this journey.

I am also deeply grateful to Isabelle, who gave me the opportunity to join her lab almost four years ago. From the moment I attended your lecture during my master's program, I was captivated by your dedication and groundbreaking work. Your continuous support and belief in me have been invaluable, and I hope to rise to the challenges ahead and meet your expectations.

To the esteemed members of my jury: thank you for accepting my invitation and for your thoughtful feedback. I extend my appreciation to Pr. Kristl Claeys and Dr. Karim Hnia for your insightful comments, as well as to Pr. Olivier Biondi and Dr. Caroline Le Guiner. It is an honor to have you as part of this process. A special thank you to Dr.

Serge Braun, who not only provided invaluable feedback during my pharmacy thesis but also graciously accepted the invitation to participate in this thesis.

I would also like to thank my thesis committee members, Dr. Daniel Stockholm and Dr. Andrea Burgo, for their guidance and advice throughout the course of my PhD.

To Laura, my PhD labmate and companion on this journey: from our internship to the completion of our PhDs, it's been the ride of a lifetime. Having you by my side, especially as part of the DMD family, made this journey so much easier. You've always pushed me to be better in the spirit of a 'healthy competition' of course, and I'll forever treasure the laughs, breaks, and moments we shared. I hope we get the chance to work together again (my offer will always stand!), but regardless, I know I've gained a lifelong friend.

I extend my heartfelt thanks to my colleagues in the DDC team, who welcomed me with open arms. A special thanks to Jérôme, my first mentor during my master's. I learned so much from you, and it has always been a pleasure working with you. To Célia, thank you for your unwavering support, you make our work so much easier! To Ai, you were one of the people I learned the most from, and I truly looked up to you. And to the pillars of the DDC: Evelyne, Carinne, Laurence, Nathalie, your collective knowledge, experience, and camaraderie are truly unmatched. I am also grateful to the other team members with whom I shared this journey: Marine, Sonia, Anthony, Elise, Maxime, Valeria, Auriane, Stephany, Eva, Tao, Louise, Cheryane, Lucie, Giorgia, Louna, Matteo, Jeanette, Djunda and Valère. Thank you to the interns I had the pleasure of mentoring, Rania and Juliane, best of luck with your future endeavors! To Elise, all the best with the remainder of your PhD, and take good care of David! To the former members of the team, special thanks to Cynthia my first labmate for all the shared moments, and to Juliette for all our good memories together. A heartfelt

thanks to Julie, Fanny, Alan, Ariane, Camille, Simone, and all others who were part of this experience.

To the Italian group—Paola, Giulia, Valeria, Matteo, Giorgia—you've added so much joy and fun to this journey. Paola, you're the best PhD student now, and I have full confidence in your success. Giulia, you're no longer the best postdoc, time to pass the baton!

Thank you to the Genethon staff, and especially the platforms that made this work possible. I am particularly grateful to the preclinical evaluation platform: Christophe, Emilie, Fanny, for their help in histology, and to Laetitia, Adeline, Béatrice, Romane and Guillaume for their help in animal experiments. Thank you also to the imaging platform, especially Daniel, Jérémie, and Simon, for your assistance with this project.

To my friends, classmates, and colleagues, thank you. A special shout-out to Habib, Rayan, Jad, and all my Lebanese French friends who have accompanied me on this long journey.

To my parents, your unwavering support has been the foundation of this work. Thank you for always believing in me. To my sisters, Solange, Ikram, and Heba, there is not much I can say to thank you, life would be dull without you. To my brother, mentor, mentee, competitor and friend of this journey in France, this one is for you too.

Sincerely,

Abbass

# CONTENT TABLE

<b>PREAMBLE</b>	<b>4</b>
<b>ACKNOWLEDGMENTS</b>	<b>6</b>
<b>LIST OF ABBREVIATIONS</b>	<b>13</b>
<b>LIST OF FIGURES</b>	<b>19</b>
<b>LIST OF TABLES</b>	<b>21</b>
<b>INTRODUCTION</b>	<b>22</b>
<b>I- The Skeletal Muscle</b>	<b>22</b>
I.1 Muscle structure	23
I.2 Myofibril structure and composition	24
I.2.1 Proteins	24
a) Contractile proteins	24
b) Regulatory proteins	25
c) Structural proteins	25
I.2.2 Sarcomere	26
I.2.3 Organelles	26
I.3 Muscle Fiber Types	28
I.4 The physiology of muscle activation: excitation-contraction coupling mechanism	29
I.5 Types of muscular actions	32
I.6 Muscle energy mechanisms	33
I.7 Satellite cells and muscle regeneration	35
I.8 Muscle function in health and disease	36
I.8.1 Sarcopenia and muscle atrophy	37
I.8.2 The impact of exercise and physical inactivity on muscle function	37
I.8.3 Muscle disorders and impairment of muscle function	38
I.9 Progressive Muscular Dystrophies	39

<b>II-</b>	<b>Duchenne Muscular Dystrophy: Pathophysiology and Therapeutic Strategies</b>	<b>42</b>
II.1	Disease description	43
II.2	Clinical presentation	44
II.3	Genetic basis of the disease: the <i>DMD</i> gene and Dystrophin	46
I.3.1	The <i>DMD</i> gene	46
I.3.2	Muscle Dystrophin	47
II.4	DMD pathophysiology	50
I.4.1	Pathological mechanisms leading to muscle cell death	52
a)	Mechanical stress and sarcolemma disruption	52
b)	Free-radical-induced muscle damage: oxidative and nitrosative stress	53
c)	Loss of calcium homeostasis	54
d)	Muscle ischemia	55
e)	Mitochondrial dysfunction	56
f)	Autophagy defects and loss of proteostasis	56
g)	Lipid abnormalities	58
I.4.2	Pathological mechanisms contributing to disease progression following myofibers death	59
a)	Inflammation and immune response	59
b)	Muscle regeneration and depletion of the muscle stem cell pool	60
c)	Fibrofatty infiltration in the dystrophic muscle	61
II.5	Therapeutic management and treatments in development for DMD	63
II.5.1	Current clinical management of DMD	63
a)	Glucocorticoids treatments	64
b)	Givinostat treatment	65
c)	Cardiac and respiratory care	65
d)	Management of other disorders	66
II.5.2	Advances and challenges in microdystrophin gene therapy for DMD	67
a)	rAAV vectors for gene therapy	67
b)	Microdystrophin gene therapy	70
II.5.3	Gene editing strategies	81
a)	Exon skipping	81
b)	CRISPR-Cas9 genome editing approaches	82
<b>III-</b>	<b>Lysosome Function in Health and Disease</b>	<b>83</b>
III.1	Lysosomal structure and function	84
III.3.1	Lysosome Structure and Composition	84

III.3.2 Lysosomal Function	88
a) Role in macromolecule degradation and recycling	88
b) Vesicular trafficking and fusion	93
c) Roles in signaling and metabolism	94
III.2 Lysosomal stress and pathological implications	101
III.2.1 Lysosomal dysfunction and consequences	102
a) Lysosomal stress and lysosomal stress response	102
b) Lysosomal dependent cell death	106
III.2.2 Lysosomal function in aging	106
III.2.3 Lysosomal function in disease	107
a) Lysosomal storage disorders	107
b) Lysosomal defects in neurodegenerative disease	107
c) Lysosomal defects implications in cardiovascular diseases	108
III.2.4 Lysosomal defects and muscle impairments	108
III.3 Endolysosomal damage response	110
III.3.1 Endo-lysosomal repair pathways	112
a) The Endosomal Sorting Complex Required for Transport (ESCRT)- mediated repair	113
b) Lipid-triggered invagination	113
c) Lipid transfer-mediated repair: phosphoinositide-initiated membrane tethering and lipid transport (PITT)	114
d) Other identified repair mechanism	115
III.3.2 Removal of damaged lysosomes	115
a) Lysophagy: degradation of damaged lysosomes	115
b) Connexin-43 mediated exocytosis	116
III.3.3 Replacement and regeneration: TFEB-mediated lysosomal biogenesis	117
<b>OBJECTIVES</b>	<b>120</b>
<b>RESULTS</b>	<b>125</b>
<b>I- Targeting lysosomal damage as a new therapeutic perspective for Duchenne Muscular Dystrophy</b>	<b>125</b>
<b>II- Detection of Lysosomal Membrane Permeabilization in Various Muscle Disorders</b>	<b>209</b>

<b>DISCUSSION</b>	<b>214</b>
<b>I- Summary</b>	<b>214</b>
<b>II- Lysosomal Damage Contributes to the Pathogenesis of Muscular Dystrophies</b>	<b>216</b>
II.1 Galectin-3 overexpression in dystrophic muscle correlates with lysosomal membrane permeabilization and lysosomal stress	216
II.2 Activation of the endo-lysosomal damage response and interpretation of autophagy defects:	219
II.3 Cathepsin overexpression and implications	221
II.4 Interplay between lysosomal damage and lipid perturbations	222
II.4.1 Cholesterol and DMD phenotype	222
II.4.2 Cholesterol accumulation in the lysosome	223
II.4.3 Implications of cholesterol accumulation	224
II.4.4 Cholesterol and lysosomal membrane permeabilization:	224
II.5 Lysosomal defects in DMD: cause, consequences and therapeutic opportunities	225
<b>III- Targeting Lysosomal Damage in DMD Improve Microdystrophin Gene Therapy</b>	<b>227</b>
III.1 Correction of LMP following gene therapy varies between the modality of gene therapy approaches in dystrophic models	227
III.2 Trehalose-mediated correction of lysosomal damage improve overall therapeutic effect of microdystrophin gene therapy	228
<b>IV- Concluding Remarks</b>	<b>231</b>
<b>BIBLIOGRAPHY</b>	<b>233</b>
<b>ANNEX</b>	<b>261</b>
<b>Scientific Productions</b>	<b>261</b>
<b>Manuscript Summary in French</b>	<b>264</b>

# LIST OF ABBREVIATIONS

## A

AAP: assembly-activating protein

AAV: adeno-associated virus

ABD: actin-binding domain

ACE: angiotensin-converting enzyme

ADCNM: Autosomal Dominant  
Centronuclear Myopathy

ADP: adenosine diphosphate

AFM: Association française contre les  
myopathies

ALIX: ALG-2 interacting protein X

ALR: autophagic lysosomal reformation

AMKP: AMP-activated protein kinase

Arp2/3: Actin Related Protein 2/3

ASM: acid sphingomyelinase

ASO: antisense oligonucleotide

ATP: adenosine triphosphate

## B

BMD: Becker muscular dystrophy

bp: base pairs

## C

cDNA: complementary DNA

CK: Creatine kinase

CLEAR: coordinated lysosomal  
expression and regulation

CMA: chaperone-mediated autophagy

CMD: Congenital Muscular Dystrophy

CP: creatine phosphate

CR: cysteine-rich

CRISPR: *clustered regularly interspaced  
short palindromic repeats*

CTGF: Connective Tissue Growth Factor

## D

DAGC: dystrophin-associated  
glycoprotein complex

Da: Dalton

DG: Dystroglycan

DHP: dihydropyridine

DMD: Duchenne Muscular Dystrophy

## E

EC: excitation-contraction

ECM: extracellular matrix

EMA: European Medicines Agency

ER: endoplasmic reticulum

ESCRT: Endosomal Sorting Complex  
Required for Transport)

## F

FAPs: fibro-adipogenic progenitors

FDA: U.S Food and Drug  
Administration

FKRP: Fukutin-related protein

## G

GA: gastrocnemius

GAA: acid alpha-glucosidase

Gal-3: Galectin-3

GSDII: Glycogen Storage Disease Type  
II

## H

H<sub>2</sub>O<sub>2</sub>: hydrogen peroxide

HDAC: histone deacetylase

HDR: homology-directed repair

HE: hematoxylin and eosin

HOPS: homotypic fusion and protein  
sorting)

HR: homologous recombination

HSC70: heat shock-cognate chaperone  
70 kDa protein

## I

IFN- $\gamma$ : Interferon gamma

IGF-1: Insulin-like Growth Factor 1

IgG: Immunoglobulin G

IKK:  $\kappa$ B kinases

IL: Interleukin

INDELS: small nucleotide insertions or deletions

INPP5K: Inositol Polyphosphate-5-Phosphatase K

ITRs: inverted terminal repeats

kDA: kilo daltons

## L

LAL: lysosomal acid lipase

LAMP: lysosome-associated membrane protein

LC3: Microtubule-associated protein 1A/1B-light chain 3

LDCD: Lysosomal-dependent cell death

LDL: low-density lipoprotein

LGMD: Limb-Girdle muscular dystrophy

LIMP: and lysosome-integral membrane protein

LLOMe : L-leucyl-L-leucine methyl este

LMP : Lysosomal membrane permeabilization

LPL : lipoprotein lipase

LSD : Lysosomal storage disorder

LTBPs: latent TGF- $\beta$  binding proteins

## M

MAAP : membrane-associated accessory protein

MAMs ; mitochondria-associated ER membranes

MAPKs: mitogen-activated kinases

MHC: Myosin Heavy Chain

miR : microRNA

ML-IV: Mucopolidosis Type IV

MMP: matrix metalloproteinase

MOMP: mitochondrial outer membrane permeabilization

mPTP: mitochondrial permeability transition pore

MRI: magnetic resonance imaging

mRNPs: messenger ribonucleoproteins

mTOR: mammalian target of rapamycin

mTORC1: mammalian target of rapamycin complex I

MuSCs: Muscle Stem Cells

MVBs: multivesicular bodies

Myf5: Myogenic Factor 5

MyoD: Myogenic Differentiation 1

## N

NCX: sodium-calcium exchanger

NF- $\kappa$ B: nuclear factor-kappa B

NHEJ: non-homologous end joining

nNOS: neuronal nitric oxide synthase

NOX: NADP(P)H oxidase

NPC: Niemann-Pick Type C

## O

OPMD: Oculopharyngeal muscular dystrophy

ORF: open reading frame

ORPs: oxysterol binding protein (OSBP)-related proteins

OSBP: oxysterol binding protein

## P

P: Phosphate

PAMPs: pathogen-associated molecular patterns

Pax: Paired box protein

PDCD6: programmed cell death protein 6

PE: phosphatidylethanolamine

PI3K: class III phosphatidylinositol 3-kinase

PI4K2A: phosphatidylinositol 4-kinase 2A

PI4P: phosphatidylinositol 4-phosphate

PITT: phosphoinositide-initiated membrane tethering and lipid transport

PM: Plasma membrane

PS: phosphatidylserine

## R

rAAV: recombinant adeno-associated virus

Rheb: Ras homolog enriched in brain

RNS: reactive nitrogen species

ROS: reactive oxygen species

RyR: ryanodine receptors

## S

SA: stretch-activated calcium channels

SAE: severe adverse events

SCAP: SREBP cleavage-activating protein

SERCA: *sarco-endoplasmic reticulum Ca<sup>++</sup> ATPase*

SG: stress granules

SG: Sarcoglycan

SNAREs: N-ethylmaleimide-sensitive factor-attachment protein (SNAP) Receptors

SOC: store-operated calcium channels

SR: sarcoplasmic reticulum

SREBP: sterol regulatory element-binding protein

## T

TA: tibialis anterior

TFEB: transcription factor EB

TGF- $\beta$ : Transforming growth factor beta

TNF alpha: Tumor necrosis factor alpha

TnI/TnC/TnT: troponin I, C and T

TPC: Two-Pore Channel

TRPML: Transient Receptor Potential Cation Channel, Mucolipin Subfamily

TSC: tuberous sclerosis complex

## U

ULK1: unc-51-like kinase 1

## V

VAMP: vesicle-associated membrane protein

v-ATPase: vacuolar H<sup>+</sup> ATPase

VP: viral protein

**Y**

vg: viral genomes

YAP: yes-associated protein

# LIST OF FIGURES

<b>Figure 1. Muscle and myofibril structure.</b>	24
<b>Figure 2. Organization of the triad in skeletal muscle and distribution of mitochondrial networks.</b>	28
<b><i>Figure 3. Muscle contraction mechanisms.</i></b>	32
<b>Figure 4. Types of muscular action.</b>	33
<b>Figure 5. Skeletal muscle regeneration and repair..</b>	36
<b>Figure 6. Overview of Myopathies.</b>	39
<b>Figure 7. Proteins implicated in muscular dystrophies.</b>	41
<b>Figure 8. Drawing of a DMD patient by Dr. Guillaume-Benjamin Duchenne de Boulogne in 1868.</b>	43
<b>Figure 9. Clinical evolution of DMD.)</b>	45
<b>Figure 10. Structure and functions of the DMD gene and dystrophin protein..</b>	49
<b><i>Figure 11. Pathophysiological mechanisms of muscular dystrophies.</i></b>	51
<b>Figure 12. Permeabilization of muscle fibers in dystrophic muscle..</b>	53
<b>Figure 13. Wild-type and recombinant AAV (rAAV) genomes..</b>	69
<b>Figure 14. rAAV production by triple transfection.</b>	70
<b>Figure 15. Truncated dystrophin expressed in a BMD patient muscle.</b>	71
<b>Figure 16. Microdystrophin constructs.</b>	72
<b>Figure 17. Localization of microdystrophin constructs in clinical trials to the DAGC.</b>	76
<b>Figure 18. Gene transfer strategies for the expression of longer constructs than microdystrophin, using several rAAV vectors and different splicing strategies.</b>	81
<b>Figure 19. Lysosome structure and function.</b>	87
<b>Figure 20. Autophagy and lysosome reformation.</b>	92
	19

<b>Figure 21. The lysosome regulates cholesterol homeostasis.</b>	<b>99</b>
<b>Figure 22. Lysosomal Stress Response.</b>	<b>105</b>
<b>Figure 23. Lysosome Membrane Permeabilization.</b>	<b>105</b>
<b>Figure 24. Identification of pathways involved in the lysosome quality control in the last 15 years.</b>	<b>112</b>
<b>Figure 25. The endolysosomal damage response.</b>	<b>118</b>
<b>Figure 26. Principle of combined therapy for DMD.</b>	<b>124</b>
<b>Figure 27. Detection of lysosome damage in different forms of LGMD.</b>	<b>212</b>
<b>Figure 28. Detection of lysosome damage in congenital myopathy and Pompe disease.</b>	<b>212</b>

## LIST OF TABLES

<b>Table 1. Types and characteristics of different muscle fibers.</b>	<b>29</b>
<b>Table 2. Non-muscular isoforms of Dystrophin</b>	<b>47</b>
<b>Table 3. Summary of ongoing clinical trials using rAAV-microdystrophin for DMD.</b>	<b>74</b>
<b>Table 4. List of FDA-approved drugs based on exon skipping strategies for the treatment of DMD.</b>	<b>82</b>

# INTRODUCTION

Duchenne muscular dystrophy (DMD) is a rare and progressive muscle-wasting disease primarily affecting boys. As an X-linked recessive genetic disorder, DMD leads to significant muscle degeneration starting in early childhood. The disease predominantly affects skeletal muscles, with cardiac muscle involvement becoming more pronounced in later stages. This introduction aims to enhance understanding of DMD by first detailing the structure and function of skeletal muscle, followed by a comprehensive overview of Duchenne muscular dystrophy itself, and then an overview of lysosomal function in health and disease.

## I- The Skeletal Muscle

Representing almost 40% of body mass <sup>[1]</sup>, skeletal muscle is one of the most dynamic and elastic tissues in the human body. Muscle tissue is composed primarily of water (75%), protein (20%) and other compounds such as salts, minerals, fat and carbohydrates <sup>[2]</sup>. It plays a crucial role in various bodily functions, both metabolic and mechanical.

From a mechanical perspective, muscle tissue converts chemical energy into mechanical energy through the hydrolysis of adenosine triphosphate (ATP). This conversion enables the generation of force, the maintenance of posture and the execution of physical movements.

Metabolically, muscle is a major contributor to basal energy metabolism, participating in heat production necessary for maintaining body temperature. It also serves as a storage site for numerous metabolites, including carbohydrates and amino acids <sup>[2]</sup>. Through its role as an amino acid reservoir, muscle supports continuous protein

synthesis in other tissues and organs, such as the brain, heart, skin and liver. During fasting, muscle-derived amino acids facilitates both protein synthesis and gluconeogenesis, thus ensuring carbohydrate and protein homeostasis [3]. Consequently, decline in muscle function or mass, particularly with aging, can impair protein synthesis, leading to an imbalance between protein synthesis and degradation, ultimately disrupting proteostasis and promoting the accumulation of protein aggregates [4].

Skeletal muscle also plays a key role in glucose homeostasis and insulin resistance. Storing nearly 80% of carbohydrates, mainly in the form of glycogen [5], skeletal muscle is essential for glucose distribution. It is stimulated by insulin, and alone is responsible for the absorption of 80% of glucose in the post-prandial period [5,6]. As a result, alterations in metabolic function in the muscle can have severe effects. Muscle desensitization to insulin (insulin resistance) is considered the hallmark of the metabolic syndrome, a precursor of prediabetes [7-9].

## **I.1 Muscle structure**

Skeletal muscle is characterized by a well-defined arrangement of muscle fibers associated with connective tissue (**Figure 1**). A muscle fiber is about 100 µm in diameter and 1 cm in length, bounded by a membrane (the sarcolemma), and contains an aqueous solution (the sarcoplasm). Each muscle fiber is enveloped by a thin connective tissue (endomysium). The fibers are grouped into bundles surrounded by a relatively loose connective tissue (perimysium). The assembly of these bundles by denser connective tissue (epimysium) constitutes the muscle. The connective tissue networks unite at each end of the muscle to form the dense connective tissue of the tendons: these are firmly attached to the outer layer of the bone and form the

mechanical link between muscle and bone <sup>[10]</sup>. These fibers themselves are composed of about 2000 myofibrils, forming elongated, cylindrical multinucleated cells.

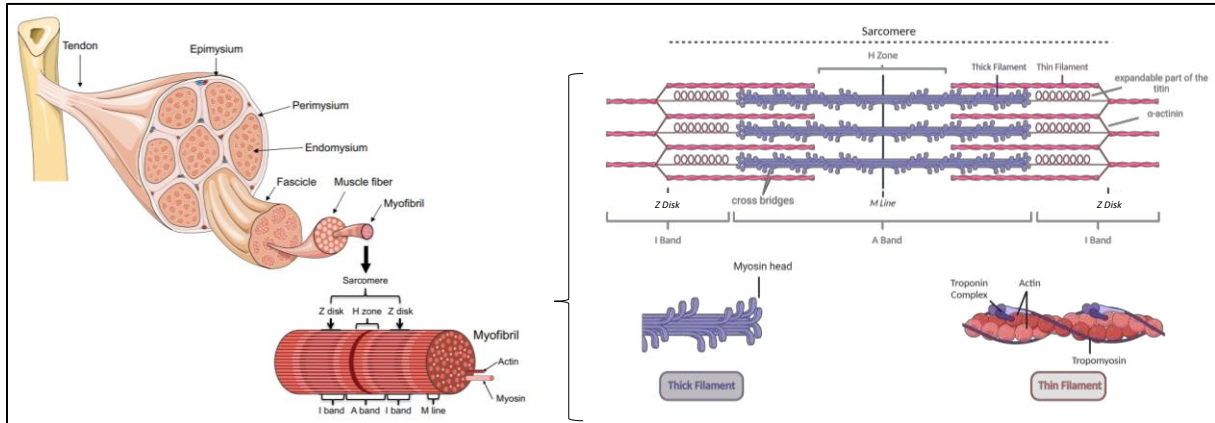


**Figure 1. Muscle and myofibril structure.** (Adapted from Bonetto & Bonewald, 2019 <sup>[10]</sup>)  
Figure created with [BioRender.com](https://www.biorender.com).

## I.2 Myofibril structure and composition

### I.2.1 Proteins

Muscle fibers are made up mainly of proteins (~80% of myofibers dry mass) <sup>[11]</sup>. There are 3 main categories of muscle protein: contractile proteins, regulatory proteins and structural proteins.

#### **a) Contractile proteins**

The two most abundant myofibrillar proteins are myosin and actin, accounting for around 70-80% of the total amount of protein in a muscle fiber <sup>[2]</sup>.

- **Myosin** is a contractile protein characterized by its ATPase activity, which allows it to hydrolyze ATP, providing the energy required for muscle contraction <sup>[12]</sup>. It is composed of multiple chains: two heavy chains (Myosin Heavy Chain, or MHC) and four light chains. Approximately 200 myosin

molecules align in an antiparallel fashion to form a thick filament. The myosin heads are oriented outward from the filament, enabling interaction with actin filaments during muscle contraction.

- **Actin** is a globular protein that polymerizes to form two intertwined helical chains, constituting the core of thin filaments. It interacts with myosin to form actomyosin complexes, which are crucial for muscle contraction. These complexes facilitate the formation of crossbridges between actin and myosin, enabling the sliding filament mechanism that drives muscle movement.

#### ***b) Regulatory proteins***

Regulatory proteins are crucial for controlling muscle contraction by preventing the constant interaction between actin and myosin and responding to signals that trigger the removal of this inhibition. The most important of these proteins are:

- **Tropomyosin:** This protein is bound along the length of the two actin chains, obstructing the sites where myosin would normally bind to actin, thereby inhibiting muscle contraction.
- **Troponins:** These proteins are positioned at regular intervals along the thin filaments and consist of three subunits: Troponin I (TnI), Troponin C (TnC), and Troponin T (TnT). TnC binds to calcium ions, which induces a conformational change in the regulatory proteins, causing them to shift towards the center of the thin filament. This movement exposes the binding sites on actin, allowing interaction with myosin and enabling muscle contraction.

#### ***c) Structural proteins***

Other structural proteins involved in the organization and stability of myofibrils include **alpha actinin**, **nebulin**, **desmin**, **vimentin** and **titin**. Alpha-actinin defines the boundaries of the sarcomere, ensuring proper alignment of the actin filaments.

Nebulin binds to actin filaments, playing a crucial role in regulating their length and maintaining the uniformity of thin filaments. Desmin and vimentin form intermediate filaments that provide structural integrity to muscle fibers and facilitate efficient force transmission across the cells. Titin, the largest known protein, interacts with both actin and myosin, maintaining the structural integrity of sarcomere components throughout contraction-relaxation cycles and contributing to the elasticity and extensibility of muscle tissues.

### **I.2.2 Sarcomere**

Thick and thin filaments are organized in a precisely regular pattern within muscle fibers. Thin filaments converge at one end, connecting via alpha-actinin to form the Z-line (**Figure 1**). Intermediate filaments, such as desmin and vimentin, create longitudinal and transverse connections between the Z-lines, enhancing structural integrity. Another structural protein, nebulin, extends along the length of the thin filament, contributing to its stability and regulation. The region between two Z-lines is defined as a sarcomere, the fundamental contractile unit of muscle (**Figure 1**).

Thick filaments are also anchored to the Z-line through the giant protein titin, which plays a crucial role in maintaining sarcomere elasticity and alignment. The sequential arrangement of sarcomeres (ranging from 100 to 400 in series) forms a myofibril, characterized by its transverse striations. These striations are created by the alternating isotropic (I) and anisotropic (A) bands, giving the muscle its distinctive striped appearance.

### **I.2.3 Organelles**

Myofibrils combine to form a fiber. The membrane of this fiber, known as the sarcolemma, periodically invaginates to create the transverse tubular system (T-tubules). These T-tubules transmit electrical excitation from the membrane to the

sarcoplasmic reticulum (SR) vesicles <sup>[13]</sup>. The connection between the T-tubules and the sarcoplasmic reticulum (SR) occurs in a specialized region called the terminal cisterna/SR junction <sup>[14]</sup>. The terminal cisternae serve as reservoirs for calcium ions. Together, a T-tubule and two adjacent terminal cisternae form a structure known as the triad <sup>[14]</sup> (**Figure 2**).

- The **Sarcoplasmic reticulum** (SR) is a key regulator of calcium homeostasis in muscle cells, laying an essential role in the coupling between electrical excitation and actin-myosin interaction. It is responsible for the storage, release, and reuptake of calcium ions. Two key proteins within the SR, SERCA (*sarco-endoplasmic reticulum Ca<sup>++</sup> ATPase*) and calsequestrin, are vital for maintaining this homeostasis. SERCA actively pumps calcium ions back into the SR, while calsequestrin binds calcium ions within the SR, ensuring a ready supply for rapid release during muscle contraction.
- **Mitochondria:** In muscle cells, mitochondria form a three-dimensional network crucial for generating the energy needed for muscle function, particularly under aerobic or endurance conditions. Their organization and abundance are dynamic and can be influenced by various physical stimuli, such as endurance exercise, which stimulates mitochondrial biogenesis. However, when the mitochondrial network becomes impaired —due to conditions such as mitochondrial diseases, metabolic syndrome, or obesity— this can lead to compromised muscle function.

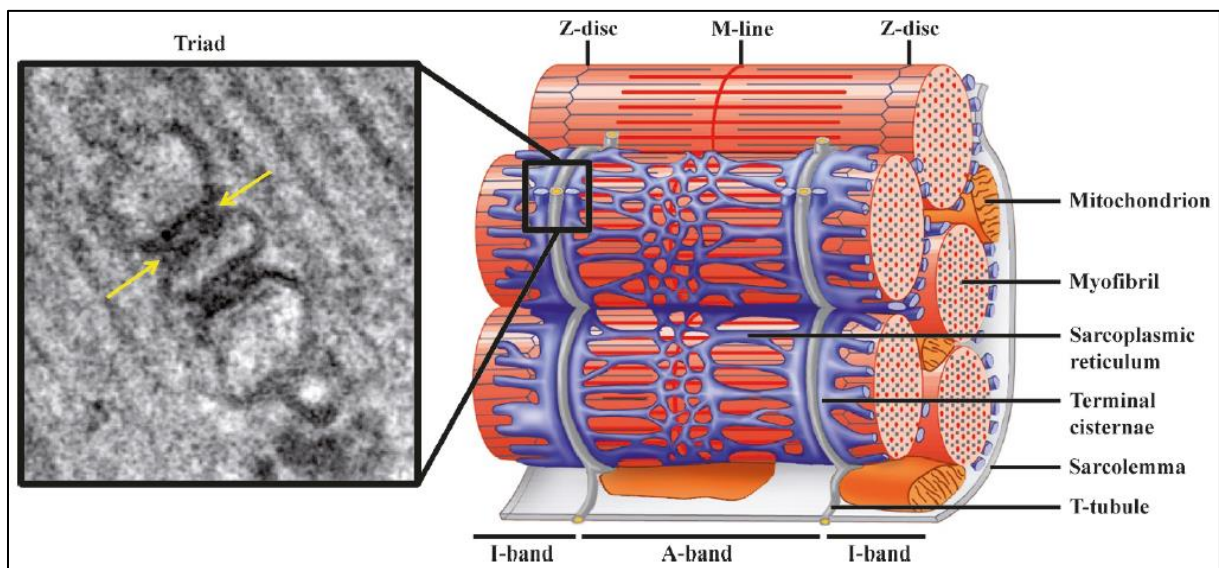


**Figure 2. Organization of the triad in skeletal muscle and distribution of mitochondrial networks.** (Adapted from Al-Qusairi & Laporte, 2011 <sup>[14]</sup>) The electron micrograph on the left illustrates the structural organization of a triad junction in skeletal muscle. The image depicts a T-tubule (transverse tubule) flanked by terminal cisternae of the sarcoplasmic reticulum, forming the triad. This arrangement is crucial for efficient excitation-contraction coupling in muscle fibers. Additionally, the distribution of mitochondrial networks can be observed on the right schematic, highlighting their strategic positioning relative to the triad for optimal energy supply during muscle contraction.

### **1.3 Muscle Fiber Types**

Skeletal muscle is a heterogeneous tissue exhibiting biochemical, mechanical, and metabolic diversity. Early work on muscle vascularization identified two types of muscle: "red" and "white". Since then, various classifications of muscle fibers have been proposed based on criteria such as contractile properties, contraction speed (fast/slow twitch), fatigue resistance during prolonged activity (fatigable/non-fatigable), predominant metabolic or enzymatic pathways (oxidative, glycolytic), and the expression of different MHC isoforms <sup>[15]</sup>.

However, muscles are rarely homogeneous; instead, they consist of varying proportions of fast and slow fibers. This fiber type variability within a single muscle reflects physiological adaptability, enabling muscles to perform a range of activities with different mechanical and metabolic demands. For simplicity, we will use the most classical classification of muscle fibers, which identifies three main (non-exclusive) types: type I, type IIa, and type IIb/IIx (**Table 1**).

Characteristic	Type 1	Type IIa	Type IIb/IIx
Contraction Speed	Slow	Fast	Fast
Predominant energy metabolism	Beta-Oxidation (aerobic pathway)	Beta-Oxidation (aerobic pathway)	Glycolysis (anaerobic pathway)
Fatigue resistance	High	Intermediate	Low
Predominant MHC isoform	I or <i>Myh7</i>	IIa or <i>Myh2</i>	IIb or <i>Myh4</i>

**Table 1. Types and characteristics of different muscle fibers.**

#### **1.4 The physiology of muscle activation: excitation-contraction coupling mechanism**

Excitation-contraction (EC) coupling represents the intricate coordination of processes required for muscle force generation: the transmission of the nerve stimulus to the triad, followed by the release of calcium from the terminal cisternae and the subsequent interaction between actin and myosin to form cross-bridges.

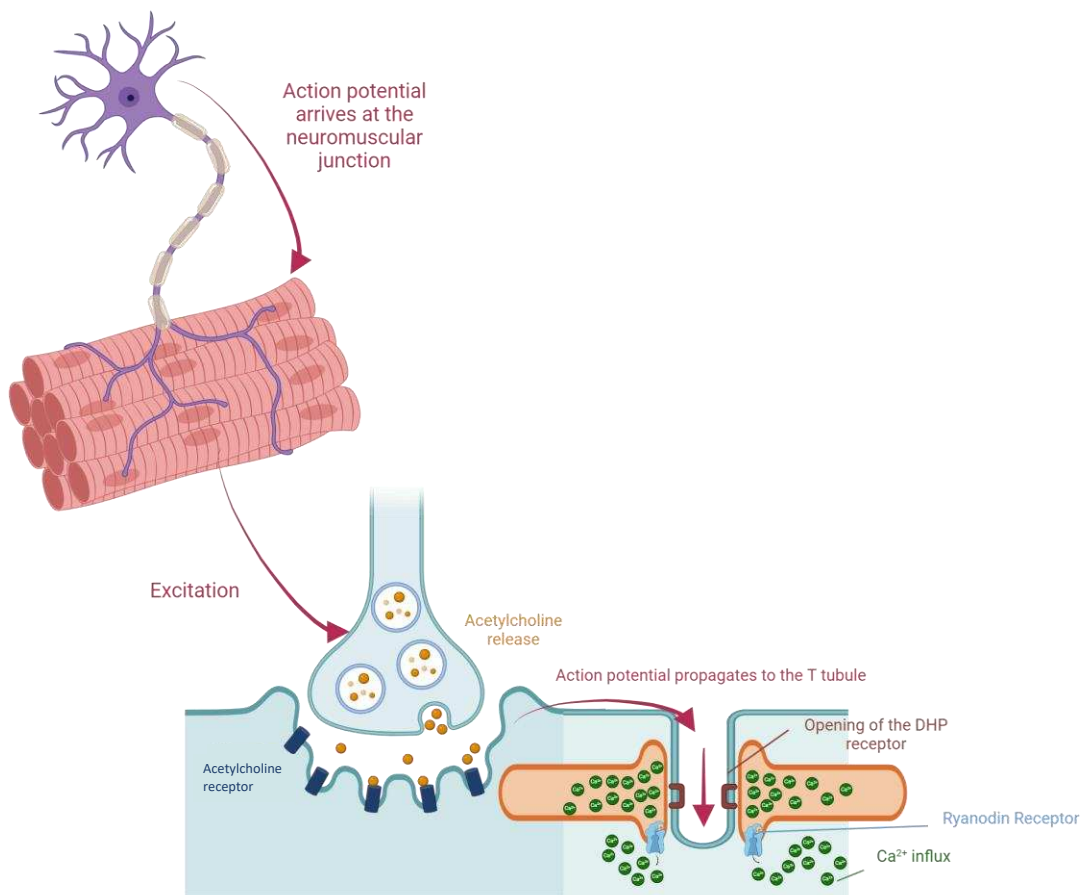
When an action potential reaches the muscle fiber membrane, it is transmitted into the myofibrils via the transverse tubular (T-tubule) system (**Figure 3A**). Upon reaching the triad, the nerve impulse activates a subunit of the dihydropyridine (DHP) receptors on the T-tubule, leading to the influx of calcium <sup>[16]</sup>. This calcium influx then

triggers the opening of ryanodine receptors (RyR) in the terminal cisternae of the SR, releasing large quantities of calcium into the sarcoplasm.

The calcium released into the sarcoplasm binds to the regulatory protein TnC on the actin thin filament. This binding initiates a series of molecular events culminating in the sliding of actin and myosin filaments and the generation of force (**Figure 3B**). The process can be summarized as follows:

- The myosin head is in the "armed" position, bound to adenosine diphosphate (ADP) and phosphate (P).
- Calcium binds to troponin, causing tropomyosin to shift and expose the binding sites on actin for myosin.
- The myosin head binds to actin, and the inorganic phosphate is released.
- The myosin heads pivot towards the center of the sarcomere, pulling the actin filaments inward.
- The ADP molecule is released from the myosin head.
- A new ATP molecule binds to the myosin head, causing it to detach from actin, while troponin and tropomyosin return to their original positions.
- The ATPase activity of myosin hydrolyzes ATP into ADP and P, rearming the myosin head for the formation of a new cross-bridge.

A.



B.

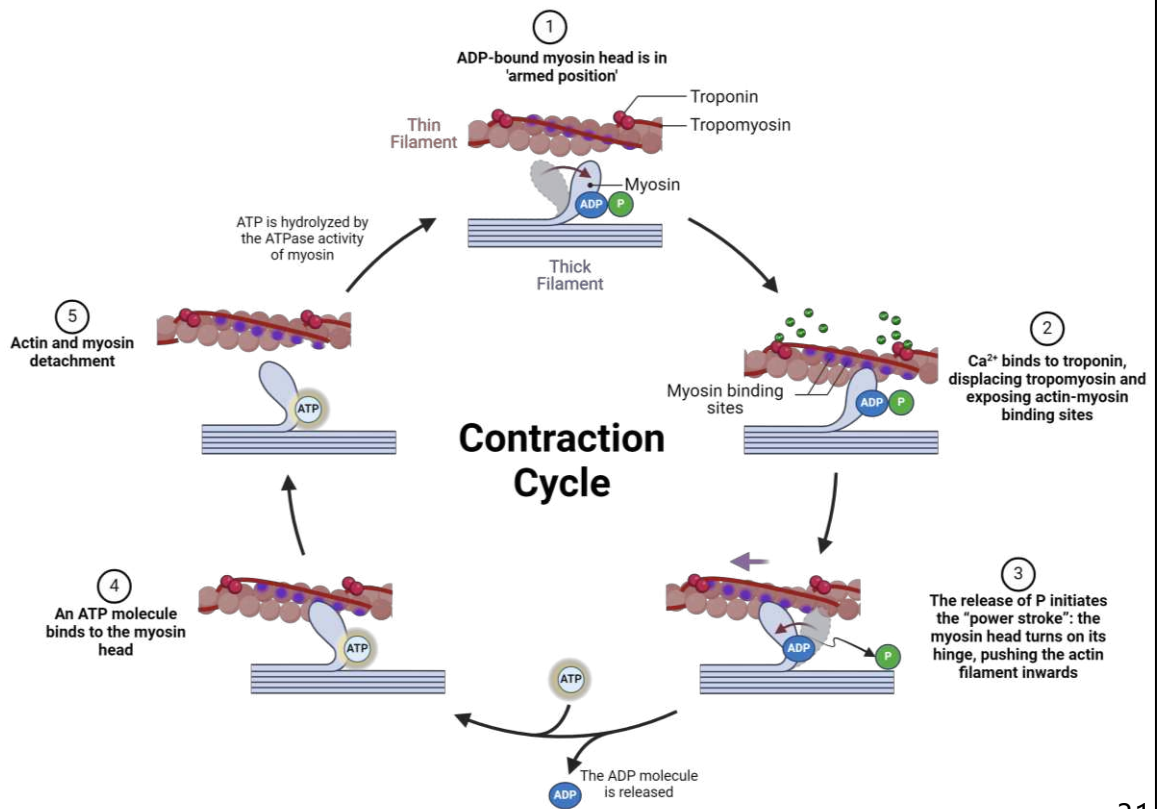


**Figure 3. Muscle contraction mechanisms. A.** The arrival of the action potential at the neuromuscular junction causes  $Ca^{2+}$  release from the SR into the sarcoplasm. **B.** Muscle contraction cycle following  $Ca^{2+}$  binding to troponin. Figure created with [BioRender.com](https://www.biorender.com).

## 1.5 Types of muscular actions

Muscular actions can be classified into three main categories: static (or isometric), dynamic concentric, and dynamic eccentric (**Figure 4**).

- **Isometric Actions:** an isometric action is characterized by the generation of force without any movement of a joint or limb. In these conditions, the resistance is greater than the force generated, resulting in no change in muscle length.
- **Dynamic (Isotonic) Actions:** A dynamic action involves both force generation and joint movement and can be further divided into concentric and eccentric actions <sup>[17]</sup>.
  - **Concentric Actions:** These occur when the muscle shortens as it generates force, causing the origin and insertion points of the muscle to move closer together, such as during elbow flexion.
  - **Eccentric Actions:** These occur when the muscle lengthens while generating force, causing the origin and insertion points of the muscle to move further apart.

The conversion of chemical energy into mechanical energy, described in 1954, is best explained by the "sliding filament" theory <sup>[18,19]</sup>. Accordingly, muscle contraction occurs as individual actin-myosin cross-bridges generate force, which is then transmitted both longitudinally and laterally within the muscle fiber. Movement is produced when this force reaches the myotendinous junction, tendons, and joints.

The force generated by a muscle depends on several factors, including:

- The degree of activation by the nervous system.
- The angle of insertion of muscle fibers into the tendon.
- The size of the muscle.
- The spacing between filaments.
- The number of cross-bridges formed.
- The quality of interaction between cellular elements.

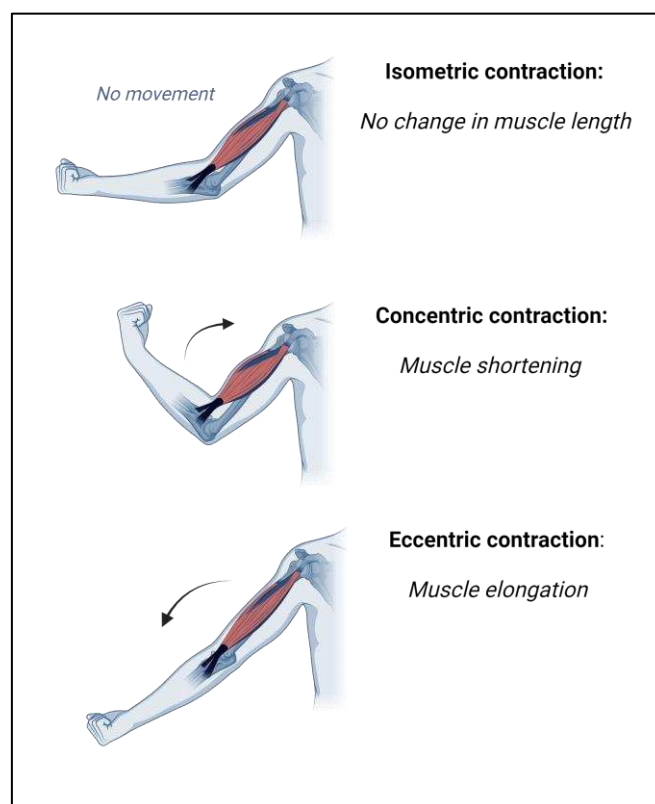


**Figure 4. Types of muscular action.** Muscles can contract isometrically, concentrically, or eccentrically. Figure created with [BioRender.com](https://www.biorender.com).

## I.6 Muscle energy mechanisms

Skeletal muscle requires energy in the form of ATP to produce force. The metabolic pathways for generating this energy vary based on the duration and intensity of the activity. Carbohydrates (blood glucose and muscle glycogen) and fats (free fatty acids in plasma and muscle triglycerides) are the primary fuels utilized by muscle fibers to produce ATP <sup>[20]</sup>. Amino acids can also contribute to energy production, though to a lesser extent <sup>[21]</sup>.

The selection of fuel type depends largely on the intensity of exercise:

- **High-Intensity Exercise:** Muscle glycogen is the preferred energy source due to its rapid availability and ability to sustain high rates of ATP production.
- **Low-Intensity, Prolonged Exercise:** Fatty acids become the primary fuel, as they provide a more sustained energy supply for longer durations.

This adaptive selection allows muscles to efficiently meet the energy demands of varying exercise intensities.

Three primary energy pathways enable muscle to perform its contractile function: ATP/CP (creatine phosphate) stores, anaerobic glycolysis, and oxidative phosphorylation. These pathways can be activated simultaneously at different points during exercise, depending on the intensity of the effort.

- **ATP/CP Stores:** The small reserves of ATP and CP in the muscle can sustain short bursts of high-intensity activity for a few seconds.
- **Anaerobic Glycolysis:** This pathway rapidly produces ATP to support muscular activity lasting a few minutes. However, its byproducts, hydrogen ions (H<sup>+</sup>) and lactate, impair muscle function and contribute to muscle fatigue.
- **Oxidative Phosphorylation:** For prolonged, intense exercise (ranging from minutes to hours), energy is supplied primarily through oxidative phosphorylation within the mitochondrial network. This pathway relies heavily

on the vascular capillary network, which delivers oxygen to active muscle fibers. The development and density of this network are influenced by the metabolic demands of each individual fiber.

By efficiently utilizing these pathways, muscles can meet the varying energy demands of different types of physical activity.

## **1.7 Satellite cells and muscle regeneration**

In healthy muscle, repetitive contractions can damage the sarcolemma, leading to muscle degeneration and inflammation. To counteract these injuries, muscle tissue can regenerate by activating resident muscle stem cells (MuSCs), also known as satellite cells. Satellite cells are located between the basal lamina and sarcolemma of muscle fibers <sup>[22]</sup>. Although these cells are quiescent in mature muscle, they retain the ability to generate myoblasts in response to muscle injury.

Small injuries, which may occur regularly during daily activities, result in minimal proliferation of satellite cells. In contrast, major injuries trigger prolonged and extensive proliferation before differentiation <sup>[23]</sup>. Activated satellite cells facilitate the replacement of damaged fibers (**Figure 5**).

Activated satellite cells can undergo two modes of division: symmetrical or asymmetrical (**Figure 5**). Asymmetrical division produces myogenic progenitors, which differentiate to regenerate and repair muscle fibers. Symmetrical division, however, maintains the pool of satellite cells. The balance between symmetrical and asymmetrical division is crucial for preserving the stem cell pool while generating enough progenitors for muscle growth and regeneration <sup>[24]</sup>.

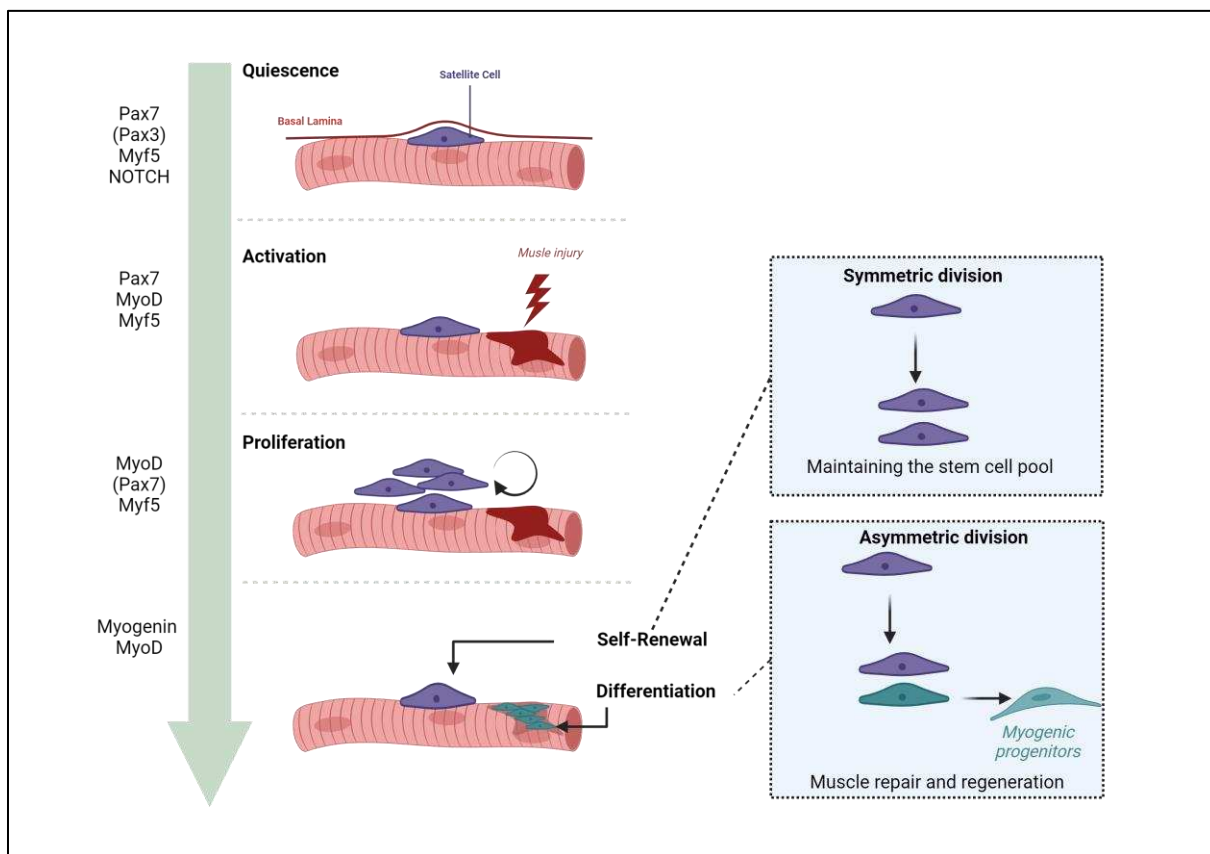


**Figure 5. Skeletal muscle regeneration and repair.** In the normal state, satellite cells remain quiescent, expressing markers such as Paired box protein-7 (Pax7) and Pax3 (in some muscles), and Myogenic Factor 5 (Myf5), while the Notch signaling pathway is active. Following an injury, satellite cells become activated and produce myogenic progenitors that express Myogenic Differentiation 1 (MyoD). These myoblasts then differentiate into myotubes, expressing myogenin. In cases of mild injury, the myotubes fuse with the damaged fiber, whereas in cases of severe injury, they fuse together to form new muscle fibers. Throughout this process, satellite cells undergo symmetrical division to self-renew, ensuring the replenishment of the stem cell pool. Figure created with [BioRender.com](https://www.biorender.com).

## I.8 Muscle function in health and disease

Skeletal muscle is a fundamental and essential tissue of the human body, performing several vital physiological and mechanical functions. These include facilitating movement and mobility, maintaining posture, supporting respiratory and cardiac function, and regulating energy and glucose metabolism. However, these functions can be influenced by various physiological, pathophysiological, and environmental disturbances.

### **I.8.1 Sarcopenia and muscle atrophy**

Ageing is frequently associated with sarcopenia <sup>[25]</sup>, which is characterized by a decline in muscle mass and strength <sup>[26]</sup>. Muscle atrophy, a hallmark of sarcopenia, is believed to adversely affect various physiological functions including thermoregulation, respiration, and metabolic homeostasis <sup>[27]</sup>. This decline in muscle function is particularly linked to reduced activity of muscle stem cells <sup>[28]</sup>, responsible for muscle regeneration, as well as atrophy of type II muscle fibers <sup>[29]</sup>. The mechanisms underlying these age-related changes remain incompletely understood; however, inflammation and oxidative stress <sup>[30]</sup>, loss of mitochondria <sup>[31]</sup>, and physical inactivity <sup>[32]</sup> are thought to contribute to sarcopenia.

### **I.8.2 The impact of exercise and physical inactivity on muscle function**

Both physical inactivity and exercise exert significant effects on muscle function. Prolonged periods of inactivity have been shown to lead to a notable decrease in muscle strength <sup>[33,34]</sup>, a phenomenon often linked with muscle fiber atrophy <sup>[35]</sup>. This atrophy is partially attributed to disruptions in proteostasis, marked by the activation of proteolysis pathways <sup>[36]</sup>.

Conversely, exercise plays a crucial role in either preventing or slowing down muscle atrophy by influencing various physiological processes. These include enhancing

organelle function, modulating signaling pathways, and regulating epigenetic mechanisms <sup>[37]</sup>.

### **I.8.3 Muscle disorders and impairment of muscle function**

Various muscle disorders can profoundly impact muscle function. These conditions may arise from hereditary factors or be secondary to other disorders, termed acquired myopathies (**Figure 6**).

Acquired myopathies often stem from endocrine imbalances (such as hyper- or hypothyroidism) or inflammatory conditions (like autoimmune diseases), manifesting as muscle weakness or fatigue. Additionally, certain drug therapies, such as statins prescribed for hypercholesterolemia, can induce myopathy.

On the other hand, hereditary muscle disorders result from genetic mutations affecting diverse aspects of muscle function. These mutations may affect muscle integrity and structure (as seen in congenital myopathies and muscular dystrophies), muscle contraction (as observed in myotonias and canalopathies), or energy metabolism (as seen in mitochondrial and metabolic myopathies). While these muscle disorders share common symptoms such as muscle weakness and wasting, they can vary in severity and age of onset.

For instance, congenital myopathies typically manifest at birth due to structural or functional alterations in muscle fibers, resulting in muscle weakness and delayed motor development <sup>[38]</sup>. Conversely, muscular dystrophies present as progressive muscle weakness, with severity and age of onset varying according to the specific type of dystrophy.

Our work focuses particularly on progressive muscular dystrophies, which will be described in more details.

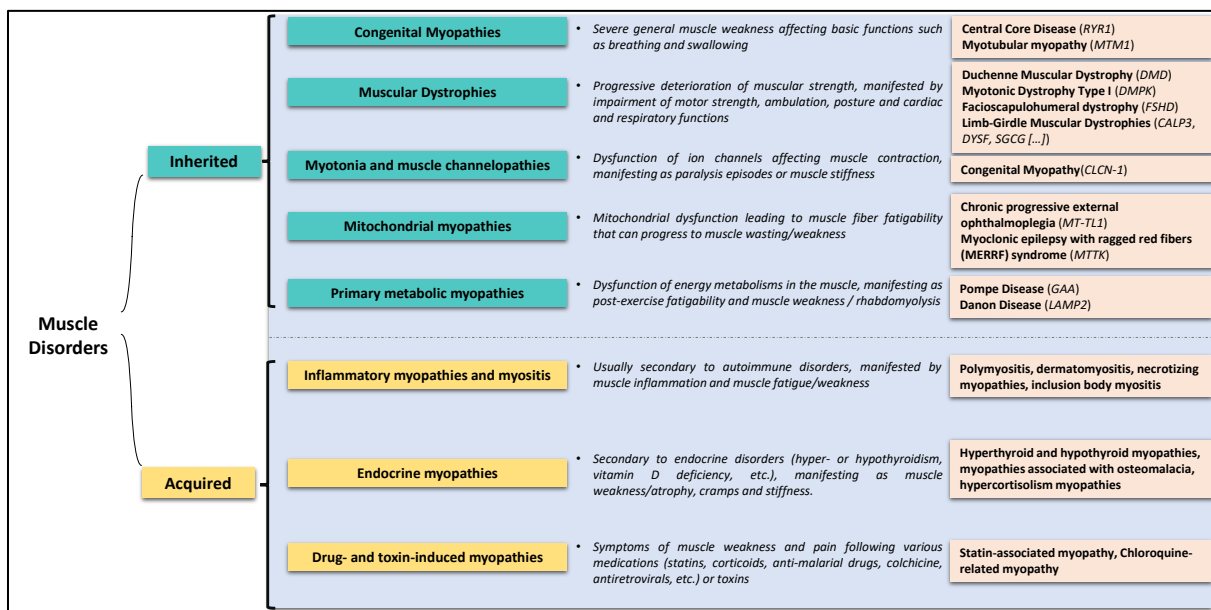


**Figure 6. Overview of Muscle Disorders.** Muscle disorders encompass a diverse range of diseases without an official classification. However, for the purpose of this discussion, we will categorize them into two main classes: inherited muscle disorders, resulting from mutations in specific genes, and acquired myopathies, which arise as secondary manifestations of other disorders or may be inherited with an unidentified or multigenic cause.

## I.9 Progressive Muscular Dystrophies

Progressive muscular dystrophies constitute a diverse group of genetic disorders primarily affecting skeletal muscle, characterized by the gradual decline of muscle strength over time. These muscle disorders typically manifest as motor weakness, compromised ambulation, posture abnormalities, and in advanced stages, impairment of cardiac and respiratory functions in certain dystrophies.

The genetic basis of muscular dystrophies involves mutations in genes encoding various proteins, which play roles in the organization of the sarcolemma or sarcomere, the extracellular matrix (ECM), the nuclear membrane, and cytoplasmic enzymes [39–41]. Severity levels of muscular dystrophies vary depending on the specific

gene affected, and mutations in the same gene can lead to different forms of dystrophy <sup>[42]</sup>. Onset may occur either at birth (for congenital muscular dystrophy), in childhood or adulthood, contingent on the dystrophy type.

Diagnosis typically relies on clinical symptoms, primarily muscle weakness, particularly in the proximal limbs, and is confirmed through histological studies revealing muscle degeneration and serological analyses detecting elevated creatine kinase (CK) levels. Genetic analysis further corroborates the diagnosis by identifying the mutated gene.

One of the earliest and most prevalent muscular dystrophies identified is Duchenne muscular dystrophy (DMD), attributed to the absence or reduction of the dystrophin protein <sup>[43]</sup>. Within skeletal muscle, dystrophin interacts directly or indirectly with various cellular components, including the sarcolemma, cytoskeleton, signaling proteins, and scaffolding proteins. Together, dystrophin and its associates form the dystrophin-associated glycoprotein complex (DAGC) (**Figure 7**).

The DAGC, essential for maintaining the structural stability and integrity of muscle cells, comprises of multiple proteins. These include dystrophin, the dystroglycan (DG) subcomplex ( $\alpha$ -dystroglycan and  $\beta$ -dystroglycan), the sarcoglycan (SG) subcomplex ( $\alpha$ -sarcoglycan,  $\beta$ -sarcoglycan,  $\gamma$ -sarcoglycan, and  $\delta$ -sarcoglycan), dystrobrevin ( $\alpha$ -dystrobrevin,  $\beta$ -dystrobrevin), syntrophin ( $\alpha$ 1-syntrophin and  $\beta$ 1-syntrophin), sarcospan and neuronal nitric oxide synthase (nNOS).

The characterization of the DAGC <sup>[44]</sup> and sub-sarcolemmal cytoskeletal networks and extracellular partners has facilitated the identification of additional muscular dystrophies beyond DMD, such as limb-girdle muscular dystrophy (LGMD) and congenital muscular dystrophy (CMD) <sup>[45]</sup>.

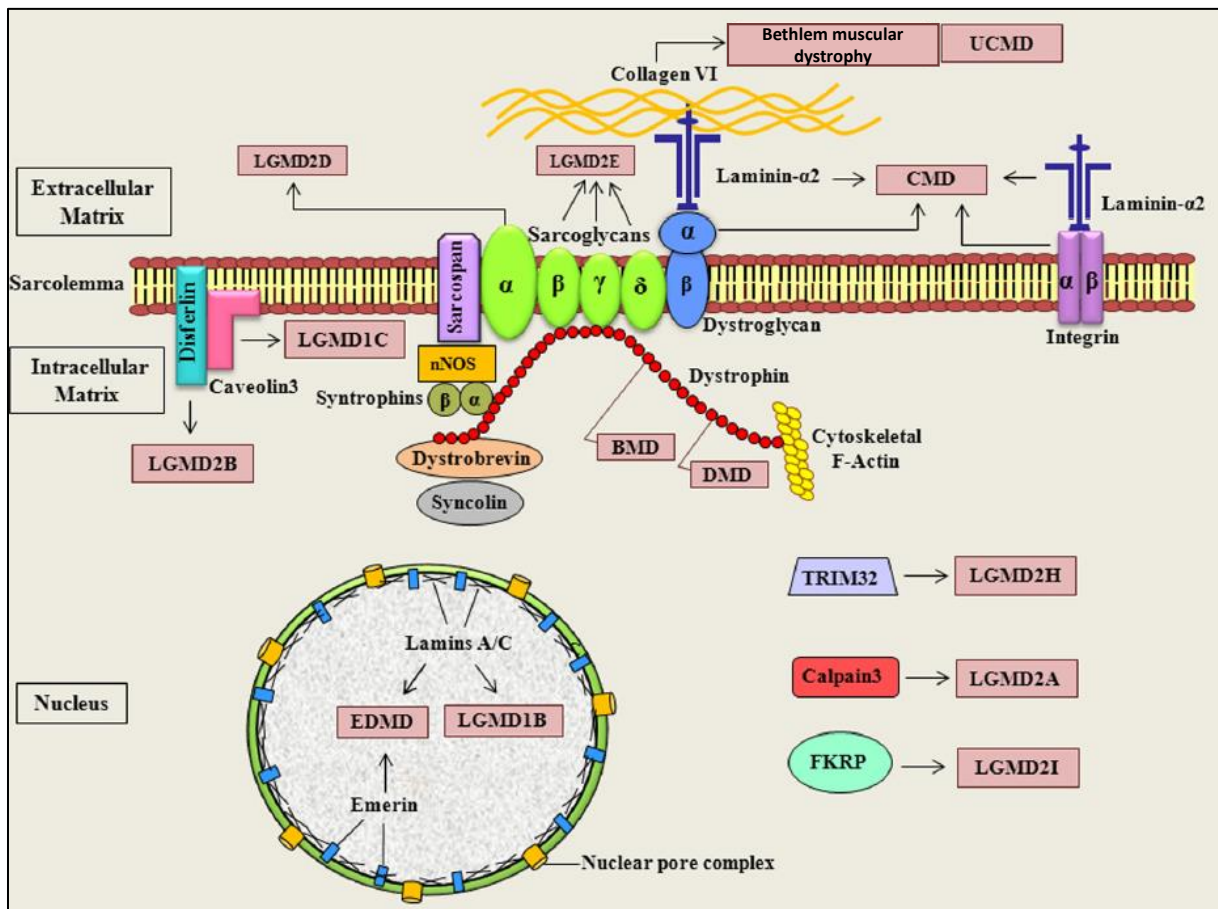


**Figure 7. Proteins implicated in muscular dystrophies.** (Adapted from Shin et al., 2013<sup>[41]</sup>) Mutations in genes encoding various proteins contribute to the development of muscular dystrophies. Numerous proteins, including those forming the DAGC, play critical roles in preserving muscle structure during contractions. Additionally, proteins located in the extracellular matrix, plasma membrane, nuclear membrane, and cytoplasmic enzymes have been implicated in the pathogenesis of muscular dystrophies.

LGMDs encompass a diverse array of muscular disorders, primarily affecting the proximal muscles in the early stages of the disease, and potentially extending to distal-proximal involvement as the myopathy progresses. Despite their heterogeneity, these dystrophies share common features, including persistent muscle fiber degeneration and regeneration, elevated serum CK levels, fibroadipose infiltration,

and degenerative alterations evident on magnetic resonance imaging (MRI) imaging of the muscle <sup>[46]</sup>.

The age of onset for LGMDs spans infancy (non-congenital) to late adulthood, with disease progression generally manifesting as symmetrical muscle weakness. However, there is considerable variability both among different types of LGMD and among patients with the same LGMD. As a result, LGMDs present a broad spectrum of muscle damage and atrophy, ranging from severe forms with rapid progression in childhood to relatively benign forms with late onset.

With over 30 genetically distinct types, LGMDs are categorized into two main groups: dominant forms (formerly designated as type 1, now designated by 'D' for dominant) and recessive forms (previously LGMD type 2, now designated by 'R' for recessive).

Among the most prevalent forms of LGMD in France, which are the focus of research and therapeutic development in our laboratory, are calpainopathy (LGMDR1) <sup>[47]</sup>, sarcoglycanopathies (LGMDR3-R4-R5-R6) <sup>[48]</sup>, Fukutin-related protein (FKRP)-related LGMDR9, and dysferlinopathy (LGMDR2) <sup>[47]</sup>.

## **II- Duchenne Muscular Dystrophy: Pathophysiology and Therapeutic Strategies**

DMD is a rare, severe, and progressive muscular disorder primarily affecting boys, for which there are currently no curative treatments. This section provides an overview of the disease, its pathophysiology, and ongoing therapeutic strategies aimed at managing its progression.

## II.1 Disease description

DMD is an X-linked recessive genetic disorder primarily characterized by the absence or dysfunction of dystrophin; a protein encoded by the *DMD* gene. With an incidence of approximately 1 in 5000 boys, it is the most prevalent infantile form of muscular dystrophy [49,50].

The initial description of the disease dates back to Edward Meryon (1807-1880), who documented the clinical cases of nine boys exhibiting progressive muscle loss, including calf muscle enlargement [51]. Dr. Duchenne de Boulogne (1806-1875) further elucidated DMD in 1861, providing a comprehensive analysis of the first patient afflicted with "progressive muscular atrophy with degeneration," later recognized as DMD, in his book entitled '*De l'électrisation localisée et de son application à la pathologie et à la thérapeutique*' [51] (**Figure 8**).

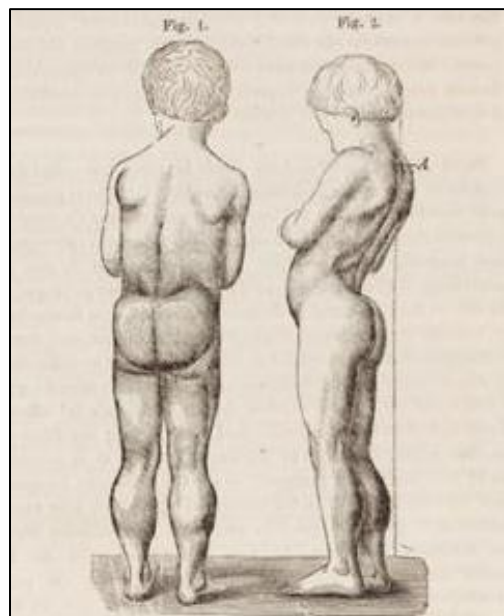


**Figure 8. Drawing of a DMD patient by Dr. Guillaume-Benjamin Duchenne de Boulogne in 1868.**

With the advent of molecular genetics, the *DMD* gene was cloned for the first time in 1987 by Koeing et al. <sup>[52]</sup>, establishing the association with the myopathy phenotype. Subsequent investigations revealed that this gene encodes for dystrophin, a crucial protein for the preservation of muscle integrity <sup>[43,52]</sup>. Consequently, DMD arises from mutations within the *DMD* gene, impairing the production of the muscular isoform of dystrophin (Dp427m) <sup>[53]</sup>.

Furthermore, mutations in the *DMD* gene can give rise to another form of muscular dystrophy, namely Becker muscular dystrophy (BMD), which typically exhibits a milder clinical course with later onset and slower progression of symptoms compared to DMD <sup>[54]</sup>.

While DMD predominantly affects males, occurring in approximately less than 1 per million females, its occurrence in women is often linked to conditions such as Turner syndrome <sup>[55–58]</sup>, a non-random X-chromosome inactivation <sup>[59,60]</sup>, or is associated with bi-allelic mutations <sup>[61]</sup>.

## **II.2 Clinical presentation**

DMD typically presents with early-onset weakness in the lower proximal limbs, accompanied by elevated levels of CK due to ongoing degradation of muscle fibers <sup>[40]</sup>. Cognitive impairment, notably in working memory and executive function, is often observed in patients, although this impairment tends to remain stable rather than progressive <sup>[62]</sup>. Cardiac and respiratory impairments typically manifest in patients during the second and third decades of life <sup>[63]</sup> (**Figure 9**).

Most patients experience loss of ambulation around the ages of 10 to 12 years <sup>[54]</sup> and may require ventilatory assistance by around 20 years of age. Despite significant advancements in care, individuals with DMD generally have a lifespan ranging from

20 to 40 years, with respiratory and/or cardiac complications being the primary causes of mortality. However, the survival rate of DMD patients has shown improvement over time, attributed to enhanced recommendations for care and better management of cardiopulmonary complications [64]. For instance, a study conducted in France demonstrated an increase in median life expectancy from 25.77 years for patients born before 1970 to 40.95 years for those born after 1970 [65].

Female carriers of *DMD* mutations on one X chromosome typically remain asymptomatic, although in rare instances, they may present with a BMD phenotype [66,67]. Approximately 2.5-19% of carriers exhibit skeletal muscle syndromes, and 7.3-16.7% develop dilated cardiomyopathy [68], although respiratory involvement is typically absent.

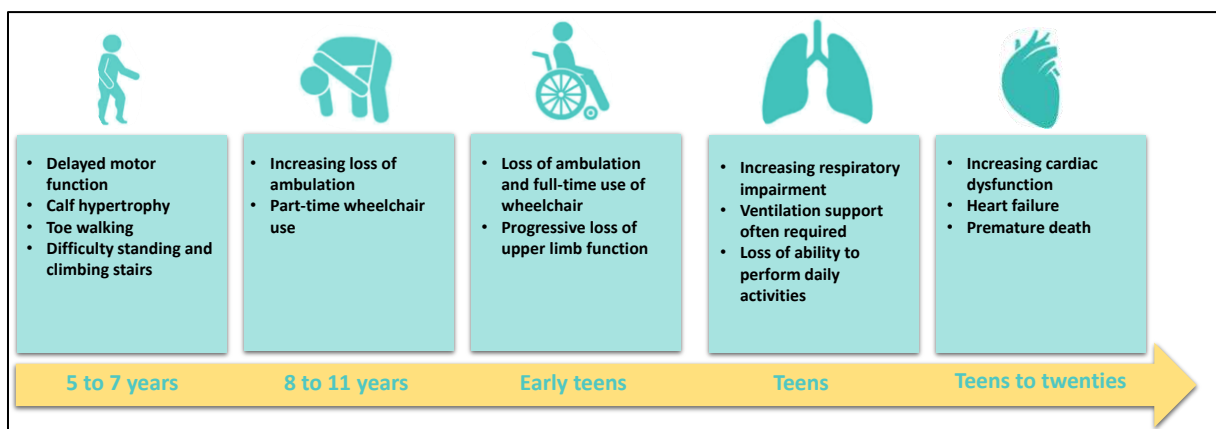


**Figure 9. Clinical evolution of DMD.** (Adapted from Asher et al., 2020 [69])

Today, the primary cause of mortality among patients is cardiovascular complications [70,71]. DMD is closely linked to dilated cardiomyopathy and cardiac rhythm irregularities, particularly supraventricular arrhythmias. The observed dilated cardiomyopathy is characterized by widespread fibrosis of the left ventricular free wall [72], with heart failure emerging as the disease advances [73]. Hence, early detection

and effective management of cardiovascular issues are pivotal for enhancing both survival rates and overall quality of life.

## **11.3 Genetic basis of the disease: the *DMD* gene and Dystrophin**

### **1.3.1 The *DMD* gene**

The *DMD* gene is the largest known coding gene, encompassing over 2.6 million base pairs (bp) and consisting of 79 exons that encode multiple dystrophin isoforms (**Figure 10A**). Given its extensive size, the gene is particularly susceptible to mutation, with thousands of mutations identified in both DMD and BMD patients <sup>[74]</sup>.

In DMD patients, various mutations lead to the complete loss of or production of nonfunctional dystrophin. Approximately 60-70% of these mutations are deletions, while 20% consist of point mutations, small deletions, or insertions <sup>[75,76]</sup>. Conversely, in BMD patients, 60-70% of mutations are deletions, 20% are duplications, and 5-10% are point mutations, small deletions, or insertions <sup>[75,77,78]</sup>. Mutations in BMD are typically in-frame, preserving the open reading frame (ORF) and allowing for the production of a partially functional, truncated dystrophin protein.

Deletions and duplications often cluster in specific 'hotspots' regions of the *DMD* gene, with around 47% of mutations in DMD patients occurring within the exons 45-55 region <sup>[79]</sup>, and 7% found between exons 3-9 <sup>[80]</sup>.

The *DMD* gene primarily encodes the muscle isoform of dystrophin (Dp427m) (**Figure 10B**), alongside two additional complete isoforms and several truncated isoforms transcribed from various internal promoters (**Table 2**).

	Dp427b	Expressed in cortical neurons <sup>[81]</sup>
	Dp427p	Expressed in cerebellar Purkinje cells, identified in mice and

<b>Complete isoforms</b>		very weakly expressed in humans during embryogenesis and postnatally <sup>[82,83]</sup>
<b>Truncated isoforms</b>	Dp260	Expressed mainly in the retina <sup>[84]</sup>
	Dp140	Expressed in the central nervous system and kidneys <sup>[85]</sup> , and highly expressed in the brain at the embryonic stage <sup>[83]</sup>
	Dp116	Expressed mainly in peripheral nerves and Schwann cells <sup>[86]</sup>
	Dp71	Ubiquitously expressed, but particularly in neuronal cells <sup>[87]</sup>
	Dp40	Derived from the same promoter as Dp71 but is polyadenylated in intron 70 <sup>[88]</sup>

**Table 2. Non-muscular isoforms of Dystrophin**

### **I.3.2 Muscle Dystrophin**

The Dp427m isoform, weighing approximately 427 kilo daltons (kDa), is predominantly expressed in skeletal and cardiac muscle tissues. It is a sub-sarcolemmal protein with several binding domains, enabling it to establish a mechanical bridge between the ECM and the cytoskeleton – a crucial link for structural integrity of the muscle.

Dystrophin is a pivotal constituent of the DAGC, crucial not only for maintaining muscle fiber rigidity <sup>[88]</sup>, but also for shielding the muscle against mechanical stress encountered during contractions <sup>[89,90]</sup>.

Muscle dystrophin contains four major domains, that enable it to bind different protein partners:

- **Actin-binding domain (ABD):** this domain binds the actin filaments.
- **The central 'rod' domain:** composed of 24 spectrin repeats (R1-R24) and four hinges (H1-H4), this domain enables dystrophin to bind several sarcomeric and

sarcolemmal components. It includes two regions of direct sarcolemma binding (R1-R3 and R10-R12), a site for actin filaments binding via electrostatic interactions (R11-R15) <sup>[91]</sup>, and two sites of interactions with microtubules (R4-R15 and R20-R23) <sup>[92,93]</sup>. Spectrins R16 and R17 host the nNOS binding site, pivotal for correct nNOS localization on the sarcolemma <sup>[94,95]</sup>. Localization of nNOS to the sarcolemma facilitates paracrine signaling by diffusing nitric oxide to blood vessels, thereby promoting vasodilatation in contractile muscles. Misplacement of nNOS could lead to functional ischemia during exercise <sup>[96,97]</sup>, or cell-damaging nitrosative stress, affecting muscle force production <sup>[98,99]</sup>.

- **The cysteine-rich domain (CR):** this domain enables dystrophin to interact with other DAGC proteins, particularly through binding with the transmembrane protein  $\beta$ -DG <sup>[100]</sup>. Additionally, the CR domain interacts with calmodulin <sup>[101]</sup>, which plays a pivotal role in calcium signaling pathways <sup>[102]</sup>.
- **The C-terminal domain:** this domain contains a direct binding site to the sarcolemma <sup>[103]</sup>, as well as interaction sites with DAGC constituents (syntrophin and dystrobrevin).  $\alpha$ -syntrophin, particularly, plays a crucial signaling role by binding several ion channels (sodium channels Na1.4 and Na1.5, potassium channels Kiv2, Kiv4.1 and calcium receptors TRPC1 and TRPC4). Furthermore, it anchors nNOS to dystrophin <sup>[103,104]</sup>.

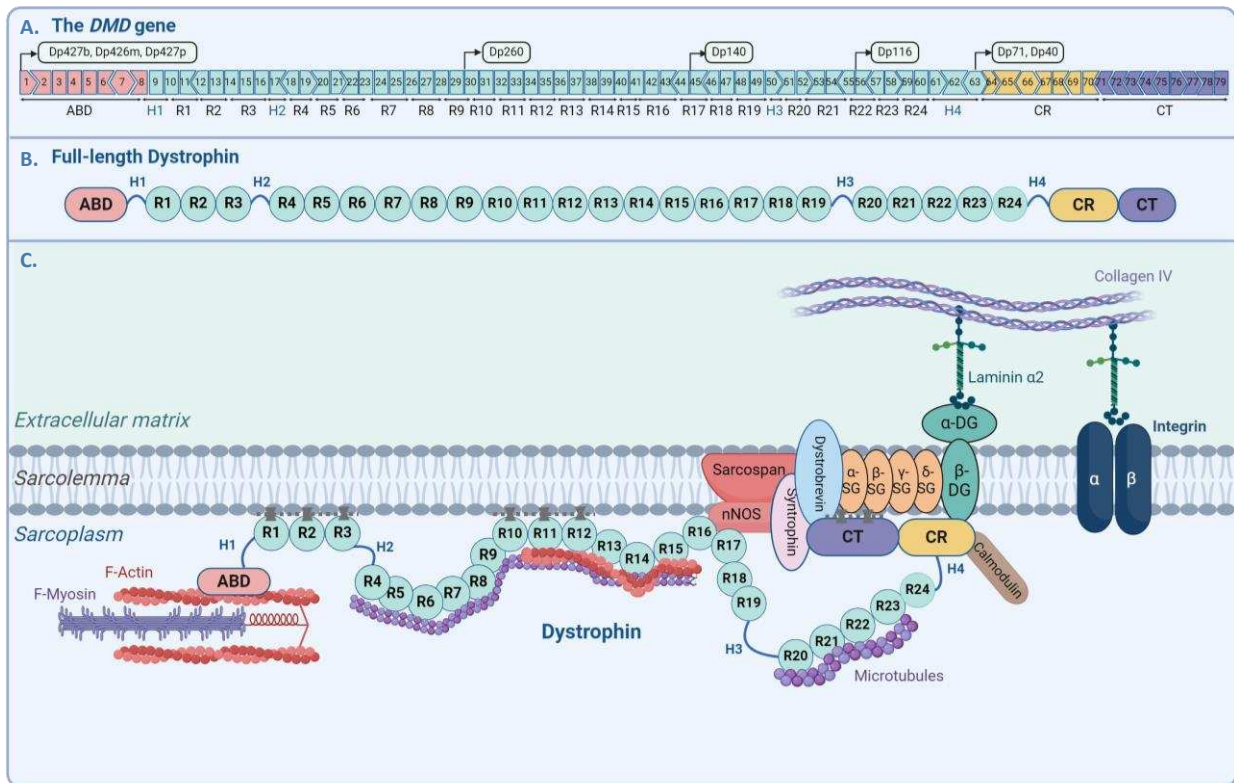


**Figure 10. Structure and functions of the DMD gene and dystrophin protein. A.** The complete DMD gene is ~2.4 Mb long and contains 8 promoters and 79 exons. Three upstream promoters (Dp427b, Dp427m and Dp427p) produce the complete cDNA of approximately 11.4 kb and the full-length protein of around 427 kDa. Additionally, four internal promoters (Dp260, Dp140, Dp116, and Dp71) produce truncated non-muscular isoforms of dystrophin. Alternative splicing at the 3' end and alternative polyadenylation contribute to the generation of further dystrophin isoforms. The primary muscle isoform is synthesized from the Dp427m promoter. **B.** The full-length dystrophin protein: complete dystrophin consists of four primary domains: the N-terminal actin-binding domain (ABD), encoded by exons 1-8; the rod domain (R), encoded by exons 8-64; the cysteine-rich domain (CR), encoded by exons 64-70; and the C-terminal (CT) domain, encoded by exons 71-79. The rod domain comprises 24 spectrin-like repeats and 4 intersecting hinges. **C.** Localization of dystrophin and the DAGC in the muscle fiber. Figure created with [BioRender.com](https://www.biorender.com).

## II.4 DMD pathophysiology

DMD has historically been perceived primarily as a muscle degenerative disease <sup>[105]</sup>, although the precise mechanisms driving muscle necrosis remain inadequately understood. Prior to the discovery of dystrophin, various hypotheses regarding muscle degeneration had been suggested, including muscle ischemia, motor-neuronal abnormalities, nutritional deficiencies, metabolic irregularities, and sarcolemma damage alongside calcium deregulation <sup>[106,107]</sup>. Among these hypotheses, the notion attributing the clinical manifestations of DMD to sarcolemma instability emerged as the most compelling. The identification of dystrophin and *DMD* as the protein and gene <sup>[43,52]</sup> involved in the myopathy bolstered this hypothesis, according to which DMD is caused by structural and functional defects in the sarcolemma.

Indeed, the absence of functional dystrophin in skeletal and cardiac muscle is believed to compromise the integrity of the sarcolemma, rendering muscle fibers more vulnerable to damage induced by contractions. This hypothesis may also elucidate the pathogenesis of several muscular dystrophies wherein proteins of the DAGC are impacted. However, it is noteworthy that some muscular dystrophies result from abnormalities in non-structural muscle proteins (such as *CALP3* for LGMDR1, *DYSF* for LGMDR2, and *HGMCR* for a recently identified dystrophy) <sup>[39,108,109]</sup>, indicating that sarcolemma destabilization may not comprehensively elucidate all mechanisms driving muscle degeneration.

Subsequently, we will elucidate the diverse molecular and cellular disruptions, both direct and indirect, responsible for muscle fiber degeneration, alongside the pathophysiological alterations dystrophic muscle undergoes consequent to muscle fiber death (**Figure 11**). While the pathophysiological mechanisms will be delineated

primarily for DMD, several mechanisms are shared among other muscular dystrophies, albeit with variations in severity and temporal progression.

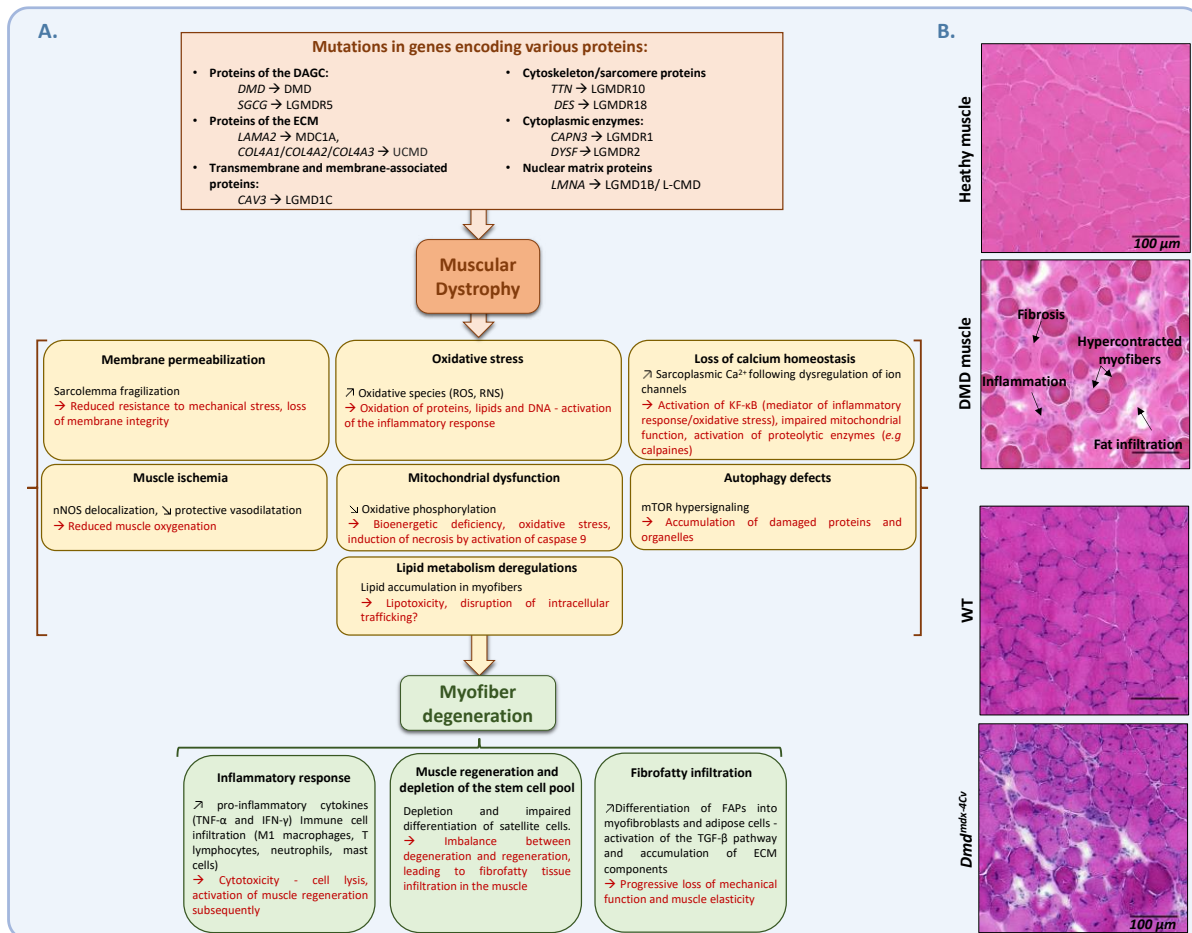


**Figure 11. Pathophysiological mechanisms of muscular dystrophies. A.** Schematic representation of the various mechanisms directly or indirectly contributing to muscle degeneration and muscular dystrophy progression. **B.** Cross-sections of skeletal muscle obtained from DMD patients and *Dmd*<sup>mdx-4Cv</sup> mouse model (and healthy and WT controls), stained with hematoxylin and eosin (HE). Dystrophic muscle exhibits a more disorganized fiber distribution compared to healthy muscle, accompanied by a loss of inter-fiber connections. Notable dystrophic features include inflammatory cell infiltration (manifested as accumulations of nuclei between fibers), fibrosis (evidenced by increased extracellular matrix components), and

*adipose infiltration (indicated by white spaces on HE sections). In  $Dmd^{mdx-4Cv}$  muscle, centronucleated fibers (with nuclei positioned at the fiber center instead of the periphery) are observed, indicative of ongoing muscle regeneration.*

#### **I.4.1 Pathological mechanisms leading to muscle cell death**

##### **a) Mechanical stress and sarcolemma disruption**

The muscular force generated by the sarcomere during contraction-relaxation cycles is transmitted through the sarcolemma, imposing significant mechanical stress on this membrane. Under normal physiological conditions, the integrity of the sarcolemma is upheld by the intricate interplay among the cytoskeleton, sarcolemma, and ECM, facilitated by the DAGC and integrin complexes. Dystrophin, notably, plays a major role, by interacting with both the filamentous F-actin <sup>[110]</sup> and the gamma cortical (costameric) actin <sup>[111,112]</sup>.

In DMD, as in many LGMDs, the breakdown of the DAGC complex compromises the sarcolemma's strength, rendering it more vulnerable to damage induced by muscle contractions. This event stands as one of the initial pivotal occurrences in DMD pathology and likely underpins subsequent pathological manifestations. Notably, sarcolemma ruptures represent a hallmark mechanism of pre-necrotic fibers <sup>[113]</sup>. These membrane disruptions, also referred to as "tears" or "delta" lesions, are discernible by the passive leakage of muscle enzymes like CK from the muscle into the bloodstream, particularly following muscle activity (e.g., post-exercise). Furthermore, compromised plasma membrane integrity is evidenced by the infiltration of dyes (e.g., Evans Blue) or circulating proteins (e.g., Immunoglobulin G - IgG, albumin) into the interior of fibers (**Figure 12**), facilitating the identification of damaged fibers within cross-sections of dystrophic muscle.

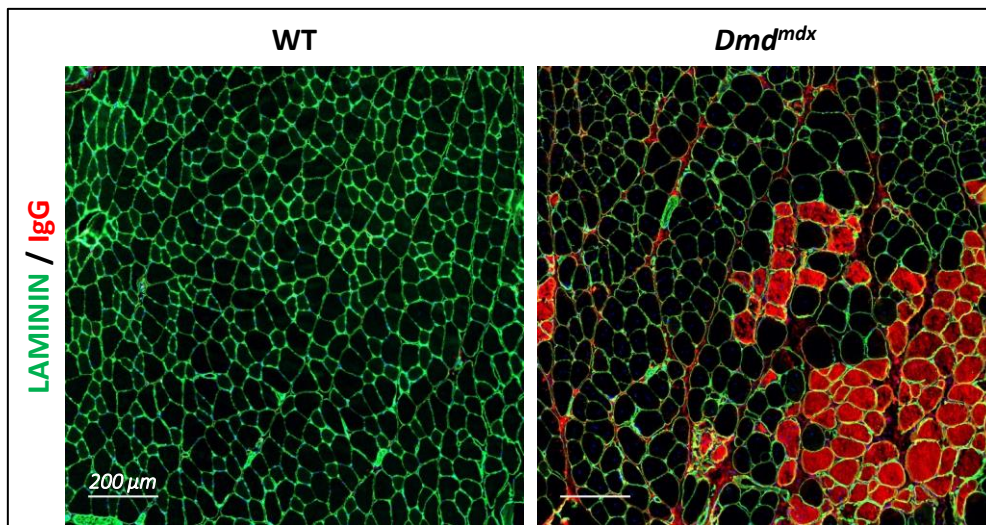


**Figure 12. Permeabilization of muscle fibers in dystrophic muscle.** Permeabilized muscle fibers, indicative of compromised membrane integrity, are highlighted by positive labeling for mouse immunoglobulin G (IgG) (depicted in red) in cross-sections of gastrocnemius muscle (GA) obtained from  $Dmd^{mdx}$  and wild-type (WT) mice. This staining pattern illustrates the infiltration of circulating IgG into the interior of fibers, a characteristic feature of damaged fibers in dystrophic muscle.

**b) Free-radical-induced muscle damage: oxidative and nitrosative stress**

Excessive oxidative stress generates superoxide anions, hydrogen peroxide, and nitric oxide. These primary oxidative species are subsequently converted into reactive oxygen species (ROS) and reactive nitrogen species (RNS), which can damage membrane lipids, sarcomere structural and regulatory proteins, and DNA.

DMD muscle is characterized by significant oxidative stress, contributing to muscle weakening. This is evidenced by elevated levels of ROS and RNS, as well as extensive oxidation of proteins, lipids, and DNA [114–117].

- **Oxidative stress and ROS**

Increased oxidative stress in muscle primarily stems from the upregulation of the ROS-generating NADP(P)H oxidase 2 (NOX2) complex within the sarcolemma [118].

Activation of NOX2 occurs via the microtubule-associated protein Tac1 in response to mechanical stretching of the muscle, culminating in the generation of ROS [119,120]. This process is notably exacerbated in DMD due to the dense and disorganized microtubule network resulting from the loss of dystrophin-microtubule interaction. Inhibition of this complex has shown promise in mitigating muscle damage in *Dmd*<sup>mdx</sup> mice [121]. More recently, NOX4 was also shown to be upregulated in dystrophic muscle, and its inhibition showed a new strategy to reduce fibrosis and other dystrophic features in animal models [122].

Additionally, infiltration of neutrophils containing myeloperoxidases and other inflammatory cells, along with mitochondrial dysfunction, represent significant contributors to ROS production in DMD muscle.

- **Nitrosative stress and RNS**

Another prominent source of free radical damage in DMD muscle arises from RNS. Disruption of nNOS binding to dystrophin leads to its detachment from the sarcolemma [98,123]. Consequently, nNOS loses its ability to release nitric oxide to the blood vessels and becomes activated within the cytoplasm, triggering nitrosative stress within the muscle tissue.

Elevated levels of oxidative stress exacerbate muscle degeneration by intensifying the inflammatory response and impeding the regeneration process [124]. Despite the pivotal role oxidative stress plays in DMD pathogenesis, conventional antioxidant therapies have demonstrated limited efficacy in patients [116].

- c) Loss of calcium homeostasis**

A hallmark of dystrophic muscle is the overload of Ca<sup>2+</sup> detected in the cytosol [125,126], particularly in the subsarcolemmal space [127]. This elevation in cytosolic

calcium is pronounced during muscle contraction but is also present in resting myotubes <sup>[128]</sup>.

Dystrophin and the DAGC form a scaffold for numerous proteins, including those involved in calcium metabolism, which are crucial for the activation, modulation, and termination of calcium signals <sup>[101,129,130]</sup>. The DAGC complex is associated with several key players in calcium homeostasis, such as store-operated calcium channels (SOC), stretch-activated (SA) channels, and the sodium-calcium exchanger (NCX) <sup>[129,131]</sup>.

Dysfunction of the SR further contributes to the increase in cytosolic calcium. Nitrosative and oxidative stress in dystrophic muscle induces nitrosation and phosphorylation of ryanodine receptors (RyRs), destabilizing their interaction with calstabin <sup>[132]</sup>. This destabilization increases the opening of RyRs during contraction, causing calcium leakage from the SR into the cytosol <sup>[133]</sup>.

Elevated cytosolic calcium is implicated in the activation of nuclear factor-kappa B (NF- $\kappa$ B), a transcription factor that plays a role in the inflammatory response and oxidative stress. Additionally, excessive calcium leads to mitochondrial calcium overload, disrupting cellular energy metabolism. Another detrimental consequence is the activation of calcium-dependent enzymes, such as calpains and phospholipase A<sub>2</sub>, which ultimately result in muscle protein degradation and fiber necrosis <sup>[134]</sup>.

Despite the critical role of calcium homeostasis deregulation in muscle fiber degeneration in muscular dystrophies, clinical trials with calcium channel blockers have not demonstrated significant benefits for DMD patients <sup>[135]</sup>.

#### ***d) Muscle ischemia***

One of the crucial roles of dystrophin is to anchor nNOS to the sarcolemma. This anchoring allows nNOS to perform a paracrine function by releasing nitric oxide into the surrounding vasculature, thereby inducing protective vasodilation <sup>[94]</sup>. When

dystrophin is absent, nNOS becomes delocalized in the cytoplasm, which impairs its ability to facilitate muscle oxygenation and leads to ischemic damage to muscle fibers [136].

#### ***e) Mitochondrial dysfunction***

Mitochondria play a key role in the bioenergetic mechanisms of skeletal muscle by synthesizing ATP through oxidative phosphorylation [137]. Additionally, they are crucial for muscle signaling, regulating calcium levels, and initiating calcium-dependent cell death [138].

In DMD, mitochondrial deficits are a hallmark of the disease's pathogenesis. Mitochondrial function in dystrophic muscle is compromised, with a significant reduction in oxidative phosphorylation [139,140], particularly affecting complex I activity [141]. These mitochondrial dysfunctions are largely attributed to  $Ca^{2+}$  overload, which is believed to cause extensive opening of the mitochondrial permeability transition pore (mPTP) and a subsequent decrease in ATP synthesis [138].

Recent studies by our team have linked the decrease in oxidative phosphorylation and ATP production to the deregulation of a cluster of microRNAs (miRs) at the Dlk1-Dio3 locus [142,143], notably including miR-379 [144]. The increase in these miRNAs in the circulation is partially attributed to regenerative muscle fibers [143].

Impaired oxidative phosphorylation contributes to oxidative stress by increasing the emission of hydrogen peroxide ( $H_2O_2$ ) [145–147]. Mitochondrial dysfunction also induces endoplasmic reticulum (ER) stress due to disrupted interactions at mitochondria-associated ER membranes (MAMs) contact sites [148,149]. Moreover, the resulting bioenergetic impairment of mitochondria is correlated with necrosis and muscle atrophy through the activation of caspase 9 [147].

#### ***f) Autophagy defects and loss of proteostasis***

The muscular damage described, notably sarcolemmal permeabilization, activation of calcium-dependent proteases, and oxidative and nitrosative stress, leads to an accumulation of defective organelles and altered cellular components in dystrophic muscle.

In healthy muscle, autophagy (or macro-autophagy) plays a crucial role in maintaining muscle mass by renewing cellular components under both normal conditions and in response to stimuli such as cellular stress and nutrient or amino acid deprivation <sup>[150,151]</sup>. Defects in autophagy can be detrimental to muscle health and are implicated in several muscle disorders, such as autophagic vacuolar myopathies <sup>[152]</sup>.

In DMD muscle, numerous studies have identified significant defects in autophagy <sup>[153–156]</sup>, evidenced by the accumulation of damaged organelles. These autophagy defects have been attributed to various factors, including the activation of the mammalian target of rapamycin (mTOR) through phosphorylation by protein kinase B (also known as *Akt*) <sup>[153]</sup>. Oxidative stress also indirectly contributes to autophagy defects by continuously activating a kinase called *Src*, which in turn activates mTOR via PI3K/Akt phosphorylation <sup>[155]</sup>.

The accumulation of damaged proteins and organelles due to impaired autophagic flux directly contributes to muscle cell degeneration in DMD muscle <sup>[154]</sup>. Therefore, targeting autophagy presents a promising therapeutic strategy for DMD. For instance, a low-protein diet in *Dmd*<sup>mdx</sup> mice has been shown to reactivate autophagy, leading to significant improvements in muscle function and structure <sup>[153]</sup>. Additionally, treatment with a pharmacological agonist of the AMP-activated protein kinase (AMPK) of *Dmd*<sup>mdx</sup> mice also activates autophagy and improves the dystrophic phenotype in the diaphragm <sup>[157]</sup>.

### **g) Lipid abnormalities**

Muscle biopsies from young DMD patients reveal notable lipid abnormalities [158]. These include the accumulation of phosphatidylcholine, cholesterol, sphingomyelin, and triglycerides, along with an abundance of monounsaturated fatty acids in the most affected muscle areas [159,160]. Additionally, studies have shown deregulation of circulating lipids in DMD patients [161,162], characterized by increased levels of triglycerides, phospholipids, and various forms of cholesterol (total, free, and esterified). Similar lipid disturbances have also been detected in patients with BMD and in healthy female carriers of the *DMD* gene [163]. These findings led to the suggestion that DMD may represent a novel form of genetic dyslipidemia [163,164].

Lipid dysregulations are primarily observed at early stages of the disease in both patients and animal models [160,163,165], indicating that these abnormalities might play a crucial role in the pathogenesis of DMD. However, the underlying mechanisms and their impact on disease progression remain poorly understood.

Recently, our team identified deregulations in cholesterol and fatty acid metabolism in DMD muscle [142]. By screening miRNAs in the serum of a cohort of DMD patients, we detected deregulated circulating miRNAs. Analysis of these miRNAs, based on their host and target genes, highlighted disruptions in the cholesterol synthesis pathway (mevalonate pathway) and the fatty acid synthesis pathway. These findings were validated by detecting cholesterol accumulation in muscle biopsies from DMD patients and *Dmd*<sup>mdx</sup> mice. This cholesterol buildup was correlated with the activation of sterol regulatory element-binding protein 1/2 (SREBP1 and SREBP2) transcription factors, which regulate endogenous cholesterol synthesis and cellular uptake.

Administering simvastatin, a known cholesterol-lowering drug, corrected muscle cholesterol accumulation in *Dmd<sup>mdx</sup>* mice [142]. Simvastatin treatment has also been shown to improve both skeletal [166] and cardiac [167] muscle function in these mice.

#### **1.4.2 Pathological mechanisms contributing to disease progression following myofibers death**

##### **a) Inflammation and immune response**

Muscle fiber damage and degeneration lead to the infiltration of inflammatory cells into the muscle tissue. This infiltration, primarily involving T lymphocytes and macrophages, is most prominent in young patients aged 2 to 8 years [168]. This early inflammatory response precedes the onset of the disease and directly contributes to the progression of dystrophy.

- **Macrophage infiltration**

At the onset of the inflammatory phase, an infiltration of pro-inflammatory M1 macrophages is observed. These activated macrophages are a major source of pro-inflammatory cytokines, such as Tumor necrosis factor alpha (TNF- $\alpha$ ) and Interferon gamma (IFN- $\gamma$ ), which activate proteolytic systems and inhibit muscle regeneration [168-170]. Notably, pro-inflammatory cytokines like TNF- $\alpha$  and interleukin 6 (IL-6) activate the  $\kappa$ B kinases (IKKs) and the mitogen-activated kinases (MAPKs), and ultimately upregulates NF- $\kappa$ B and activator protein 1 (AP-1) signaling pathways. These transcription factors induce the expression of pro-inflammatory genes, including chemokines, cytokines, cell adhesion molecules and enzymes. Additionally, the production of nitric oxide by these macrophages promotes cell lysis. Macrophages are also responsible for the phagocytosis of damaged fibers and the activation of T lymphocytes through antigen presentation.

In the subsequent stage, M1 macrophages are replaced by M2 macrophages, which are activated by anti-inflammatory cytokines such as IL-4 and IL-10. M2 macrophages promote fibrosis and muscle regeneration by stimulating satellite cell proliferation [171].

- **Lymphocyte T role**

CD4+ lymphocytes in dystrophic muscle are a significant source of cytokines, aiding in the activation of other immune cells, particularly CD8+ T lymphocytes [172]. Cytotoxic CD8+ lymphocytes contribute to cell death through perforin-dependent cytotoxicity [173,174].

- **Infiltration of other immune cells**

Neutrophil infiltration is also observed in dystrophic muscle, serving as a significant source of superoxide anions [175]. Mast cells contribute to the immune response in dystrophic muscle as well [176,177]. Their degranulation around damaged fibers promotes membrane lysis through the action of specific proteases, such as chymases, tryptases, and carboxypeptidases. Additionally, mast cells release histamines and TNF- $\alpha$ , which can exacerbate muscle fiber necrosis.

The high prevalence of immune cells in dystrophic muscle has led to trials using immunosuppressants in DMD patients. However, these trials have not demonstrated significant improvement [178,179].

- b) Muscle regeneration and depletion of the muscle stem cell pool***

In the early stages of DMD, muscle fiber degeneration is counteracted by active muscle regeneration. However, as continuous cell death persists, an imbalance arises between degeneration and regeneration. This imbalance is marked by a decline in the number of satellite cells over the course of degeneration-regeneration cycles.

Consequently, there is a progressive replacement of functional muscle fibers by fibro-adipocyte tissue, leading to impaired mechanical function of the muscle <sup>[180,181]</sup>.

Several studies have proposed that the DAGC directly influences muscle regeneration. Muscle repair, facilitated by the asymmetric division of satellite cells, is believed to rely on the interaction of DAGC complex proteins such as dystrophin-PAR1b and  $\beta$ 1-syntrophin-p38 $\gamma$ /Carm1 <sup>[182,183]</sup>. Disruption of the DAGC complex may compromise the myogenic engagement of activated satellite cell, thereby impairing muscle repair. Moreover, studies have demonstrated the expression of dystrophin in satellite cells <sup>[184]</sup>. Notably, M. Rudnicki's team suggested a role for dystrophin in maintaining polarity through its association with serine-threonine protein kinase 2 (MARK2), which is crucial for cell polarity. Consequently, the absence of dystrophin in DMD patients could lead to a decrease in asymmetrical divisions, resulting in a reduced generation of myogenic progenitors essential for muscle regeneration <sup>[184,185]</sup>. However, further research is needed to fully elucidate the "stem cell phenotype" theory in DMD <sup>[186]</sup>, particularly to demonstrate how impaired asymmetric division contributes to regeneration defects in animal models and patients.

### ***c) Fibrofatty infiltration in the dystrophic muscle***

Fibrosis, defined as the replacement of healthy tissue by scar tissue primarily composed of fibrous connective tissue following injury or damage <sup>[187]</sup>, is a hallmark feature of dystrophic muscle. As degenerated muscle fibers are replaced, fibrosis progressively develops throughout degeneration-regeneration cycles. This process involves the activation of fibroblasts, which secrete ECM proteins like collagens and fibronectin <sup>[188]</sup>.

The main contributors to fibrogenesis are myofibroblasts <sup>[189]</sup>, which arise from the differentiation of fibro-adipogenic progenitors (FAPs). FAPs are resident cells in

muscle with the capacity to differentiate into myofibroblasts or adipocytes <sup>[190]</sup>. In healthy muscle, FAPs play a supportive role for muscle progenitors during regeneration. However, in muscular dystrophies, the balance is disrupted, leading to a chronic elevation of FAPs and impairment of their apoptosis program due to persistent degeneration <sup>[191]</sup>. Consequently, FAPs progressively differentiate into myofibroblasts <sup>[192]</sup> and white adipose cells <sup>[193]</sup>, directly contributing to the fibro-adipocytic transformation of dystrophic muscle.

- **Signaling and regulatory pathways in muscle fibrosis**

Several signaling pathways modulate the progression of fibrosis in dystrophic muscle.

The primary pro-fibrotic signal is mediated by Transforming growth factor beta (TGF- $\beta$ ) <sup>[194]</sup>, which triggers the activation of fibroblasts and the expression of ECM proteins <sup>[195]</sup>. In the muscle of DMD patients, the expression of TGF- $\beta$  and its receptors correlates with the degree of muscle fibrosis <sup>[196]</sup>, directly contributing to the pathogenesis of muscular dystrophies <sup>[197]</sup>. TGF- $\beta$  and its receptors are predominantly localized in the ECM, forming complexes with latent TGF- $\beta$  binding proteins (LTBPs) within inflammatory and fibrotic areas of dystrophic muscle <sup>[196,198]</sup>. Activation of TGF- $\beta$  requires its release from the complex by proteases, such as ECM matrix metalloproteinases MMP2 and MMP0. Once activated, TGF- $\beta$  isoforms bind to their transmembrane receptors, initiating the canonical TGF- $\beta$  pathway. This results in the activation of SMAD and its translocation into the nucleus, where it regulates the expression of various target genes, including those encoding ECM proteins <sup>[199–201]</sup>, ECM receptors on the cell surface <sup>[202]</sup>, and other profibrotic genes amplifying the action of TGF- $\beta$ , such as Connective Tissue Growth Factor (CTGF) <sup>[203]</sup>.

In addition to molecular signaling pathways, muscle stiffness has emerged as a critical fibrogenic signal in various tissues <sup>[123,204]</sup>. Skeletal muscle, being mechanosensitive

<sup>[205]</sup>, responds to changes in stiffness. One of the mechanosensitive transcription factors implicated in this process is YAP (yes-associated protein), which is dysregulated in muscular dystrophies <sup>[206]</sup>. YAP translocates into the nucleus in response to rigid substrates and targets CTGF and other factors involved in the fibrogenic program <sup>[206]</sup>.

The fibroadipocytic transformation of muscle and the increased ECM density eventually impair muscle motor function, directly correlating with the age of ambulation loss in patients <sup>[207]</sup>. Moreover, fibrosis exacerbates profibrotic cytokine production and perpetuates a chronic inflammatory state in the muscle.

## **II.5 Therapeutic management and treatments in development for DMD**

DMD therapeutic care requires an early multidisciplinary approach. Despite significant therapeutic strides in the last three decades, curative treatments remain elusive. Present management primarily focuses on symptom alleviation, aiming to decelerate disease advancement and enhance patients' quality of life. Concurrently, various therapeutic strategies, particularly those targeting the restoration of functional dystrophin expression, are undergoing development. Notably, some approaches have recently gained regulatory approval in both the United States and Europe.

First, we will discuss the current routine clinical management of DMD, and approved pharmacological treatments, followed by an introduction to various dystrophin restoration strategies, such as gene transfer and gene editing.

### **II.5.1 Current clinical management of DMD**

The current clinical management of DMD involves a multidisciplinary approach addressing both muscular (both skeletal and cardiac) and extra-muscular manifestations of the disease. Consequently, guidelines have been published to ensure optimal care, aiming to enhance both the duration and quality of life for patients [208–210].

#### **a) Glucocorticoids treatments**

Treatment with glucocorticoids, such as Deflazacort and Prednisone (and the recently approved Vamorolone), is currently recommended to begin as early as possible [211] and continue throughout the patient's life [53,208,212]. These treatments have demonstrated significant improvements in strength and motor function and can delay the loss of ambulation [212,213]. Additionally, glucocorticoids slow the onset of pulmonary [214] and cardiac damage [215] and reduce the risk of scoliosis [216].

The effects of glucocorticoids vary according to the treatment regimen, with daily treatment resulting in a greater delay (up to two years) compared to on/off regimens (approximately one year) [217]. However, these treatments come with problematic side effects. Glucocorticoids have mineralocorticoid activity, which may lead to hypertension, weight gain, and skin atrophy [53]. They are also associated with delayed growth and puberty, bone demineralization, behavioral changes, cataracts, and renal failure [211].

In late 2023, a new drug, Vamorolone, received approval from both the U.S Food and Drug Administration (FDA) and the European Medicines Agency (EMA), for the treatment of DMD. Vamorolone is a first-in-class dissociative steroidal anti-inflammatory drug that has demonstrated efficacy similar to glucocorticoids in treating DMD [218–220], with reduced safety concerns in comparison with traditional corticosteroids. Notably, it has been shown to reverse bone morbidities associated

with prednisone, such as stunting of growth <sup>[221]</sup>, when patients transitioned treatment to Vamorolone.

### ***b) Givinostat treatment***

In March 2024, the FDA approved Givinostat (Duvyzat, Italfarmaco) for the treatment of DMD in patients six years and older. Notably, Givinostat is the first non-steroidal treatment approved by the FDA for DMD and functions as a histone deacetylase (HDAC) inhibitor, which can stimulate myogenesis <sup>[222]</sup> and improve various dystrophic parameters, including fibrosis, fat infiltration, inflammation and muscle strength and performance <sup>[223,224]</sup>. Clinical data confirmed initial studies, showing significant improvement in muscle histology for young DMD patients (ages 7-1) treated with Givinostat <sup>[225]</sup>, as well as better preservation of functional performance over time compared to placebo, with no severe adverse effects reported <sup>[226]</sup>. While Givinostat is approved for all patients with DMD regardless of mutation, it is not expected to cure the disease but to slow its progression. Additionally, current preclinical and clinical data indicate that Givinostat is most effective in the early stages of disease progression when compensatory regeneration is still active. Its effect on older patients remains to be determined.

### ***c) Cardiac and respiratory care***

Impaired respiratory function in DMD patients is often associated with sleep-disordered breathing and nocturnal hypoventilation <sup>[227]</sup>. Management of respiratory failure involves regular assessment of respiratory function starting from diagnosis. When hypoventilation occurs, respiratory assistance through mechanical ventilation is implemented <sup>[209]</sup>.

The cardiac phenotype of DMD primarily involves progressive dilated cardiomyopathy and cardiac rhythm disorders <sup>[73]</sup>. Management includes early

detection of heart failure symptoms and arrhythmias through annual check-ups. Upon the appearance of these symptoms, patients are typically prescribed angiotensin-converting enzyme (ACE) inhibitors and  $\beta$ -blockers. Prophylactic treatment with ACE inhibitors, in particular, may delay the onset of cardiac symptoms [228–230].

#### ***d) Management of other disorders***

DMD patients present other disorders as the disease progresses, requiring individualized management strategies.

- **Orthopedic management:** DMD patients are prone to muscular deformities, scoliosis, and fractures. Preventative measures, including physiotherapy, are essential to maintain stability and ambulation [53]. In cases of scoliosis, surgery may be necessary.
- **Endocrinological management:** Endocrinological disorders are common, particularly with glucocorticoid use. Dietary interventions can help manage weight gain and altered glucose and lipid metabolism. Calcium and vitamin D supplementation is prescribed to address bone demineralization.
- **Neuropsychological and neurodevelopmental management:** DMD patients may experience cognitive impairment, attention deficit/hyperactivity disorder, obsessive-compulsive disorder, and autism spectrum disorder. Psychological and educational support is provided, with treatments tailored to the specific disorder.
- **Gastrointestinal and urological management:** In advanced stages of DMD, gastrointestinal and urological disorders become more prevalent and require appropriate pharmacological treatment.

## **II.5.2 Advances and challenges in microdystrophin gene therapy for DMD**

DMD is the focus of several gene therapy strategies aimed at curing the disease by restoring dystrophin expression via gene transfer. This approach involves delivering a healthy copy of the targeted gene to restore the expression of the deficient protein. Various gene delivery vectors have been developed for this purpose, with recombinant adeno-associated virus (rAAV) vectors being the most widely used for neuromuscular diseases. The most promising advancement to date in treating DMD involves delivering a truncated version of dystrophin, referred to as microdystrophin, via a recombinant rAAV vector. In this context, we will briefly explain the concept of rAAV gene therapy and present current trials utilizing this approach for DMD treatment.

### ***a) rAAV vectors for gene therapy***

Adeno-associated viruses (AAVs) were first discovered accidentally in an adenovirus preparation <sup>[231]</sup> and were later also detected in human tissues <sup>[232]</sup>. With advancements in molecular genetics and the understanding of genetic diseases, AAVs were first studied as potential vectors for gene transfer in 1984 <sup>[233]</sup>. Since then, six drugs utilizing rAAV vectors for gene transfer have been approved by the regulatory authorities:

- **Glybera**: approved by the EMA in 2012 for the treatment of familial lipoprotein lipase (LPL) deficiency <sup>[234]</sup> (later abandoned by the sponsor company in 2017).
- **Luxturna**: approved in 2017 for the treatment of an inherited retinal disease <sup>[235]</sup>.
- **Zolgensma**: approved by the FDA in 2019 for the treatment of a form of spinal muscular atrophy <sup>[236]</sup>.
- **Hemgenix**: approved in 2022 by the FDA for certain types of hemophilia B.

- **Roccatavian:** approved in 2023 for treating severe hemophilia A.
- **Elevidys:** approved in 2024 by the FDA for treating DMD.

- **Wild-Type AAV**

AAVs belong to the *Parvoviridae* family and the *Dependovirus* genus. These non-enveloped viruses have an icosahedral capsid approximately 25 nm in diameter, containing a 4.7 kb single-stranded DNA genome <sup>[237]</sup>. Flanking the single-stranded DNA are non-coding inverted terminal repeats (ITRs), palindromic motifs around 145 base pairs long, which form hairpin loops at the 5' and 3' ends <sup>[238]</sup>. ITRs are crucial for the encapsidation of the genome into viral particles, as well as for the replication and integration of the virus into the host genome <sup>[239]</sup>.

The AAV genome consists of two main ORFs: the *Rep* gene, which encodes replication proteins, and the *Cap* gene, which encodes viral structural proteins (VP). Additionally, alternative ORFs encode three accessory proteins: assembly-activating protein (AAP), membrane-associated accessory protein (MAAP), and protein X (**Figure 13**).

To date, numerous AAV variants have been identified from human and primate tissues <sup>[240]</sup>, including at least 12 major serotypes (AAV1 to AAV13) and over 100 variants studied as gene transfer vectors <sup>[241]</sup>. Epidemiological studies indicate that between 40% and 80% of the human population has antibodies against AAV, suggesting widespread exposure to various AAV serotypes <sup>[242]</sup>.

- **Recombinant AAV**

rAAVs are derived from wild-type (WT) AAV. In these engineered vectors, only the cis-acting ITR sequences from the WT AAV are retained for transgene encapsidation and expression <sup>[243]</sup>. The *Rep* and *Cap* genes are replaced by an expression cassette

containing the transgene of interest <sup>[244]</sup>. This cassette typically ranges from 4.1 to 4.9 kb and includes a promoter, the complementary DNA (cDNA) of the therapeutic gene, and a polyadenylation signal (**Figure 13**).

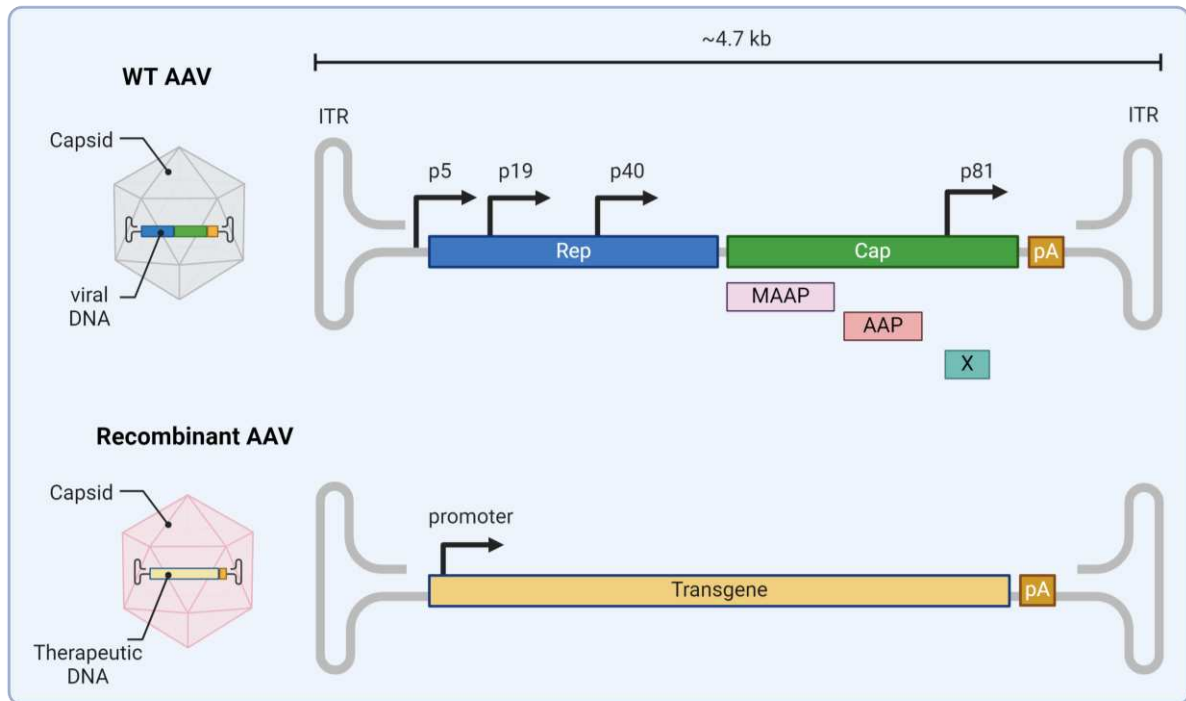


**Figure 13. Wild-type and recombinant AAV (rAAV) genomes.** The rAAV genome is assembled by deleting the *Rep*, *Cap*, *Maap* and *Aap* genes and replacing them with a transgene expression cassette comprising a promoter, a complementary DNA (cDNA) sequence of the transgene and a polyA signal sequence. The ITRs are the only remaining elements of the wild-type AAV genome, ensuring replication and encapsidation of the rAAV. Figure created with [BioRender.com](https://www.biorender.com).

A common method for producing rAAV involves transfecting producer cells, either adherent or in suspension, with three plasmids (**Figure 14**). The first plasmid supplies the *Rep* and *Cap* gene sequences in trans, necessary for replication and virion assembly <sup>[245]</sup>. The second plasmid provides the transgene flanked by the ITRs in cis. The third plasmid, known as the helper plasmid, encodes adenovirus genes that

enhance the production of rAAV particles. Following production, rAAVs are purified using techniques such as column chromatography or gradient centrifugation [246].

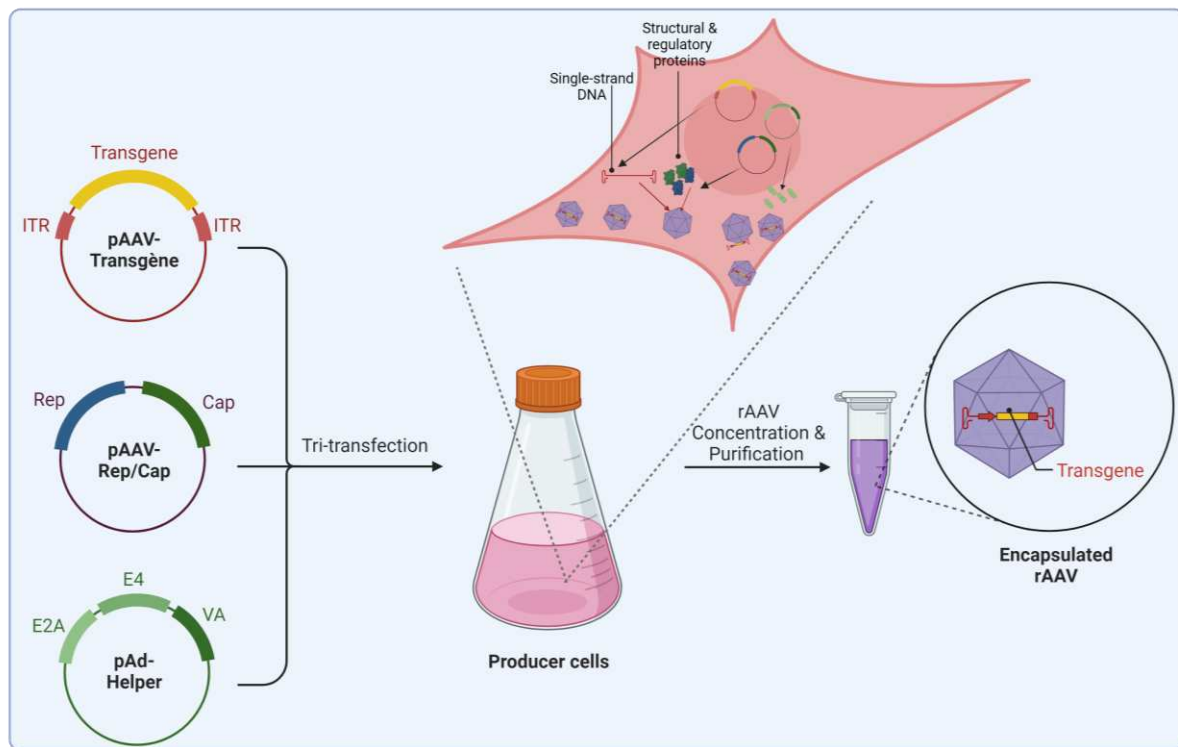


**Figure 14. rAAV production by triple transfection.** Producer cells (usually HEK297T) are co-transfected with 3 plasmids. The Rep gene (required for replication) and the Cap gene (encoding the virion capsid) are provided in trans in one plasmid. The transgene surrounded by the ITRs is provided in cis in a second plasmid. A third plasmid containing Adenovirus sequences is also used to enhance the production of rAAV particles. The rAAV particles are then harvested and purified. Figure created with [BioRender.com](https://www.biorender.com).

### **b) Microdystrophin gene therapy**

The *DMD* gene's mRNA open reading frame spans about 11.5 kb, surpassing the encapsidation capacity of rAAVs. To circumvent this limitation, various microdystrophins have been designed by retaining essential domains of the dystrophin [247,248]. This strategy is based in particular on observations made in

patients with BMD where the expression of truncated dystrophin forms appears to mitigate the condition's severity compared to DMD [97,249,250] (**Figure 15**). More importantly, this approach is theoretically applicable to all DMD patients, whatever mutations they carry.

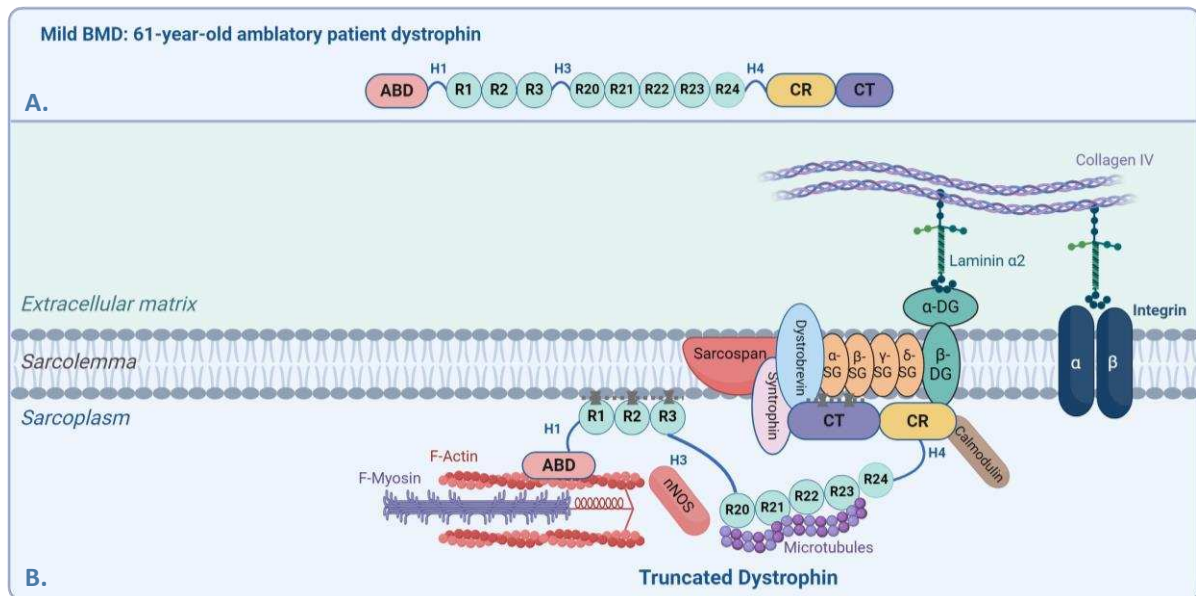


**Figure 15. Truncated dystrophin expressed in a BMD patient muscle. A.** In BMD patients, a truncated dystrophin is expressed (case first reported by England et al., 1990 [251], illustration adapted from Asher et al., 2020 [69]). **B.** As shown, this truncated dystrophin retains essential domains necessary for binding to actin filaments and the extracellular matrix, thereby enabling partial dystrophin function. Figure created with [BioRender.com](https://www.biorender.com).

Several clinical trials are currently undergoing, sponsored by various pharmaceutical companies, including Sarepta Therapeutics, Pfizer, Solid Biosciences and Regenxbio in the USA, and Généthon in Europe (**Table 3**). Each trial employs a slightly distinct microdystrophin construct (see **Figure 16**). Although the drug developed by Sarepta Therapeutics (Elevidys) has been granted accelerated marketing approval by the FDA in June 2023 for patients aged 4-5 years, and expanded approval in June 2024, debates persist as to its efficacy, particularly concerning functional improvements in

patients for whom the primary functional outcomes have not been met [252,253]. Approval was granted based on surrogate endpoints, evoked by the level of microdystrophin expression. The rationale posited was that the generation of microdystrophin could reasonably anticipate an enhancement in muscle function [254].

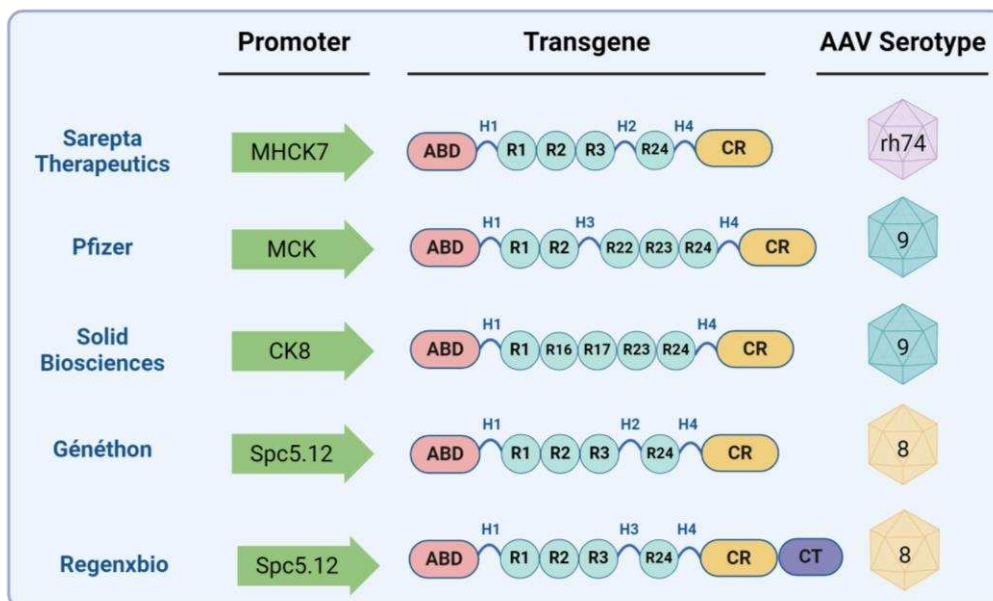


**Figure 16. Microdystrophin constructs.** The promoters used in these constructs (shown in green) are specific to muscle and heart tissues. Each transgene includes coding sequences for domains deemed clinically relevant and functional. The choice of AAV serotype is based on tissue tropism, with these serotypes specifically targeting muscle and heart. Figure created with [BioRender.com](https://www.biorender.com).

<b>Sarepta</b>	<b>Clinical trials:</b>
	<p><b>NCT03375164:</b> Phase I/II, 2017→completed  <b>NCT03769116</b> (Study 101,102): Phase I/II, 4-7y, 2018→completed  <b>NCT04626674</b> (ENDEAVOR-Study 103, 301): Phase Ib, 4-8y, 2020→ongoing  <b>NCT05096221</b> (EMBARC): Phase III, 4-8y, 2021→ongoing  <b>NCT06270719</b> (ENDURE): Phase IV, observational study</p>
	<b>Highlights:</b>

<p><b>Therapeutics</b> [SRP-9001/ Elevidys]</p>	<p>First cohort dosed at 2E14vg/kg, second cohort dosed at 1.33E14 vg/kg and showed satisfying safety profile (chosen dose for phase III). Phase I/II showed robust microdystrophin expression <sup>[255,256]</sup>, and improvement of functional parameters, but primary outcomes (i.e significant increase of NSAA* score) were not met in latest studies (ENDEAVOR/EMBARK).</p> <p><b>Major SAE**:</b> SAE reported for 4 patients in Phase II, later resolved.</p> <p>→ <b>Conditional FDA approval granted in June-2023 for 4–5-year-old patients</b> → <b>Expanded approval in June-2024 for 4y and older patient, and accelerated approval for non-ambulatory patients</b></p>
<p><b>Pfizer</b> [PF-06939926]</p>	<p><b>Clinical trials:</b> <b>NCT03362502:</b> Phase I, 2018 <b>NCT05429372 (DAYLIGHT):</b> Phase II, 2-4y <b>NCT04281485 (CIFEEO):</b> Phase III, 2022-ongoing (4-8y)</p> <p><b>Highlights:</b> Dose escalation study (1<sup>st</sup> cohort dosed at 1E14vg/kg, 2<sup>nd</sup> cohort at 3E14vg/kg). Robust microdystrophin expression at higher dose, improvement of NSAA score 1year post-treatment for 2 patients <sup>[257]</sup>.</p> <p><b>Major SAE:</b> Kidney toxicity reported for 2 patients in phase Ib, later resolved, myocarditis reported for 2 patients. Immune reactions related SAE reported for all 5 patients in phase Ib. Trial suspended in December 2021 following a patient’s death, resumed in April 2022 after protocol modification. Death of a patient in May 2024, more than 1-year post-injection (Daylight study) due to cardiac arrest, CIFEEO missed its primary endpoint in motor function improvement.</p> <p>→ <b>Dosing posed in May 2024, Program terminated in July 2024</b></p>
<p><b>Solid Biosciences</b> [SGT-001]</p>	<p><b>Clinical trials:</b> <b>NCT03368742 (IGNITE):</b> Phase I/II, 2017-ongoing, 4-17y</p> <p><b>Highlights:</b> Dose ascending study (5E13 vg/kg – 2E14vg/kg). Variable microdystrophin expression levels (5-50%), improvement of respiratory function reported. Trial suspended in October 2020; protocol amended before trial resumption.</p> <p><b>Major SAE:</b> Thrombocytopenia reported for 1 patient and complement pathway activation</p>

	reported for 2 patients.
<b>Généthon</b> [GNT0004]	<p><b>Clinical trials:</b> <b>2020-002093-27:</b> Phase I/II/III, (I/II= dose determination study, III=pivotal) 2020-ongoing, 6-10y</p> <p><b>Highlights:</b> First patient dosed in April 2021 for whom a SAE occurred (later resolved), trial was suspended and resumed at the end of 2022. As of May 2024, 5 patients were treated (2 patients at 1E13vg/kg, 3 patients at higher dose of 3E13 vg/lg), and showed robust microdystrophin expression, decrease in CK. A positive trend of functional improvement observed for a patient dosed with the lower dose 1-year post-treatment. <b>→ Pivotal phase under preparation</b></p>
<b>RegenXbio</b> [RGX-202]	<p><b>Clinical trials:</b> <b>NCT05693142</b> (AFFINITY): Phase I/II, dose escalation study (doses: 1E14 vg/kg, 2E14vg/kg)</p> <p><b>Highlights:</b> 5 patients treated as of March 2024. Robust microdystrophin expression in 12y old patient, initial evidence of functional improvement, no SAE reported.</p>

**Table 3. Summary of ongoing clinical trials using rAAV-microdystrophin for DMD.**

\*NSAA = North Star Ambulatory Assessment - \*\*SAE = Severe Adverse Event.

- **Major hurdles for microdystrophin gene therapy**

Gene therapy for muscle diseases using rAAV vectors is predominantly systemic, aiming to target skeletal muscle, which accounts for around 40% of body mass. Achieving significant therapeutic efficacy in conditions like DMD requires administering very high doses of viral vectors, often  $\geq 1E14$  viral genomes per kilogram (vg/kg) [258]. This approach presents several challenges, including the potential risk of hepatotoxicity due to rAAVs' natural affinity for the liver and the daunting industrial task of large-scale vector production, which demands substantial capacity and incurs exorbitant costs. On the other hand, microdystrophin lacks certain functional domains of dystrophin, limiting its efficacy. Additionally, immune responses against both rAAV vectors and specific microdystrophin epitopes pose

significant obstacles that need to be addressed. Moreover, concerns over cardiac overexpression of microdystrophin have been recently brought to light.

- **Dystrophin versus microdystrophin**

The muscle isoform of dystrophin (Dp427m) consists of multiple binding domains that enable it to establish a critical mechanical connection between the ECM and the cytoskeleton, as well as interact with DAGC proteins. This function is essential for protecting muscle against mechanical stress during contraction. Beyond its mechanical role, dystrophin interacts with various proteins involved in vital signaling pathways. For instance, spectrin repeats R16 and R17 contain the binding site for nNOS, essential for the precise localization of nNOS in the sarcolemma <sup>[94]</sup>. The CR domain interacts with calmodulin, playing a crucial role in calcium signaling pathways (See section **I.3.2 Muscle Dystrophin**).

Since the first shortened dystrophin constructs were developed in 1995 <sup>[259,260]</sup>, over 30 microdystrophin configurations have been published. Optimizations have been made as the binding domains of dystrophin have been characterized, and their functions have been defined. However, the limited packaging capacity of rAAV vectors means only the most essential parts of dystrophin can be retained. Most microdystrophin designs include the ABD, responsible for anchoring to the cytoskeleton, and the CR domain, essential for interaction with  $\beta$ -dystroglycan and thus the DAGC (**Figure 16** , **Figure 17**).

Despite promising results in preclinical studies, clinical trials with microdystrophin have not replicated these successes. This discrepancy raises questions about the importance of the missing domains in microdystrophins. Constructs may lack crucial interaction domains, such as the central rod domain and the C-terminal domain,

suggesting that the expression of a larger dystrophin may be necessary to achieve more complete phenotype correction.

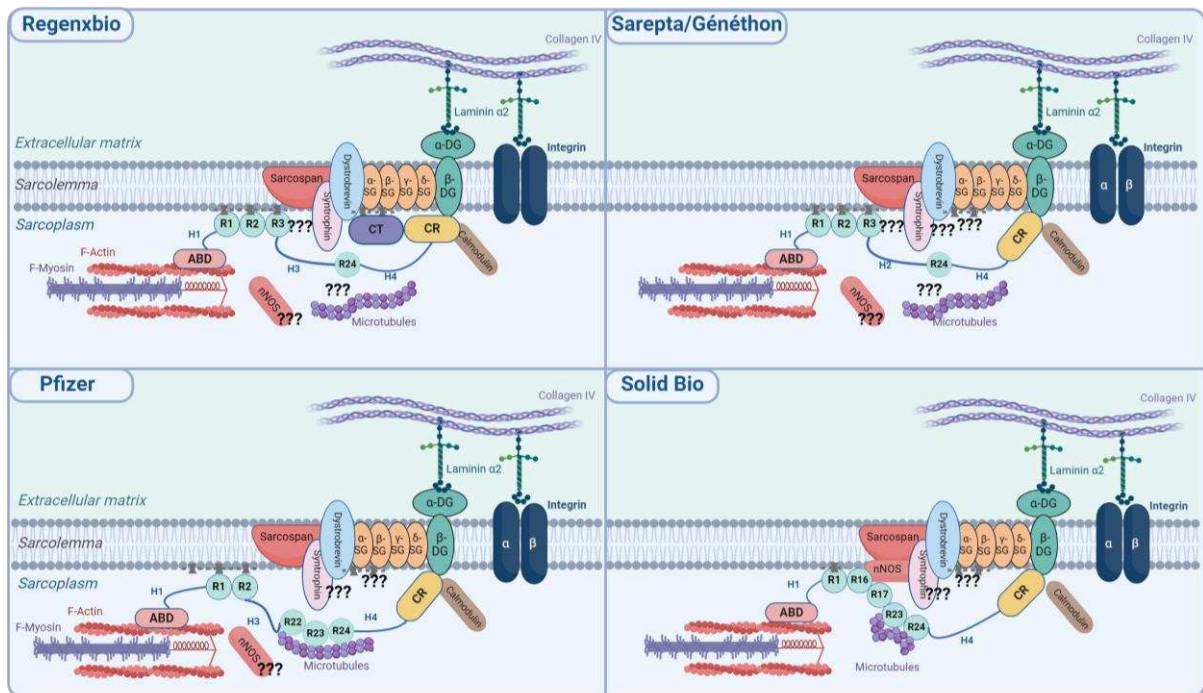


**Figure 17. Localization of microdystrophin constructs in clinical trials to the DAGC.** The 'MD1' microdystrophin used by Sarepta and Genethon binds actin filaments to the DAGC. The microdystrophin used by Regenxbio retains additionally the C-terminal domain, ensuring direct binding to the membrane and dystrobrevin. Pfizer's construct provides microtubule binding via the R22-R24 domain. The construct used by Solid Biosciences includes the R16-R17 spectrins, necessary for nNOS binding and localization to the membrane. Figure created with [BioRender.com](https://www.biorender.com/).

- **rAAV and anti-capsid immune response**

One of the major limitations of gene therapy using rAAV vectors is the immune response directed against the viral capsid. A significant challenge arises from pre-existing immunity, as up to 80% of the human population is seropositive for AAV [242]. Patients can mount a humoral response mediated by anti-capsid antibodies and a

cytotoxic response mediated by CD8+ T lymphocytes. Consequently, patients with neutralizing antibodies to rAAV are excluded from these studies, limiting the number of eligible participants. Additionally, all patients in clinical trials are screened for a humoral response and treated with high doses of glucocorticoids to mitigate the immune reaction against the viral capsids.

Post-injection immune responses can also occur, leading to severe reactions such as thrombotic microangiopathy or acute renal failure due to complement pathway activation. An innate immune response can be triggered immediately after injection by recognizing pathogen-associated molecular patterns (PAMPs), which may include capsid proteins, the DNA content of rAAVs, or protein/DNA contaminants in the rAAV batch. An adaptive immune response may also develop, involving the activation of B and T lymphocytes, which limits transduction efficiency. The generation of memory B and T lymphocytes further complicates future reinjections with the same vector, as they prevent its effective use again.

- **Transgene and immunogenicity**

In addition to the immune response against rAAV capsids, it is now recognized that immune reactions can also occur against the transgene in certain patients <sup>[261]</sup>. Recent collaboration among the four companies conducting clinical trials has led to a better understanding of the serious adverse effects observed in some patients. It was discovered that specific epitopes present in microdystrophin constructs, particularly those encoded by exons 8 to 11, could trigger a cytotoxic immune response against non-self-antigens in patients with deletions in the exons encoding these epitopes. Severe effects are notably observed in patients with deletions from exon 8 to exon 21 <sup>[262]</sup>.

This improved understanding of the immune response against the transgene paves the way for more targeted measures to avoid adverse effects and for the exclusion of patients with specific mutations. For example, in the case of the FDA approval for Sarepta Therapeutics' treatment, patients with deletions of exons 8 and/or 9 were excluded. Nevertheless, further immunological studies on microdystrophin epitopes are needed to better predict immunological risks in patients with genomic deletions in these regions.

- **Cardiac toxicity concerns**

The effects of microdystrophin expression in the heart have been debated for some time <sup>[263,264]</sup>, with limited data on its long-term impact on cardiomyopathy progression. A study by Piepho et al. (2023) demonstrated that microdystrophin treatment could prevent cardiomyopathy up to 18 months post-injection in a utrophin/dystrophin double knockout mouse model <sup>[265]</sup>. However, a more recent study from Lee Sweeney's lab evaluated different microdystrophin constructs used in clinical trials at a high dose similar to clinical levels (2E14 vg/kg) in a severe DMD mouse model (DBA2Jmdx) <sup>[266]</sup>. Despite the constructs showing long-term improvements in muscle force and histology, an accelerated progression of dilated cardiomyopathy and cardiac-related death was observed, with the severity depending on the construct rather than the cardiac level of expression. This cardiomyopathy correlated with significantly high expression levels of microdystrophin in the heart (55 times more than the native dystrophin expression level in WT controls), displacement of utrophin, and saturation of the ubiquitin-proteasome system <sup>[266]</sup>.

This study is particularly noteworthy in light of the recent death of a patient in Pfizer's Daylight study due to cardiac arrest, which occurred more than a year after treatment <sup>[267]</sup>. The delayed onset of this fatality, unlike previous deaths in rAAV clinical trials, suggests a direct effect on cardiac function rather than immune rejection. A thorough

investigation is necessary to fully understand the impact of microdystrophin on cardiac function. Meanwhile, it is essential to closely monitor the cardiac status of all treated patients, and the prophylactic use of cardio-protective drugs should be considered <sup>[266]</sup>.

- **Undergoing efforts to improve microdystrophin gene therapy**

Recent efforts have focused on optimizing rAAV vectors for muscle gene therapy. To better target muscle tissue and reduce transfer to other tissues, such as the liver, our laboratory and other research teams have developed several myotropic hybrid capsid <sup>[268-271]</sup>. These hybrid capsids are designed to reduce the amount of vector needed for effective muscle transduction, thereby minimizing the risks of immunotoxicity and hepatotoxicity. While these new vectors are still in the development and preclinical stages, their advancement towards clinical trials holds promise for not only improving the efficacy of gene therapy for muscle diseases but also enhancing its safety.

Currently, microdystrophin treatment is administered at a stage when dystrophy is already established, and significant muscle fibrosis has occurred. This approach faces the challenge of reversing all the pathological mechanisms, particularly since microdystrophin cannot fully replace the function of dystrophin and is not expressed in all muscle fibers, as evidenced by clinical results to date. Moreover, recent research in our laboratory has shown that even when microdystrophin is expressed in nearly 100% of muscle fibers in dystrophic mice, the transcriptomic profile is not completely restored <sup>[271]</sup>. This finding suggests that microdystrophin alone is insufficient to restore all the disrupted molecular mechanisms in dystrophic muscle.

- **Development of longer dystrophin constructs:**

Since gene therapy using microdystrophin can only mitigate the disease, theoretically progressing to a milder but still disabling form akin to BMD, a major challenge is

delivering a longer version of microdystrophin. One approach involves using multiple rAAV vectors, each carrying a fragment of the *DMD* gene, which can reconstitute the complete therapeutic gene when the vectors simultaneously infect the same myofiber (**Figure 18**). Various reconstitution mechanisms, such as DNA trans-splicing, homologous recombination (HR), and protein trans-splicing, can be employed depending on the gene sequence.

Studies have demonstrated proof-of-principle for transferring longer forms of dystrophin through DNA trans-splicing <sup>[272,273]</sup> and HR <sup>[274,275]</sup> in DMD mouse models. However, these approaches have shown limited transgene reconstitution efficiency, necessitating higher doses of rAAV. The protein trans-splicing approach, utilizing the split-intein system, presents a promising avenue for DMD treatment. This system involves two polypeptides that, through post-translational processing, fuse into a single functional protein. Initial studies <sup>[276,277]</sup> have shown efficacy in both young and old DMD mouse models.

The main limitation of these approaches is the need for even higher rAAV doses to achieve therapeutic efficacy. Therefore, it is crucial to maximize reconstitution efficiency and test these methods with more effective myotropic vectors.

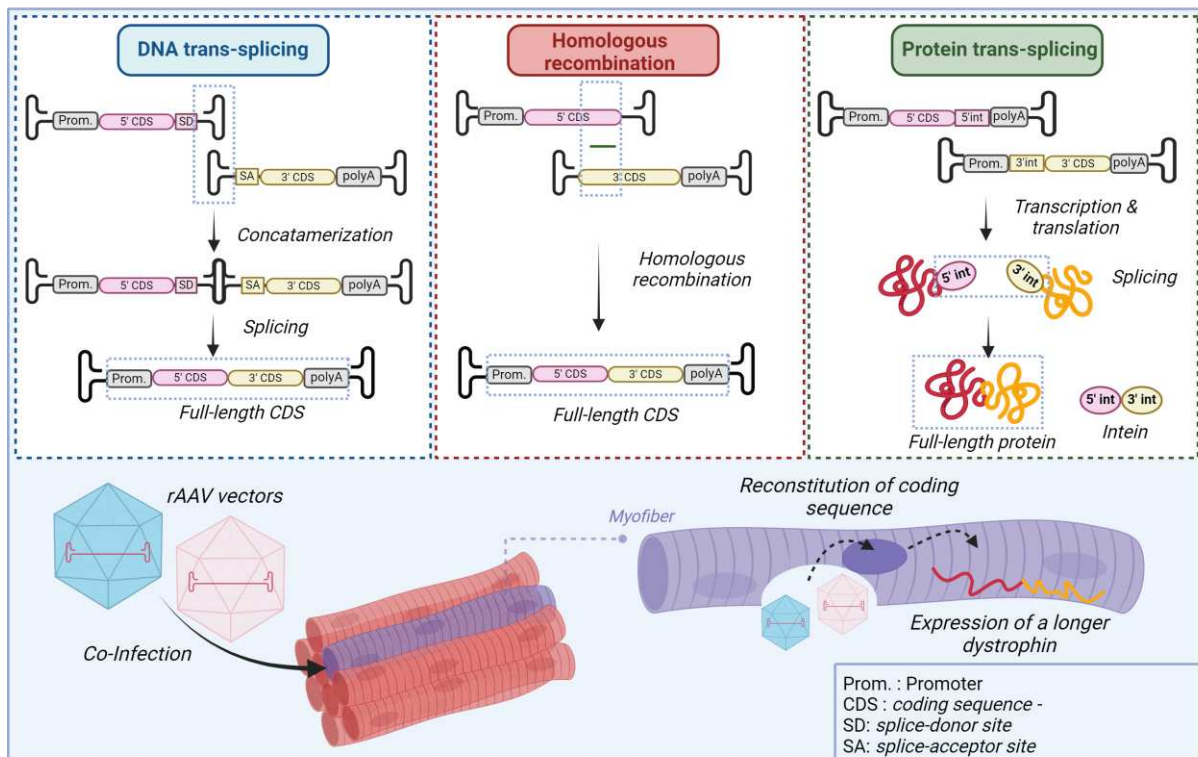


**Figure 18. Gene transfer strategies for the expression of longer constructs than microdystrophin, using several rAAV vectors and different splicing strategies.** Figure created with [BioRender.com](https://www.biorender.com/).

### II.5.3 Gene editing strategies

#### a) Exon skipping

Therapeutic exon skipping is a technique aimed at restoring the reading frame of dystrophin transcripts, resulting in partially functional proteins similar to those found in BMD patients. This method uses antisense oligonucleotides (ASOs) that bind to the target exon during pre-mRNA splicing, preventing its inclusion in the mature mRNA [278].

These strategies are tailored to specific genetic mutations, particularly those located in the hotspots of the *DMD* gene. Currently, four FDA-approved drugs utilize this approach, targeting deletions in exons 51 [279,280], 53 [281,282], and 45 [283] (**Table 3**).

However, these treatments require repeated administration due to the constant turnover of ASOs, transcripts, and proteins. Additionally, the rates of dystrophin restoration achieved by these ASOs are relatively low: 1% for Golodirsen <sup>[284]</sup>, 2.8% for Viltolarsen <sup>[285]</sup>, and 1.74% for Casimersen <sup>[286]</sup>.

Drug	Formulation	Target exon	Company	Approval Date
<b>Eteplirsen</b>	PMO*	51	Sarepta Therapeutics	2016
<b>Golodirsen</b>	PMO	53	Sarepta Therapeutics	2019
<b>Viltolarsen</b>	Morpholino ASO	53	NS Pharma	2020
<b>Casimersen</b>	PMO	45	Sarepta Therapeutics	2021

**Table 4. List of FDA-approved drugs based on exon skipping strategies for the treatment of DMD.** \*PMO = Phosphorodiamidate morpholino oligomer

### **b) CRISPR-Cas9 genome editing approaches**

The development of genome editing systems has enabled new therapeutic approaches for correcting various mutations found in DMD, particularly with the CRISPR-Cas9 system (*clustered regularly interspaced short palindromic repeats* - CRISPR-associated Cas protein). This system uses RNA guides that recognize specific complementary DNA regions, allowing the Cas9 enzyme to create a double-stranded cut at the targeted location <sup>[287]</sup>. These cuts are then repaired by the host cell's DNA repair systems: non-homologous end joining (NHEJ) and homology-directed repair (HDR) <sup>[288]</sup>. HDR is predominant in dividing cells and repairs the double-strand break by inserting an error-free template DNA sequence, while NHEJ is predominant in

post-mitotic cells and is more error-prone, often generating small nucleotide insertions or deletions (INDELs) at the break site.

Genome-editing approaches in DMD aim to restore the reading frame to produce a functional form of dystrophin. This can be achieved through several strategies: exon deletions, exon skipping, reading frame repair via NHEJ, using the HDR system to correct mutations with donor DNA sequences, or single base editing to correct point mutations (base editing) [289].

Proof of concept for these strategies has been demonstrated in cellular and animal models [289–291]. Research is also ongoing for broader approaches that can target more mutations, such as deleting exons 45–55 [292] or exons 47–58 [293]. Other strategies aim to target all DMD mutations by modulating the expression of genes homologous to dystrophin, like utrophin [294].

However, genome-editing approaches face several challenges, including optimizing the delivery system, managing the risk of immune response, and addressing the risk of off-target editing. To date, only one DMD patient has received experimental treatment using a CRISPR-Cas9 system. Unfortunately, this patient died shortly after treatment, likely due to an innate immune response triggered by the high dose of rAAV [295].

### **III- Lysosome Function in Health and Disease**

A central focus of this thesis is the characterization of lysosomal function in dystrophic muscle and its correlation with previously identified lipid perturbations. To provide context for the project and facilitate understanding of the various experiments and analyses conducted, this section of the introduction will present an

overview of lysosomal function in both health and disease. We will begin with a discussion on lysosomal structure and function, followed by an examination of lysosomal stress and its physiological implications in diseases and muscle disorders. Finally, we will explore the lysosomal damage response and the mechanisms that cells employ to cope with lysosomal damage.

### **III.1 Lysosomal structure and function**

Lysosomes are single-membrane cell organelles, first described by Christian de Duve in 1959. Initially thought to be merely cellular waste bins or "suicide bags" of the cell, this view has evolved significantly with recent discoveries. It is now recognized that lysosomes are crucial players in balancing catabolic and anabolic processes, thereby maintaining cellular homeostasis.

Lysosomes are involved in a wide array of cellular functions. Beyond their role in terminal degradation, lysosomes participate in plasma membrane repair, immunity, metabolic signaling, gene regulation and cell adhesion and migration. They form an integral part of the larger endolysosomal system, which also includes endosomes, multivesicular bodies (MVBs), autophagosomes, and autophagolysosomes. Endosomes and lysosomes are often collectively referred to as endolysosomes, highlighting their interconnected roles in the cell.

#### **III.3.1 Lysosome Structure and Composition**

Lysosomes are heterogeneous in terms of morphology, composition, pH and intracellular distribution <sup>[296]</sup>. Their sizes range from 200 to 600 nm in diameter. The lysosome contains an acid lumen filled with more than 60 hydrolytic enzymes, including proteases, nucleases, phosphatases, lipases, and glycosidases, which are essential for breaking down macromolecules (**Figure 19**). Among these, the cathepsin

family of proteases is particularly abundant, encompassing serine cathepsins (A and G), aspartic cathepsins (D and E), and cysteine cathepsins (B, C, F, H, L, K, O, S, W, X). Additional luminal factors, such as saposins and granulins, contribute to degradation of macromolecules <sup>[297]</sup>.

A critical luminal enzyme is the lysosomal acid lipase (LAL), responsible for hydrolyzing lipoprotein cholesteryl esters and triglycerides, which are delivered to the lysosome through endocytosis of lipoproteins or autophagy (lipophagy) <sup>[298]</sup>, releasing free cholesterol and fatty acids <sup>[299]</sup>.

This acidic environment is enclosed by a single phospholipid bilayer membrane, which hosts various proteins crucial for lysosomal function. Maintaining the acidic pH of the lysosomal lumen is vital and is facilitated by specific membrane proteins, particularly the vacuolar H<sup>+</sup> ATPase (v-ATPase), which hydrolyzes ATP to actively transport protons into the lysosome, ensuring optimal conditions for enzyme activity and efficient degradation processes <sup>[300,301]</sup>.

Other membrane proteins include structural proteins such as the highly glycosylated lysosome-associated membrane proteins (LAMPs) and lysosome-integral membrane proteins (LIMPs), which form a glycocalyx lining the inner surface of the limiting membrane, protecting it from the hostile luminal environment. LAMP1 and LAMP2 notably, are often used as lysosomal markers, since they constitute about 50% of the lysosomal membrane protein content <sup>[296]</sup>.

Additionally, the lysosome membrane contains proteins involved in organelle trafficking and fusion, such as members of the N-ethylmaleimide-sensitive factor-attachment protein receptors (SNAREs) family, including vesicle-associated membrane proteins 7 (VAMP7) and 8 (VAMP8). Proteins involved in lipid trafficking, such as oxysterol-binding-related proteins (ORPs), and those that transport various

macronutrients and micronutrients, including ions, sugars, lipids, nucleosides, and amino acids, are also present.

Lysosomal membrane proteins also play roles in significant signaling pathways. For example, solute carrier family 38 member 9 (SLC38A9) is involved in cholesterol sensing and mechanistic target of rapamycin complex I (mTORC1) signaling <sup>[302]</sup>.

Lysosomes are dynamic organelles broadly distributed throughout the cytosol of the cell. In non-polarized cells, they often accumulate in a central region, forming a "perinuclear cloud", but they are also many peripheral lysosomes which can reach the plasma membrane. Their positioning within the cell can change in response to various stimuli, such as plasma membrane damage, ion imbalances, and changes in pH (acidification or alkalinization) <sup>[303]</sup>. Lysosomes move along microtubules in both anterograde (toward the cell periphery) and retrograde (toward the nucleus) directions <sup>[304]</sup>.

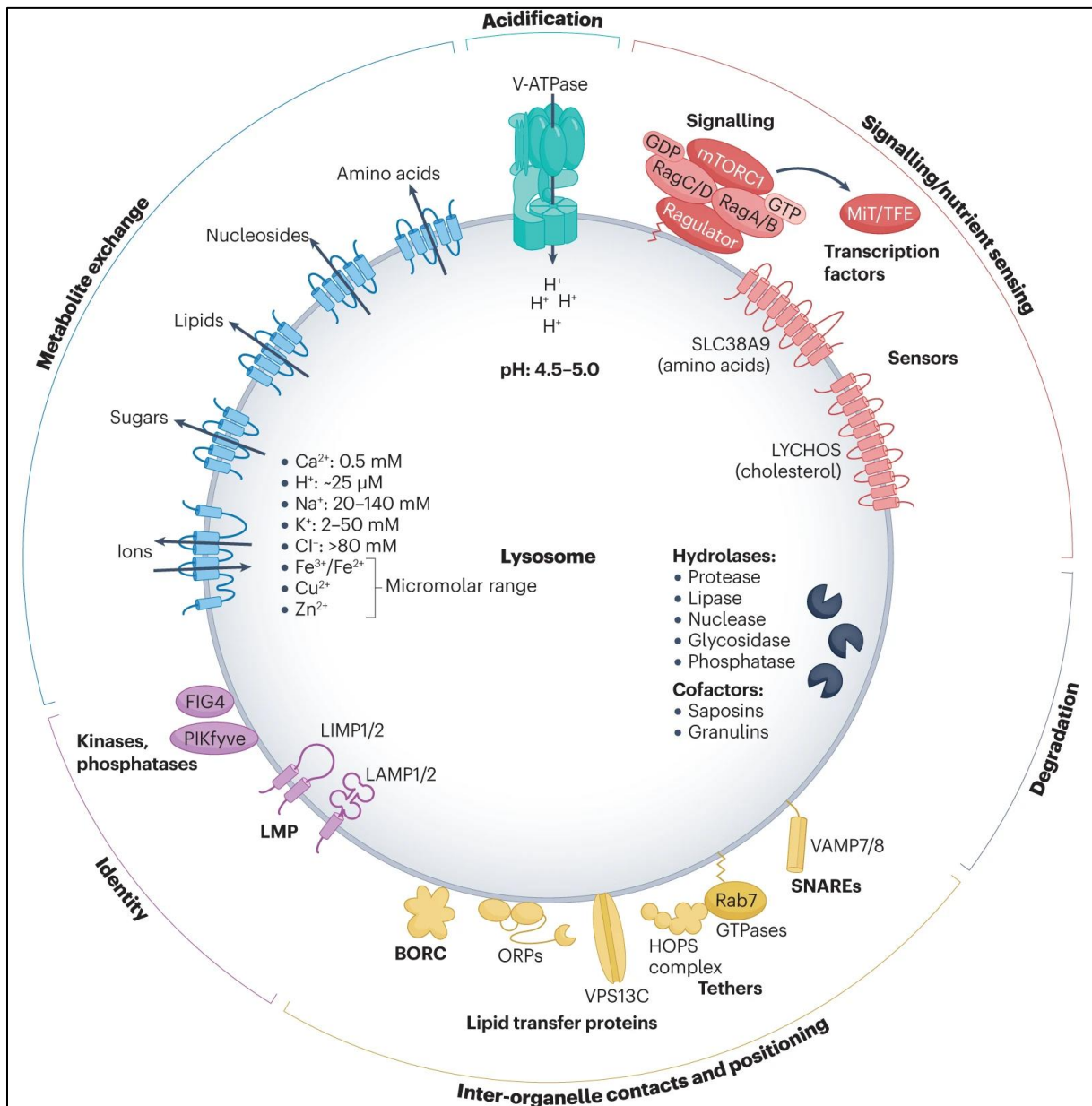


**Figure 19. Lysosome structure and function.** (Adapted from Settembre & Perera, 2024 <sup>[297]</sup>). The lysosome contains luminal hydrolases, integral-membrane proteins and membrane-associated proteins. The lumen of the lysosome has an acidic pH, mediating the degradative capacity of more than 60 hydrolases. Cofactors such as saposins and granulins aid in macromolecular breakdown. The luminal acidic pH is maintained by a vacuolar ATPase (v-ATPase) embedded in the lysosomal membrane. The structural lysosomal membrane proteins (LMPs), such as the highly glycosylated lysosome-associated membrane proteins (LAMPs) and

*lysosome-integral membrane proteins (LIMPs), form a protective glycocalyx shielding. The lysosomal membrane contains ion channels and transporters that participate in ion homeostasis, as well as macronutrient transporters of lipids, sugars, nucleosides and amino acids. The cytosolic face of the lysosome associates many protein complexes involved in cell signaling and nutrient sensing, including the mammalian target of rapamycin complex 1 (mTORC1) and various transcription factor such as TFEB that regulate lysosome biogenesis and autophagy. Many proteins involved in inter-organelle contacts and positioning localize to the lysosomal membrane, such as the soluble N-ethylmaleimide-sensitive factor-attachment protein receptors (SNAREs) involved in membrane tethering, the oxysterol-binding protein-related proteins (ORPs) involved in intermembrane lipid transfer and the homotypic fusion and vacuole protein sorting (HOPS) complex involved in vesicular fusion.*

### **III.3.2 Lysosomal Function**

Since their discovery, the lysosome's myriad crucial roles have been increasingly elucidated. Beyond their central function in the degradation and recycling of cellular components, lysosomes are integral to various cell signaling pathways, nutrient sensing, and energy metabolism, most notably mTORC1 signaling. They play a central role in the autophagy pathways and are essential for organelle trafficking processes such as endocytosis, exocytosis, and MVB sorting. Additionally, lysosomes have specialized functions in certain cell types, including pathogen defense in immune cells and bone remodeling through lysosomal exocytosis. Lysosomes are also involved lysosomal-dependent cell death.

#### **a) Role in macromolecule degradation and recycling**

Lysosomes serve as the terminal degradative organelles for autophagy, where the breakdown of macromolecules (proteins, lipids, nucleic acids, etc.) occurs. This process allows for the recycling of cellular components, which is essential for cellular

renewal and repair. There are three types of autophagy described in mammalian cells: macroautophagy, chaperone-mediated autophagy (CMA), and microautophagy. All these processes rely directly on lysosomal function (**Figure 20**).

### **Chaperone-Mediated Autophagy (CMA) and Microautophagy:**

- **CMA** involves the selective degradation of specific cytosolic proteins that possess a recognition sequence motif (KFERQ). This motif binds to a transmembrane protein complex composed of heat shock-cognate chaperone 70 kDa protein (HSC70), LAMP-2A, and the luminal form of HSC70 <sup>[305]</sup>.
- **Microautophagy** involves the direct engulfment of cytoplasmic materials by lysosomal membrane invagination <sup>[306]</sup>.

### **Macroautophagy:**

Macroautophagy, often referred to simply as autophagy, is the most studied and common form. It involves an additional organelle: the double-membrane autophagosome, which encapsulates cytoplasmic contents before fusing with the lysosome to form the autolysosome, where the cargo is degraded. Various cargos, including lipids, complex sugars, nucleic acids, misfolded proteins, and whole organelles, can be targeted to the autophagosome before delivery to the lysosome for degradation.

#### ○ **Selective autophagy processes:**

Selective autophagy maintains cellular homeostasis by constantly recycling damaged or superfluous components. This includes over a dozen pathways such as lysophagy (degradation of lysosomes)<sup>[307]</sup>, reticulophagy (degradation of the ER) <sup>[308]</sup>, mitophagy (degradation of mitochondria) <sup>[309]</sup>, nucleophagy (degradation of nuclei) <sup>[310]</sup>, lipophagy (degradation of lipid droplets) <sup>[311]</sup>, and pexophagy (degradation of peroxisomes) <sup>[312]</sup>.

- **Autophagy and cellular stress:**

Autophagy occurs at basal levels in most tissues <sup>[313,314]</sup>, and is tailored to respond to various stress stimuli to preserve organelle health and cell homeostasis. Autophagy flux increases notably in response to stress, nutrient starvation, organelle damage, and abnormal protein aggregation.

- **Autophagy process:**

Autophagy is a multistep, coordinated pathway requiring a complex vesicular trafficking network to recruit and assemble multiple autophagy-related protein complexes. Initial steps of autophagy consist of the formation and maturation of the autophagosome, which have been the focus of autophagy studies for a long time. However, recently more and more interest has been given to the later steps of autophagy, particularly membrane fusion and membrane-sorting events defining the life cycle of the autolysosome <sup>[314]</sup>. Briefly, the main steps include:

- **Initiation:** Formation of the phagophore (isolation membrane) coordinated by the unc-51-like kinase 1 (ULK1) complex, activated by mTORC1 and AMPK pathways <sup>[315,316]</sup>.
- **Nucleation:** Occurs at ER-specific sites called omegasomes, regulated by the class III phosphatidylinositol 3-kinase (PI3K) complex <sup>[317]</sup>.
- **Expansion:** Involves elongation and closure of the phagophore to form a complete autophagosome, facilitated by two ubiquitin-like conjugation systems <sup>[317,318]</sup>:
  - **ATG12-ATG5-ATG16L1 complex:** ATG12 is conjugated to ATG5, and this complex then associates with ATG16L1. This complex localizes to the expanding phagophore and is necessary for the recruitment of LC3 <sup>[319]</sup>.

- **LC3 conjugation system:** Microtubule-associated protein 1A/1B-light chain 3 (LC3), initially synthesized as pro-LC3, is cleaved by ATG4 to form LC3-I. LC3-I is then conjugated to phosphatidylethanolamine (PE) by the action of ATG7 (an E1-like enzyme) and ATG3 (an E2-like enzyme), forming LC3-II, which is incorporated into the autophagosome membrane <sup>[320]</sup>.
- **Maturation:** As the autophagosome matures, it sequesters cytoplasmic components, including damaged organelles and misfolded proteins. The maturation process involves further elongation and the eventual closure of the autophagosome, forming a double-membrane structure.
- **Lysosome-Autophagosome Fusion:** The autophagosome fuses with the lysosome to form the autolysosome. This fusion is mediated by several factors, including SNARE proteins <sup>[321]</sup>, Rab GTPases <sup>[322]</sup>, and the HOPS (homotypic fusion and protein sorting) complex <sup>[323]</sup>. Once fused, the lysosomal enzymes degrade the autophagic cargo, allowing the breakdown products to be recycled back into the cytoplasm.
- **Autophagy Regulation:**

Autophagy is tightly regulated by two major signaling pathways:

- **mTORC1:** Inhibits autophagy under nutrient-rich conditions by phosphorylating and inhibiting the ULK1 complex, thus suppressing autophagosome formation <sup>[315,324,325]</sup>.
- **AMPK:** Activates autophagy in response to low energy levels and cellular stress by phosphorylating the ULK1 complex on alternative residues <sup>[315,316,326]</sup>.

The lysosome also plays a regulatory role, particularly through its interaction with mTORC1 <sup>[327]</sup>. Under nutrient-rich conditions, mTORC1 localizes to the lysosome <sup>[328,329]</sup>, where it becomes activated and launch growth-promoting processes while

suppressing macroautophagy by inhibiting the autophagy initiation complex [327] and the inhibition of the nuclear translocation of transcription factor EB (TFEB), which is the master transcription regulator of lysosomal and autophagy genes [330,331].

In contrast, during starvation, mTORC1 dissociates from the lysosomal membrane, inducing autophagy [327]. mTORC1 reactivation is later necessary to replenish the lysosomal pool, in a process termed autophagic lysosomal reformation (ALR) [332,333] in which lysosomal membrane components, shaping into tubular structures, form small vesicles named proto-lysosomes (**Figure 20D**). These vesicles would later acquire lysosomal luminal proteins and mature into new intact lysosomes. Defects in ALR were notably reported to be involved in a muscular dystrophy [334].

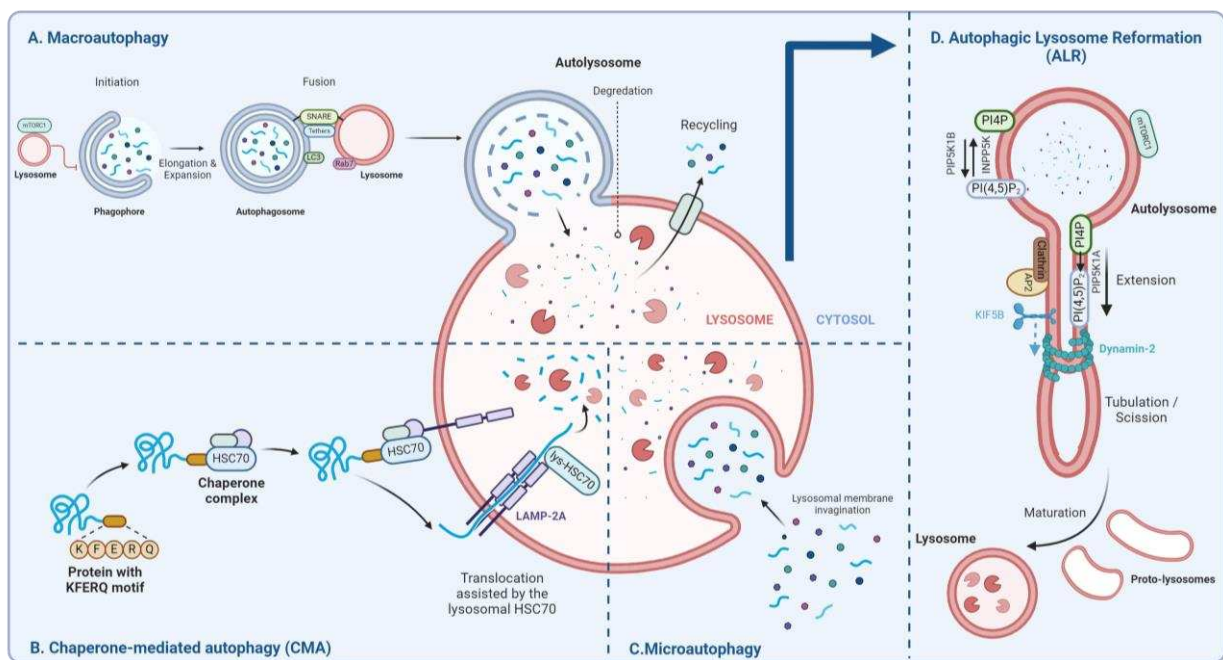


**Figure 20. Autophagy and lysosome reformation.** **A.** Macroautophagy is characterized by the sequestration of targeted materials into the double-membrane autophagosome. The autophagosome fuse with the lysosome, exposing its content to the hydrolases of the lysosomal lumen. Resulting metabolites are transported into the cytosol for recycling. mTORC1 activation, depicted by its localization to the lysosome inhibits macroautophagy. At the end of the process,

*mTORC1 is reactivated, and lysosome membranes are recycled in a process termed autophagic lysosome reformation (ALR). **B.** Chaperone-mediated autophagy (CMA) allows the degradation of specific proteins carrying the pentapeptide KFERQ-like sequence, which is recognized by the HSC70 chaperone. This chaperone associates the lysosomal membrane protein LAMP-2A, causing its translocation into the lysosomal lumen through a process requiring the lysosomal HSC70. **C.** Microautophagy consists of invagination of the lysosomal membrane allowing the sequestration of targeted components for degradation. **D.** Following macroautophagy, autophagic lysosome reformation is initiated by membrane budding on autolysosomes, mediated by Phosphatidylinositol 4,5-bisphosphate (PIP(4,5)P<sub>2</sub>), Clathrin and the adapter complex 2 (AP2). The kinesin family member 5B (KIF5B) drives the elongation of membrane tubules along microtubules and dynamin-2 allows the scission of proto-lysosomes. The generation of PIP(4,5)P<sub>2</sub> from PIP4P is controlled by PIP4P 5-kinase 1B (PIP5K1B) on autolysosome membranes and PIP5K1A on protolysosomal tubules. The balance between PIP(4,5)P<sub>2</sub> and PIP4P is also regulated by inositol polyphosphate-5-phosphatase K (INPP5K). Figure created with [BioRender.com](https://BioRender.com).*

### **b) Vesicular trafficking and fusion**

The lysosome plays a crucial role in organelle trafficking and turnover within the cell, mediating the degradation and recycling of cellular components, and coordinating the movement and function of other organelles. Lysosomes are directly involved in endocytosis, receiving endocytic vesicles containing extracellular material and plasma membrane components that need to be degraded. These vesicles fuse with lysosomes, allowing their contents to be broken down and recycled.

Additionally, lysosomes participate in exocytosis, where they fuse with the plasma membrane to release their contents outside the cell. This process is vital for various cellular physiological processes, such as bone resorption, cell signaling and notably plasma membrane (PM) repair which is crucial in muscle cells.

### **Plasma membrane repair:**

The selective permeability of the PM is crucial for maintaining cell homeostasis. Cells, especially muscle cells, are constantly subjected to physical stress, making rapid membrane repair essential to prevent ion efflux, cytoplasmic leakage, and cell death [335]. The process of PM resealing is initiated by an influx of  $\text{Ca}^{2+}$  to the injured membrane, which quickly recruits intracellular vesicles to fuse at the damage site. Among these vesicles, lysosomes play a major role in plasma membrane repair [336,337].

Upon membrane injury, lysosomes undergo  $\text{Ca}^{2+}$ -triggered exocytosis, releasing proteases and acid sphingomyelinase (ASM). ASM is a crucial enzyme for membrane resealing, acting extracellularly on the outer leaflet of the PM to cleave sphingomyelin and generate ceramides, which form inward budding structures that aid in repair [338,339]. Additionally, cathepsins were reported to be secreted upon PM injury, degrading surface cell proteins to facilitate membrane access and ASM activation [340]. Alongside lysosome exocytosis, massive endocytosis is essential for promoting PM resealing by removing the damaged membrane. This process involves  $\text{Ca}^{2+}$ - and cholesterol-dependent endosomes and the recruitment of caveolins, proteins that form caveolae structures [341–343].

The importance of these mechanisms is underscored in muscle fiber integrity, where mutations in caveolae proteins can lead to muscular dystrophy [343]. Mutations in ASM, which cause a neurodegenerative disease called Niemann-Pick disease type A, have shown an impaired sarcolemma repair and muscle function following injury in knock-out mouse model [344]. Thus, the coordinated actions of lysosome exocytosis and endocytosis are critical for maintaining cellular integrity under stress, which is crucial specially in the skeletal myofibers.

### ***c) Roles in signaling and metabolism***

New emerging roles of the lysosome have recently placed this organelle at the center of metabolic regulation. Here we discuss a few of its most important role in regulation of cellular signaling and metabolism.

### 1) Nutrient sensing and mTORC1 regulation

The lysosome is a crucial regulator of nutrient sensing through its close physical and functional association with the master growth regulator mTORC1. A significant advancement in this field was the discovery that mTORC1 localizes to the lysosome [329,345]. This finding positioned the lysosome as a central hub for nutrient signaling, where it orchestrates various downstream cellular programs in response to nutrient availability, thus maintaining cellular homeostasis.

The lysosome integrates signals related to the availability of nutrients such as amino acids [346], glucose [347], and lipids [348]. Amino acids are particularly important for mTORC1 activation. When amino acids are abundant, they are transported into the lysosome, where they activate mTORC1. Conversely, cellular starvation inhibits mTORC1, causing the activation of the master transcription factor EB (TFEB), responsible for lysosomal biogenesis.

#### **Activation mechanism:**

Several complexes localizing to the membrane of the lysosome play a direct role in mTORC1 regulation:

- **Rag GTPases:** these proteins are located on the lysosomal surface and play a pivotal role in amino acid sensing. When amino acids are present, Rag GTPases become activated and recruit mTORC1 to the lysosomal membrane [349].
- **Ragulator Complex:** this complex anchors Rag GTPases to the lysosomal membrane and is essential for the proper localization and activation of mTORC1 [329].

- **V-ATPase:** The vacuolar H<sup>+</sup>-ATPase (V-ATPase) also participates in the amino acid sensing process by interacting with the Ragulator complex [345].

Many growth signals converge upstream of mTORC1 on the tuberous sclerosis complex (TSC), which negatively regulates kinase activity of mTORC1 [350]. Conversely, amino acids signal independently of TSC via the Rag GTPases [328,351]. Amino acids induce a conformational change in the Rag GTPases, switching them to an active state capable of recruiting mTORC1 to the lysosome. This lysosomal localization facilitates the interaction of mTORC1 with *Rheb* (Ras homolog enriched in brain), a small GTPase [328,350]. *Rheb*, in its active GTP-bound form, directly activates the kinase activity of mTORC1, enabling it to phosphorylate downstream substrates. Under nutrient-rich conditions, the TSC complex is inhibited, allowing *Rheb* to stay in its active state, thus promoting the recruitment and activation of mTORC1 at the lysosome.

#### **mTORC1-mediated regulation of cellular processes:**

Active mTORC1 promotes anabolic processes such as protein synthesis, lipid synthesis, and nucleotide synthesis. This is achieved through the phosphorylation of key downstream targets, including S6 kinase (S6K) [352] and the eukaryotic initiation factor 4E-binding protein (4E-BP) [353]. In contrast, mTORC1 activation inhibits autophagy, by phosphorylating and inhibiting the ULK1 complex, which is essential for autophagosome formation, and by the inhibition of the nuclear translocation of TFEB.

#### **Regulation under nutrient-deprived conditions:**

When nutrients are scarce, mTORC1 dissociates from the lysosomal membrane. This is due to the activation of the TSC complex, which inhibits *Rheb*, leading to the inactivation of mTORC1. Following the dissociation and inactivation of mTORC1, its

suppressive effect on the ULK1 complex and TFEB nuclear translocation is lifted <sup>[354]</sup>. This initiates autophagy, enabling the cell to survive under nutrient-deprived conditions by breaking down and recycling cell nutrients to maintain energy homeostasis.

## 2) Lipid trafficking and cholesterol homeostasis:

The lysosome plays a pivotal role in lipid trafficking and cholesterol homeostasis through its involvement in the breakdown, recycling, and distribution of lipids and cholesterol within the cell.

### ○ **Lipid Trafficking:**

- **Degradation of lipids:** Lysosomes contain various lipases and hydrolases that degrade complex lipids into simpler molecules such as free fatty acids, glycerol, and cholesterol <sup>[355]</sup>. This degradation is essential for the recycling and redistribution of lipids within the cell.
- **Formation of lipids droplets:** After degradation, the resulting lipids can be re-esterified and stored in lipid droplets. These lipid droplets serve as reservoirs of energy and can be mobilized when needed by the cell. Tight regulation of lipid metabolism by lipid droplets is notably crucial in skeletal muscle <sup>[356]</sup>.

### ○ **Cholesterol homeostasis:**

- **Cholesterol trafficking:** Cholesterol is delivered to lysosomes primarily through the endocytosis of low-density lipoprotein (LDL) particles. These particles bind to LDL receptors on the cell surface and are internalized into endosomes, which then fuse with lysosomes <sup>[357]</sup>. Within lysosomes, LDL particles are degraded by acid hydrolases, releasing free cholesterol (**Figure 21A**).

- **Role of Niemann-Pick Type C (NPC) proteins:** NPC1 and NPC2 are essential proteins in the lysosome that facilitate the transport of free cholesterol out of the lysosome to other cellular compartments. NPC2 binds to cholesterol and transfers it to NPC1, which then exports it to the lysosomal membrane <sup>[358]</sup>. Mutations in the genes encoding NPC1 or NPC2 lead to Niemann-Pick disease type C, characterized by the accumulation of cholesterol and other lipids in lysosomes (**Figure 21B**).
- **Regulation of cholesterol levels:** The lysosome is integral to the regulation of cellular cholesterol levels. When intracellular cholesterol levels are low, the transcription factor sterol regulatory element-binding protein (SREBP) is activated. SREBP is transported from the ER to the Golgi, where it is processed and then moves to the nucleus to upregulate the expression of genes involved in cholesterol synthesis and uptake <sup>[358]</sup>. Conversely, when cholesterol levels are sufficient, cholesterol binds to SREBP cleavage-activating protein (SCAP), retaining it in the ER and preventing the activation of SREBP, thereby reducing cholesterol synthesis and uptake.

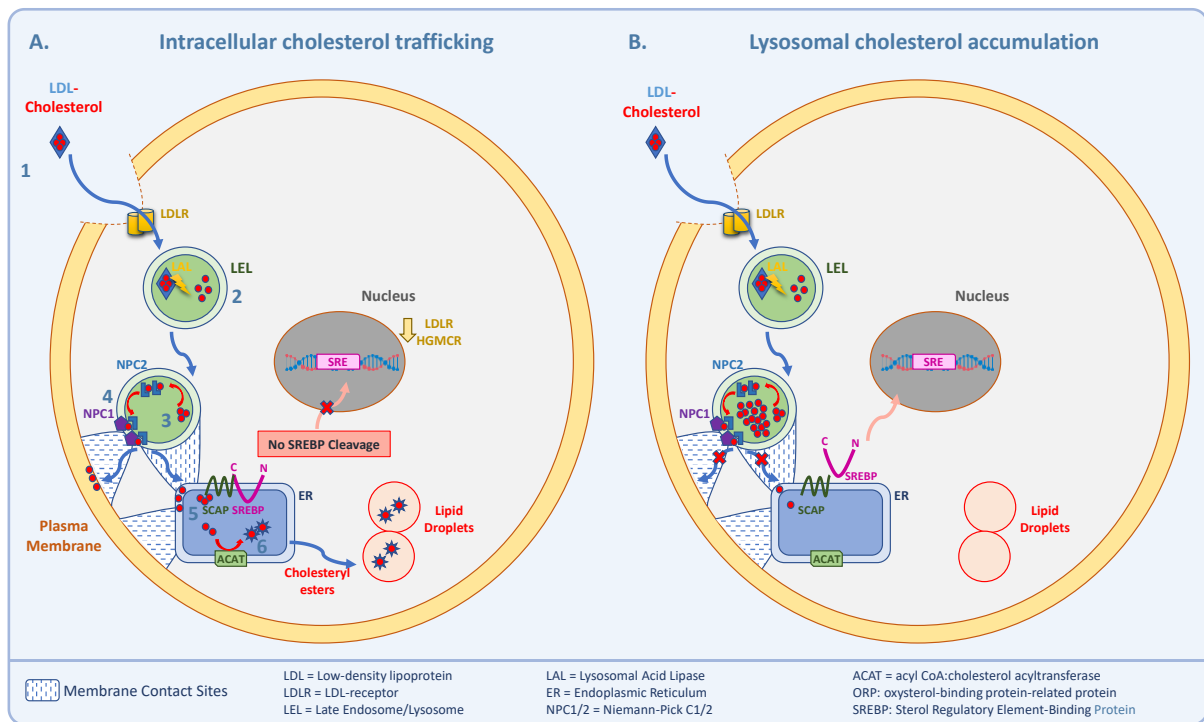


**Figure 21. The lysosome regulates cholesterol homeostasis. A.** 1) LDL-cholesterol binds to the LDL receptor (LDLR) and enters the cell via clathrin-pit-mediated endocytosis. 2) LDL-cholesterol is converted into free cholesterol by lysosomal acid lipase (LAL). 3) Free cholesterol binds to NPC2 inside the lysosome. 4) The cholesterol is then transferred to NPC1 on the lysosomal membrane and delivered to other cellular compartments (plasma membrane, ER). 5) Cholesterol overload in the ER retains the Scap/SREBP complex in the ER. SREBP is not cleaved in the Golgi apparatus and cannot activate transcription of the LDLR and HMGCR genes, causing a decrease in cholesterol uptake and biosynthesis. 6) Excess cholesterol in the ER is esterified by ACAT and then stored in lipid droplets. Cholesterol accumulation in the lysosome disrupts intracellular cholesterol trafficking. As a result, the Scap/SREBP complex detaches due to the lack of cholesterol feedback in the ER. SREBP is then translocated to the nucleus, where it activates the pathways for cholesterol uptake and synthesis. **B.** Cholesterol accumulation in the lysosome disrupts intracellular cholesterol trafficking. As a result, the Scap/SREBP complex detaches due to the lack of cholesterol feedback in the ER. SREBP is then translocated to the nucleus, where it activates the pathways for cholesterol uptake and synthesis.

### 3) Calcium signaling:

The lysosome plays a significant role in calcium signaling within mammalian cells, serving as the second largest store of  $\text{Ca}^{2+}$ , with concentrations in the range of 500-600  $\mu\text{M}$ , which is approximately 5000 times higher than cytosolic  $\text{Ca}^{2+}$  levels [359]. This high concentration of calcium in lysosomes makes it a major calcium reservoir, playing a pivotal role in cellular calcium signaling. The ability of the lysosome to release calcium in response to different stimuli underscores its importance in mediating various cellular processes, including vesicular trafficking, signal transduction, transcription regulation, and lysosome reformation.

#### **Lysosome calcium channels:**

Lysosomal calcium is regulated through specific calcium channels located on the lysosomal membrane. There are three known families of these channels in mammals:

- 1- **Transient Receptor Potential Cation Channel, Mucolipin Subfamily (TRPML):** These are non-selective cation channels that allow the passage of multiple ions, including  $\text{Ca}^{2+}$ ,  $\text{Na}^+$ ,  $\text{K}^+$ ,  $\text{Fe}^{2+}$ , and  $\text{Zn}^{2+}$ , and consists of three channels (TRPML1-3) [360]. TRPML1 (or MCOLN1) is exclusively localized to lysosomes and is found ubiquitously in mammalian cells, while TRPML2 is primarily localized to endosomes and TRPML3 is found on both lysosomes and endosomes.
- 2- **Two-Pore Channels (TPC):** These channels (TPC1-2) are involved in calcium release from the lysosome and play a role in various signaling pathways.
- 3- **P2X4 Receptors:** These ion channels are also implicated in lysosomal calcium signaling, mainly promoting endo-lysosomal membrane fusion in  $\text{Ca}^{2+}$ /calmodulin dependent manner [361].

#### **Role of lysosomal calcium:**

Lysosomal calcium ( $\text{Ca}^{2+}$ ) is crucial for several key cellular functions, acting as a primary mediator of vesicular fusion [362]. This includes the fusion of lysosomes with other vesicular compartments, such as endosomes and autophagosomes, as well as lysosomal exocytosis [363,364]. Additionally, lysosomal calcium is involved in various signaling pathways. For instance, during starvation and exercise, mucolipin 1 (MCOLN1, or TRPML1) channel releases  $\text{Ca}^{2+}$ , which activates calcineurin [365]. Calcineurin then dephosphorylates TFEB, promoting its translocation to the nucleus, where it activates the transcription of genes involved in autophagy and lysosome biogenesis [365].

MCOLN1 also acts as a sensor for various cellular stresses, mediating the activation of TFEB. Calcium signaling through MCOLN1 can be triggered in response to ROS stress [366]. Moreover, lysosome membrane damage can activate MCOLN1 calcium signaling through its interaction with LC3, which is recruited to the lysosome during such damage [367].

Calcium signaling through MCOLN1 is also crucial for lysosome reformation following their fusion with other organelles. Mutations in *MCOLN1* cause mucopolidosis type IV, a lysosomal storage disorder characterized by morphological and functional defects of lysosomes [368]. More notably in the context of skeletal muscle, MCOLN1 is essential for sarcolemma repair, and a knockout of MCOLN1 in mice results in early-onset muscular dystrophy [369]. Overexpression or activation of MCOLN1 in a DMD mouse model has been shown to alleviate dystrophic features [369,370].

### **III.2 Lysosomal stress and pathological implications**

The pathogenesis of lysosome dysfunction was initially described in the context of lysosomal storage disorders (LSD), which are caused by inherited mutations in genes

involved in lysosomal function or structure. However, recent studies have revealed that lysosome dysfunction also plays a significant role in a wide range of other diseases, including neurodegenerative disorders, cancer, cardiovascular disease and metabolic disorders. In this section, we'll first explore lysosomal dysfunction and its cellular consequence, followed by a discussion of its pathophysiological implication in various diseases. Additionally, we will examine the connection between lysosomal dysfunction and muscle pathogenesis.

### **III.2.1 Lysosomal dysfunction and consequences**

#### ***a) Lysosomal stress and lysosomal stress response***

Lysosomal dysfunction is characterized by the progressive accumulation of undegraded substrates within lysosomes, leading to a state known as lysosomal stress. This stress results from various internal or external stimuli that challenge the lysosome's capacity to maintain cellular homeostasis <sup>[371]</sup> (**Figure 22**). Stimuli that can induce lysosomal stress include:

- **The accumulation of LDL cholesterol:** Cholesterol accumulation in the lysosome is closely correlated with lysosomal dysfunction, as most notably observed in Niemann Pick type C disease. In these lysosomal storage disorders, mutations in the lysosomal cholesterol export transporters NPC1/2 cause an accumulation of lysosomal cholesterol <sup>[372]</sup>, leading to an autophagic stress <sup>[373]</sup> and a pronounced proteolytic impairment with hydrolase depletion <sup>[348]</sup>.
- **Reactive oxygen species:** Lysosomes lack the most common antioxidant enzymes found in other organelles. When ROS levels are high, they can cross and damage the lysosomal membrane <sup>[374,375]</sup>. Lysosomal luminal is rich in free iron (resulting from the degradation of iron-containing proteins), which will

catalyze the conversion of hydrogen peroxide into highly reactive hydroxyl radicals that can damage and destabilize lysosomal membrane further <sup>[376]</sup>.

- **Therapeutic agents such as chloroquine and hydroxychloroquine:** These drugs diffuse into the lysosome where they undergo a protonation and alkalinize intraluminal pH <sup>[377,378]</sup> and cause defects of lysosome-autophagosome fusion <sup>[379]</sup>.
- **Drugs of abuse like methamphetamine and opioids:** These weak-base drugs are up-taken into the lysosome, where they would increase luminal pH, cause vacuolization, permeabilize the lysosomal membrane and disrupt iron homeostasis <sup>[380–382]</sup>.

The concept of the lysosomal stress response (LSR), a relatively recent addition to cellular stress responses, was proposed by Lakpa et al. (2021) to describe how lysosomes respond to these stress-inducing stimuli <sup>[371]</sup>. Several criteria define the lysosomal stress response:

- **Increase in pH:** Lysosome de-acidification is the most critical indicator, affecting many lysosomal characteristics and functions, and directly impacting cellular homeostasis. This can impair the hydrolytic activity of luminal enzymes and alter lysosome positioning <sup>[383]</sup>.
- **Increase in Lysosome Size:** Accumulation of undigested materials leads to a morphological increase in lysosome size <sup>[296]</sup>.
- **Lysosome Membrane Permeabilization (LMP):** Damage to the lysosomal membrane results in the release of luminal contents into the cytosol <sup>[384,385]</sup> (**Figure 23**). This can be detected by the Galectin-3 puncta assay <sup>[386]</sup>, as galectins are recruited to the inner layer of the lysosomal membrane to coordinate repair and removal pathways <sup>[387]</sup>. An immunofluorescence of Galectin-3 (LGALS3 or Gal-3) thus allows for the detection of damaged

lysosome, seen as puncta of Gal-3 co-localizing with lysosomal membrane markers like LAMP1 and LAMP2. LMP can be caused by ROS, excessive phagocytic uptake, or neurotoxic aggregates like tau, alpha-synuclein, or beta-amyloid fibrils [388,389]. Lysomotropic compounds like L-leucyl-L-leucine methyl ester (LLOMe) are commonly used to study lysosomal function and repair pathways [390].

- **Cationic Efflux:** Upon de-acidification, calcium and other cations such as iron are released from the lysosome. Calcium release can notably activate lysosomal biogenesis through the calcineurin-TFEB axis [365]. Iron release affects iron homeostasis [391] and lead to oxidative stress [392].
- **Intracellular Repositioning:** Lysosomes move within the cell in response to various factors, including cell type and intraluminal pH. Highly acidic endolysosomes are typically found in the perinuclear region, while de-acidified lysosomes move toward the cell periphery [304,383].
- **Misfolded Protein Aggregation:** Accumulation of intraluminal protein aggregates due to impaired hydrolytic activity of luminal enzymes.
- **LDL-Cholesterol Accumulation:** Lysosome de-acidification and decreased activity of lipases can cause the accumulation of LDL-cholesterol.
- **Redox Catastrophe:** De-acidification promotes the efflux of redox-active iron into the cytosol, generating ROS through the Fenton reaction [392,393].
- **Bioenergetic Crisis:** Compromised energy metabolism, particularly affecting mitochondrial quality, has been linked with impairment of lysosome-autophagosome fusion [394].

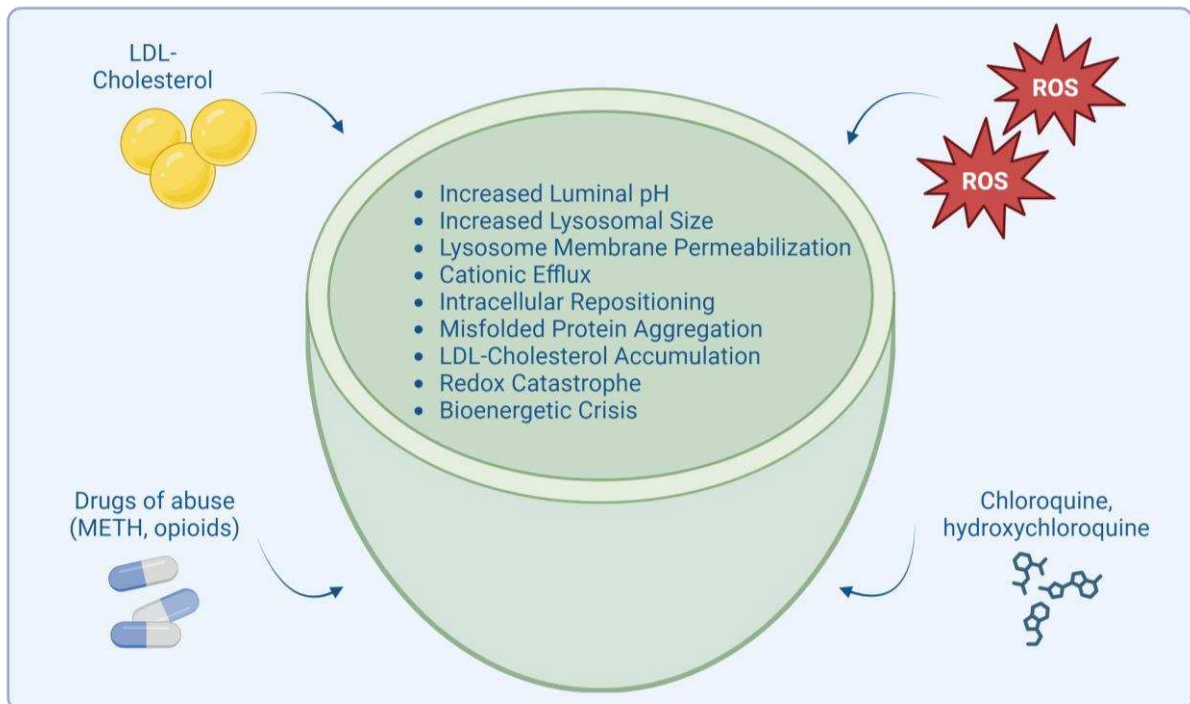


**Figure 22. Lysosomal Stress Response.** (Adapted from Lakpa et al., 2021) Figure created with [BioRender.com](https://www.biorender.com).

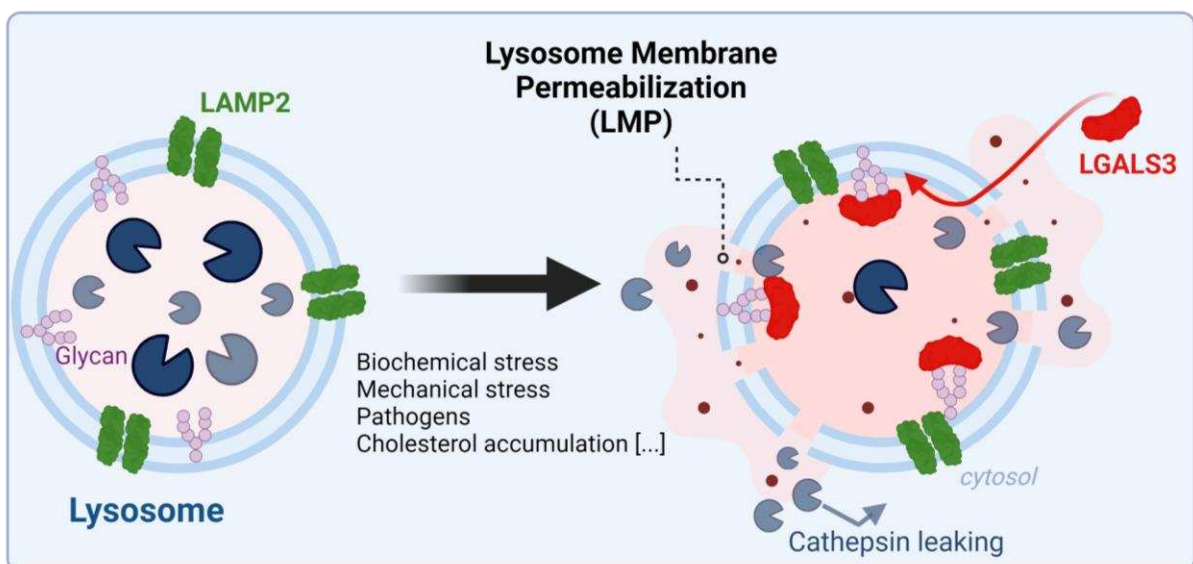


**Figure 23. Lysosome Membrane Permeabilization.** Various mechanisms can induce lysosome membrane permeabilization (LMP), such as mechanical stress, certain drugs or cholesterol accumulation. Galectin-3 (LGALS3) is recruited to the exposed inner layer of the

lysosomes where it binds the glycans. Cathepsin leaking from the lysosomal lumen to the cytosol through the damaged membrane causes perturbation of cellular homeostasis, potentially leading to lysosomal-dependent cell death (LDCD). Figure created with [BioRender.com](https://www.biorender.com).

### ***b) Lysosomal dependent cell death***

Lysosomal-dependent cell death (LDCD) is a cell death pathway directly resulting from LMP <sup>[385]</sup>. LMP causes the release of cathepsins into the cytosol, where they act as executors of cell death <sup>[395,396]</sup>. In addition to their direct effects, cathepsins can induce the proteolytic activation of substrates such as *Bid* and *Bax*, promoting mitochondrial outer membrane permeabilization (MOMP) and caspase activation <sup>[396,397]</sup>. LDCD occurs in various physiological contexts, including tissue remodeling and homeostatic mechanisms to eliminate intracellular pathogens, such as viruses, by removing infected cells <sup>[398]</sup>. One approach to block LDCD is through the inhibition of cathepsin activity, either by using protease inhibitors or by upregulating endogenous cathepsin inhibitors like serpin and cystatin <sup>[399]</sup>.

### **III.2.2 Lysosomal function in aging**

Lysosomal function declines with aging, primarily due to oxidative stress, which causes lysosomal damage and subsequent LMP. This damage results in decreased acidification and lysosomal enzyme activity, leading to the accumulation of undegraded substrates and defects in autophagy. This impairment is particularly pronounced in the central nervous system, predisposing individuals to late-onset neurodegenerative disorders <sup>[400,401]</sup>. Additionally, lysosomal dysfunction directly impacts mitochondrial function by deregulating the balance between mitophagy and general autophagy processes <sup>[402]</sup>. Targeting lysosomal function has emerged as a promising strategy to promote longevity, as it helps improve autophagy, proteostasis,

and mitochondrial quality, thereby maintaining cellular health and function during aging.

### **III.2.3 Lysosomal function in disease**

#### ***a) Lysosomal storage disorders***

Lysosomal storage disorders (LSDs) are a group of inherited monogenic diseases caused by mutations in genes encoding lysosomal resident proteins or proteins involved in lysosomal function. These genetic mutations result in defects in lysosome-mediated degradation and recycling processes, leading to the accumulation of undigested substrates <sup>[403,404]</sup>. 'Simple LSDs' arise from mutations in specific hydrolases, such as in Wolman disease, where a mutation in the *LAL* enzyme-coding gene causes lipid accumulation. In contrast, mutations in genes encoding lysosomal membrane proteins lead to broader cellular consequences. For example, mutations in the *TRPML1* gene, which cause Mucopolipidosis type IV (MLIV), are associated with significant intracellular trafficking defects.

LSDs are typically characterized by early-onset neurodegeneration, and they are severe and life-limiting. Current therapies are limited and mostly non-curative, relying on enzyme replacement therapies for many LSDs.

Certain LSDs, such as Pompe disease (caused by a mutation in the *GAA* gene leading to glycogen accumulation) and Danon disease (caused by mutations in the *LAMP2* gene), are particularly noteworthy for their severe impact on skeletal and cardiac muscles, highlighting the importance of lysosomal function in the muscle.

#### ***b) Lysosomal defects in neurodegenerative disease***

Lysosomal defects are increasingly recognized as significant contributors to neurodegenerative diseases, including Alzheimer's disease, Parkinson's disease,

Huntington's disease, amyotrophic lateral sclerosis, and Charcot-Marie-Tooth (CMT) disease. In these disorders, lysosomes exhibit disrupted and insufficient proteolysis, as well as defective autophagosome-lysosome fusion, leading to autophagic defects [405]. LDCD has been notably observed in neurodegenerative conditions, such as Parkinson's disease, where ROS-mediated lysosomal damage causes LMP and the release of cathepsins into the cytoplasm, triggering cell death. This process exacerbates neuronal loss and contributes to the progression of neurodegenerative diseases. Understanding the role of LDCD in these conditions highlights the importance of lysosomal health in neuronal survival and offers potential therapeutic targets for mitigating neurodegeneration [406,407].

### ***c) Lysosomal defects implications in cardiovascular diseases***

Lysosomal defects have significant implications in cardiovascular diseases, particularly in the context of drug-induced cardiotoxicity. Doxorubicin, a well-known anticancer drug, is notorious for causing dilated cardiomyopathy, a condition characterized by an enlarged and weakened heart. Research by Bartlet et al. (2016) demonstrated that doxorubicin represses the expression of TFEB, a master regulator of lysosomal biogenesis and function [408]. This repression is associated with impaired cathepsin proteolytic activity, reduced autophagic flux, and the activation of cell death pathways, all of which contribute to cardiac dysfunction. However, recent studies by Santin et al. (2023) suggest that treatment with acidic nanoparticles can counteract the cardiotoxic effects of doxorubicin [409]. These nanoparticles improve lysosomal function, thereby mitigating the deleterious impacts on the heart [409]. This therapeutic approach highlights the critical role of lysosomal health in maintaining cardiac function and offers a promising avenue for preventing drug-induced cardiomyopathy.

## **III.2.4 Lysosomal defects and muscle impairments**

Lysosomal dysfunction is increasingly recognized as a significant factor in various muscle impairments and muscle disorders. Lysosomes are essential for cellular waste degradation and recycling, and their malfunction can lead to severe muscle-related symptoms. Here we explore a few examples in which mutations in specific lysosomal function or structure involved genes can lead to an impairment of muscle function:

- **Pompe Disease**, also known as Glycogen Storage Disease Type II (GSDII), is caused by a deficiency in the enzyme acid alpha-glucosidase (GAA). This deficiency leads to the accumulation of glycogen in lysosomes within muscle cells, resulting in muscle weakness and respiratory issues.
- **Danon Disease** is characterized by mutations in the *LAMP2* gene, leading to a deficiency in lysosome-associated membrane protein-2. This deficiency causes skeletal myopathy, cardiomyopathy, and intellectual disabilities.
- **INPP5K-Related Muscular Dystrophy** arises from mutations in the *Inositol Polyphosphate-5-Phosphatase K (INPP5K)* gene, disrupting the function of the INPP5K enzyme. This enzyme plays a crucial role in regulating phosphoinositide levels in cells. Affected individuals typically present with congenital muscular dystrophy, characterized by muscle weakness and hypotonia from birth or early infancy. Recent studies highlight the importance of INPP5K in autophagic lysosome reformation <sup>[334]</sup>, emphasizing the role of lysosome recycling in muscle health.
- **VCP Disease** is caused by mutations in the *Valosin Containing Protein (VCP)* gene, which is involved in various cellular processes, including protein degradation and DNA repair. These mutations impair VCP's function, leading to alterations in protein and organelle homeostasis. This results in inclusion body myopathy, characterized by progressive muscle weakness and atrophy, particularly in the proximal muscles. A recent study has shown early defects in

the lysosomal system when *VCP* is inactivated in the skeletal muscle, with detection of LMP in the muscle, setting *VCP* as central mediator of both lysosomal clearance and biogenesis in skeletal muscle <sup>[410]</sup>.

- **Mucopolysaccharidosis Type IV (ML-IV)** is caused by mutations in the *MCOLN1* gene. These mutations affect the *MCOLN1* channel, crucial for maintaining lysosomal ion homeostasis, which is necessary for proper lysosomal function, including the degradation of macromolecules. Additionally, *MCOLN1* was reported to play a major role in sarcolemma repair <sup>[369]</sup>. ML-IV is characterized by muscle weakness and hypotonia from infancy, delayed motor development, and movement difficulties. Interestingly, the overexpression or activation of *MCOLN1* in a DMD mouse model has been shown to alleviate dystrophic features <sup>[369,370]</sup>.
- **Niemann-Pick Disease Type C (NPC)** results from mutations in the *NPC1* or *NPC2* genes, disrupting cholesterol and lipid trafficking within cells. This disruption leads to the accumulation of lipids in lysosomes, impairing degradation processes and overall cellular function. Individuals with NPC often exhibit muscle weakness and hypotonia, symptoms that can appear in infancy or later in childhood and progressively worsen over time. Interestingly in the context of DMD, a transgenic expression of *NPC1* in the *Dmd*<sup>*mdx*</sup> mouse model was reported to ameliorate muscular dystrophy, suggesting a potential compensatory gene for muscular dystrophy <sup>[411]</sup>.

### III.3 Endolysosomal damage response

Lysosomes are pivotal organelles at the crossroads of catabolic and anabolic processes, ensuring the degradation and recycling of various materials. However, this critical function makes lysosomes susceptible to LMP, which poses a significant threat

to cellular homeostasis due to the potential loss of lysosomal function and degradative capacity. To counteract LMP, cells have developed a set of coordinated set of pathways and mechanisms collectively referred to as the endolysosomal damage response <sup>[412]</sup> or lysosomal quality control pathways <sup>[413]</sup>. Initially, different repair mechanisms are activated to restore lysosomal membrane integrity, varying in their kinetics and response to the extent of LMP (**Figure 25**). When damage is too severe for repair, lysophagy—a selective autophagy of injured lysosomes—is triggered, followed by the recycling of lysosomal membranes through a process called autophagic lysosomal reformation (**Figure 25**). This process is mediated by the mTORC1-TFEB axis, which activates lysosomal biogenesis. These responses are tightly regulated by various factors recruited to the damaged lysosomal membrane, with Galectin-3 (Gal-3) being one of the first identified and extensively studied. In this section, we will first describe the various repair pathways and then the elimination and replacement pathways, noting that this is a relatively new field in cell biology with ongoing research revealing new actors, repair pathways, and mechanisms (**Figure 24**).

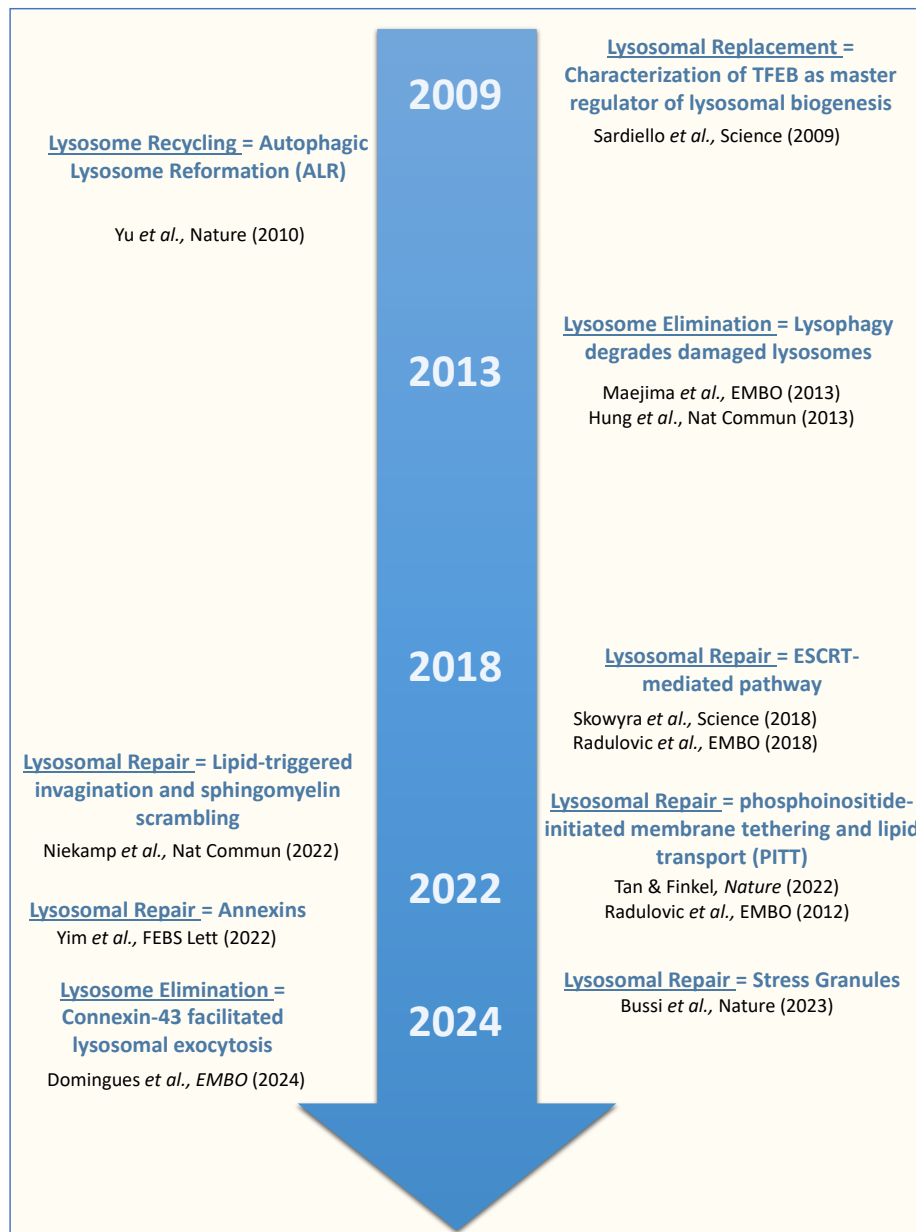


**Figure 24. Identification of pathways involved in the lysosome quality control in the last 15 years.** Since the identification of TFEB as a master regulator of lysosomal biogenesis and quality control, many pathways involved in lysosome quality control have been identified, with more research in the last few years. These pathways include lysosome recycling, repair, replacement and removal.

### III.3.1 Endo-lysosomal repair pathways

Lysosomal function is crucial to maintain cellular homeostasis. In order to preserve lysosomal function in response to various stress stimuli, the cell has developed various mechanisms to quickly repair the lysosomal membrane and prevent detrimental cellular damages. These mechanisms were mostly recently identified, with research still ongoing to better understand and characterize further lysosomal repair pathways (**Figure 24**).

**a) The Endosomal Sorting Complex Required for Transport (ESCRT)-mediated repair**

The ESCRT (Endosomal Sorting Complex Required for Transport) machinery plays a crucial role in lysosomal repair, a mechanism first reported by Radulovic et al. (2018) and Skowyra et al. (2018) <sup>[414,415]</sup>. Known for its functions in the formation of intraluminal vesicles at endolysosomes <sup>[416]</sup>, the ESCRT machinery comprises several complexes: ESCRT-0, -I, -II, and -III. Upon LMP, ESCRT-III is rapidly recruited to the lysosomal membrane within minutes. This recruitment is triggered by the leakage of  $\text{Ca}^{2+}$ , which activates the programmed cell death protein 6 (PDCD6), a calcium-binding protein (**Figure 25A**). PDCD6 then recruits ALIX (ALG-2 interacting protein X) to the membrane, which subsequently recruits additional ESCRT-III subunits such as CHMP2A, CHMP3, and CHMP4B. This orchestrated assembly of the ESCRT-III complex facilitates the repair of the lysosomal membrane, thereby restoring lysosomal integrity and preventing cell death.

**b) Lipid-triggered invagination**

Lysosome membrane repair can be mediated by lipid processing, specifically through a recently identified sphingomyelin-based repair pathway <sup>[417]</sup>. In this mechanism, membrane damage activates a calcium-dependent scramblase, which flips sphingomyelin from the luminal to the cytosolic leaflet of the lysosomal membrane.

The exposed sphingomyelin is then targeted by cytosolic neutral sphingomyelinase, which generates ceramide on the cytosolic surface of the lysosome <sup>[417]</sup> (**Figure 25A**). This ceramide production facilitates membrane bending towards the lumen of the lysosome, effectively mediating the repair of the injured lysosomal membrane <sup>[412,417]</sup>. This lipid-triggered invagination mechanism is a critical process for maintaining lysosomal integrity and cellular homeostasis, however the specific scramblase which activates this mechanism is still to be determined.

**c) Lipid transfer-mediated repair: phosphoinositide-initiated membrane tethering and lipid transport (PITT)**

The recently identified phosphoinositide-initiated membrane tethering and lipid transport (PITT) lysosome repair pathway is mediated by lipid transport to injured lysosomal membranes, a mechanism discovered independently by two research groups <sup>[418,419]</sup>. LMP triggers the calcium-dependent activation of phosphatidylinositol 4-kinase 2a (PI4K2A), leading to the generation of phosphatidylinositol 4-phosphate (PI4P) on the damaged membranes. PI4P facilitates the formation of ER–lysosome contact sites, accompanied by the recruitment of various lipid transfer enzymes, particularly the oxysterol binding protein (OSBP)-related proteins (ORPs) (**Figure 25A**). These ORPs assist in tethering the ER and lysosome together. OSBP selectively transfers cholesterol from the ER to the lysosomal membrane in exchange for PI4P, which is subsequently dephosphorylated in the ER. The transferred cholesterol intercalates into the lipid bilayer of the damaged lysosomal membrane, aiding its repair. Additionally, other ORPs such as ORP9, ORP10, and ORP11 transfer phosphatidylserine (PS) to the lysosomal membrane in exchange for PI4P (**Figure 25A**). Both PS and cholesterol contribute to lysosomal membrane repair and stability. The presence of PS also promotes the recruitment of other repair factors, notably ATG2, which facilitates lipid scrambling within the lipid bilayer through its

hydrophobic central groove. This pathway is emerging as an essential mechanism for rapid lysosomal repair.

***d) Other identified repair mechanism***

- **Annexins**

Annexins are a group of calcium responding membrane repair proteins. In the context of lysosome membrane repair, ANXA1 and ANXA2 particularly have been reported to play a selective role in lysosomal repair, especially larger pores sizes injuries that cannot be repair by the ESCRT machinery <sup>[420]</sup>.

- **Stress granules plug- mediated membrane stabilization**

A recently identified mechanism involves the recruitment of stress granules <sup>[421]</sup>. In fact, lysosomal damage induces the formation of stress granules (SGs) <sup>[422]</sup>. These SGs are condensates of non-translating messenger ribonucleoproteins (mRNPs) and a diverse group of proteins <sup>[423]</sup>. When membrane damage occurs, pores form, making the vesicles unstable and prone to collapse if the ruptured area cannot be sealed. It was reported that following endolysosomal damage, stress granules form near the sites of endomembrane damage and create localized condensates, or protective plugs <sup>[421]</sup>. These stress plugs stabilize the ruptured membrane, promoting efficient repair and preventing the collapse of the damaged vesicles. This mechanism highlights the crucial role of stress granules in maintaining cellular integrity under stress conditions.

### **III.3.2 Removal of damaged lysosomes**

***a) Lysophagy: degradation of damaged lysosomes***

Lysophagy is a specialized form of autophagy that is activated when lysosomes are damaged beyond repair, preventing further cellular damage from leaking cathepsins.

The term lysophagy was first coined in 2007 to describe the pathogenesis of Pompe disease, with an apparent accumulation of swollen lysosomes inside the autophagosomes <sup>[424]</sup>. Only later in 2013 was lysophagy contextualized within lysosomal repair processes <sup>[425,426]</sup>.

In this mechanism, damaged lysosomes are selectively sequestered by autophagosomes for degradation by intact lysosomes <sup>[425,426]</sup>. This process is mediated by the ubiquitylation of damaged lysosomes, involving ubiquitylation factors such as TRIM16, which is recruited by LGALS3 <sup>[427]</sup> (**Figure 25B**). Additionally, LGALS9 plays a crucial role in the overall ubiquitylation of damaged lysosomes <sup>[428]</sup>. Following ubiquitylation, various autophagy receptors, including TAX1BP1, SQSTM1/p62, and optineurin (OPT), are recruited <sup>[429]</sup>. This is followed by the recruitment of the autophagy initiation complex ULK1-ATG13-FIP200 <sup>[412]</sup>, leading to the formation of a phagophore that engulfs the damaged lysosome. Once the autophagosome formation is complete, it fuses with an intact lysosome, where the damaged lysosome is degraded, thus maintaining cellular health and preventing further damage.

#### ***b) Connexin-43 mediated exocytosis***

Some studies have suggested that aggregated materials in damaged lysosomes may be secreted via exocytosis <sup>[430,431]</sup>. While these studies did not establish a direct link to lysosomal quality control, a more recent study proposed lysosomal exocytosis as a part of the endolysosomal damage response when repair and degradation are inhibited <sup>[432]</sup>. This mechanism involves the recruitment of Connexin43 to damaged lysosomes, which triggers actin cytoskeletal remodeling mediated by the interaction between Connexin43 and the Actin Related Protein 2/3 (Arp2/3) complex, and also results in a decrease of cell stiffness (**Figure 25B**). Subsequently, extracellular vesicles

are secreted following the fusion of damaged lysosomes with the plasma membrane, occurring in a  $\text{Ca}^{2+}$ -independent manner.

### **III.3.3 Replacement and regeneration: TFEB-mediated lysosomal biogenesis**

Lysosomal biogenesis, a crucial component of the endo-lysosomal damage response, is essential for restoring the cellular pool of lysosomes following damage. This process is primarily regulated by the major transcription factor EB (TFEB), a member of the microphthalmia (MiT/TFE) family of leucine zipper transcription factors. TFEB binds to promoter regions with coordinated lysosomal expression and regulation (CLEAR) elements, governing the expression of lysosomal genes <sup>[433]</sup>. Under normal conditions, TFEB is phosphorylated by mTORC1 and retained in the cytoplasm <sup>[354,433,434]</sup>. However, upon lysosomal permeabilization, TFEB becomes dephosphorylated and translocates to the nucleus <sup>[330]</sup> (**Figure 25C**). This dephosphorylation is facilitated by the dissociation of mTORC1 from the lysosome following its inhibition <sup>[354,434]</sup> and by the activation of calcineurin in response to calcium efflux <sup>[365]</sup>. mTORC1 activation is dependent on nutrient signaling in intact lysosomes; thus, lysosomal stressors, such as proton pump inhibition, lysosomal membrane damage <sup>[387]</sup>, or nutrient starvation, can inactivate mTORC1, leading to TFEB activation <sup>[433]</sup>. Once in the nucleus, TFEB drives the expression of lysosomal genes, promoting the biogenesis of new lysosomes to maintain cellular homeostasis.

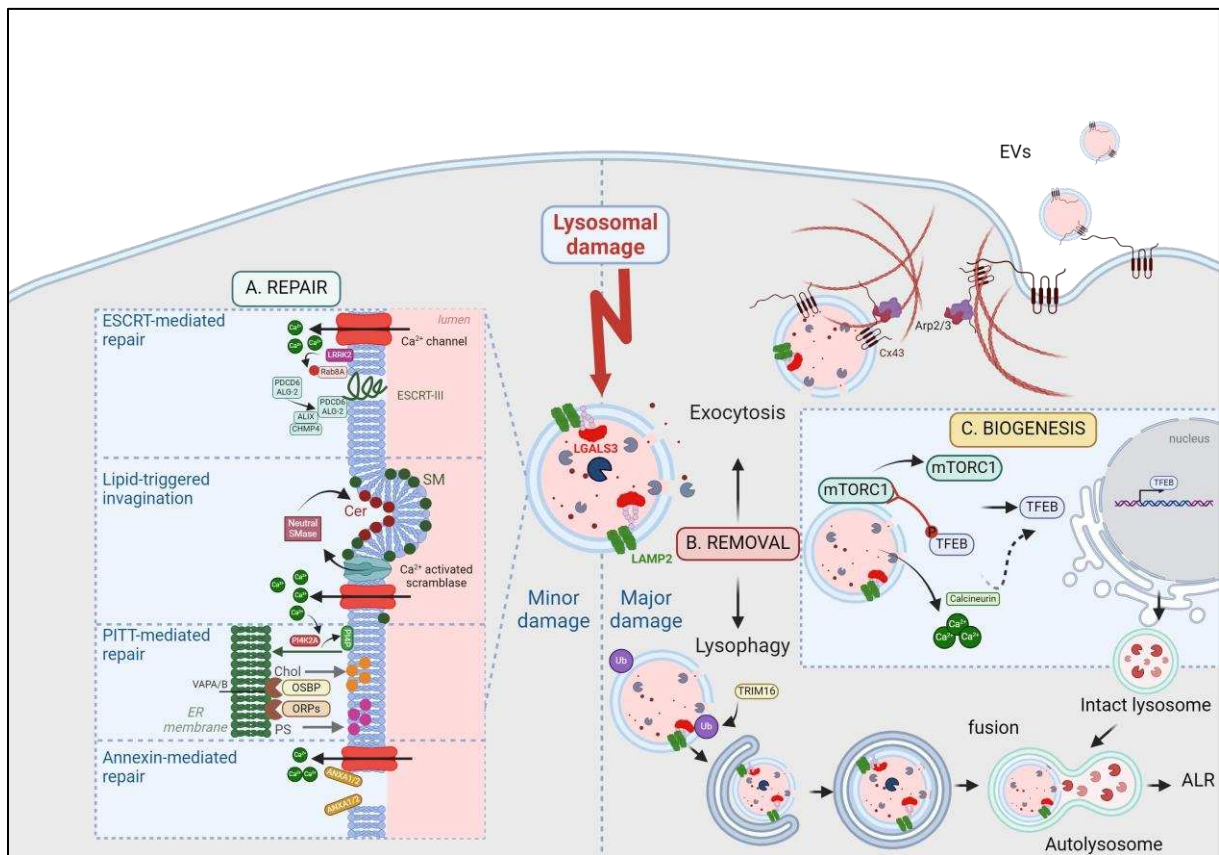


**Figure 25. The endolysosomal damage response.** Following the permeabilization of lysosomal membrane, various repair pathways are activated to restore membrane integrity. When damage is extensive or repair mechanisms fail, lysosomes undergo a form of selective macroautophagy, termed lysophagy, or are secreted out of the cell through a Connexin43 (Cx43)-dependent exocytosis. Simultaneously, lysosomal biogenesis is initiated through TFEB translocation to replenish the lysosomal pool. **A.** ESCRT machinery is rapidly recruited to the lysosome membrane following  $Ca^{2+}$  efflux. Programmed cell death protein 6 (PDCD6)/apoptosis-linked gene 2 (ALG2) are initially recruited, followed by ESCRT-III subunits such as ALG-2 interacting protein X (ALIX) and Charged Multivesicular Body Protein 4 (CHMP4). These subunits assemble into filament spirals that remodel the lysosomal membrane and push damaged membranes into the lysosomal lumen. Lipid-triggered invagination is mediated by  $Ca^{++}$  activated scramblase, which translocates sphingomyelin (SM) from the inner luminal leaflet of the membrane to the cytosolic leaflet. SM is then digested by neutral sphingomyelinase (SMAse) to produce ceramide (Cer), driving inward budding. Calcium efflux

also activates Phosphatidylinositol 4-Kinase Type 2 Alpha (PI4K2A), generating Phosphatidylinositol 4-phosphate (PI4P) on the limiting membrane. PI4P recruits lipid transfer proteins tethered to the VAMP-Associated Protein A/B on the ER membrane at ER-lysosome contact sites. OSBP mediates PI4P and cholesterol (Chol) counter-transport between the ER and damaged lysosomes, while ORPs mediate PI4P/phosphatidylserine (PS) exchange. Annexins ANXA1 and ANXA2 are also recruited by  $Ca^{++}$  efflux, aiding in the resealing of larger membrane pores. **B.** Damaged lysosomes are ubiquitinated by Tripartite Motif Containing 16 (TRIM16) and engulfed by the double-membrane autophagosome. After autophagosome closure, fusion with an intact lysosome occurs, resulting in the degradation of the damaged lysosome. Cx43 is recruited to the damaged lysosome, mediating exocytosis by remodeling the actin cytoskeleton through interaction with the Actin-Related Protein 2/3 (Arp2/3) complex. **C.** Damage signaling on the lysosomal membrane triggers the dissociation of mTORC1, leading to TFEB dephosphorylation and translocation to the nucleus.  $Ca^{2+}$ -mediated activation of calcineurin also contributes to TFEB dephosphorylation. In the nucleus, TFEB binds to coordinated lysosomal expression and regulation (CLEAR) motifs, promoting the transcription of lysosomal and autophagy genes. This process results in lysosome biogenesis, autophagosome formation, and lysosomal exocytosis. Figure created with [BioRender.com](https://www.biorender.com).

## OBJECTIVES

The work presented in the manuscript was conducted in the 'Progressive Muscular Dystrophies' laboratory led by Dr. Isabelle Richard. This team is dedicated to developing innovative treatments for rare muscular dystrophies, which currently lack effective therapies. Among their achievements, the team has developed several experimental gene therapies, including one that is currently in clinical trials for limb-girdle muscular dystrophy associated with FKRP deficiency (LGMDR9).

This project primarily investigates the pathophysiological mechanisms of DMD, some of which are shared with other muscular dystrophies. The primary goal is to identify new therapeutic targets by elucidating these mechanisms. This would allow to develop combined therapies, integrating gene therapy to restore the expression of the deficient gene with additional treatments addressing cellular and metabolic perturbations in the muscle. This dual approach aims to lower the required dose of rAAV vectors, thereby reducing the risks of toxicity and immune response while enhancing the gene therapy's therapeutic effects.

Recently, the team identified perturbations in cholesterol metabolism in DMD. We hypothesized that these perturbations are linked to defects in the endolysosomal system. The first objective of this project was to characterize the endolysosomal system in the dystrophic muscle and its link with the disrupted cholesterol metabolism. The second objective was to develop a combined therapy involving microdystrophin transfer via rAAV vectors alongside the correction of secondary metabolic disorders.

### **Objective 1: Characterization of the endolysosomal system in DMD**

- **Evidence and hypothesis of lysosomal defects in DMD**

It is increasingly appreciated that the absence of dystrophin leads to both mechanical instability of skeletal muscle fibers and a wide range of metabolic disruptions [107]. Notably, plasma dyslipidemia and disturbances in lipid metabolism have been observed [163]. In a recent study examining circulating miRNAs expression in a large cohort of DMD patients, we demonstrated alterations in cholesterol metabolism within dystrophic muscle [142].

However, the molecular mechanisms linking cholesterol overload to muscle degeneration in DMD remain unclear. Previous studies have indicated that cholesterol accumulation in muscle, particularly in sarcolemmal T-tubules and triad structures, can adversely affect muscle metabolism [435]. This is primarily due to reduced efficiency in muscle excitation-contraction coupling and glucose endocytosis, contributing to insulin resistance.

Increasing evidence suggests that excess lipids can disrupt lysosomal functions, including acidification [436,437], trafficking [438–441], exosome release [442], autophagy [373,441,443–445], and activation of the mTOR pathway [348]. Similar disruptions are observed in many LSDs, such as Niemann-Pick disease [372]. We hypothesized that, similar to LSDs, excess cholesterol might also accumulate in the endolysosomal system in dystrophic muscle, leading to lysosomal dysfunction.

This hypothesis is supported by previous studies reporting abnormalities in lysosome structure and activity long ago [446–448], and again more recently [449,450]. Notably, *Dmd*<sup>mdx</sup> mice exhibit lysosomal abnormalities at a very early stage (10 days) [451]. At this age, there are no detectable histological disturbances in *Dmd*<sup>mdx</sup> mice, suggesting that lysosomal dysfunction may be an early event in the DMD pathological cascade.

However, few studies have considered lysosomal defects as primary contributors to the pathophysiology of DMD. Instead, research has largely focused on disruptions in autophagy <sup>[153,156,452]</sup>. Autophagy and lysosomal activity are closely linked functional processes, and autophagy dysfunction has been identified in several LSDs, where the primary defect is attributed to the lysosomes and autophagy dysfunction is clearly secondary <sup>[453,454]</sup>. Recently, secondary autophagy disturbances due to lysosomal defects have been detected in muscular dystrophies, both in skeletal <sup>[455]</sup> and cardiac muscle <sup>[456]</sup>. It remains to be determined whether the autophagy disturbances observed in DMD are secondary to underlying lysosomal defects.

- **Galectin-3: A potential biomarker of lysosomal damage in DMD**

To investigate the hypothesis that cholesterol accumulation in the dystrophic muscle could be associated with impaired lysosomal function, we needed a method to quantify lysosomal damage. Several studies have recently focused on lysosomal dysfunction, in which LMP plays a central role <sup>[371]</sup>. However, few studies have investigated lysosome damage in muscle. One identified marker of LMP is Gal-3 (or LGALS3), which belongs to a family of lectins that specifically bind to carbohydrates <sup>[457]</sup>. These lectins are present in the cytosol, nucleus, and extracellular matrix (ECM) and are translocated to the membrane of damaged lysosomes <sup>[386]</sup> prior to their removal by the autophagy machinery <sup>[307,387]</sup>.

Interestingly, Gal-3 upregulation was previously reported in the dystrophic muscle <sup>[458]</sup>, with a correlation with the severity of the dystrophic phenotype in animal models and the degree of dystrophin expression <sup>[459]</sup>. Additionally, Gal-3 is linked to inflammation <sup>[460]</sup>, with its upregulation in DMD primarily attributed to infiltrating macrophages <sup>[461]</sup>. However, recent studies suggest that Gal-3 is expressed within muscle cells themselves, rather than solely in infiltrating immune cells, and plays a significant role in muscle regeneration <sup>[462,463]</sup>.

These indications suggest that Gal-3 could serve as a biomarker of lysosomal damage in DMD. To explore this hypothesis, we first focused on studying the expression and localization of Gal-3 in the context of DMD and other muscular dystrophies. We also set out to characterize various aspects of lysosomal function and structure in the dystrophic muscle.

### **Objective 2: Developing new combined therapeutic approaches for the treatment of muscular dystrophies**

The second focus of this thesis was the development of innovative therapeutic strategies for DMD. Over the past 25 years, significant efforts have been directed towards developing gene therapies for DMD, but there has been comparatively less focus on understanding and targeting the disease's secondary pathological mechanisms. Currently, microdystrophin treatment is administered when the dystrophy is already well-established, often with significant muscle fibrosis. This approach faces the challenge of reversing all pathological mechanisms, especially since microdystrophin does not fully replicate dystrophin's function and is not expressed in all muscle fibers, as demonstrated by clinical results to date.

Recent research in our laboratory has revealed that even when microdystrophin is successfully expressed in nearly 100% of muscle fibers of dystrophic mice, the transcriptomic profile is not fully restored <sup>[271]</sup>. This suggests that microdystrophin alone may not be sufficient to restore all disrupted molecular mechanisms in dystrophic muscle. Therefore, a comprehensive therapeutic strategy that addresses the various pathological aspects of DMD remains essential.

Exploring these secondary mechanisms can help reduce the required doses of rAAV needed to achieve a significant therapeutic effect, while simultaneously enhancing the molecular correction of dystrophy. Several therapeutic strategies have already

been proposed, such as reducing muscle degeneration and stimulating muscle regeneration through the activation of Insulin-like Growth Factor 1 (IGF-1) [464], or attenuating fibrosis [465].

Our approach thus involves combining a suboptimal dose of rAAV delivering microdystrophin with complementary treatments to enhance the efficacy of gene therapy by addressing uncorrected secondary muscle alterations (**Figure 26**).

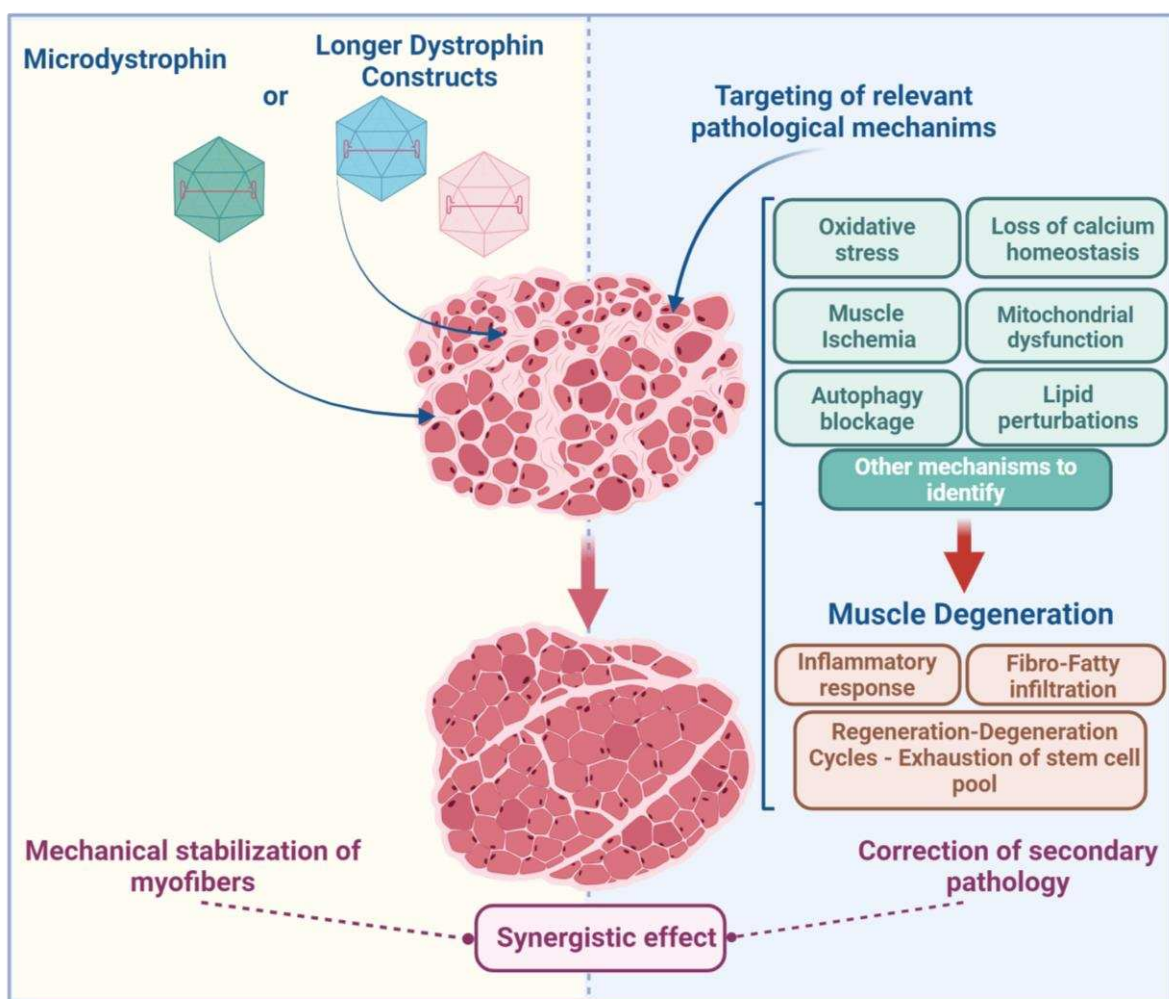


**Figure 26. Principle of combined therapy for DMD.** Gene therapy would be combined with complementary treatment that address the various pathophysiological mechanisms in the dystrophic muscle. Figure created with [BioRender.com](https://www.biorender.com).

# RESULTS

The results of this thesis will be presented in a manuscript currently under submission. Additionally, supplemental results not included in the manuscript will be presented in a separate section.

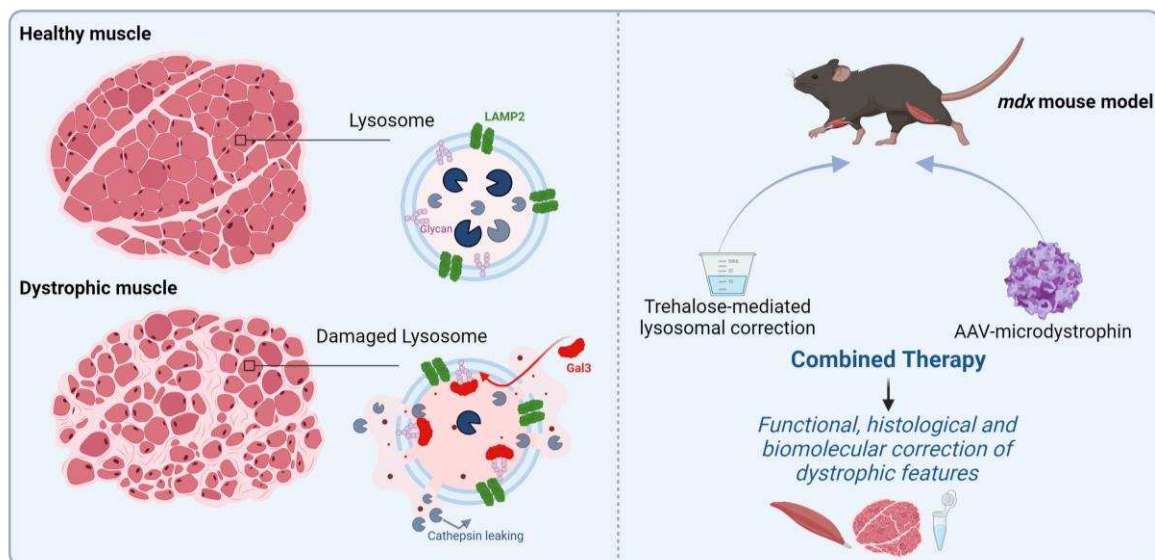
## I- Targeting lysosomal damage as a new therapeutic perspective for Duchenne Muscular Dystrophy

**Questions:** Building on our previous work showing perturbations of cholesterol metabolism in DMD, we hypothesized a potential interplay between cholesterol accumulation and lysosomal perturbations in DMD pathogenesis. We set out to characterize the lysosomal system in the dystrophic muscle.

**Findings:** We identified an upregulation of Gal-3, a known biomarker of LMP, in the dystrophic muscle of DMD patients and animal models, indicating the occurrence of LMP within dystrophic myofibers. We also detected significant lysosomal stress in the dystrophic muscle, evidenced by changes in lysosome number, morphology, positioning and activation of lysosomal biogenesis, repair and removal pathways. We then showed that a cholesterol-rich high fat diet induces an increase of lysosomal damage in *Dmd*<sup>mdx-4Cv</sup> mice, as well as an exacerbation of muscle fibrosis, linking cholesterol accumulation in the muscle to lysosomal damage and exacerbation of dystrophic features. Subsequently, treatment of the *Dmd*<sup>mdx</sup> mice with an optimal dose of rAAV encapsulating a  $\mu$ -dystrophin sequence demonstrated only partial correction of lysosomal damage. To address this limitation, we administered trehalose, a dietary supplement known to mitigate lysosomal damage, either alone or in combination with a suboptimal dose of AAV- $\mu$ -dystrophin. Our findings revealed

that the combined treatment of AAV  $\mu$ -dystrophin and trehalose yielded the most substantial correction of lysosomal damage and amelioration of dystrophic muscle features, including motor function, muscle histology and transcriptomic signature. Our study underscores the significance of lysosomal damage in DMD pathophysiology and suggests that a synergistic approach combining trehalose supplementation with a suboptimal dose of AAV  $\mu$ -dystrophin holds promise for enhancing therapeutic outcomes in DMD.

### Graphical Abstract:



Created with [BioRender.com](https://BioRender.com)

**Contribution:** I am the first author of this study. I designed, performed and analyzed most of the experiments. I constructed and wrote the manuscript with guidance from IR and DI.

1 **Targeting lysosomal damage is a new therapeutic perspective for Duchenne Muscular**  
2 **Dystrophy**

3 Abbass Jaber<sup>1,2</sup>, Laura Palmieri<sup>1,2</sup>, Rania Bakour<sup>1,2</sup>, Elise Lachiver<sup>1,2</sup>, Ai Vu Hong<sup>1,2</sup>, Nathalie Bourg<sup>1,2</sup>, Jérôme  
4 Poupiot<sup>1,2</sup>, Sonia Albini<sup>1,2</sup>, Daniel Stockholm<sup>1,3</sup>, Laetitia Van Wittenberghe<sup>1,2</sup>, Adeline Miranda<sup>1,2</sup>, Nathalie  
5 Daniele<sup>1,2</sup>, Inés Barthélémy<sup>4</sup>, Stephan Blot<sup>4</sup>, Mai Thao Bui<sup>5</sup>, Teresinha Evangelista<sup>5</sup>, Isabelle Richard<sup>1,2,6</sup> &  
6 and David Israeli<sup>1,2,\*</sup>

7 <sup>1</sup>Genethon, 91000 Evry, France

8 <sup>2</sup>Université Paris-Saclay, Univ Evry, Inserm, Généthon, Integrare research unit UMR\_S951, 91000, Evry-  
9 Courcouronnes, France.

10 <sup>3</sup>Ecole Pratique des Hautes Etudes, PSL Research University, Sorbonne Université, INSERM, CRSA, Paris,  
11 75012, France.

12 <sup>4</sup>Univ Paris-Est Créteil, INSERM U955 IMRB, Ecole Nationale Vétérinaire d'Alfort, EFS, IMRB, Team BNMS,  
13 Maisons-Alfort, France

14 <sup>5</sup>Muscle Pathology Unit, Institut de Myologie and Neuropathology department, Sorbonne Université, Pitié-  
15 Salpêtrière Hospital, APHP, Paris, France

16 <sup>6</sup>Atamy Therapeutics, 1, bis rue de l'internationale, Evry, France

17

18 **Key words:** Duchenne Muscular Dystrophy, Cholesterol, Lysosome, Gene therapy, Microdystrophin,  
19 Trehalose

20 \* Corresponding author: David Israeli, [israeli@genethon.fr](mailto:israeli@genethon.fr)

21

## 22 **ABSTRACT**

23 Duchenne Muscular Dystrophy (DMD) is a muscle degenerative disease primarily affecting young boys,  
24 characterized by the loss of functional dystrophin expression. While gene therapy targeting the restoration  
25 of a functional truncated form of dystrophin, known as  $\mu$ -dystrophin, has shown promise in preclinical  
26 studies, its therapeutic efficacy in treated DMD patients remains limited, necessitating urgent  
27 improvements. Our recent investigations into plasma microRNAs profiles of a large DMD cohort have  
28 revealed dysregulations of cholesterol metabolism, a phenomenon frequently associated with lysosomal  
29 dysfunction in neurodegenerative disorders. Building upon this association, we hypothesized a potential  
30 interplay between cholesterol accumulation and lysosomal perturbations in DMD pathogenesis. Our study  
31 identified an upregulation of Galectin-3 (LGALS3), a known biomarker of lysosome membrane  
32 permeabilization (LMP), in the dystrophic muscle of DMD patients and animal models, indicating the  
33 occurrence of LMP within dystrophic myofibers. We also detected significant lysosomal stress in the  
34 dystrophic muscle, evidenced by changes in lysosome number, morphology, positioning and activation of  
35 lysosomal biogenesis, repair and removal pathways. We then showed that a cholesterol-rich high fat diet  
36 induces an increase of lysosomal damage in *Dmd*<sup>*mdx-4Cv*</sup> mice, as well as an exacerbation of muscle fibrosis,  
37 linking cholesterol accumulation in the muscle to lysosomal damage and exacerbation of dystrophic  
38 features. Subsequently, treatment of the *Dmd*<sup>*mdx*</sup> mouse model with an optimal dose of recombinant  
39 Adeno-Associated Virus (rAAV) encapsulating a  $\mu$ -dystrophin sequence demonstrated only partial  
40 correction of lysosomal damage. To address this limitation, we administered trehalose, a dietary  
41 supplement known to mitigate lysosomal damage, either alone or in combination with a suboptimal dose  
42 of AAV- $\mu$ -dystrophin. Our findings revealed that the combined treatment of AAV  $\mu$ -dystrophin and  
43 trehalose yielded the most substantial correction of lysosomal damage and amelioration of dystrophic  
44 muscle features, including motor function, muscle histology and transcriptomic signature. Our study  
45 underscores the significance of lysosomal damage in DMD pathophysiology and suggests that a synergistic

46 approach combining trehalose supplementation with a suboptimal dose of AAV  $\mu$ -dystrophin holds  
47 promise for enhancing therapeutic outcomes in DMD.

48

## 49 INTRODUCTION

50 Duchenne muscular dystrophy (DMD) is an X-linked recessive muscle disease due to the absence of  
51 dystrophin, the protein encoded by the DMD gene. It affects roughly 1/5000 boys and is the most common  
52 form of childhood muscular dystrophy. The loss of dystrophin in the skeletal myofiber leads to a  
53 destabilization of the dystrophin-associated glycoprotein complex, which connects the cytoskeleton to the  
54 extracellular matrix (Duan et al., 2021). This disruption triggers a cascade of pathological events including  
55 perturbations of calcium homeostasis, oxidative stress, mitochondrial dysfunction, chronic inflammation,  
56 fibro-adipocytic transformation, and consequently loss of muscle mechanical function (Allen et al., 2016).  
57 Current clinical management of DMD involves a multidisciplinary approach to address both muscular and  
58 extra-muscular manifestations of the disease (Roberts et al., 2023). Approved treatments include mainly  
59 glucocorticoids, which are recommended as early as possible (Zhang & Kong, 2021) and throughout the  
60 patient's life (Bushby et al., 2010). Although glucocorticoids have shown a significant improvement in  
61 motor function, they remain merely a symptomatic treatment and can at best delay disease progression  
62 (McDonald et al., 2018). Besides, several therapeutic approaches under investigation aim at restoring a  
63 functional form of dystrophin. One of the most advanced and promising approaches is microdystrophin  
64 ( $\mu$ -dystrophin) gene therapy, which involves delivering a shortened but functional variant of the dystrophin  
65 gene using a recombinant Adeno-Associated Vector (rAAV) (Chamberlain et al., 2023). This approach faces  
66 a key challenge, which is optimizing the therapeutic dosage. High doses may trigger severe immune  
67 responses and organs' toxicity (Bradbury et al., 2023), while low doses may fail to achieve the desired  
68 therapeutic effect. Although one  $\mu$ -dystrophin gene therapy (*delandistrogene moxeparvovec*) has recently  
69 gained FDA approval for ambulatory patients, functional improvements for patients have not replicated  
70 preclinical results (Mullard, 2023; Rind, 2024). The limited functional improvement observed in the clinical  
71 trials with  $\mu$ -dystrophin could be attributed to several factors, primarily including the lack of certain  
72 functional domains found in full-length dystrophin (Mirouse, 2023). Therefore,  $\mu$ -dystrophin gene transfer

73 may not be able to reverse all the pathological mechanisms in the muscle. Identifying specific pathological  
74 mechanisms that remain uncorrected by  $\mu$ -dystrophin gene therapy and exploring combinatorial  
75 approaches with complementary treatments targeting these mechanisms is crucial.

76 It is increasingly appreciated that the lack of dystrophin results not only in the mechanical instability of the  
77 skeletal myofiber but also in a vast spectrum of metabolic perturbations (Timpani et al., 2015). Among  
78 these, plasma dyslipidemia and perturbation of lipid metabolism were identified (White et al., 2020),  
79 whereas, in an investigation of expression of circulating microRNA in a large DMD cohort, we have recently  
80 showed perturbations of cholesterol metabolism in the dystrophic muscle in DMD (Amor et al., 2021;  
81 Israeli et al., 2022). Excessive cholesterol levels have frequently been associated with impaired lysosomal  
82 function, particularly in neurodegenerative diseases (Betuing et al., 2022; Udayar et al., 2022). We  
83 therefore hypothesized that cholesterol accumulation in the dystrophic muscle could be associated with  
84 impaired lysosomal function. To assess lysosomal function in DMD, we first evaluated the expression and  
85 localization of galectin-3 (Gal-3 or LGALS3), a known biomarker of lysosomal membrane permeabilization  
86 (LMP). We found that Gal-3 is significantly upregulated in the skeletal myofibers of DMD patients and  
87 various animal models, localizing to the lysosomes. LMP was also detected in a Limb-Girdle Muscular  
88 Dystrophy Type R5 (LGMDR5) mouse model and patient, suggesting a common perturbation across  
89 different types of muscular dystrophy. Using the *Dmd*<sup>mdx-4Cv</sup> mice, we detected and characterized various  
90 lysosomal perturbations in the dystrophic muscle, such as enlargement and increased number of  
91 lysosomes. Additionally, we observed activation of the endolysosomal damage response, which includes  
92 lysosomal replacement, repair and removal, and a perturbation of autophagy. Remarkably, LMP was  
93 exacerbated in dystrophic mice fed a cholesterol-rich diet and was not fully corrected by  $\mu$ -dystrophin  
94 gene therapy. In contrast, gene therapy showed better corrected in the LGMDR5 mouse model when  
95 delivering the complete sequence of the missing gamma-sarcoglycan coding sequence, suggesting that the  
96 corresponding lysosomal dysfunction is reversible in other muscular dystrophies, but not by the sole  $\mu$ -

97 dystrophin in DMD. Subsequently, we selected trehalose, an FDA-approved compound known to restore  
98 lysosomal function, for use in combination with a suboptimal dose of AAV- $\mu$ -dystrophin gene therapy. The  
99 combined treatment resulted in improved correction of dystrophic parameters, including motor function,  
100 muscle histology, and transcriptome signature, compared to  $\mu$ -dystrophin suboptimal gene therapy alone.

101

102 **RESULTS**

103 **Lysosome membrane permeabilization impairs lysosome function in muscle cells and can be detected**  
104 **with LGALS3 puncta assay:**

105 To investigate the hypothesis that cholesterol accumulation in the dystrophic muscle could be associated  
106 with impaired lysosomal function, we needed a method to quantify lysosomal damage. Several studies  
107 have recently focused on lysosomal dysfunction, in which LMP plays a central role (Lakpa et al., 2021).  
108 However, very few studies have investigated lysosome damage in muscle. One identified marker of LMP  
109 is gal-3 (or LGALS3), which is part of the galectins, a family of lectins that bind specifically to carbohydrates  
110 (Barondes et al., 1994). These lectins are present in the cytosol, nucleus, and extracellular matrix (ECM)  
111 and are translocated to the membrane of damaged lysosomes prior to their removal by the autophagy  
112 machinery (Aits et al., 2015). To analyze LGALS3 expression in a myogenic environment and its capacity to  
113 detect LMP, healthy human immortalized myoblasts were differentiated into elongated myotubes for 7  
114 days, and then immune-stained for LGALS3. A diffuse expression of LGALS3 was observed in the cells  
115 (**Figure S1a**). Treatment with L-leucyl-L-leucine methyl ester (LLOMe), a lysomotropic agent that induces  
116 lysosome-specific membrane damage (Uchimoto et al., 1999), for 30 minutes at 2,5 mM, triggered the  
117 formation of LGALS3 positive puncta, a characteristic of damaged lysosomes. An overexpression of LGALS3  
118 was also detected by western blot after 30 minutes to 1 hour of LLOMe treatment (**Figure S1b-c**).  
119 Interestingly, LGALS3 puncta were drastically reduced 3 hours after treatment, and LGALS3 expression was  
120 restored to control level, demonstrating an efficient lysosomal repair by the cells. This pattern correlated  
121 inversely with the amount of LGALS3 released in the media, detected by enzyme-linked immunosorbent  
122 assay (ELISA) assay (**Figure S1d**), where a significant increase was detected in the media only after 3 hours  
123 of LLOMe treatment. We then aimed to check the effect of LMP on lysosomal function after LLOMe  
124 treatment. For that, we performed pH probing using a combination of two dextran conjugates (MW =  
125 10 kDa), which are endocytosed by the cells, and accumulate selectively in the lysosomes. One dextran is

126 conjugated with Oregon Green, whose emission is quenched under acidic environments such as the  
127 lysosomal lumen, and the other is conjugated with Tetramethylrhodamine (TMRM), whose emission in the  
128 red spectrum is pH independent (Fernandez-Mosquera et al., 2019). Monitoring the ratio between the  
129 green and red dextran-coupled fluorophores demonstrated a decrease of acidification after treatment  
130 with LLOMe for 30 minutes (higher green/red ratio), indicating an impact of LMP on lysosomal function in  
131 myotubes. Collectively, these data indicate that LGALS3 is expressed in muscle cells and is recruited  
132 specifically to damaged lysosomes. Immunostaining for LGALS3 could be therefore applied to detect LMP  
133 in skeletal muscle and to provide an insight into lysosomal function.

134 **LGALS3 is overexpressed in dystrophic muscle and correlates with lysosomal membrane**  
135 **permeabilization and lysosomal stress:**

136 After validating LGALS3 as a biomarker for LMP in muscle cells, we aimed at studying its expression and  
137 localization in DMD. First, Gal-3 expression at the mRNA and protein levels was evaluated in young 7-week-  
138 old *Dmd*<sup>mdx-4Cv</sup> mice. A significant upregulation was observed in both mRNA transcripts and protein in the  
139 gastrocnemius (GA) (mRNA: FC=32; protein: FC=14.4), tibialis anterior (TA) (mRNA: FC=21; protein:  
140 FC=22.6) and diaphragm (mRNA: FC=10; protein: FC=41.2) muscles of dystrophic mice compared to Wild-  
141 Type (WT) mice (**Figure 1a-c**). In addition, a significant increase of LGALS3 was also detected in the serum  
142 of *Dmd*<sup>mdx-4Cv</sup> mice compared to control mice (FC=1.8) (**Figure 1d**), suggesting a release of LGALS3 from the  
143 muscle. To evaluate whether LGALS3 is recruited to the damaged lysosomes in the context of LMP in the  
144 dystrophic muscle, cross-sections of TA muscles were immunostained for LGALS3 and the lysosome-  
145 associated membrane proteins 2 (LAMP2) which is commonly used as lysosome marker (Barral et al., 2022)  
146 (**Figure 1e**). Confocal immunofluorescence images showed a colocalization of LGALS3 puncta with LAMP2  
147 inside the myofibers of young *Dmd*<sup>mdx-4Cv</sup> mice, indicating a substantial amount of LMP. Quantification of  
148 the double positive puncta (LAMP2+LGALS3+) per myofiber showed a significant increase in the dystrophic

149 muscle compared to WT control, where very few puncta were detected (Mean = 9 for *Dmd*<sup>mdx-4Cv</sup> versus 1  
150 for control).

151 Positive areas of LGALS3 and LAMP2 were also detected outside the muscle fibers of dystrophic mice, and  
152 do not indicate myofiber lysosomal damage. This staining corresponds to area of inflammatory infiltrates  
153 classically seen in dystrophic muscles and is consistent with previously reports, where overexpression of  
154 Gal-3 at the mRNA level in animal models of DMD was mainly attributed to LGALS3 positive infiltrating  
155 immune cells such as macrophages (Coulis et al., 2023; Marotta et al., 2009; van Putten et al., 2012). To  
156 confirm that these areas correspond indeed to inflammatory infiltrating cells, a co-immunostaining of  
157 LGALS3 and CD11b was performed on serial cross sections of dystrophic TA muscles (**Figure 1g**). An overlay  
158 of both staining (CD11b and LGALS3) was observed between the myofibers, indicating infiltrating  
159 macrophages. This confirms that LGALS3 overexpression in the muscle of *Dmd*<sup>mdx-4Cv</sup> is not only due to  
160 infiltrating macrophages, but also to a myogenic upregulation of LGALS3 and recruitment to the lysosomes,  
161 indicating substantial LMP. After confirmation of LMP incidence in the dystrophic muscle, we sought to  
162 evaluate parameters of lysosomal stress. First, we evaluated lysosome number with a WB for LAMP2 in  
163 WT and *Dmd*<sup>mdx-4Cv</sup> muscles (**Figure 1h & S2a**). An overexpression of LAMP2 was observed in both GA  
164 (FC<sub>GA</sub>=3.9) (**Figure 1i**) and TA (FC<sub>TA</sub>=4.1) (**Figure S2a**). Moreover, a quantification of LAMP2 spots on  
165 transversal sections from TA muscles immunolabeled with LAMP2 showed a significant increase of spot  
166 number (mean=14.3 and 12.2 for *Dmd*<sup>mdx-4Cv</sup> and WT respectively) (**Figure S2b-c**), and spot size (FC=1.7)  
167 [**Figure S2d**], two main criteria of lysosomal stress. To further analyze lysosome morphology and number  
168 at the single myofiber level, Flexor Digitorum Brevis (FDB) muscle fibers were isolated from *Dmd*<sup>mdx-4Cv</sup> and  
169 WT mice, and immunostained for LAMP2 and LGALS3 (**Figure 1j**). Three Dimension re-construction of  
170 confocal stack images showed a significant accumulation of lysosomes in the *Dmd*<sup>mdx-4Cv</sup> myofibers, which  
171 co-localized with LGALS3, especially around the nuclei, indicating a substantial amount of LMP. However,  
172 not all lysosomes (LAMP+ spots) were positive for LGALS3, indicating the existence of a population of non-

173 damaged lysosomes. A 3D modeling of LAMP2 spots (**Figure 1k**), showed a significant increase of lysosome  
174 number ( $FC_{\text{number}}=3.4$ ) (**Figure 1l**) and a denser distribution in the *Dmd*<sup>mdx-4Cv</sup> myofibers, as indicated by the  
175 distance to the 5 nearest spots ( $FC_{5 \text{ nearest spots}}=-1.65$ ) (**Figure 1m**). An increase of the average spot diameter  
176 ( $FC_{\text{Diameter}}=1.2$ ) was observed in the *Dmd*<sup>mdx-4Cv</sup> myofibers (**Figure 1n**). When plotting the spots diameter on  
177 a density plot, three populations of LAMP2 spots were distinguished in the *Dmd*<sup>mdx-4Cv</sup> myofibers versus  
178 one main population in the WT myofibers (**Figure 1o**). Both WT and *Dmd*<sup>mdx-4Cv</sup> myofibers displayed a  
179 population of average size spots. *Dmd*<sup>mdx-4Cv</sup> myofibers showed additionally a population of enlarged spots,  
180 corresponding to typical damaged enlarged lysosomes, indicative of lysosomal stress and accumulation of  
181 undegraded materials. Interestingly, an additional population of smaller spots was detected in *Dmd*<sup>mdx-</sup>  
182 <sup>4Cv</sup>myofibers. These smaller spots may correspond to newly generated lysosomes and/or to proto-  
183 lysosomes, which are fragments of recycled lysosomal membranes following the elimination of damaged  
184 lysosomes (Y. Chen & Yu, 2017).

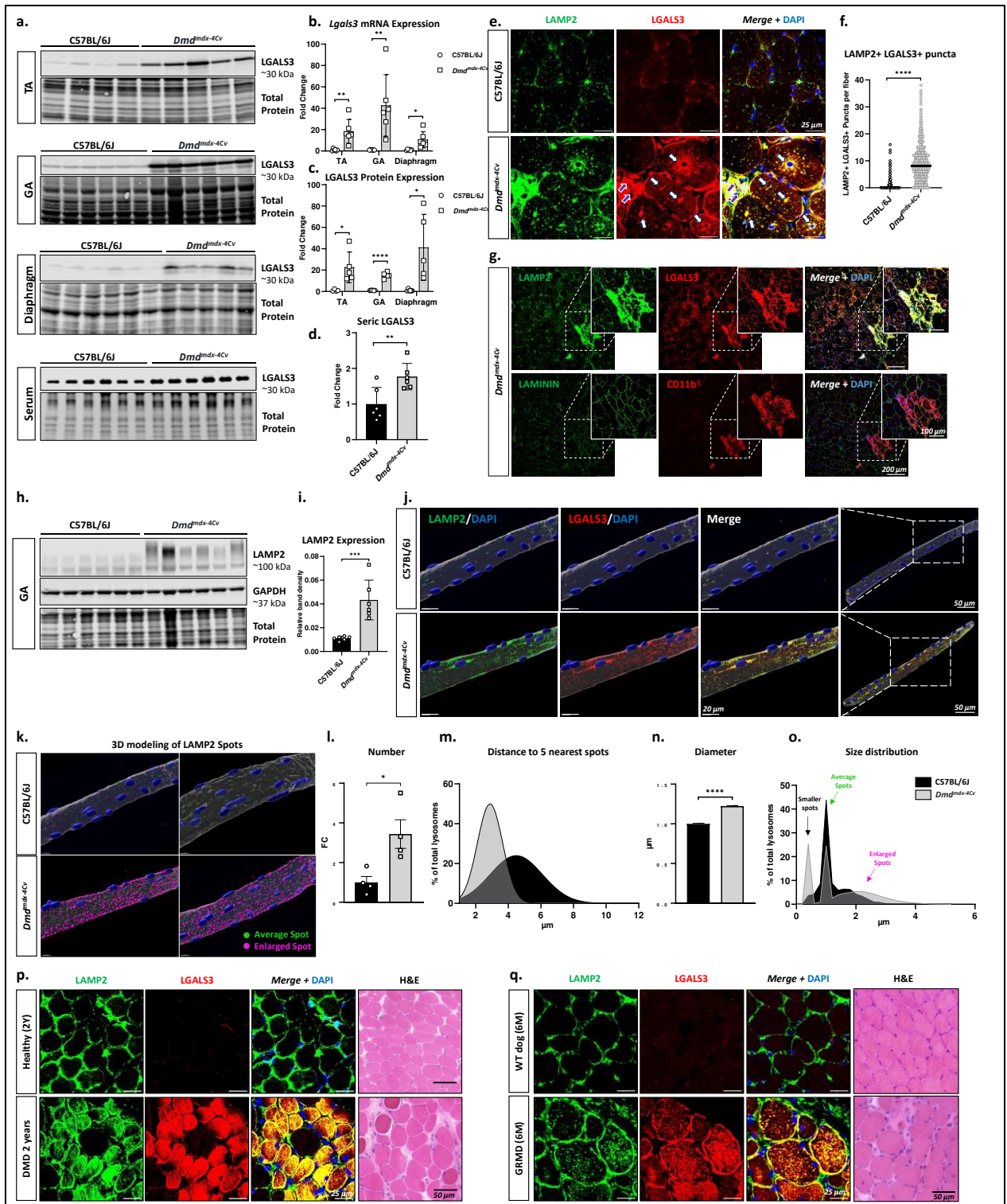
185 Collectively, these data indicate that LMP occurs in dystrophic muscle of *Dmd*<sup>mdx-4Cv</sup> as detected by  
186 LGALS3+LAMP2+ puncta quantification. Furthermore, various signs of lysosomal stress, including lysosome  
187 enlargement and increased number and density, were detected in the myofibers of dystrophic mice,  
188 further supporting the hypothesis of lysosomal dysfunction in the dystrophic muscle.

189 **Lysosome membrane permeabilization persist with age, and is a common feature across different**  
190 **muscular dystrophies and models:**

191 To address whether LMP is only an early process in dystrophic pathogenesis since only young mice were  
192 evaluated above, or a persistent feature with disease evolution, 1 year-old *Dmd*<sup>mdx-4Cv</sup> and control mice  
193 were also studied. An upregulation of *Lgals3* transcripts ( $FC=29$  for TA and 6.5 for GA) (**Figure S3a**), an  
194 overexpression of LGALS3 ( $FC=52$  for TA and 23 for GA) (**Figure S3b-c**), and a high number of  
195 LGALS3+LAMP2+ puncta (**Figure S3d-g**), were detected in both TA and GA muscle (Mean =10.7 and 9.1 in

196 *Dmd*<sup>mdx</sup> versus 3.9 and 3.1 in WT, for TA and GA respectively). Interestingly, older WT mice displayed more  
197 LMP compared to young WT mice, indicating a possible degradation of lysosomal function overtime.  
198 Overexpression of LGALS3 in muscle fibers was also confirmed on biopsies of DMD patients of different  
199 ages (2 years and almost 4 years) (**Figure 1o & S3h**) and of 6-month-old *golden retriever muscular*  
200 *dystrophy* (GRMD) dogs (**Figure 1p**), with all biopsies showing a colocalization of LGALS3 and LAMP2 in the  
201 majority of myofibers of dystrophic muscles.

202



203  
 204 **Figure 1: LGALS3 overexpression in dystrophic muscle correlates with LMP and lysosomal stress. a)**  
 205 **Western blot analysis of TA, GA, Diaphragm muscles and serum samples of WT and *Dmd<sup>mdx-4Cv</sup>* 7 weeks-old**  
 206 **mice (n=4-6) for LGALS3. Total protein staining was used as loading control. b) Relative *Lgals3* mRNA**

207 expression in the TA, GA, and diaphragm, normalized to Rplp0. Scatter plots represent average  $\pm$  SD of Fold  
208 change compared to WT mice (n=6). **c)** Band intensity quantification of LGALS3 relative to total protein  
209 staining in TA, GA, and diaphragm muscles. Scatter plots show average  $\pm$  SD of Fold change compared to  
210 WT mice (n=4-6). **d)** Band intensity quantification of LGALS3 relative to total protein staining in serum. Data  
211 are represented as scatter plot of average  $\pm$  SD of fold change relative to WT mice (n=6). **e)** Representative  
212 confocal Images of TA muscle cross-sections immunostained for LAMP2 (green) and LGALS3 (red). White  
213 arrows indicate LAMP2+LGALS3+ puncta inside the myofibers, purple arrows indicate immune cells  
214 infiltration between the myofibers. **f)** Quantification of double positive puncta (LAMP2+LGALS3+) in the  
215 myofibers of TA muscles of WT and *Dmd*<sup>mdx-4Cv</sup> mice. Data are represented as scatter plots with median  
216 (>400 myofibers from n=6). **g)** Confocal images of serial transversal sections of TA muscles from *Dmd*<sup>mdx-4Cv</sup>  
217 mouse immunostained for LAMP2/LGALS3 and LAMININ/CD11b. Zoomed in images show inflammatory  
218 area of the dystrophic muscle. **h)** Western blot analysis of GA muscle for LAMP2 (n=6). **i)** Band density  
219 quantification of LAMP2 relative to GAPDH (n=6), represented as scatter plots (average  $\pm$  SD). **j)**  
220 Reconstructed 3D images of isolated myofibers from the flexor digitorum brevis (FDB) muscle of *Dmd*<sup>mdx-4Cv</sup>  
221 and WT mice, immunostained for LAMP2 and LGALS3. **k)** 3D modeling of LAMP2 spots in single myofibers.  
222 Green spots show average sized lysosome (diameter <1.5  $\mu$ m) and purple spots show enlarged lysosomes  
223 (diameter >1.5  $\mu$ m). **l)** Analysis of number of lysosomes per myofiber (n=4) (average  $\pm$  SD of Fold-Change  
224 are represented). **m)** Analysis of 5 nearest spots to each spot, represented as density plot (with non-linear  
225 fit gaussian curve applied). **n)** Quantification of LAMP2 spots diameter (average + SEM). **o)** Density plot  
226 showing distribution of LAMP2 spots diameter. **p-q)** Representative confocal images of transversal sections  
227 from muscles of a DMD patient and a healthy control (**p**), and a GRMD dog and a WT control (**q**),  
228 immunostained for LAMP2 and LGALS3. Left panels show H&E labeling from the same muscle biopsies. An  
229 unpaired two-tailed t.test was used for statistical comparisons of WT and *Dmd*<sup>mdx-4Cv</sup> groups. T.test p-value  
230 \**p* < 0.05, \*\**p*<0.01, \*\*\*\**p*<0.0001.

231  
232 To evaluate if lysosomal degradation was a specific DMD feature, or whether it might be a common feature  
233 in muscular dystrophies, transversal GA muscle sections from a limb-girdle muscle dystrophy type R5  
234 (LGMDR5 or gamma-Sarcoglycanopathy) mouse model (*Sgcg*<sup>-/-</sup>) were immunostained for LAMP2 and  
235 LGALS3 (**Figure S4a**). A significant increase of LAMP2+LGALS3+ puncta was observed in *Sgcg*<sup>-/-</sup> muscle  
236 compared to WT control (mean = 8.3 vs 1.9 for control) (**Figure S4a-b**), indicating a substantial amount of

237 lysosomal damage. Additionally, a muscle biopsy from an LGMDR5 patient was analyzed. A positive pattern  
238 of LAMP2+/LGALS3+ staining was detected inside the myofibers, although to a lesser extent than DMD  
239 muscle, possibly correlating the level of lysosomal damage and the severity of the dystrophic phenotype.  
240 Taken together, these findings show that LMP, which can be detected with LGALS3 recruitment to the  
241 lysosomes, might be a common cellular perturbation in muscular dystrophies.

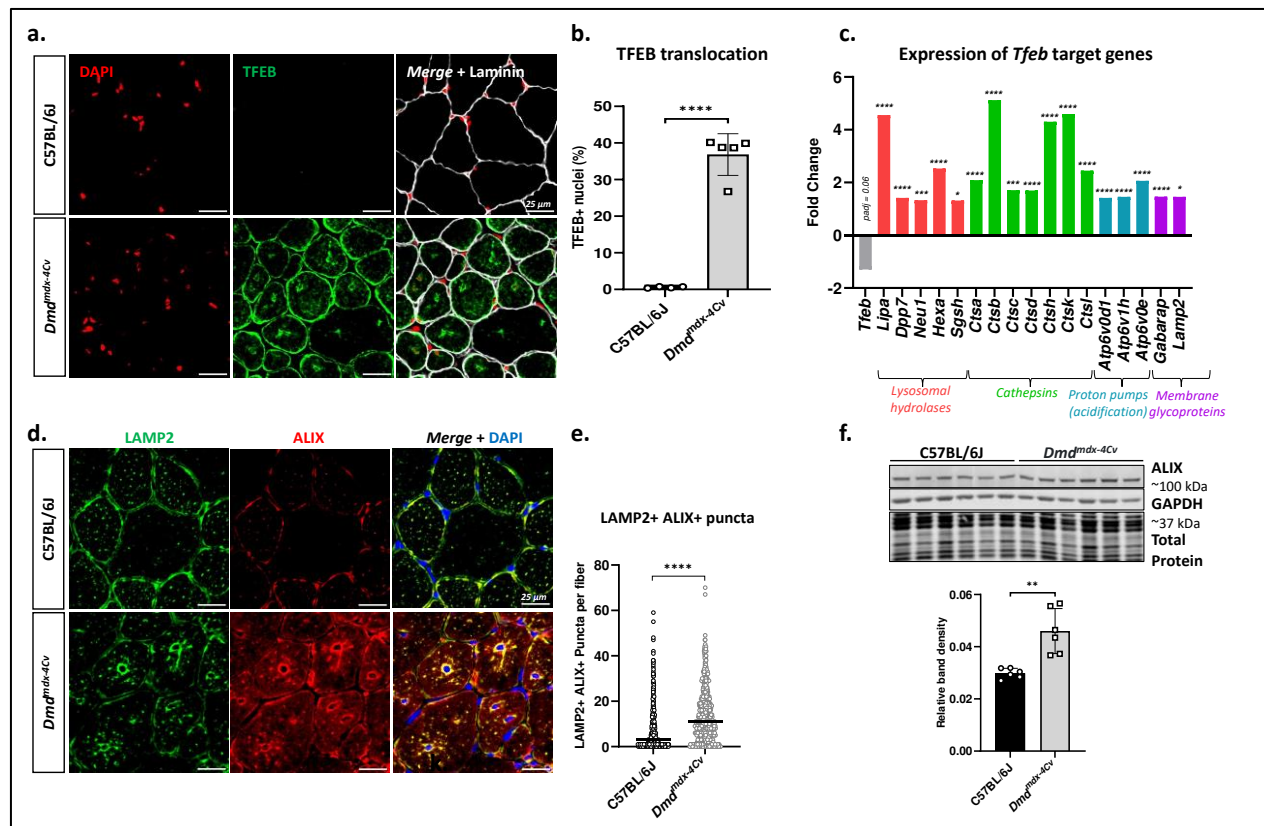
242 **Activation of the endolysosomal damage response in *Dmd*<sup>mdx-4Cv</sup> muscles:**

243 Lysosomal stress, characterized by LMP and increase of lysosome size, is an activator of the endolysosomal  
244 damage response, which is coordinated, among other proteins, by LGALS3 (Jia et al., 2020). In physiological  
245 conditions, this response includes lysosomal replacement, repair and removal. We sought out to  
246 investigate whether and to which extent this response is activated in the dystrophic muscle.

247 First, we evaluated the lysosomal biogenesis pathway, mediated by the master transcription factor EB  
248 (TFEB). For that, we performed an immunostaining TFEB on muscle cross-sections of 7-week-old *Dmd*<sup>mdx-</sup>  
249 <sup>4Cv</sup> mice and WT controls (**Figure 2a**). Interestingly, a nuclear localization of TFEB was observed more  
250 abundantly in dystrophic mice compared to control (**Figure 2a-b**), indicating a translocation of TFEB into  
251 the nuclei and hence an activation of the lysosomal biogenesis machinery. Bulk RNA sequencing was  
252 performed on GA muscle of 7-weeks old WT and *Dmd*<sup>mdx-4Cv</sup> mice and analyzed to determine the expression  
253 of genes involved in lysosome function and structure. An upregulation of various TFEB target genes was  
254 observed in *Dmd*<sup>mdx-4Cv</sup> mice compared to WT controls, that include lysosomal enzymes, cathepsins,  
255 protons pumps and lysosomal membrane glycoproteins (**Figure 2c**). Among the cathepsins we further  
256 immunodetected the overexpression in the TA muscle of *Dmd*<sup>mdx-4Cv</sup> mice of cathepsins B and D (*CTSB* and  
257 *CTSD*) (**Figure S5a**). While cathepsins overexpression in the dystrophic muscle had been previously shown,  
258 it remained mechanistically poorly understood (Kimura et al., 2024; Tjondrokoesoemo et al., 2016;  
259 Whitaker et al., 1983). Our data support that this upregulation may result from lysosomal stress activation

260 of the TFEB pathway (Jia et al., 2020; Settembre et al., 2011). In addition to overexpression, in WT muscle  
261 cathepsins B and D exhibited a punctate pattern co-localizing with LAMP2, confirming their confinement  
262 within the lysosomes, while in dystrophic muscle, a higher expression of CTSB and CTSD was detected,  
263 with a more diffuse pattern, only partially co-localizing with LAMP2. This observation suggests a leakage  
264 of cathepsins from the lysosomal lumen, a hallmark of LMP, which can have a detrimental effect on cell  
265 homeostasis by promoting protein degradation, cellular damage, inflammation, and cell death (Xie et al.,  
266 2023).

267 Second, we evaluated the *Endosomal Sorting Complex Required for Transport* (ESCRT)-mediated lysosome  
268 repair, which is responsible for the quick repair of acute lysosomal leakages (Skowyra et al., 2018). Upon  
269 LMP, several subunits of the ESCRT complex are recruited to the lysosomal membrane in a Ca<sup>2+</sup> dependent  
270 manner (Radulovic et al., 2018; Skowyra et al., 2018). Two of the recruited subunits are ALIX (ALG-2-  
271 Interacting Protein X or *Programmed Cell Death 6 Interacting Protein* - PDCD6IP) and the *Charged*  
272 *Multivesicular Body protein 4B* (CHMP4B). To evaluate this pathway, we performed an immunostaining of  
273 ALIX and LAMP2 on TA cross-sections (**Figure 2d**). A significant accumulation of ALIX puncta in *Dmd*<sup>*mdx-4Cv*</sup>  
274 mice, co-localizing with LAMP2, was detected (mean =13.9 and 6.8 for *Dmd*<sup>*mdx-4Cv*</sup> and WT respectively)  
275 (**Figure 2e**). An overexpression of ALIX protein was also detected in WB in TA muscles (**Figure 2f**). In  
276 addition, an increased colocalization of LAMP2 and CHMP4B was observed on TA muscle cross-sections  
277 compared to WT (**Figure S5c-d**), even though no overexpression of CHMP4B was detected at the protein  
278 level (**Figure S5e**). Together, these results suggest that lysosomal repair is active in the dystrophic muscle,  
279 through recruitment of the ESCRT complex.

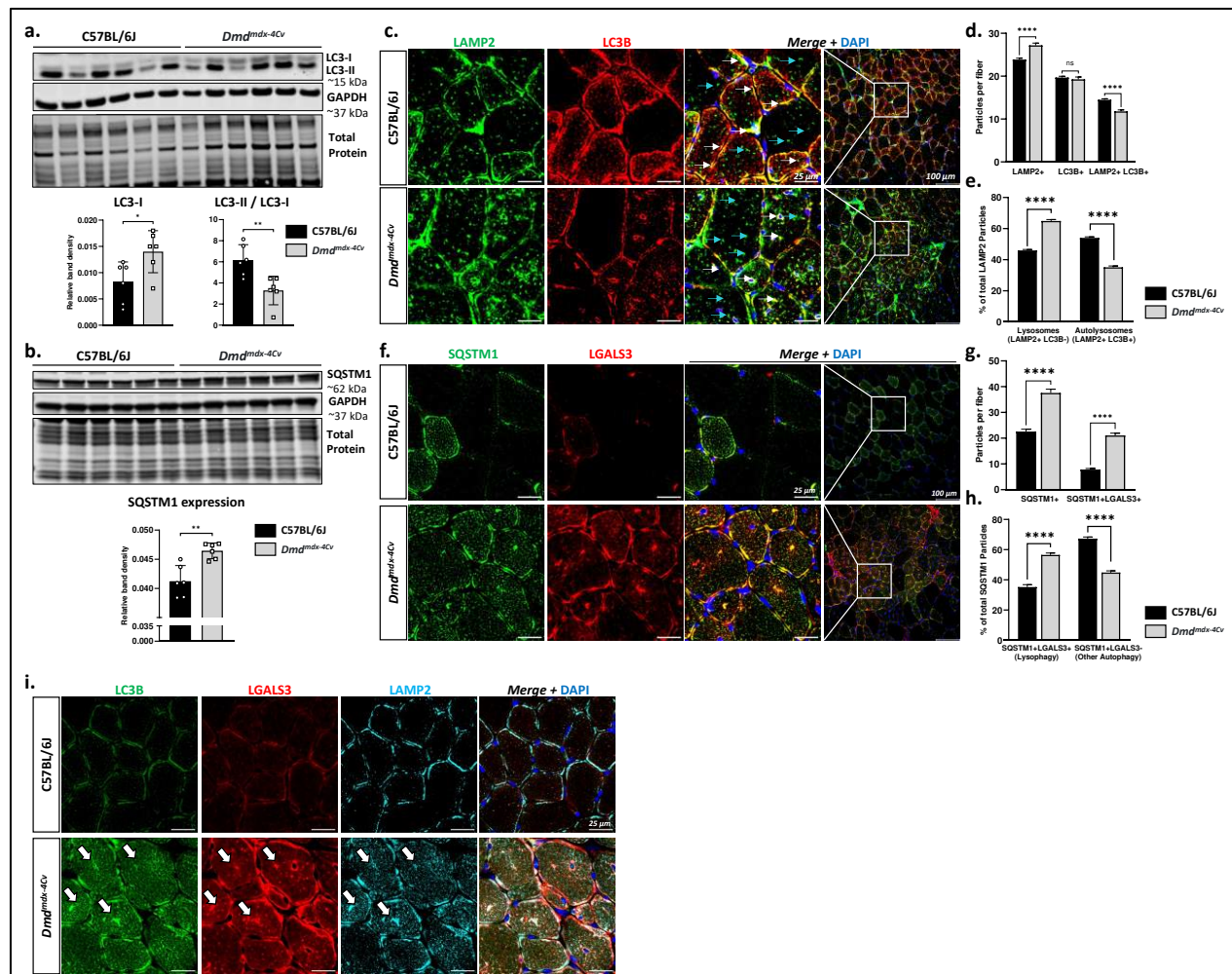


280  
 281 **Figure 2. Activation of lysosomal biogenesis and repair pathways in Dmd<sup>mdx-4Cv</sup> mice.** **a)** Confocal images  
 282 of serial transversal sections of GA muscle immunostained for TFEB and laminin. **b)** Quantification of TFEB  
 283 positive nuclei (n=5). **c)** RNA sequencing analysis of GA muscle from 7-weeks old Dmd<sup>mdx-4Cv</sup> and control  
 284 mice, displaying the expression of certain genes under the control of TFEB. Data are presented as fold  
 285 change to WT controls (n=5). **d)** Representative confocal images of TA transversal sections immunostained  
 286 for ALIX and LAMP2. **e)** Quantification of LAMP2+ ALIX+ positive puncta per myofiber. Data are presented  
 287 scatter plots with median (>692 myofibers analyzed from n=6). **f)** Western blot of TA muscle for ALIX, and  
 288 band density quantification of ALIX relative to GAPDH (n=6), represented as scatter plots (average ± SD).  
 289 An unpaired two-tailed t.test was used for statistical comparisons of WT and Dmd<sup>mdx-4Cv</sup> groups. T.test p-  
 290 value \*p < 0.05, \*\*\*p<0.001 \*\*\*\*p<0.0001.

291  
 292 Third, we aimed at evaluating lysophagy, which is the selective autophagy of damaged lysosomes where  
 293 they are selectively captured by autophagosomes and subsequently degraded after fusion with intact  
 294 lysosomes. As lysophagy is dependent on overall autophagic flux, we first aimed at assessing the general

295 autophagy process. Whereas defects in autophagy have been previously reported in DMD, with a main  
296 role attributed to mTOR hyper-signaling (De Palma et al., 2012; Pal et al., 2014; You et al., 2024), no  
297 correlation with impaired lysosome function or structure was described. We performed a western blot on  
298 the TA for the *Microtubule Associated Protein 1 Light Chain 3 Beta* (MAP1LC3B or LC3B). An increase of  
299 LC3-I in the *Dmd<sup>mdx-4Cv</sup>* muscle (FC=1.7) was observed. However, the ratio between the lipidated form (LC3-  
300 II), generated during the autophagosome formation and representing active autophagy, and the non-  
301 lipidated LC3-I, was significantly reduced in *Dmd<sup>mdx-4Cv</sup>* muscles (FC=-1.9) (**Figure 3a**). This correlated with  
302 the increase of *Sequestosome 1* expression (SQSTM1 or p62) (**Figure 3b**), an autophagy substrate cargo  
303 protein known to be integrated into the autophagosomes and degraded during autophagy. These results  
304 confirmed a previous report in the mdx model (De Palma et al., 2012) and support the hypothesis of a  
305 decrease of the autophagic flux in the dystrophic muscle. To better understand the autophagy defects in  
306 dystrophic muscle, we performed an immunostaining of LAMP2 and LC3B on TA cross-sections (**Figure 3c**).  
307 A co-localization of LAMP2 and LC3B was notably detected around the nuclei in both WT and *Dmd<sup>mdx-4Cv</sup>*  
308 muscles, indicating lysosome-autophagosome fusion (Li et al., 2016; Yim & Mizushima, 2020). Analyses of  
309 LAMP2 and LC3B particles showed an increase of LAMP2+ (mean = 27 for *Dmd<sup>mdx-4Cv</sup>* vs 23.9 for WT) but  
310 not of LC3B+ particles (mean = 19.3 for *Dmd<sup>mdx-4Cv</sup>* vs 19.7 for WT, non-significant difference) in *Dmd<sup>mdx-4Cv</sup>*  
311 muscle compared to WT (**Figure 3d**). However, the number of LAMP2+LC3B+ particles, representing  
312 autolysosomes, was significantly decreased in *Dmd<sup>mdx-4Cv</sup>* muscle compared to WT (mean = 12.8 for *Dmd<sup>mdx-</sup>*  
313 *4Cv* vs 17.1 for WT). This analysis confirmed an increase of lysosomes (LAMP2+ LC3B- particles) ratio in the  
314 *Dmd<sup>mdx-4Cv</sup>* muscle compared to WT control (65% for *Dmd<sup>mdx-4Cv</sup>* vs 46% for WT) (**Figure 3e**), and a decrease  
315 of autolysosomes (LAMP2+ LC3B+ particles) ratio (35% for *Dmd<sup>mdx-4Cv</sup>* vs 54% for WT), which suggests a  
316 defect in lysosome-autophagosome fusion in the *Dmd<sup>mdx-4Cv</sup>* muscle. Moreover, to assess lysophagy  
317 specifically, we performed a co-immunostaining of SQSTM1 (labeling the autophagosomes (Pankiv et al.,  
318 2007)) and LGALS3 (labeling the damaged lysosomes) (**Figure 3f**). The increase of SQSTM1+ (mean= 37.6

319 for *Dmd*<sup>mdx-4Cv</sup> vs 22.6 for WT) and SQSTM1+LGALS3+ particles (mean= 21.1 for *Dmd*<sup>mdx-4Cv</sup> vs 7.8 for WT) in  
320 *Dmd*<sup>mdx-4Cv</sup> muscle indicated a significant activation of lysophagy (**Figure 3g**), and recruitment of the  
321 autophagic machinery to damaged lysosomes. Ratio analyses of total SQSTM1 particles (**Figure 3h**)  
322 confirmed an increase of lysophagy, represented by percentage of SQSTM1+LGALS3+ particles (55.2% for  
323 *Dmd*<sup>mdx-4Cv</sup> vs 32.8%), and a decrease of other autophagy-related pathways (percentage of  
324 SQSTM1+LGALS3-) in *Dmd*<sup>mdx-4Cv</sup> mice (44.8.% for *Dmd*<sup>mdx-4Cv</sup> vs 67.2%). Additionally, a co-immunostaining  
325 of LAMP2, LGALS3 and LC3B on TA cross-sections (**Figure 3i**) showed a colocalization of LAMP2 and LGALS3  
326 with the autophagosome marker LC3B, indicating an ongoing lysophagy process, where damaged  
327 lysosomes are sequestered by the double membrane of the autophagosome, before fusing with remaining  
328 intact lysosomes (Maejima et al., 2013; Yang & Tan, 2023). Taken together, these data confirm an  
329 autophagy perturbation in the dystrophic muscle of *Dmd*<sup>mdx-4Cv</sup> mice, and notably a defect in lysosome-  
330 autophagosome fusion. Since, the fusion of autophagosome-lysosome requires intact acidic lysosomes,  
331 the substantial number of damaged lysosomes and the recruitment of the autophagic machinery to these  
332 damaged lysosomes in the context of lysophagy might be contributing to the autophagy blockage.



333

334 **Figure 3. Autophagy and Lysophagy evaluation in *Dmd<sup>mdx-4Cv</sup>* muscle.** **a)** Western blot analysis of TA  
 335 muscle for LC3, GAPDH and total protein staining are used as loading controls. Graphs show band density  
 336 quantification of LC3-I and LC3-II/LC3-I ratio, normalized to GAPDH. Data are presented as scatter plots  
 337 (average  $\pm$  SD) (n=6). **b)** Western blot analysis of TA muscle for SQSTM1, with GAPDH and total protein  
 338 staining used as loading controls. Graph shows band density quantification of SQSTM1, normalized to  
 339 GAPDH (average  $\pm$  SD) **c)** Representative confocal images of TA transversal sections immunostained for  
 340 LAMP2 and LC3B. White arrowheads depict LAMP2+LC3B+ particles representing autolysosomes, and blue  
 341 arrowheads depict LAMP2+LC3B- particles representing lysosomes **d)** Bar plot (average + SEM) showing  
 342 quantification of LAMP2+, LC3B+ and LAMP2+LC3B+ particles in the myofibers (>1045 myofibers analyzed  
 343 from n=6 per group). **e)** Lysosomes and autolysosomes ratios were estimated by quantification of the  
 344 percentages of LAMP2+LC3B- (lysosomes) and LAMP2+LC3B+ (autolysosomes) particles of total LAMP2+  
 345 particles per myofiber **f)** Representative confocal images of TA transversal sections immunostained for

346 SQSTM1 (p62) and LGALS3. **g)** Bar plot (average + SEM) showing quantification of SQSTM1+ and  
347 SQSTM1+LGALS3+ particles from immunostaining of TA muscle (>552 myofibers analyzed from n=6). **h)**  
348 Ratios of active lysophagy and non-lysophagy related autophagy were estimated from the quantification  
349 of the percentages of SQSTM1+LGALS3+ (Lysophagy) and SQSTM1+LGALS3- (non-lysophagy autophagy)  
350 particles of total SQSTM1+ particles per myofiber. **i)** Representative confocal images of TA transversal  
351 sections immunostained for LC3B, LGALS3 and LAMP2. White arrowheads depict LAMP2+LC3B+LGALS3+  
352 representing damaged lysosomes sequestered by autophagosomes. An unpaired two-tailed t.test was used  
353 for statistical comparisons of WT and *Dmd*<sup>mdx-4Cv</sup> groups. T.test ns=non-significant, p-value \*p < 0.05,  
354 \*\*p<0.01, \*\*\*\*p<0.0001.

355

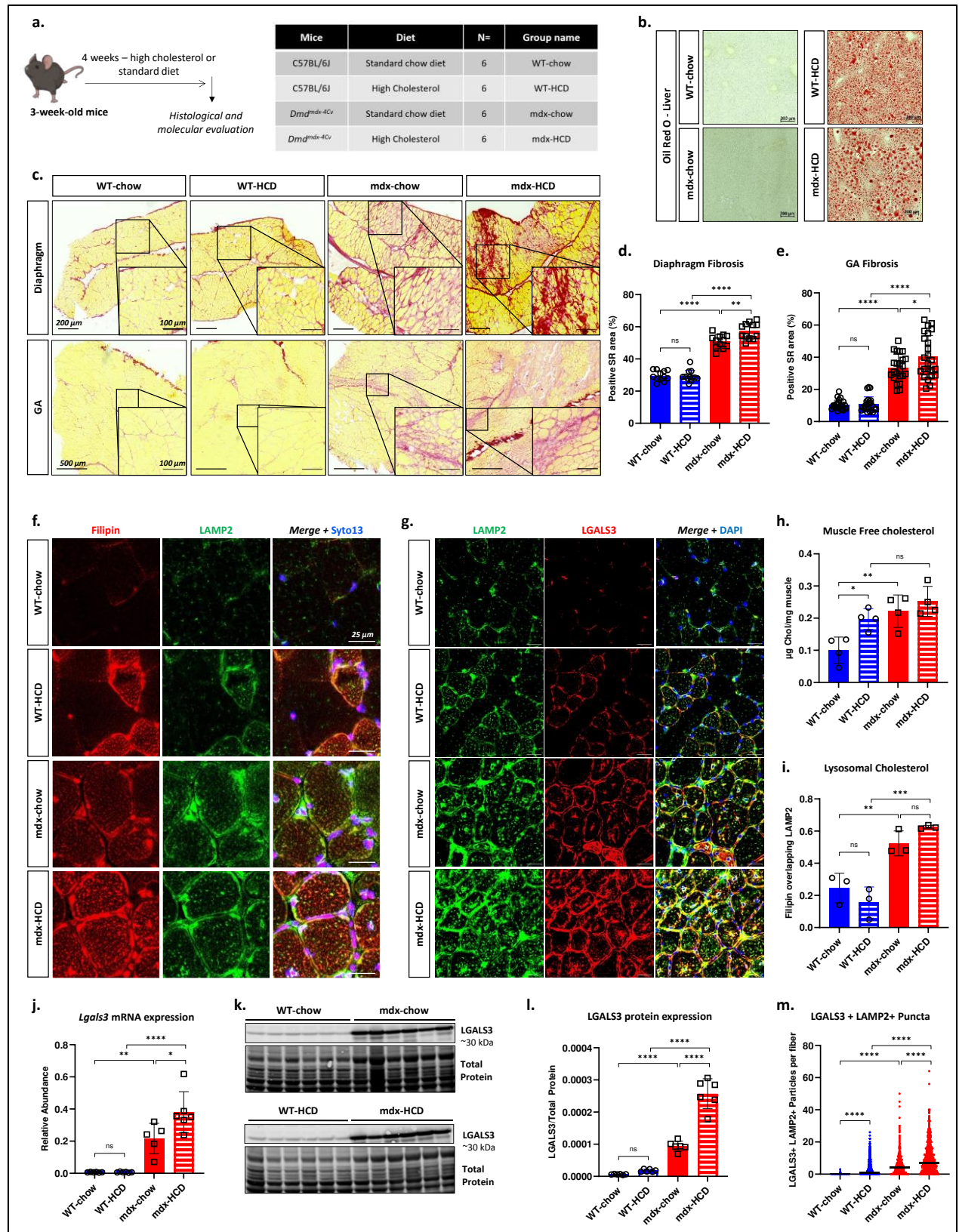
### 356 **Lipid perturbations in *Dmd*<sup>mdx-4Cv</sup> mice correlate with damaged lysosomal system:**

357 We have previously shown perturbation of lipid metabolism, and especially accumulation of cholesterol in  
358 the dystrophic myofiber in DMD (Amor et al., 2021); but the consequences of these perturbations and  
359 their contribution to disease pathogenesis, including in relationship to lysosomal dysfunction, remained  
360 elusive. To further clarify the nature of these lipid perturbations, we evaluated muscle biopsies of young  
361 *Dmd*<sup>mdx-4Cv</sup> mice and a young DMD patient. Consistence with our previous study (Amor et al., 2021),  
362 significant accumulation of cholesterol was detected in the dystrophic muscle by filipin (free cholesterol)  
363 staining (**Figure S6a**). We additionally performed a lipidomic study in the GA muscle of young *Dmd*<sup>mdx-4Cv</sup>  
364 mice, which confirmed the cholesterol accumulation observed with filipin labelling (**Figure S6b-e**). Indeed,  
365 elevations of cholesterol, cholesterol esters and sphingomyelin were detected compared to WT mice  
366 (**Figure S6c-e**). Moreover, qPCR analysis in GA muscles of *Dmd*<sup>mdx-4Cv</sup> mice showed a dysregulation of major  
367 genes related to cholesterol homeostasis, such as HMG-CoA reductase (*Hmgcr*) involved in cholesterol  
368 synthesis, or the ATP-binding cassette transporter (*Abca1*) and apolipoprotein E (*ApoE*) involved in  
369 cholesterol efflux (**Figure S6f**). These data confirmed the perturbation of lipid metabolism and showed  
370 that cholesterol accumulation is an early process in DMD pathogenesis.

371 To better elucidate the effect of cholesterol accumulation on the pathogenesis of DMD, and its potential  
372 link with lysosomal damage, young WT and *Dmd*<sup>mdx-4Cv</sup> mice were fed with either a cholesterol-rich high-  
373 fat diet or normal diet for 4 weeks (**Figure 4a**). An oil red O staining confirmed lipid accumulation in the  
374 liver of WT and *Dmd*<sup>mdx-4Cv</sup> mice under the high-cholesterol diet (HCD) (**Figure 4b**), but the HCD did not  
375 affect the body weight of the mice or the weight of muscles, liver, or heart (**Figure S7a-b**). Next, we  
376 evaluated the effect of the diet on the severity of the dystrophic phenotype. For that, muscle fibrosis in  
377 the diaphragm and the GA was analyzed by Sirius red labeling (**Figure 4c**). Quantification of Sirius red  
378 positive area showed a significant increase in fibrosis in *Dmd*<sup>mdx-4Cv</sup> mice on HCD compared to dystrophic  
379 mice on a standard diet (**Figure 4d-e**). However, no significant difference in fibrosis was observed between  
380 WT mice on HCD or standard diet in both the diaphragm and the GA (**Figure 4c-e**). This suggests that excess  
381 cholesterol in the diet may contribute to the exacerbation of the dystrophic phenotype. Nevertheless, no  
382 increase in muscle inflammation or sarcolemma permeabilization was caused by the HCD, as shown with  
383 CD11b and IgG labeling on GA cross-sections (**Figure S7c-e**). Additionally, we quantified the free  
384 cholesterol in the GA muscle (**Figure 4h**). *Dmd*<sup>mdx-4Cv</sup> mice on standard diet displayed higher muscle  
385 cholesterol accumulation than WT controls ( $FC_{\text{mdx-chow}/\text{WT-chow}}=2.2$ ), as expected. Interestingly, the  
386 cholesterol load increased in WT mice on HCD ( $FC_{\text{WT-HCD}/\text{WT-chow}}=2$ ), suggesting an accumulation of muscle  
387 cholesterol even in WT muscle. However, co-labeling of filipin (free cholesterol) and LAMP2 (lysosome)  
388 showed no significant localization of cholesterol in the lysosomes of WT muscle, contrary to *Dmd*<sup>mdx-4Cv</sup>  
389 muscle (**Figure 4f**), where a colocalization of filipin and LAMP2 was detected (**Figure i**). These results  
390 showed that HCD increases muscle cholesterol in both healthy and dystrophic muscles, but this  
391 accumulation was detected inside the lysosome only in the *Dmd*<sup>mdx-4Cv</sup> mice, suggesting an interplay  
392 between cholesterol accumulation and lysosomal dysfunction in dystrophic muscle. To further explore this  
393 hypothesis, we evaluated LMP following HCD with an immunostaining of LGALS3 and LAMP2 in the GA  
394 muscle of WT and *Dmd*<sup>mdx-4Cv</sup>. An increase of LAMP2+LGALS3+ puncta was detected in *Dmd*<sup>mdx-4Cv</sup> mice on

395 HCD compared to the group on standard diet ( $FC_{\text{mdx-HCD/mdx-chow}}=1,8$ ) (**Figure 4g&m**), which correlated with  
396 an upregulation of *Lgals3* ( $FC_{\text{mdx-HCD/mdx-chow}}=1.75$ ) and protein expression ( $FC_{\text{mdx-HCD/mdx-chow}}=14.25$ ) (**Figure**  
397 **4j-l**). Interestingly, LAMP2+LGALS3+ spots were also detected in WT mice on HCD compared to the one on  
398 standard diet (mean = 3.2 and 0.1 for WT-HCD and WT-chow respectively), although these puncta were  
399 significantly less than those detected in the dystrophic muscle. Nonetheless, no significant increase of Gal-  
400 3 at the protein or mRNA level was observed in WT mice on HCD, suggesting that lysosomal damage may  
401 be minimal in WT mice on HCD. Taken together, these data indicate that excess cholesterol contributes to  
402 lysosomal damage in the muscle of both WT and dystrophic mice. However, the effect of the HCD on LMP  
403 is more significant in the dystrophic muscle, where lysosomal damage is already present and exacerbated  
404 further by cholesterol excess.

405

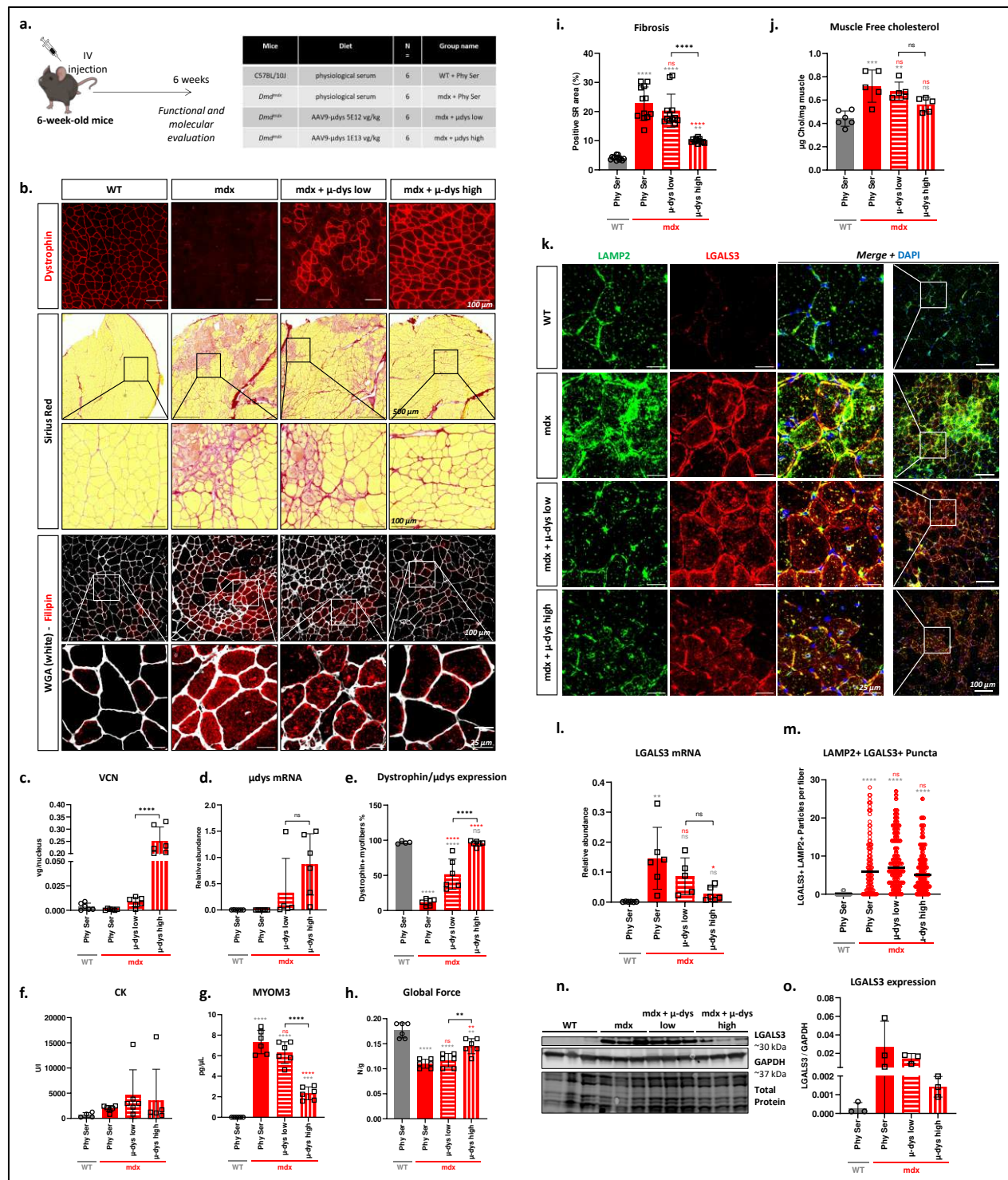


407 **Figure 4. Lipid perturbations in *Dmd*<sup>mdx-4Cv</sup> mice correlate with LMP.** **a)** Schematic representation of study  
408 set-up. 3-week-old WT and *Dmd*<sup>mdx-4Cv</sup> mice were fed with a standard chow diet or a high cholesterol/high  
409 fat diet for 4 weeks. **b)** Cross-sections of livers stained with Oil Red O, labeling non-polar lipids. **c)** Sirius red  
410 staining of diaphragm and GA muscles cross-sections. **d-e)** Quantification of fibrosis (Sirius red positive  
411 area) (n=12 for diaphragm, and n=24 for GA). **f)** Left Panel: representative confocal images of serial  
412 transversal sections of GA muscle labeled with filipin (Free cholesterol), Syto13 (nuclei) and immunostained  
413 with LAMP2 (green). Right Panel: Representative confocal images of transversal sections of GA muscle  
414 immunostained for LAMP2 (green) and LGALS3 (red). **g)** Scatter plot (average  $\pm$  SD) displaying free  
415 cholesterol quantification in whole GA muscle lysates (n=4). ANOVA p-value \*p<0.05 \*\*<0.01 ns=non-  
416 significant. **h)** Co-localization analysis of Filipin signal overlapping LAMP2 signals, represented as scatter  
417 plot (average  $\pm$  SD) of Manders' Overlap coefficient (MOC) (n=3). **i)** Relative *Lgals3* mRNA expression in the  
418 GA normalized to *Rplp0*. Scatter plots represent average  $\pm$  SD. **j)** Western blot analysis of GA muscles (n=6)  
419 for LGALS3. Total protein staining is used as loading control. **k)** Band intensity quantification of LGALS3  
420 relative to total protein staining. Data are represented as scatter plot of average  $\pm$  SD of fold change  
421 relative to WT mice (n=6). **m)** Quantification of double positive puncta (LAMP2+LGALS3+) in the myofibers  
422 of GA muscles. Data are represented as scatter plots with median (>784 myofibers analyzed from n=6). An  
423 ANOVA test with Tukey multiple comparison, or a Kruskal-Wallis with Dunn's multiple comparisons (when  
424 values didn't follow a normal distribution), were used for statistical comparisons. p-value \*p<0.05,  
425 \*\*p<0.05, \*\*\*p<0.001, \*\*\*\*p<0.0001, ns=non-significant.

426  
427 **Correction of LMP following gene therapy varies between the modality of gene therapy approaches in**  
428 **dystrophic models:**

429 Following the identification of LMP in DMD, we set out to evaluate the effect of a current therapeutic  
430 approach to correct these damages, namely  $\mu$ -dystrophin gene therapy. Six-week-old *Dmd*<sup>mdx</sup> mice were  
431 injected with an AAV9 viral vector encapsulating a  $\mu$ -dys coding sequence under the control of a muscle  
432 promoter (spc5.12), and the analyses were conducted 6 weeks later. Two vector doses were used, a  
433 suboptimal dose (low) and a higher dose (high) known to be effective in this model (Bourg et al., 2022)  
434 (**Figure 5a**). A dose effect was noticed in terms of vector transduction assessed by quantification of viral

435 copy number (VCN) (**Figure 5c**), transgene expression at the mRNA (**Figure 5d**) and protein levels (**Figure**  
436 **5b&e**), with the high dose transducing nearly all GA muscle fibers (~95% of positive myofibers) (**Figure**  
437 **5b&e**). Additionally, a partial normalization of circulating biomarkers, creatine kinase (CK) and myomesin  
438 3 fragments (MYOM3) was achieved, albeit not to WT levels (**Figure 5f-g**). A dose-dependent effect was  
439 observed in the reduction of fibrosis in the GA muscle, which was quantified from Sirius red labeling (**Figure**  
440 **5b&i**). Still, even with the high dose of  $\mu$ -dys, fibrotic area was not reduced to WT level in the GA muscle.  
441 Partial restoration of fibrosis correlated also with the rescue of global muscle force as evaluated with an  
442 escape test (**Figure 5h**). Indeed, the low dose did not increase muscle force compared to *Dmd*<sup>mdx</sup> controls,  
443 while the high dose resulted in a significant increase compared to non-treated mice, albeit not to WT level.  
444 Next, we investigated the correction of metabolic dysregulations. Labeling (**Figure 5b**) and quantification  
445 of free cholesterol (**Figure 5j**) were performed on GA muscles. An overcharge of free cholesterol was  
446 observed in *Dmd*<sup>mdx</sup>, as expected. Treatment with a low dose of AAV-microdystrophin resulted in a small  
447 but non-significant reduction in cholesterol. This reduction was greater with the high dose of AAV, where  
448 a non-significant difference from WT mice was obtained (**Figure 5j**). We then assessed the level of  
449 lysosomal damage following gene transfer. A 5.5-fold decrease of *Lgals3* mRNA expression in the GA was  
450 observed for mice treated with the high dose of  $\mu$ -dys ( $FC_{mdx-\mu-dys/mdx-Phy-ser} = -5.5$ ). A noticeable decrease of  
451 gal-3 at the protein level was also observed, but not to WT level. An immunostaining for LGALS3 and  
452 LAMP2 on GA cross-sections showed no reduction of LAMP2+LGALS+ puncta after treatment with low  
453 dose  $\mu$ -dys, and only a subtle decrease after treatment with high dose  $\mu$ -dys, compared with untreated  
454 mice (**Figure 5k&m**) (mean=7.8 for mdx versus 6.3 for mdx- $\mu$ -dys-high), indicating no or partial correction  
455 of LMP. These results suggests that treatment with a suboptimal dose of  $\mu$ -dys is not sufficient to correct  
456 lysosomal damage, and a high dose of  $\mu$ -dys can only reduce lysosomal damage but is still not sufficient  
457 for complete lysosomal correction. Following these results, we suspected that using  $\mu$ -dys, rather than full  
458 length dystrophin, may result in incomplete lysosomal correction.



459

460 **Figure 5.  $\mu$ -dystrophin gene therapy does not entirely correct lysosomal damage in *Dmdmdx* muscle. a)**  
 461 *Schematic representation of study set-up. 6-week-old *Dmdmdx* mice were injected intravenously with a rAAV*  
 462 *encapsulating a  $\mu$ -dystrophin encoding sequence under the control of *spc512* promoter, at 2 doses of 5e12*  
 463 *vg/kg (low dose) and 1e13 vg/kg (high dose). b) Histological characterization of GA muscle. Top panel:*

464 *Dystrophin staining of GA cross-sections (DYSB antibody recognizes N-terminal part of dystrophin). Middle*  
465 *Panel: Sirius Red labeling of GA cross-sections. Bottom panel: Filipin (free cholesterol) and Wheat Germ*  
466 *Agglutinin (WGA) (labeling of nuclear and sarcolemma membranes) labeling of GA cross-sections. c) Viral*  
467 *copy numbers (VCN) quantification in GA muscle. Data are presented as Scatter plot (average  $\pm$  SD) of*  
468 *relative abundance to Rplp0. d) Quantification of  $\mu$ -dys transcripts in GA muscle. Data are presented as*  
469 *Scatter plot (average  $\pm$  SD) of relative abundance to Rplp0. e) Quantification of dystrophin positive fibers*  
470 *in GA muscle (The antibody used, DYSB, recognize the N-terminal of the  $\mu$ -dys protein as well as the WT*  
471 *murine dystrophin). f) Dosage of CK in serum of mice 6-weeks post-injection. Data are presented as scatter*  
472 *plot (average  $\pm$  SD). g) ELISA quantification of MYOM3 in the serum of the mice 6-weeks post injection.*  
473 *Data are presented scatter plot (average  $\pm$  SD). h) Global force evaluation by an escape test before sacrifice*  
474 *of mice. Data are presented as scatter plot (average  $\pm$  SD) of global force normalized to mice body weight.*  
475 *i) Quantification of fibrosis in the GA (Sirius red positive area) (n=12). j) Scatter plot (average  $\pm$  SD)*  
476 *displaying free cholesterol quantification in whole GA muscle lysates (n=5). j) Quantification of fibrosis*  
477 *(Sirius red positive area) in GA muscle. k) Representative confocal images of transversal sections of GA*  
478 *muscle immunostained for LAMP2 (green) and LGALS3 (red). l) Relative Lgals3 mRNA expression in the GA*  
479 *normalized to Rplp0. Scatter plots represent average  $\pm$  SD. m) Quantification of double positive puncta*  
480 *(LAMP2+LGALS3+) in the myofibers of GA muscles. Data are represented as scatter plots with median. n)*  
481 *Western blot analysis of GA muscles (n=3) for LGALS3. GAPDH is used as loading control. o) Band intensity*  
482 *quantification of LGALS3 relative to GAPDH. Data are represented as scatter plot of average  $\pm$  SD (n=3). An*  
483 *ANOVA test with Tukey multiple comparison, or a Kruskal-Wallis with Dunn's multiple comparisons (when*  
484 *values didn't follow a normal distribution), were used for statistical comparisons. p-value \*p<0.05,*  
485 *\*\*p<0.05, \*\*\*p<0.001, \*\*\*\*p<0.0001, ns=non-significant. Grey Asterix represents relative comparison to*  
486 *'WT+Phy Ser' group, red Asterix represent comparison to 'mdx+Phy Ser' group.*

487

488 To investigate this hypothesis, we evaluated the effect of gene therapy on lysosomal correction in another  
489 model for muscular dystrophy, notably LGMDR5, which in terms of pathophysiology is close to DMD. Of  
490 note, the gene therapy in that case is through the transfer of the entire gene and this investigation will  
491 help to define whether lysosomal dysfunction could be fully restored when using a complete copy of the  
492 missing gene. Using the *Sgcg*<sup>-/-</sup> KO mouse model, we delivered a complete copy of the human gamma-

493 sarcoglycan gene and sought. *Sgcg*<sup>-/-</sup> KO mice were injected with a previously established optimal dose of  
494 2e13 vg/kg (Israeli et al., 2019), which transduced nearly all muscle fibers with the human copy of the  
495 SGCG protein (**Figure S8a-e**). Histological, molecular, and functional evaluation showed the efficacy of the  
496 treatment, with correction of circulating biomarkers (**Figure S8f-g**) and muscle force (**Figure S7h**).  
497 Expression of *Lgals3* was also restored to WT levels after gene transfer. Number of LAMP2+LGALS3+ in the  
498 GA was also greatly decreased upon gene transfer (**Figure S7j-k**) (median= 5 for *Sgcg*<sup>-/-</sup> + PBS versus 1 for  
499 *Sgcg*<sup>-/-</sup> + AAV). Importantly, overall correction of dystrophic features and LMP was more effective in this  
500 model than  $\mu$ -dys gene therapy in the *Dmd*<sup>mdx</sup> model.

501 Taken together, it appears that  $\mu$ -dys gene therapy can only partially correct the muscle lysosomal  
502 damage, even when all myofibers are expressing  $\mu$ -dys. This is of particular interest when compared to  
503 LGMDR5, where the transduction of all myofibers with the complete gamma-sarcoglycan protein is more  
504 effective at correcting LMP. It is therefore interesting to target specifically these damages in DMD, in  
505 combination with  $\mu$ -dys gene therapy, in order to achieve lysosomal correction and improve overall  
506 reversion of dystrophy, as seen in gene therapy for *Sgcg*<sup>-/-</sup> KO mice.

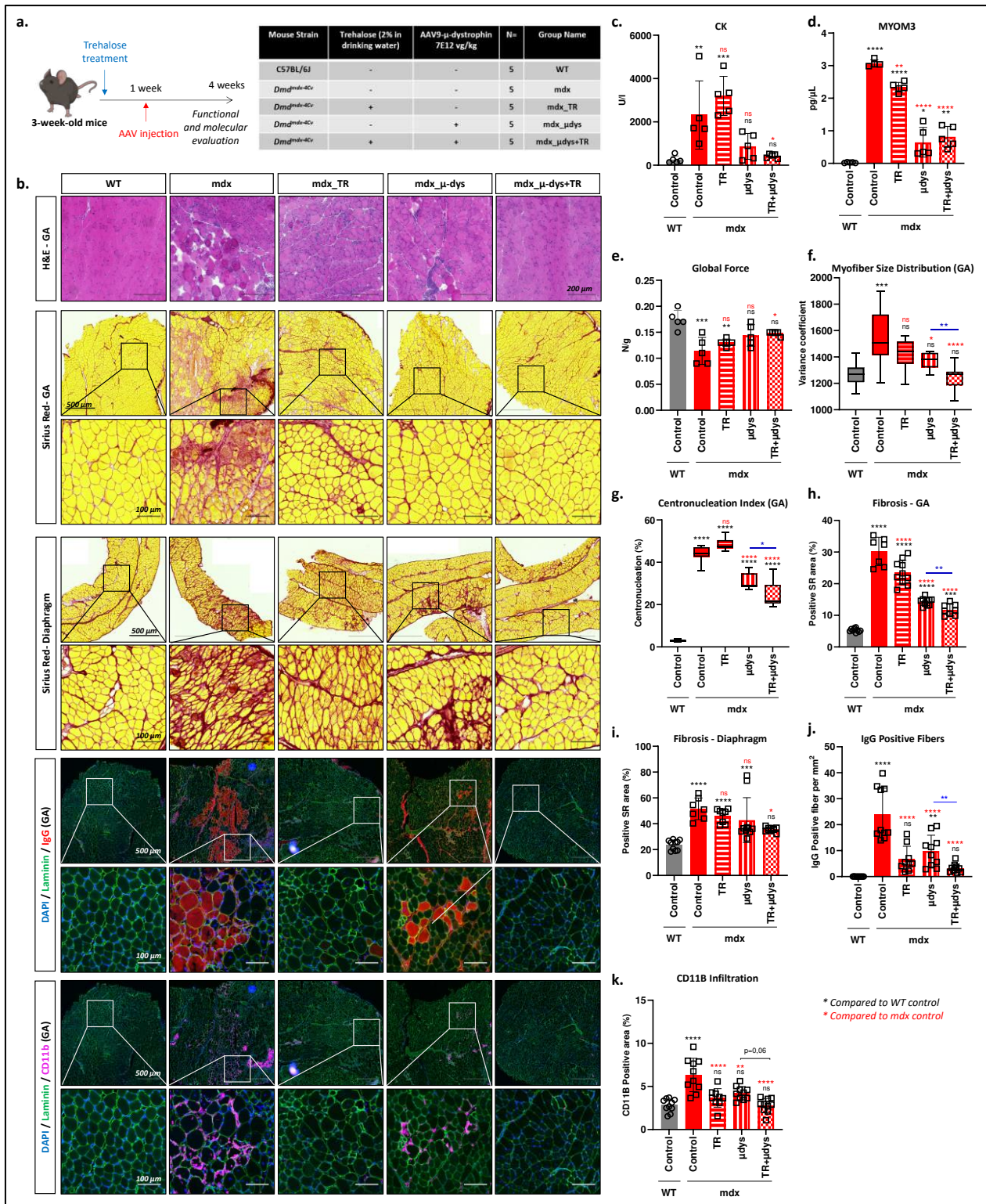
507 **Trehalose-mediated lysosomal correction improves  $\mu$ -dystrophin gene therapy at a suboptimal dose in**  
508 **a combined therapy setup:**

509 After the identification of lysosomal damage in the dystrophic muscle, and the insufficiency of the  $\mu$ -dys  
510 gene therapy alone to correct these damages, we designed a combined therapy setup where a suboptimal  
511 dose of rAAV- $\mu$ -dys would be administrated with a drug capable of alleviating lysosomal dysregulations.  
512 For that, trehalose, an FDA-approved dietary disaccharide was selected, as it has been shown to activate  
513 lysosomal biogenesis and alleviate lysosomal damage in various neurodegenerative diseases (Palmieri et  
514 al., 2017; Rusmini et al., 2019). Trehalose was administered alone (2% in drinking water) and in  
515 combination with a suboptimal dose of rAAV- $\mu$ -dys in *Dmd*<sup>mdx-4Cv</sup> mice. To this end, five groups of male

516 mice were included in this study (**Figure 6a**). Trehalose was diluted in the drinking water and administered  
517 from three weeks of age until the end of the study four weeks later. Recombinant AAV- $\mu$ -dys was injected  
518 intravenously (IV) one week after the beginning of treatment with trehalose. First, we assessed whether  
519 trehalose treatment affected muscle transduction or transgene expression. Quantification of VCN and  
520 mRNA transcripts in the GA and TA muscles showed no significant differences between the 2 groups  
521 injected with the vector with or without trehalose (**Figure S9a-b**). No significant difference was noticed in  
522 the number of dystrophin positive fibers as well (**Figure S9c-d**). Serum was collected at the end of the  
523 study before functional evaluation, and different circulating biomarkers were quantified. CK levels were  
524 decreased significantly compared to control *Dmd*<sup>mdx-4Cv</sup> reaching non-significant difference from WT mice  
525 only for mice treated with the combined therapy (FC<sub>mdx- $\mu$ -dys/mdx</sub>=-2.7, FC<sub>mdx- $\mu$ -dys+TR/mdx</sub>=-5.5) (**Figure 6c**).  
526 MYOM3 levels were significantly decreased with Trehalose treatment alone (FC<sub>mdx-TR/mdx</sub>=-1.3), but still not  
527 normalized to WT level even with the combined therapy (**Figure 6d**). As for the global muscle strength  
528 assessed by an escape test, a slight improvement in muscle strength compared to *Dmd*<sup>mdx-4Cv</sup> was observed  
529 in mice treated with trehalose alone or AAV-microdystrophin alone (**Figure 7e**), albeit not significantly  
530 (**Figure 6e**). Importantly, only mice treated with the combined therapy showed a significant improvement  
531 in muscle strength compared to the untreated *Dmd*<sup>mdx-4Cv</sup> mice and showed no longer a significantly  
532 different strength from the WT group (**Figure 6e**). We then performed a histological characterization,  
533 following the different treatments (**Figure 6b**). H&E staining of GA transversal section showed  
534 improvement of muscle histology for both trehalose and  $\mu$ -dys only treated mice compared to non-treated  
535 *Dmd*<sup>mdx-4Cv</sup> mice (**Figure 6b**). However, a better correction was achieved in the combined therapy group,  
536 where myofiber size distribution was best restored (**Figure 6f**), and the centronucleation index decreased  
537 (**Figure 6g**). Fibrosis was assessed by Sirius red labeling in the diaphragm and GA, which are among the  
538 most fibrotic muscles in this mouse model (**Figure 6b**). As for fibrosis in the GA, the trehalose treated mice  
539 showed a significant reduction, and the combined therapy group had a significantly lower fibrosis than the

540  $\mu$ -dys only treated group (**Figure 6b&h**). In the diaphragm, neither Trehalose nor  $\mu$ -dys treatments alone  
541 decreased fibrosis (**Figure 6b&i**). Only the combination of treatments reduced fibrosis significantly in this  
542 muscle. In addition, myofiber necrosis was evaluated in the GA by mouse IgG labeling (**Figure 6b&j**). A  
543 significant reduction of IgG positive myofibers was observed in both trehalose and  $\mu$ -dys treated mice,  
544 with a better correction in trehalose treated mice versus  $\mu$ -dys-only (non-significant difference from WT  
545 controls). The best correction was attained in the combined therapy group, where very few IgG positive  
546 myofibers were detected, indicating a better integrity of myofibers sarcolemma. CD11b staining was also  
547 performed to assess the inflammation level in the GA muscle (**Figure 6b**). A significant decrease of  
548 inflammatory areas was observed with both trehalose and  $\mu$ -dys treatments, with the combined therapy  
549 reaching the best correction (most significant decrease compared to non-treated *Dmd<sup>mdx-4Cv</sup>*).

550



551

552 **Figure 6. Trehalose treatment restore some dystrophic parameters and improve  $\mu$ -dystrophin gene**  
 553 **therapy in *Dmd*<sup>mdx-4Cv</sup> mice. a) Schematic representation of study set-up. *Dmd*<sup>mdx-4Cv</sup> mice were started on**

554 trehalose treatment (2% dilution in drinking water) at 3-weeks. For Group 4 and 5, mice were injected  
555 intravenously with a rAAV9 encapsulating the  $\mu$ -dys sequence at a  $7e12$  vg/kg dose. **b)** Histological  
556 characterization of muscles. Top panel: H&E labeling of GA muscle cross-sections. Middle Panel: Sirius red  
557 labeling of diaphragm and GA muscle cross-sections. Bottom Panel: Representative images of GA muscle  
558 serial cross sections immunostained for mouse immunoglobulin (IgG), laminin and CD11b. **c)** Dosage of CK  
559 in serum of mice before escape test. Data are presented as scatter plot (average  $\pm$  SD). **d)** ELISA  
560 quantification of MYOM3 in the serum of the mice before escape test. Data are presented scatter plot  
561 (average  $\pm$  SD). **e)** Global force evaluation by an escape test before sacrifice of mice. Data are presented as  
562 scatter plot (average  $\pm$  SD) of global force normalized to mice body weight (N/g). **f)** Analysis of myofiber  
563 size distribution in the GA muscle. Data presented as box plots (Median + minimum/maximum) show  
564 variance coefficient calculated as [standard deviation of the muscle fiber size/mean of muscle fiber  
565 size]\*1000. **g)** Centronucleation Index in the GA muscle. Data are presented as box plots (Median +  
566 minimum/maximum). **h-i)** Fibrosis analysis of GA and diaphragm, done by quantification of Sirius red  
567 positive area on transversal sections. Data are presented as scatter plots (average  $\pm$  SD). **j)** Quantification  
568 of permeabilized fibers positive for mouse IgG staining. Data are presented as scatter plot (average  $\pm$  SD)  
569 of number of positive fibers normalized to muscle cross-sectional area. **k)** Evaluation of CD11b+ cells  
570 infiltration in the muscle, done by quantifying CD11b area normalized to muscle cross-sectional area. Data  
571 are presented as a scatter plot (average  $\pm$  SD). An ANOVA test with Tukey multiple comparison was used  
572 for statistical comparisons (compared to WT control and mdx control). ANOVA p-value \* $p < 0.05$ , \*\* $p < 0.05$ ,  
573 \*\*\* $p < 0.001$ , \*\*\*\* $p < 0.0001$ , ns=non-significant. Black Asterix represents relative comparison to 'WT  
574 control' group, red Asterix represent comparison to 'mdx control' group. An unpaired two-tailed t.test was  
575 used for statistical comparisons between mdx- $\mu$ -dys and mdx- $\mu$ -dys+TR groups. T.test p-value \* $p < 0.05$ ,  
576 \*\* $p < 0.01$ .

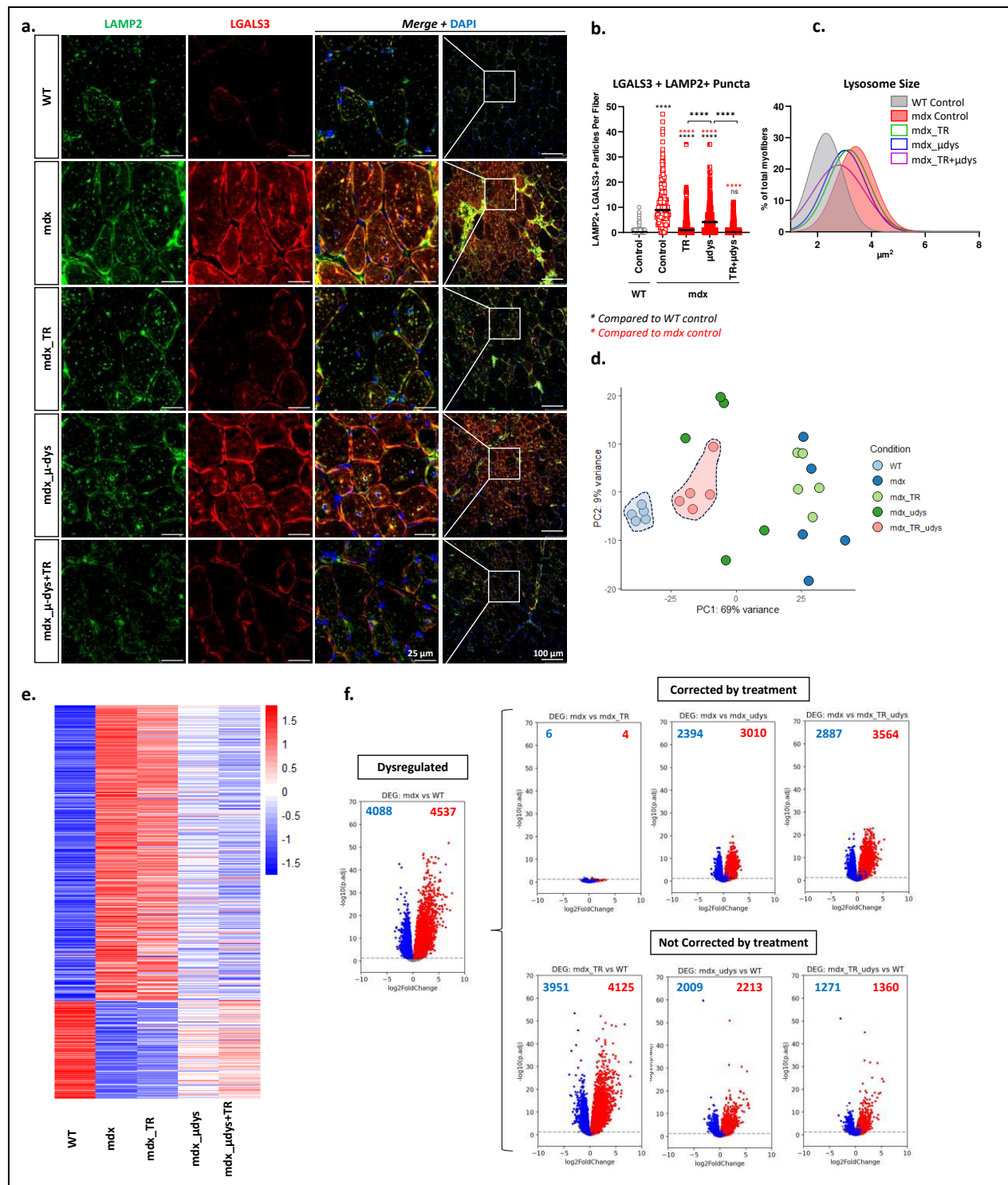
577

578 Following the demonstration of better outcomes with the combined treatment, we wanted to assess the  
579 effect of trehalose on lysosomal damage and dysregulated molecular pathways. To this end, we  
580 immunostained LAMP2 and LGALS3 on TA muscle transversal sections (**Figure 7a**). A clear increase in  
581 LAMP2+LGALS3+ puncta was detected in *Dmd*<sup>mdx-4cv</sup> muscle (mean = 10.4 and 0.5 for mdx and WT  
582 respectively), (**Figure 7b**). These puncta were decreased with  $\mu$ -dys treatment (mean = 4.7) but decreased

583 more significantly with the trehalose treatment (mean = 2.3). A correction to WT level was only achieved  
584 for the group with the combined therapy (mean = 1.1) (**Figure 7b**). Analyses of lysosomal enlargement  
585 were also done from LAMP2 immunostaining (**Figure 7c**). A clear enlargement was observed in *Dmd*<sup>mdx-4Cv</sup>  
586 muscle compared to WT, as seen on the density plot. Lysosomal size was significantly reduced with  $\mu$ -dys  
587 or trehalose treatments. Nevertheless, the best correction was also best obtained in the mice treated by  
588 the combined therapy.

589 To assess the effects of different treatments on the reversion of transcriptomic perturbations in the  
590 dystrophic muscle, we performed analysis of bulk RNA-sequencing on the GA muscles. On the first two  
591 principal components (PCs) of the PCA (**Figure 7d**), the group treated with trehalose clustered around the  
592 untreated *Dmd*<sup>mdx-4Cv</sup> group, and the group treated only with  $\mu$ -dys were widely distributed on the PCA.  
593 Importantly, only the group treated with  $\mu$ -dys+Trehalose was tightly clustered close to the WT group.  
594 Next, we investigated the evolution of all differentially expressed genes found in *Dmd*<sup>mdx-4Cv</sup> untreated  
595 group (DEGs, comparison: untreated *Dmd*<sup>mdx-4Cv</sup> versus WT, padj<0.05) upon different treatments (**Figure**  
596 **7e-f**). Similar to PCA, heatmap of the total 8625 DEGs showed comparable profiles between the trehalose  
597 treated and untreated *Dmd*<sup>mdx-4Cv</sup> group while  $\mu$ -dys-alone treatment shifted the heatmap signature closer  
598 to WT (**Figure 7e**). Strikingly, the closest profile to WT was achieved with the combined therapy. Among  
599 the 4088 downregulated and 4537 upregulated DEGs identified in *Dmd*<sup>mdx-4Cv</sup> muscle, only 6 (0.15%)  
600 upregulated and 4 (0.08%) downregulated DEGs were restored by trehalose, while  $\mu$ -dys alone restored  
601 2394 (58.5%) upregulated and 3010 (66.3%) downregulated DEGs. Importantly, the combination of  
602 trehalose and  $\mu$ -dys restored 2887 (70%) downregulated and 3564 (78.5%) upregulated DEGs. In addition,  
603 expression of more genes was partially or completely normalized by the treatment of  $\mu$ -dys+trehalose  
604 compared to  $\mu$ -dys alone. A total number of 2009 downregulated and 2213 upregulated DEGs were  
605 incompletely restored with  $\mu$ -dys, compared to 1271 downregulated and 1360 upregulated DEGs for  $\mu$ -  
606 dys+trehalose. We also performed gene set enrichment analysis (GSEA) to evaluate the correction of

607 known dysregulated pathways in the dystrophic muscle, such as inflammatory response, calcium signaling,  
608 nitrogen species metabolic process  
609



610

611 **Figure 7. Trehalose treatment corrects lysosomal damage and improve transcriptome correction with  $\mu$ -**  
 612 **dys. a)** Representative confocal Images of transversal sections of TA muscle immunostained for LAMP2  
 613 (green) and LGALS3 (red). **b)** Quantification of double positive puncta (LAMP2+LGALS3+) in the myofibers

614 of TA muscle. Data are represented as scatter plots with median ( $n > 538$ ). **c)** Density plot with non-linear fit  
615 gaussian curve applied, showing distribution of average spot size per myofiber ( $> 538$  myofibers analyzed  
616 from  $n = 5$ ). **d-f)** Comparison of global transcriptomic changes in GA muscle. **d)** Principal Component Analysis  
617 (PCA) plot using the expression level of 10000 genes with highest variance. Gene expression was first  
618 normalized by size factors and transformed by variance stabilizing transformation using the DESeq2  
619 RStudio package. **e)** Heatmap presenting the  $\log_2$  fold change ( $\log_2FC$ ) in comparison to WT muscle for all  
620 8625 DEG found in mdx muscle (compared to WT). The  $\log_2FC$  values are illustrated in row Z-scores, colored  
621 from blue to red, arranged from lowest to highest. **f)** Volcano plots of multiple comparisons illustrating  
622 transcriptomic changes before and after different treatments. As a reference, 4088 downregulated and  
623 4537 upregulated DEGs found in mdx control were colored blue and red, respectively, in all volcano plots.  
624 Among these DEGs, the number of DEGs found to be significantly different in each pair-wise comparison  
625 were labeled in the upper corners. Right upper panel shows volcano plots comparing mdx control to treated  
626 groups, in which DEGs are correctly restored after treatment. Right lower panel shows treated groups  
627 compared to WT control, in which significant DEGs are the genes that are not or incompletely restored  
628 after treatment. An ANOVA test with Tukey multiple comparison was used for statistical comparisons in (b)  
629 and (c). ANOVA  $p$ -value \*\*\*\* $p < 0.0001$ . Black Asterix represents relative comparison to 'WT control' group,  
630 red Asterix represent comparison to 'mdx control' group

631  
632 and apoptosis (**Figure S10a-b**). Metabolic pathways like cholesterol homeostasis, lipid storage, endocytosis  
633 and MTORC1 signaling (**Figure S10c**) were also evaluated. Strikingly, these pathways were all significantly  
634 closer to normal with the combined treatment of  $\mu$ -dys+Trehalose compared to  $\mu$ -dys alone. Taken  
635 together, these data suggest that combining trehalose and  $\mu$ -dys treatments significantly improve  
636 pathophysiology, lysosomal damage and transcriptomic dysregulation compared to suboptimal dosed  
637 gene therapy standalone treatment.

638

639 **DISCUSSION**

640 The prevailing dogma of DMD pathophysiology emphasizes the mechanical destabilization of the skeletal  
641 myofiber (Bez Batti Angulski et al., 2023; Duan et al., 2021). Accordingly, in the absence of dystrophin,  
642 skeletal myofibers are prone to contraction-induced damage, leading to sarcolemma disruption. Recently,  
643 however, there has been growing interest in the metabolic disturbances associated with DMD (Timpani et  
644 al., 2015), particularly mitochondrial dysfunction (Casati et al., 2024; Sanson et al., 2020; Timpani et al.,  
645 2015; Vu Hong et al., 2022). Additionally, several studies noted lysosomal perturbations in DMD (Gelman  
646 et al., 1981; Kominami et al., 1987; Pal et al., 2014; Sano et al., 1988), although the nature and  
647 consequences of these disturbances remained poorly understood. Interestingly, perturbations of lipid  
648 metabolism were also reported (Sun et al., 2023). Particularly, we and other have recently detected  
649 perturbations of cholesterol metabolism (Amor et al., 2021; Srivastava et al., 2017; White et al., 2021).  
650 Such disruptions of cholesterol metabolism are often linked with lysosomal damage, in both  
651 neurodegenerative and lysosomal storage diseases (Betuing et al., 2022; Kacher et al., 2022; Schulze &  
652 Sandhoff, 2011; Udayar et al., 2022; Whyte et al., 2017). The lysosomal damage biomarker LGALS3 (Aits et  
653 al., 2015) has been found to be upregulated in the dystrophic muscle in the *Dmd<sup>mdx</sup>* mouse model (Marotta  
654 et al., 2009). This upregulation was initially attributed to invading inflammatory mononucleated cells (van  
655 Putten et al., 2012), because Gal-3 is highly expressed in inflammatory macrophages (Coulis et al., 2023).  
656 However, recent studies suggest the expression of Gal-3 in muscle fibers and its requirement for efficient  
657 muscle regeneration (Cerri et al., 2021). We therefore set in the present study to investigate the expression  
658 of LGALS3 in the dystrophic muscle and confirmed not only its upregulation but also its localization to the  
659 enlarged lysosome of dystrophic myofibers. This pattern was observed in both DMD animal models and  
660 patients, as well as in LGMDR5 mouse model and patients, indicating that lysosomal damage may be a  
661 common feature across different muscular dystrophies. We further validated and characterized lysosomal  
662 perturbations in dystrophic muscle, revealing increased number and size of lysosomes, activation of

663 endolysosomal damage response, including replacement, repair and removal of damaged lysosomes.  
664 These processes are coordinated not only by the upregulation of LGALS3 (Jia et al., 2020) but also by the  
665 nuclear translocation of the TFEB transcription factor (Settembre et al., 2011) and the upregulation of its  
666 lysosomal target genes, such as the cathepsins, which happen to be upregulated in the dystrophic muscle  
667 (Kimura et al., 2024; Sano et al., 1988; Tjondrokoesoemo et al., 2016; Whitaker et al., 1983). Additionally,  
668 we identified autophagy defects in the dystrophic muscle. Although previous studies have already  
669 reported autophagy defects in DMD, these were mainly attributed to mTOR hyperactivation (De Palma et  
670 al., 2012; Pal et al., 2014; You et al., 2024). We found that autophagy defects correlated with a reduced  
671 rate of autophagosome-lysosome fusion, as well as increased lysophagy. Of note, lysosomal perturbations  
672 in skeletal muscle have been more widely studied before in the context of glycogen storage type II  
673 (GSDII/Pompe) disease. Interestingly, GSDII muscle is characterized by a blockage of autophagic flux with  
674 an impaired autophagosome-lysosome fusion (Do et al., 2024), despite a drastic downregulation of mTOR  
675 signaling. This autophagic blockade in GSDII can be reversed by the overactivation of TFEB (Spampanato  
676 et al., 2013). This suggests that also in DMD the autophagic disruption may result not only from mTOR  
677 upregulation but also be secondary to lysosomal dysfunction, principally due to reduced autophagosome-  
678 lysosome fusion. Collectively, our data support a model where compromised autophagic flux in dystrophic  
679 DMD muscle results from a decreased availability of functional lysosomes, which should serve for  
680 autophagosome-lysosome fusion. This deficiency is partially mitigated by TFEB-induced lysosomal  
681 biogenesis. Additionally, we showed that lysophagy, aiming to remove compromised lysosomes, is highly  
682 activated in the dystrophic muscle. The upregulation of one selective form of autophagy, in this case  
683 lysophagy, could be limiting the capacity of other selective autophagy (Germain et al., 2024) .

684 To directly investigate the link between cholesterol accumulation and lysosomal damage, mice were fed a  
685 high-cholesterol diet (HCD). While increased cholesterol load in the skeletal muscle of HCD-fed mice were  
686 observed in both WT and dystrophic mice, abnormal cholesterol accumulation, lysosome damage and

687 fibrosis were significantly more pronounced in the muscle of the HCD-fed dystrophic mice compared to  
688 those fed a standard diet, and HCD-fed healthy control mice. This indicates a direct causative relationship  
689 in this DMD model between elevated cholesterol, lysosomal damage and the exacerbation of the  
690 dystrophic parameters.

691 We then set out to test the effect of gene therapy on muscle lysosomal damage. As expected, a dose  
692 response relationship was observed, with LMP, evaluated by the LGALS3+LAMP2+ puncta, decreasing as  
693 the injected dose of AAV  $\mu$ -dys increased. However, significant residual lysosomal damage persisted even  
694 in mice treated with a high dose of AAV  $\mu$ -dys, which transduces nearly 100 % of the myofibers. Strikingly,  
695 similar gene therapy treatment of the LGMDR5 model, with the full-length gamma sarcoglycan transgene  
696 (Israeli et al., 2019) resulted in nearly complete reversion of LMP, indicating highly efficient lysosomal  
697 correction by gene therapy in this model.

698 Trehalose was selected for the combined therapy setup due to its good safety profile and affordability as  
699 a dietary disaccharide (A. Chen & Gibney, 2023), and more importantly its previous testing in clinical trials  
700 for neurodegenerative disease (Pupyshev et al., 2022) and Oculopharyngeal muscular dystrophy (OPMD)  
701 (Argov et al., 2015; Davies et al., 2006). Additionally, recent studies have shown that trehalose promotes  
702 lysosomal biogenesis and autophagy (Rusmini et al., 2019). Our experimental design enabled a comparison  
703 between the administration of trehalose alone, a suboptimal dose of AAV- $\mu$ -dys alone, and their  
704 combination. Notably, trehalose alone demonstrated significant benefits, particularly in reversing LMP  
705 (LAMP2+LGALS3+ puncta) and reducing myofiber permeabilization and necrosis (IgG staining). This  
706 highlights the positive effect of trehalose on lysosomal dysfunction and suggests a direct association  
707 between lysosomal damage and myofiber necrosis. Importantly, the combination of  $\mu$ -dys gene therapy  
708 and trehalose yielded the best therapeutic results. In the GA muscle of treated mice, we observed  
709 correction of myofibers' size distribution, improvement in the centronucleation index, regression of  
710 fibrosis and inflammation, and significant improvement of global muscle force compared to untreated

711 dystrophic mice. Transcriptomic analysis of the GA muscle further supported the efficacy of the combined  
712 therapy, showing enhanced transcriptomic correction when  $\mu$ -dys was combined with trehalose compared  
713 to  $\mu$ -dystrophin treatment alone. Notably, the inclusion of trehalose in the combined therapy promoted  
714 transcriptomic normalization across various signaling pathways and biological processes, including  
715 immune/inflammatory response, calcium homeostasis, cell death pathways, lipid metabolism,  
716 endocytosis, and the mTOR pathway. It is however noteworthy that trehalose alone did not have a striking  
717 effect on transcriptomic correction, suggesting that it may be acting synergistically with  $\mu$ -dys in the  
718 combined therapy set-up. Additionally, in models of neurodegenerative diseases, trehalose has been  
719 shown to modulate the intestine microbiota, oxidative stress, and inflammation (Khalifeh et al., 2021), all  
720 which are dysregulated in DMD. Therefore, it is possible that the beneficial effects of trehalose observed  
721 in this study are mediated through one or more of these pathways in addition to its action on the  
722 endolysosomal system.

723 One intriguing observation in this study is the partial resolution of lysosomal damage achieved through  
724 the expression of the  $\mu$ -dys protein. This contrasts sharply with the high-level correction of lysosomal  
725 damage seen with gene therapy in the LGMDR5 model, where the expression of the complete gamma-  
726 sarcoglycan protein is achieved. This discrepancy is particularly notable given the pathophysiological  
727 similarities between these closely related muscular dystrophies. A key difference between the two gene  
728 therapies is the restoration of the full-length gamma-sarcoglycan protein in the LGMDR5 model, compared  
729 to the expression of a shorter, partially functional form of dystrophin ( $\mu$ -dys), which lack most of the  
730 spectrin-repeat rod domain, in the *Dmd*<sup>mdx</sup> model. This suggests that the missing portion of  $\mu$ -dys may play  
731 a crucial role in regulating lysosomal functions in skeletal myofibers.

732 In addition to DMD and LGMDR5, we have recently detected lysosomal damage in muscle biopsies from  
733 patients and animal models across a wide spectrum of muscle diseases (manuscript in preparation). This

734 may suggest that lysosomal damage is a previously underestimated but crucial pathological feature and  
735 potential therapeutic target in various muscle diseases.

736 In summary, our investigation highlights a previously overlooked critical role of lysosomal damage in the  
737 pathophysiology of DMD. In the *Dmd<sup>mdx</sup>* mouse model, this damage is only partially corrected by  $\mu$ -dys  
738 gene therapy. We demonstrate that this damage can be alleviated with trehalose, especially when used in  
739 combination with gene therapy to restore a functional form of dystrophin expression. The combination of  
740 the restoration of dystrophin expression and the correction of lysosomal damage may offer a new  
741 therapeutic perspective in DMD.

## 742 MATERIAL AND METHODS

### 743 Patients' biopsies:

744 Open muscle biopsies were obtained for diagnostic purposes from the quadriceps (patient 1) or the deltoid  
745 muscles (patients 2, 3, 4 and 5) (see biopsies' details in **Supplementary Table S1**). The muscle location was  
746 not available for patient six. All patients consented for usage of the biological samples for research  
747 purposes. The specimens were snap frozen in isopentane cooled in liquid nitrogen for histoenzymology  
748 and immunohistochemistry. Transversal cryosections were stained using standard histological and  
749 histoenzymological methods. Histologically normal muscles served as controls. The genetic confirmation  
750 was done by sanger sequencing.

751

### 752 Animal experimentation and tissue sampling

753 Wild-Type (WT) (C57BL/10J and C57BL/6J) mice, *Dmd<sup>mdx</sup>* (C57BL/10ScSn-Dmdmdx/J) and *Dmd<sup>mdx-4Cv</sup>*  
754 (B6Ros.Cg-Dmdmdx-4Cv/J) mice were supplied by Charles Rivers Laboratories, Miserey-France. Animals  
755 were housed in cages with regular 12-hour day/12-hour night cycles, in a specific-pathogen free (SPF)  
756 barrier facility and provided with water and food ad libitum. All animal experimentation procedures were

757 conducted according to French and European guidelines for the care and use of animals for experimental  
758 purposes. All procedures were approved by ethical committee CEEA-51 and the French Ministry of Higher  
759 Education, Research, and Innovation under APAFIS numbers #19736 (DAP2018-024-B) and #35896  
760 (DAP2022-004-C). Only male mice were used for our studies. The high-fat cholesterol-rich diet was  
761 supplied by SAFE (260HF diet supplemented with 20g cholesterol/kg). Trehalose was supplied by sigma  
762 (ref. T9449) in powder form and dissolved in the mice's drinking water at a 2% concentration, which was  
763 changed twice a week. For rAAV injections, 100  $\mu$ L of viral vectors diluted in saline solution were injected  
764 intravenously into the tails of the mice. For blood sampling, mice were anesthetized with isoflurane, or a  
765 mixture of ketamine (100mg/kg) / xylazine (10mg/kg), and blood was collected from the retro-orbital vein  
766 on dry capillaries and centrifuged at 10000 rpm for 10 minutes. Serum was then collected and stored at -  
767 80°C until analysis. Mice were sacrificed by cervical dislocation at the end of the studies, and tissues were  
768 either dissected, mounted transversely on corks and frozen in cooled isopentane, or frozen directly in  
769 liquid nitrogen. Samples were stored at -80°C until molecular and histological analyses.

#### 770 **Dogs' biopsies**

771 The dogs included in this study were housed and cared for according to current EU regulations. Muscle  
772 biopsies were sampled in the context of a project authorized by the the ethical committee ComEth ANSES-  
773 EnvA-UPEC (national registration number #16) under the approval number #11-01-11/06. Muscle biopsies  
774 from GRMD and WT littermates were surgically sampled from the tibialis cranialis muscle under general  
775 anesthesia (IV propofol induction, maintenance isoflurane in 100 % O<sub>2</sub>) with an adapted analgesia (IV  
776 morphine). The muscle biopsies were immediately snap-frozen in isopentane cooled in liquid nitrogen,  
777 and subsequently stored at -80°C until cryosectioning.

#### 778 **Functional Evaluation**

779 An escape test was performed to measure the overall muscular force of mice according to standard  
780 procedures. Briefly, mice were placed in a 30 cm-long tube with both ends open, and their tails, which  
781 were connected to a force transducer, were pinched to induce escape. The force exerted was then  
782 measured by the detector. The procedure was performed 5 times, and the average of the 5 measured  
783 forces was normalized to the mouse's weight.

#### 784 **Transgene constructs and rAAV production**

785 The  $\mu$ -dys construct has been previously described (Bourg et al., 2022). The  $\mu$ -dys coding sequence was  
786 inserted into a transcription cassette under the control of the muscle promoter Spc5.12, flanked by our  
787 optimized sequences of the inverted-terminal repeats (ITR) (referred to as ITR-GNT), and encapsulated in  
788 a serotype 9 AAV. The  $\gamma$ -sarcoglycan (*SGCG*) construct has been previously described (Israeli et al., 2019).  
789 The sequence of the human copy of *SGCG* was inserted into a transcription cassette under the control of  
790 the desmin muscle promoter, flanked by the WT ITR sequences (ITR-2), and encapsulated in a serotype  
791 AAV 9 vector.

792 All rAAV in our studies were produced in HEK 293-T cells using the triple transfection protocol. For that,  
793 HEK 293-T cells were grown in suspension (seeded at 0.25x10<sup>6</sup> cells/mL) under agitation (37°C, 5% CO<sub>2</sub>)  
794 in Freestyle F17 medium (Life technologies, ref. A13835-01), supplemented with GlutaMAX-I at 4nM (Life  
795 technologies, ref. 35050-038), Pluronic F-68 at 0.08% (Life technologies, ref. 24040-032) and Anti-clumping  
796 agent (Life technologies, ref. 01-0057AE). Three days after seeding, cells were transfected with three  
797 plasmids encoding adenovirus helper proteins (pAd Helper), AAV Rep and Cap proteins, and the transgene  
798 expression cassette flanked by ITRs. Three days after transfection, cells were harvested, chemically lysed,  
799 treated with benzonase (Millipore) and filtered. Viral capsids were purified by affinity chromatography,  
800 formulated in sterile PBS and stored at -80°C.

801 Titers of rAAV vector stocks were determined using real-time PCR (qPCR). Viral DNA was extracted using  
802 MagNA Pure 96 DNA and the NA small volume viral kit (Roche Diagnostics) according to the manufacturer's  
803 instructions. PCR was performed with Absolute ROX mix (Taqman, Thermo Fisher Scientific), using ITR-  
804 specific primers (List in Supplementary **Table S2**).

## 805 **Cell Culture**

806 Immortalized human myoblasts were generated from a healthy donor (C25 cell line) at the Myoline  
807 platform (Institut of Myology, Paris). Immortalized myoblasts were grown in skeletal muscle growth  
808 medium (Promocell, ref. C-23060), supplemented with a supplement mix (Promocell ref. C-39365), 15%  
809 fetal bovine serum (Gibco 10270-106), 1% GlutaMAX (Thermo Scientific, ref. 35050061) and 1%  
810 gentamycin (Life technologies, ref. 15750-037). For myotube generation, myoblasts were grown until  
811 confluency, and growth medium was then replaced by a differentiation medium (Promocell, ref. C-23061),  
812 and cells were differentiated for 6 to 7 days before read-outs.

813 For lysosomal injury assays, myoblasts were plated on a clear-bottomed microscopy dish (Ibidi, ref. 81158)  
814 (~60,000 cells/cm<sup>2</sup>) or in 6-well plates and differentiated into myotubes. Myotubes were then treated with  
815 a solution of L-Leucyl-L-leucine methyl ester (LLOMe) (Santacruz, ref. sc-285992) at a final concentration  
816 of 2.5 mM in the medium and incubated for the indicated time at 37°C, after which the medium was  
817 collected, and the cells were either pelleted and frozen at -80°C for western blotting or fixed for  
818 immunofluorescence assays.

819 For immunofluorescence, cells were briefly washed 2 times with HBSS buffer (Hanks' Balanced Salt  
820 Solution, calcium & magnesium, Gibco), fixed with 4% ice-cold paraformaldehyde (PFA) solution (Thermo  
821 Scientific, ref. 28906) for 15 min, then washed with PBS 3 times and permeabilized for 10 min with 0.25%  
822 Triton X-100 (Sigma). Immunofluorescence was performed according to protocol described below.

823 For LGALS3 measurement in the media, media was collected after LLOMe treatment and frozen at -80°C.  
824 An ELISA for human LGALS3 (Invitrogen, kit BMS279-4) was performed according to the manufacturer's  
825 instructions.

826 Dextran pH probing was performed as described before (Fernandez-Mosquera et al., 2019). Briefly,  
827 myotubes were loaded with a with mix of Dextran Tetramethylrhodamine (10 000 MW, Invitrogen D1817)  
828 and Dextran Oregon Green (10 000 MW, Invitrogen D7171) at a final concentration of 100 µg/mL and  
829 incubated for 6h at 37°C. Cells were then washed with HBSS and incubated overnight in fresh media  
830 (chasing of the dextran into the lysosomes). Later, LLOMe was diluted in the media at 2.5 mM  
831 concentration for 30 min, after which the cells were washed twice with HBSS, fixed in 4% ice-cold PFA and  
832 mounted in DAPI-Fluoromount-G (Southern Biotech, ref. 0100-20).

### 833 **Molecular Analysis:**

#### 834 **Viral genomes copy number quantification:**

835 Genomic DNA (gDNA) was extracted from frozen muscle and organ samples or sections. Briefly, samples  
836 (frozen muscle and tissue sections) were lysed using the Beadmill (FisherBrand) machine with RIPA  
837 solution (ThermoFisher Scientific, ref. 89901) for 40 seconds (speed =6 m/s), then centrifuged for 10  
838 minutes (2000g, 4°C). DNA was later extracted from the recovered supernatant with the NucleoMag  
839 Pathogen extraction kit (Macherey-Nagel, ref. 744210.4) using the KingFisher machine (ThermoFisher  
840 Scientific, ref. 5400640). DNA concentrations were quantified by Nanodrop (NanoDrop™ 8000) and stored  
841 at -20°C. For VCN analysis, multiplex channel reactions were performed with the digital droplet PCR  
842 (ddPCR) Probe system. Extracted DNA (50 ng) was used with the following PCR amplification  
843 conditions: initial denaturation at 95°C for 10 minutes, followed by 40 cycles of denaturation at 94°C for  
844 10 seconds, annealing at 60°C for 10 seconds, and transcript extension at 72°C for 1 minute and 30  
845 seconds. Following this, fluorescent dye stabilization was performed at 98°C for 10 minutes. VCN values

846 were calculated using the ratio with the *Rplp0* gene amplification. For this analysis, multiplex channels  
847 were analyzed, depending on the type/concentration of probe. Primers and probes that were used are  
848 listed in **Supplementary Table S2**. The analysis was performed using the Quantasoft analysis pro software.

#### 849 **RNA isolation and RT-qPCR**

850 Total RNA was extracted from frozen muscle samples or sections. 400µL of Nucleozol solution (Macherey-  
851 Nagel ref.740404) were added per sample, and the tissues were lysed using the BeadMill 24 (Fisherbrand)  
852 (6m/s – 40s). Next, 160µL of DNase/RNase free water were added, and the tubes were mixed vigorously  
853 and incubated at RT for 10 minutes. Samples were then centrifuged (1000g, 15min, 20°C) and total RNA  
854 was extracted from the supernatant using magnetic beads (Macherey-Nagel, Ref. 744503.12) with the  
855 Ideal-32 system (ID solutions). RNA samples were then treated with DNase (30min ,37°C) (TURBO DNA-  
856 free kit, ThermoFisher Scientific), and 1 µg of RNA per sample was used for reverse transcription reaction  
857 using the RevertAid H Minus First Strand cDNA synthesis kit (ThermoFisher Scientific, K1632) according to  
858 the manufacturer's instructions. The cDNA samples were then diluted (1:9) and analyzed by qPCR using a  
859 LightCycler 480° (Roche), with either SYBR Green PCR assays (ThermoFisher Scientific, ref.4309155) or  
860 taqman gene expression assays (ThermoFisher). The primer sequences used are shown in **Supplementary**  
861 **Table S2**. Each reaction was performed in duplicate, and the Ct values for *Rplp0* were used to normalize  
862 gene expression using Livak's secondary derivation method (Livak & Schmittgen, 2001).

#### 863 **Protein isolation and western blotting:**

864 Frozen tissues were cut using a cryostat into 10 µm sections, and lysed with RIPA lysis buffer (Thermofisher  
865 Scientific, Ref-89901) using the the Beadmill 24 (Fisherbrand) for 40 seconds at 6m/s. Samples were then  
866 centrifuged for 10 minutes (2000g, 4°C), after which the supernatant was collected and treated with  
867 DNase (1:1000, Millipore) and a protease inhibitor cocktail (Roche) for 45 minutes. Total protein  
868 concentration was measured using the Pierce® BCA Protein Assay kit (Thermo Fisher Scientific, ref. 23225).

869 Equal amounts of protein (between 20 and 30  $\mu\text{g}$ ) were loaded and separated on NuPAGE pre-cast gels  
870 (Thermo Fisher Scientific). Proteins were transferred to nitrocellulose membranes using the iBlot 2 Dry  
871 Blotting system (Thermo Fisher Scientific), and total protein quantification was performed using the Revert  
872 Total protein Stain kit (Li-Cor). Membranes were later incubated with a blocking solution (Odyssey Blocking  
873 Buffer, Li-Cor) for 1h at room temperature (RT). Primary antibodies incubation was done overnight at 4°C  
874 (dilutions and details of primary antibodies are presented in **Supplementary Table S3**). Membranes are  
875 then washed in a TTBS solution 3 times and incubated with secondary antibodies (1:10 000, Listed in  
876 **Supplementary Table S5**). Membranes are washed again with TTBS and scanned using the Odyssey CLx  
877 scanner (Li-Cor). Images were analyzed using Image Studio Lite (ver. 5.2), pixels of selected bands were  
878 quantified, and the signal was normalized to either reference protein (GAPDH) or to total protein staining.

#### 879 **Lipidomic analysis**

880 Muscle sections were weighted and lysed in PBS, then diluted to 5 mg/mL. Shotgun lipidomic analysis was  
881 performed by Lipotype (Dresden, Germany). This technique involves automated sample extraction,  
882 automated direct sample perfusion and high-resolution mass spectrometry to capture lipid class-specific  
883 internal standards. Briefly, lipid extraction was performed using chloroform and methanol (Surma et al.,  
884 2021). Samples were spiked with lipid class-specific internal standards prior to extraction. After drying and  
885 resuspension in the mass spectrometry acquisition mixture, the lipid extracts were subjected to mass  
886 spectrometry analysis. Mass spectra were acquired on a hybrid quadrupole/Orbitrap mass spectrometer  
887 equipped with an automated nano-flow electrospray ion source in positive and negative ion modes.  
888 LipotypeXplorer' software is used for lipid identification on mass spectra. Data processing and analysis are  
889 carried out using the Lipotype information and management system and the LipotypeZoom web software.

#### 890 **Quantification of free muscle cholesterol:**

891 Muscle sections were weighed (between 10-20 mg) then lysed using a mix of chloroform/Isopropanol/NP-  
892 40 (7 : 11 : 0.1) for 1 minute with the Beadmill 24 (Fisherbrand). Samples were then centrifuged at 15,000  
893 g for 10 minutes, and supernatants were transferred to new tubes, dried at 50°C and centrifuged under  
894 vacuum for 30 min. The pellet is then re-suspended in cholesterol quantification kit buffer (Invitrogen, ref.  
895 A12216) at a concentration of 20 µg/µL, and vortexed vigorously. Free cholesterol quantification was  
896 performed in duplicate using the Amplex Red Cholesterol kit (Invitrogen, ref. A12216), following the  
897 manufacturer's instructions. Cholesterol concentrations were normalized to tissue weight for each  
898 sample.

### 899 **RNA sequencing**

900 Essentially as described previously (Vu Hong, 2023), RNA was extracted from muscle sections, and purified  
901 RNA samples were first checked for RNA quality using the Bioanalyzer 2100 (Agilent). Samples with an RNA  
902 integrity index greater than 8 were then used for RNA sequencing (Genewiz). The Stranded Total RNA  
903 Library Prep Kit (Illumina) was used to create sequencing libraries, which were sequenced according to  
904 Illumina protocol on the NovaSeq instrument (Illumina), yielding around 20 million paired end reads per  
905 library. Paired reads were filtered and subjected to quality-control using fastp. They were then mapped  
906 onto the GRCm38/mm10 genome using HISAT2 and count tables generated using htseq-count  
907 Differentially expressed genes (DEGs) were identified using the DESeq2 R package. Pathway analysis was  
908 carried out in R-Studio (version 4.0.4) using either over-representation methods with Gene Ontology or  
909 functional class scoring with Gene Set Enrichment Analysis (GSEA). GSEA was performed using the  
910 *clusterprofile* R package.

### 911 **Serum biomarkers analyses:**

912 **Creatine kinase:** Quantification of creatine kinase (CK) in serum was performed using a FUJI DRI-Chem  
913 nx500 analyzer (DMV Imaging). 10 µL of diluted serum was deposited on FUJI DRI-CHEM CPK-PIII plates

914 (DMV Imaging, ref.15809463), and CK concentrations were automatically generated in international units  
915 per liter of serum (U/L).

916 **Myomesin-3 fragments:** Fragments of the myofibrillar structural protein myomesin-3 (MYOM3) have been  
917 identified as being abnormally present in the sera of dystrophic animal models (Rouillon et al., 2015). To  
918 quantify these fragments in mouse serum, a Meso Scale Discovery (MSD) enzyme-linked immunosorbent  
919 assay (ELISA) was performed. Anti-MYOM3 polyclonal capture antibody (Proteintech Lab, ref. 17692-1-AP)  
920 was coated to the wells of a multi-array plate containing electrodes (MSD, ref. L15XA-3) (overnight, 4°C).  
921 The plate was then washed 3 times with a washing solution (PBS + 0.05% Tween 20), and the wells were  
922 saturated with a 3% bovine serum albumin (BSA) solution (1h, RT). After 3 washes, diluted sera were added  
923 (1:50 dilution in 1% BSA solution) and the plate was incubated for 2 h at room temperature under rigorous  
924 agitation. A standard range of MYOM3 peptide was also used to calculate concentrations. Revelation was  
925 carried out using a mouse monoclonal antibody (Anti-51r20, developed by Proteogenix©) coupled to a  
926 sulfo-tag (Mesoscale, ref. R31AA-2). The plate was incubated for a further 2 hours under agitation, then  
927 washed 3 times. Finally, 150 µL of MSD-Gold reading buffer (MSD, ref. R92TG-2) was added and the  
928 electro-chemiluminescence was read using the MESO QuickPlex SQ 120 (MSD). MYOM3 concentrations  
929 were calculated using the MYOM3 standard range and expressed in pg/µL.

### 930 **Single Myofiber isolation and immunostaining**

931 The two Flexor Digitorum Brevis (FDB) muscles were surgically isolated from euthanized *Dmd<sup>mdx-4Cv</sup>* and  
932 C57BL/6J male mice (6 weeks old), rinsed in PBS and placed in a digestion solution (collagenase 2.5U/mL  
933 in DMEM, Sigma-Aldrich, United States, 11088793001) for 1h30 at 37°C on a rotated wheel. The  
934 collagenase solution was removed by fiber sedimentation (10 min, RT) and the isolated muscle fibers were  
935 transferred in 2 mL tube and fixed with an ice-cold 4% PFA solution for 20 minutes. Fixed myofibers were  
936 then washed 3 times with PBS (10 min – RT) and permeabilized with 0.5% Triton-X-100 (Sigma) for 10

937 minutes. Afterwards, 10% goat serum (GS) (Agilent, ref. X090710) was used for blocking (30 min – RT),  
938 before a second blocking with ‘mouse-on-mouse’ blocking solution (Invitrogen, ref. R37621). Primary  
939 antibodies (listed in **Supplementary table S4**) were incubated overnight at 4°C on an inclined agitator.  
940 Myofibers were then washed 3 times with a Tween-Tris-buffered saline (TTBS) solution (10 min – RT),  
941 before the incubation with secondary antibodies (Listed in **Supplementary Table S5**, 1:200 dilution).  
942 Finally, myofibers were washed 3 times with PBS and mounted on glass slides with a DAPI-Fluoromount-G  
943 mounting medium (Southern Biotech, ref. 0100-20).

944 Stack images were acquired with a LEICA TCS SP8 spectral confocal microscope (Leica, Germany) running  
945 LASX software (Leica, Germany), using a HC PL APO CS2 20X 0.75 NA dry objective. A stack image was taken  
946 every  $z=0.3\ \mu\text{m}$ , and 3D myofibers images were reconstructed using Imaris software (version 9.9.1). All  
947 myofibers images were treated similarly, and LAMP2 spot analyses was performed using spot modeling  
948 function (average spot diameter =  $1\ \mu\text{m}$ ).

#### 949 **Histological studies and image analyses:**

950 For all histological studies, muscles were dissected, fixed on corks and frozen in isopentane cooled in liquid  
951 nitrogen, then stored at  $-80^{\circ}\text{C}$ . Transverse cryosections ( $8\ \mu\text{m}$  thick) were prepared from frozen muscles,  
952 air-dried, and stored at  $-80^{\circ}\text{C}$ .

#### 953 **Histochemistry:**

954 **H&E staining** was carried out in accordance with standard procedures. This staining combines nuclear  
955 staining with hematoxylin and cytoplasmic staining with eosin. Analysis of myofiber size distribution and  
956 centronucleation index was performed as previously described in (Reinbigler et al., 2022).

957 **Oil Red O** staining identifies hydrophobic lipids in the liquid phase. The colored body, called Lysochrome,  
958 moves from the solvent in which it is found to the tissue lipid, and the lipid droplets are colored red and  
959 the nuclei blue.

960 **Sirius Red staining** was used to assess tissue fibrosis, combining red staining for collagen fibers with yellow  
961 staining for cytoplasm. Briefly, slides were treated with acetone for 1 hour, fixed in formalin for 5 minutes,  
962 then incubated in Bouin's solution for 10 minutes. Slides were then rinsed twice with water and stained in  
963 Sirius Red solution (Sigma, ref. 365548) (diluted in 0.1% picric acid) for 1 hour, washed with water and  
964 dehydrated with ethanol (70% 1 min, 95% 1 min, 100% for 2 min) and then cleared in a xylene bath (2  
965 washes for 1 min). Slides were mounted in mounting medium and air-dried.

966 All bright-field histological labeling images were digitized using an Axioscan Z1 slide scanner (Zeiss,  
967 Germany) under a Zeiss Plan-Apochromat 10X/0.45 M27 dry lens (ZEISS, Germany). Tiled scanner images  
968 were reconstructed using ZEN software (ZEISS, Germany) (pixel size = 0.45  $\mu\text{m}$ ).

969 QuPath (version 0.4.3) software was used for muscle fibrosis quantification from sirus red staining. For  
970 each muscle scan, a small artificial neural network was trained to classify positive and negative fibrotic  
971 pixels, and subsequently used to quantify fibrotic areas.

## 972 **Immunofluorescence:**

### 973 **Galectin-3 and all co-immunostainings of LAMP2**

974 Slides were fixed in ice-cold 4% PFA (Thermo Scientific, ref-28906) for 3 minutes and washed 2 times in  
975 PBS, then permeabilized in an ice-cold methanol gradient (10 min 70%; 10 min 95%, 20 min 100%). After  
976 3 washes with PBS, a 10% goat serum (GS) solution (Agilent, ref. X090710) was used for blocking (RT, 30  
977 min). A second 'Mouse-on-Mouse' blocking solution (Invitrogen, ref. R37621) was also used to block  
978 endogenous binding to mouse immunoglobulins (RT, 30min), for all immunostainings with mouse primary

979 antibodies on mouse muscles. Slides were then incubated with primary antibodies at 4°C overnight  
980 (diluted in 1% GS, see **Table S3** for specific dilutions). Next, slides were washed in TTBS solution 3 times,  
981 before incubation with secondary antibodies for 2h at 4°C (Molecular Probes Alexa Fluor secondary  
982 antibodies were used, 1:200 dilution, see **Supplementary Table S5**). Finally, the slides were washed in PBS  
983 solution 3 times for 5 minutes, rinsed in milliQ water and mounted with DAPI-Fluoromount-G mounting  
984 medium (Southern Biotech, ref. 0100-20).

#### 985 **Other immunostainings:**

986 Slides were fixed for 10 minutes in 4% methanol-free ice-cold PFA solution (Thermo Scientific, ref. 28906),  
987 permeabilized in 0.1% Triton for 5 minutes and blocked for 45 minutes in 10% goat serum solution (Agilent,  
988 ref. X090710). For staining using primary mouse antibodies, an additional 30-minute blocking was done  
989 with 'mouse on mouse' solution (Invitrogen R37621). Next, slides were incubated with the primary  
990 antibody solution at 4°C overnight (diluted in 1% GS, references and dilutions are listed in **Supplementary**  
991 **Table S4**). Slides were then washed 3 times in PBS and incubated 2h at 4°C with a secondary antibody  
992 solution (Molecular Probes Alexa Fluor secondary antibodies were used, 1:200 dilution, listed in  
993 **Supplementary Table S5**). Finally, the slides were washed in PBS solution 3 times for 5 minutes, rinsed in  
994 milliQ water and mounted with DAPI-Fluoromount-G mounting medium (Southern Biotech, ref. 0100-20)  
995 or Fluoromount-G medium (Southern Biotech, ref. 0100-01).

#### 996 **Detection of free cholesterol by filipin staining:**

997 Free cholesterol was detected using the fluorophore filipin (Sigma, Ref. SAE008). Filipin was incubated with  
998 the secondary antibody solution at a concentration of 100µg/mL, along with Syto13 (Invitrogen, S7575)  
999 for nuclear staining.

#### 1000 **Image acquisition**

1001 Once the slides have been dried, they were imaged with a LEICA TCS SP8 spectral confocal microscope  
1002 (Leica, Germany) running LASX software (Leica, Germany), using a HC PL APO CS2 20X 0.75 NA dry  
1003 objective. Acquired images were processed with Fiji ImageJ for final figures.

1004 For dystrophin, IgG and CD11B staining, images were digitized using the Axioscan Z1 slide scanner (Zeiss,  
1005 Germany) under a Zeiss Plan-Apochromat 10X/0.45 M27 dry lens (Zeiss, Germany) and using an ORCA-  
1006 Flash4.0 CMOS digital camera (Hamamatsu, Japan). Tile scanner images were reconstructed with ZEN  
1007 software (ZEISS, Germany) (pixel size = 0.65  $\mu\text{m}$ ).

#### 1008 **Image Analyses:**

1009 **Myofiber segmentation:** For images with laminin or wheat germ agglutinin (WGA) labeling for the  
1010 membranes, the Cellpose2 *cyto2* model (Stringer et al., 2021) was fine-tuned on manually myofiber-  
1011 labeled images (hyperparameters: *n\_epochs*=200, *learning\_rate*=0.05, *weight\_decay*=0.0001). The  
1012 labeled dataset used in fine-tuning was prepared in such a way that the model can simultaneously segment  
1013 myofibers and ignore low-quality staining areas. Fine-tuned models were then used to extract myofiber  
1014 masks. Reconstruction of myofiber masks of whole-scan images was done using the *cellpose* package  
1015 (Stringer et al., 2021). Reconstructed masks were then converted into Regions of Interest (ROIs) for  
1016 subsequent quantification (each ROI corresponds to an individual myofiber) using the *Labels\_To\_Rois.py*  
1017 Fiji plugin (Waisman et al., 2021). For all images acquired with the confocal, the cellpose2 *cyto2* model  
1018 was fine-tuned on manually labeled images based on the background noise of the A488 channel.

1019 **Puncta Quantification:** all images from the same experiment or panel were processed uniformly using Fiji  
1020 ImageJ. Median filters were applied to reduce noise and thresholding was performed to select the puncta  
1021 to be analyzed. For overlay quantification, the image calculator function 'AND' was used. Various  
1022 parameters of puncta were quantified within each individual region of interest (ROI), where 1 ROI  
1023 corresponds to 1 myofiber.

1024 **Overlay analyzes:** ImageJ's JaCOP plug-in was used to analyze colocalization by calculating Manders  
1025 coefficients. These coefficients indicate the fraction of the fluorescence signal from one channel localized  
1026 in the fluorescence pixels of a second channel.

1027 **Statistical Analysis:**

1028 Statistical analysis was performed using Graphpad Prism 10 (GraphPad Software, Inc., La Jolla, CA, USA), R  
1029 4.2.2. or Python 3.10. Variances were assumed to be equal; a Shapiro-Wilk test was used to check  
1030 normality. A Student's t test was used to compare the mean of two groups. A one-way ANOVA test was  
1031 used to compare more than two groups when values followed a normal distribution, accompanied by  
1032 Tukey's multiple comparison test, otherwise a non-parametric Kruskal-Wallis test with Dunn's multiple  
1033 comparisons was used. Error bars on graphs represent standard deviation (SD) unless specified otherwise.  
1034 Results were considered significant when p-values or adjusted p-values were less than 0.05.

1035

1036

1037

1038

- 1040 Aits, S., Krickler, J., Liu, B., Ellegaard, A. M., Hämälistö, S., Tvingsholm, S., Corcelle-Termeau, E., Høgh, S.,  
1041 Farkas, T., Jonassen, A. H., Gromova, I., Mortensen, M., & Jäättelä, M. (2015). Sensitive detection of  
1042 lysosomal membrane permeabilization by lysosomal galectin puncta assay. *Autophagy*, *11*(8), 1408–  
1043 1424. <https://doi.org/10.1080/15548627.2015.1063871>
- 1044 Allen, D. G., Whitehead, N. P., & Froehner, S. C. (2016). Absence of Dystrophin Disrupts Skeletal Muscle  
1045 Signaling: Roles of Ca<sup>2+</sup>, Reactive Oxygen Species, and Nitric Oxide in the Development of Muscular  
1046 Dystrophy. *Physiological Reviews*, *96*(1), 253–305. <https://doi.org/10.1152/physrev.00007.2015>
- 1047 Amor, F., Vu Hong, A., Corre, G., Sanson, M., Suel, L., Blaie, S., Servais, L., Voit, T., Richard, I., Israeli, D.,  
1048 Hong, A. V., Corre, G., Sanson, M., Suel, L., Blaie, S., Servais, L., Voit, T., Richard, I., Israeli, D., ... Israeli,  
1049 D. (2021). Cholesterol metabolism is a potential therapeutic target in Duchenne muscular dystrophy.  
1050 *Journal of Cachexia, Sarcopenia and Muscle*, *12*(3), 677–693. <https://doi.org/10.1002/jcsm.12708>
- 1051 Argov, Z., Vornovitsky, H., Blumen, S., & Caraco, Y. (2015). First Human Use of High Dose IV Trehalose:  
1052 Safety, Tolerability and Pharmacokinetic Results from the Oculopharyngeal Muscular Dystrophy  
1053 (OPMD) Therapy Trial (P7. 068). *Neurology*, *84*(14 Supplement).
- 1054 Barondes, S. H., Castronovo, V., Cooper, D. N. W., Cummings, R. D., Drickamer, K., Felzi, T., Gitt, M. A.,  
1055 Hirabayashi, J., Hughes, C., Kasai, K. ichi, Leffler, H., Liu, F. T., Lotan, R., Mercurio, A. M., Monsigny,  
1056 M., Pillai, S., Poirer, F., Raz, A., Rigby, P. W. J., ... Wang, J. L. (1994). Galectins: a family of animal beta-  
1057 galactoside-binding lectins. *Cell*, *76*(4), 597–598. [https://doi.org/10.1016/0092-8674\(94\)90498-7](https://doi.org/10.1016/0092-8674(94)90498-7)
- 1058 Barral, D. C., Staiano, L., Guimas Almeida, C., Cutler, D. F., Eden, E. R., Futter, C. E., Galione, A., Marques,  
1059 A. R. A., Medina, D. L., Napolitano, G., Settembre, C., Vieira, O. V., Aerts, J. M. F. G., Atakpa-Adaji, P.,  
1060 Bruno, G., Capuozzo, A., De Leonibus, E., Di Malta, C., Escrevente, C., ... Seabra, M. C. (2022). Current  
1061 methods to analyze lysosome morphology, positioning, motility and function. *Traffic (Copenhagen,*  
1062 *Denmark)*, *23*(5), 238–269. <https://doi.org/10.1111/TRA.12839>
- 1063 Betuing, S., Pikuleva, I. A., & Castellano, J. M. (2022). Editorial: Cholesterol and Neurodegenerative  
1064 Diseases - Pressing Questions and How to Address Them. *Frontiers in Aging Neuroscience*, *14*.  
1065 <https://doi.org/10.3389/FNAGI.2022.948153>
- 1066 Bez Batti Angulski, A., Hosny, N., Cohen, H., Martin, A. A., Hahn, D., Bauer, J., & Metzger, J. M. (2023).  
1067 Duchenne muscular dystrophy: disease mechanism and therapeutic strategies. *Frontiers in*  
1068 *Physiology*, *14*. <https://doi.org/10.3389/FPHYS.2023.1183101>
- 1069 Bourg, N., Hong, A. V., Lostal, W., Jaber, A., Guerchet, N., Tanniou, G., Bordier, F., Bertil-Froidevaux, E.,  
1070 Georger, C., Daniele, N., Richard, I., & Israeli, D. (2022). Co-Administration of Simvastatin Does Not  
1071 Potentiate the Benefit of Gene Therapy in the mdx Mouse Model for Duchenne Muscular Dystrophy.  
1072 *International Journal of Molecular Sciences* 2022, Vol. 23, Page 2016, *23*(4), 2016.  
1073 <https://doi.org/10.3390/IJMS23042016>

- 1074 Bradbury, A., Markusic, D., Muhuri, M., & Ou, L. (2023). Editorial: Immunogenicity and toxicity of AAV gene  
1075 therapy. *Frontiers in Immunology*, 14. <https://doi.org/10.3389/FIMMU.2023.1227231>
- 1076 Bushby, K., Finkel, R., Birnkrant, D. J., Case, L. E., Clemens, P. R., Cripe, L., Kaul, A., Kinnett, K., McDonald,  
1077 C., Pandya, S., Poysky, J., Shapiro, F., Tomezsko, J., Constantin, C., & DMD Care Considerations  
1078 Working Group. (2010). Diagnosis and management of Duchenne muscular dystrophy, part 1:  
1079 diagnosis, and pharmacological and psychosocial management. *The Lancet Neurology*, 9(1), 77–93.  
1080 [https://doi.org/10.1016/S1474-4422\(09\)70271-6](https://doi.org/10.1016/S1474-4422(09)70271-6)
- 1081 Casati, S. R., Cervia, D., Roux-Biejat, P., Moscheni, C., Perrotta, C., & De Palma, C. (2024). Mitochondria and  
1082 Reactive Oxygen Species: The Therapeutic Balance of Powers for Duchenne Muscular Dystrophy.  
1083 *Cells*, 13(7). <https://doi.org/10.3390/CELLS13070574>
- 1084 Cerri, D. G., Rodrigues, L. C., Alves, V. M., Machado, J., Bastos, V. A. F., Carmo Kettelhut, I., Alberici, L. C.,  
1085 Costa, M. C. R., Stowell, S. R., Cummings, R. D., & Dias-Baruffi, M. (2021). Endogenous Galectin-3 is  
1086 required for skeletal muscle repair. *Glycobiology*. <https://doi.org/10.1093/GLYCOB/CWAB071>
- 1087 Chamberlain, J. S., Robb, M., Braun, S., Brown, K. J., Danos, O., Ganot, A., Gonzalez-Alegre, P., Hunter, N.,  
1088 McDonald, C., Morris, C., Tobolowsky, M., Wagner, K. R., Ziolkowski, O., & Duan, D. (2023).  
1089 Microdystrophin Expression as a Surrogate Endpoint for Duchenne Muscular Dystrophy Clinical  
1090 Trials. *Human Gene Therapy*, 34(9–10), 404–415. <https://doi.org/10.1089/HUM.2022.190>
- 1091 Chen, A., & Gibney, P. A. (2023). Dietary Trehalose as a Bioactive Nutrient. *Nutrients*, 15(6).  
1092 <https://doi.org/10.3390/NU15061393>
- 1093 Chen, Y., & Yu, L. (2017). Recent progress in autophagic lysosome reformation. *Traffic (Copenhagen,  
1094 Denmark)*, 18(6), 358–361. <https://doi.org/10.1111/TRA.12484>
- 1095 Coulis, G., Jaime, D., Guerrero-Juarez, C., Kastenschmidt, J. M., Farahat, P. K., Nguyen, Q., Pervolarakis, N.,  
1096 McLinden, K., Thurlow, L., Movahedi, S., Hughes, B. S., Duarte, J., Sorn, A., Montoya, E., Mozaffar, I.,  
1097 Dragan, M., Othy, S., Joshi, T., Hans, C. P., ... Villalta, S. A. (2023). Single-cell and spatial  
1098 transcriptomics identify a macrophage population associated with skeletal muscle fibrosis. *Science  
1099 Advances*, 9(27). <https://doi.org/10.1126/SCIADV.ADD9984>
- 1100 Davies, J. E., Sarkar, S., & Rubinsztein, D. C. (2006). Trehalose reduces aggregate formation and delays  
1101 pathology in a transgenic mouse model of oculopharyngeal muscular dystrophy. *Human Molecular  
1102 Genetics*, 15(1), 23–31. <https://doi.org/10.1093/HMG/DDI422>
- 1103 De Palma, C., Morisi, F., Cheli, S., Pambianco, S., Cappello, V., Vezzoli, M., Rovere-Querini, P., Moggio, M.,  
1104 Ripolone, M., Francolini, M., Sandri, M., & Clementi, E. (2012). Autophagy as a new therapeutic target  
1105 in Duchenne muscular dystrophy. *Cell Death & Disease*, 3(11), e1363.  
1106 <https://doi.org/10.1038/CDDIS.2012.159>
- 1107 Do, H., Meena, N. K., & Raben, N. (2024). Failure of Autophagy in Pompe Disease. *Biomolecules*, 14(5), 573.  
1108 <https://doi.org/10.3390/BIOM14050573>

- 1109 Duan, D., Goemans, N., Takeda, S., Mercuri, E., & Aartsma-Rus, A. (2021). Duchenne muscular dystrophy.  
 1110 In *Nature Reviews Disease Primers* (Vol. 7, Issue 1). Nature Research.  
 1111 <https://doi.org/10.1038/s41572-021-00248-3>
- 1112 Fernandez-Mosquera, L., Yambire, K. F., Couto, R., Pereyra, L., Pabis, K., Ponsford, A. H., Diogo, C. V., Stagi,  
 1113 M., Milosevic, I., & Raimundo, N. (2019). Mitochondrial respiratory chain deficiency inhibits  
 1114 lysosomal hydrolysis. *Autophagy*, 15(9), 1572–1591.  
 1115 <https://doi.org/10.1080/15548627.2019.1586256>
- 1116 Gelman, B. B., Davis, M. H., Morris, R. E., & Gruenstein, E. (1981). Structural changes in lysosomes from  
 1117 cultured human fibroblasts in Duchenne’s muscular dystrophy. *Journal of Cell Biology*, 88(2), 329–  
 1118 337. <https://doi.org/10.1083/jcb.88.2.329>
- 1119 Germain, K., So, R. W. L., DiGiovanni, L. F., Watts, J. C., Bandsma, R. H. J., & Kim, P. K. (2024). Upregulated  
 1120 pexophagy limits the capacity of selective autophagy. *Nature Communications*, 15(1).  
 1121 <https://doi.org/10.1038/S41467-023-44005-4>
- 1122 Israeli, D., Cosette, J., Corre, G., Amor, F., Poupiot, J., Stockholm, D., Montus, M., Gjata, B., & Richard, I.  
 1123 (2019). An AAV-SGCG Dose-Response Study in a  $\gamma$ -Sarcoglycanopathy Mouse Model in the Context of  
 1124 Mechanical Stress. 13, 494–502. <https://doi.org/10.1016/j.omtm.2019.04.007>
- 1125 Israeli, D., Vu Hong, A., Corre, G., Miagoux, Q., & Richard, I. (2022). Deciphering the Molecular Mechanism  
 1126 of Incurable Muscle Disease by a Novel Method for the Interpretation of miRNA Dysregulation. *Non-  
 1127 Coding RNA*, 8(4), 48. <https://doi.org/10.3390/NCRNA8040048>
- 1128 Jia, J., Claude-Taupin, A., Gu, Y., Choi, S. W., Peters, R., Bissa, B., Mudd, M. H., Allers, L., Pallikkuth, S., Lidke,  
 1129 K. A., Salemi, M., Phinney, B., Mari, M., Reggiori, F., & Deretic, V. (2020). Galectin-3 Coordinates a  
 1130 Cellular System for Lysosomal Repair and Removal. *Developmental Cell*, 52(1), 69-87.e8.  
 1131 <https://doi.org/10.1016/j.devcel.2019.10.025>
- 1132 Kacher, R., Mounier, C., Caboche, J., & Betuing, S. (2022). Altered Cholesterol Homeostasis in Huntington’s  
 1133 Disease. *Frontiers in Aging Neuroscience*, 14. <https://doi.org/10.3389/FNAGI.2022.797220>
- 1134 Khalifeh, M., Barreto, G., & Sahebkar, A. (2021). Therapeutic potential of trehalose in neurodegenerative  
 1135 diseases: the knowns and unknowns. *Neural Regeneration Research*, 16(10), 2026–2027.  
 1136 <https://doi.org/10.4103/1673-5374.308085>
- 1137 Kimura, S., Miyake, N., Ozasa, S., Ueno, H., Ohtani, Y., Takaoka, Y., & Nishino, I. (2024). Increase in  
 1138 cathepsin K gene expression in Duchenne muscular dystrophy skeletal muscle. *Neuropathology :  
 1139 Official Journal of the Japanese Society of Neuropathology*. <https://doi.org/10.1111/NEUP.12995>
- 1140 Kominami, E., Ii, K., & Katunuma, N. (1987). Activation of the intramyofibrillar autophagic-lysosomal system  
 1141 in muscular dystrophy. *American Journal of Pathology*, 127(3), 461–466.  
 1142 [/pmc/articles/PMC1899763/?report=abstract](https://pubmed.ncbi.nlm.nih.gov/1899763/)
- 1143 Lakpa, K. L., Khan, N., Afghah, Z., Chen, X., & Geiger, J. D. (2021). Lysosomal Stress Response (LSR):  
 1144 Physiological Importance and Pathological Relevance. In *Journal of Neuroimmune Pharmacology*

1145 (Vol. 16, Issue 2, pp. 219–237). *J Neuroimmune Pharmacol.* [https://doi.org/10.1007/s11481-021-](https://doi.org/10.1007/s11481-021-09990-7)  
1146 09990-7

1147 Li, X., Rydzewski, N., Hider, A., Zhang, X., Yang, J., Wang, W., Gao, Q., Cheng, X., & Xu, H. (2016). A molecular  
1148 mechanism to regulate lysosome motility for lysosome positioning and tubulation. *Nature Cell*  
1149 *Biology*, 18(4), 404–417. <https://doi.org/10.1038/NCB3324>

1150 Livak, K. J., & Schmittgen, T. D. (2001). Analysis of relative gene expression data using real-time  
1151 quantitative PCR and the  $2^{-\Delta\Delta CT}$  method. *Methods*, 25(4), 402–408.  
1152 <https://doi.org/10.1006/meth.2001.1262>

1153 Maejima, I., Takahashi, A., Omori, H., Kimura, T., Takabatake, Y., Saitoh, T., Yamamoto, A., Hamasaki, M.,  
1154 Noda, T., Isaka, Y., & Yoshimori, T. (2013). Autophagy sequesters damaged lysosomes to control  
1155 lysosomal biogenesis and kidney injury. *The EMBO Journal*, 32(17), 2336–2347.  
1156 <https://doi.org/10.1038/EMBOJ.2013.171>

1157 Marotta, M., Ruiz-Roig, C., Sarria, Y., Peiro, J. L., Nuñez, F., Ceron, J., Munell, F., & Roig-Quilis, M. (2009).  
1158 Muscle genome-wide expression profiling during disease evolution in mdx mice. *Physiological*  
1159 *Genomics*, 37(2), 119–132. <https://doi.org/10.1152/physiolgenomics.90370.2008>

1160 McDonald, C. M., Henricson, E. K., Abresch, R. T., Duong, T., Joyce, N. C., Hu, F., Clemens, P. R., Hoffman,  
1161 E. P., Cnaan, A., Gordish-Dressman, H., Vishwanathan, V., Chidambaranathan, S., Biggar, W. D.,  
1162 McAdam, L. C., Mah, J. K., Tulinius, M., Morgenroth, L. P., Leshner, R., Tesi-Rocha, C., ... Karachunski,  
1163 P. (2018). Long-term effects of glucocorticoids on function, quality of life, and survival in patients  
1164 with Duchenne muscular dystrophy: a prospective cohort study. *The Lancet*, 391(10119), 451–461.  
1165 [https://doi.org/10.1016/S0140-6736\(17\)32160-8](https://doi.org/10.1016/S0140-6736(17)32160-8)

1166 Mirouse, V. (2023). Evolution and developmental functions of the dystrophin-associated protein complex:  
1167 beyond the idea of a muscle-specific cell adhesion complex. *Frontiers in Cell and Developmental*  
1168 *Biology*, 11. <https://doi.org/10.3389/FCELL.2023.1182524>

1169 Mullard, A. (2023). FDA approves first gene therapy for Duchenne muscular dystrophy, despite internal  
1170 objections. *Nature Reviews. Drug Discovery*, 22(8), 610. <https://doi.org/10.1038/D41573-023-00103->  
1171 Y

1172 Pal, R., Palmieri, M., Loehr, J. A., Li, S., Abo-Zahrah, R., Monroe, T. O., Thakur, P. B., Sardiello, M., & Rodney,  
1173 G. G. (2014). Src-dependent impairment of autophagy by oxidative stress in a mouse model of  
1174 Duchenne muscular dystrophy. *Nature Communications*, 5(1), 1–10.  
1175 <https://doi.org/10.1038/ncomms5425>

1176 Palmieri, M., Pal, R., & Sardiello, M. (2017). AKT modulates the autophagy-lysosome pathway via TFEB.  
1177 *Cell Cycle (Georgetown, Tex.)*, 16(13), 1237–1238. <https://doi.org/10.1080/15384101.2017.1337968>

1178 Pankiv, S., Clausen, T. H., Lamark, T., Brech, A., Bruun, J. A., Outzen, H., Øvervatn, A., Bjørkøy, G., &  
1179 Johansen, T. (2007). p62/SQSTM1 binds directly to Atg8/LC3 to facilitate degradation of ubiquitinated  
1180 protein aggregates by autophagy. *The Journal of Biological Chemistry*, 282(33), 24131–24145.  
1181 <https://doi.org/10.1074/JBC.M702824200>

- 1182 Pupyshev, A. B., Klyushnik, T. P., Akopyan, A. A., Singh, S. K., & Tikhonova, M. A. (2022). Disaccharide  
1183 trehalose in experimental therapies for neurodegenerative disorders: Molecular targets and  
1184 translational potential. *Pharmacological Research*, 183.  
1185 <https://doi.org/10.1016/J.PHRS.2022.106373>
- 1186 Radulovic, M., Schink, K. O., Wenzel, E. M., Nähse, V., Bongiovanni, A., Lafont, F., & Stenmark, H. (2018).  
1187 ESCRT-mediated lysosome repair precedes lysophagy and promotes cell survival. *The EMBO Journal*,  
1188 37(21). <https://doi.org/10.15252/EMBJ.201899753>
- 1189 Reinbigler, M., Cosette, J., Guesmia, Z., Jimenez, S., Fetita, C., Brunet, E., & Stockholm, D. (2022). Artificial  
1190 intelligence workflow quantifying muscle features on Hematoxylin-Eosin stained sections reveals  
1191 dystrophic phenotype amelioration upon treatment. *Scientific Reports*, 12(1).  
1192 <https://doi.org/10.1038/S41598-022-24139-Z>
- 1193 Rind, D. M. (2024). The FDA and Gene Therapy for Duchenne Muscular Dystrophy. *JAMA*.  
1194 <https://doi.org/10.1001/JAMA.2024.5613>
- 1195 Roberts, T. C., Wood, M. J. A., & Davies, K. E. (2023). Therapeutic approaches for Duchenne muscular  
1196 dystrophy. *Nature Reviews Drug Discovery* 2023 22:11, 22(11), 917–934.  
1197 <https://doi.org/10.1038/s41573-023-00775-6>
- 1198 Rouillon, J., Poupiot, J., Zocevic, A., Amor, F., Léger, T., Garcia, C., Camadro, J.-M., Wong, B., Pinilla, R.,  
1199 Cosette, J., Coenen-Stass, A. M. L., McClorey, G., Roberts, T. C., Wood, M. J. a, Servais, L., Udd, B.,  
1200 Voit, T., Richard, I., & Svinartchouk, F. (2015). Serum proteomic profiling reveals fragments of  
1201 MYOM3 as potential biomarkers for monitoring the outcome of therapeutic interventions in  
1202 muscular dystrophies. *Human Molecular Genetics*, 24(17), 4916–4932.  
1203 <https://doi.org/10.1093/hmg/ddv214>
- 1204 Rusmini, P., Cortese, K., Crippa, V., Cristofani, R., Cicardi, M. E., Ferrari, V., Vezzoli, G., Tedesco, B., Meroni,  
1205 M., Messi, E., Piccolella, M., Galbiati, M., Garrè, M., Morelli, E., Vaccari, T., & Poletti, A. (2019).  
1206 Trehalose induces autophagy via lysosomal-mediated TFEB activation in models of motoneuron  
1207 degeneration. *Autophagy*, 15(4), 631–651. <https://doi.org/10.1080/15548627.2018.1535292>
- 1208 Sano, M., Wada, Y., Ii, K., Kominami, E., Katunuma, N., & Tsukagoshi, H. (1988). Immunolocalization of  
1209 cathepsins B, H and L in skeletal muscle of X-linked muscular dystrophy (mdx) mouse. *Acta*  
1210 *Neuropathologica*, 75(3), 217–225. <https://doi.org/10.1007/BF00690529>
- 1211 Sanson, M., Hog Vu, A., Massourides, E., Bourg, N., Suel, L., Amor, F., Corre, G., Bénil, P., Barthelemy, I.,  
1212 Blot, S., Bigot, A., Pinset, C., Rustin, P., Servais, L., Voit, T., Richard, I., Israeli, D., Vu Hong, A.,  
1213 Massourides, E., ... Israeli, D. (2020). miR-379 links glucocorticoid treatment with mitochondrial  
1214 response in Duchenne muscular dystrophy. *Scientific Reports*, 10(1), 9139.  
1215 <https://doi.org/10.1038/s41598-020-66016-7>
- 1216 Schulze, H., & Sandhoff, K. (2011). Lysosomal lipid storage diseases. *Cold Spring Harbor Perspectives in*  
1217 *Biology*, 3(6), 1–19. <https://doi.org/10.1101/CSHPERSPECT.A004804>

- 1218 Settembre, C., Di Malta, C., Polito, V. A., Arencibia, M. G., Vetrini, F., Erdin, S., Erdin, S. U., Huynh, T.,  
1219 Medina, D., Colella, P., Sardiello, M., Rubinsztein, D. C., & Ballabio, A. (2011). TFEB links autophagy  
1220 to lysosomal biogenesis. *Science (New York, N.Y.)*, 332(6036), 1429–1433.  
1221 <https://doi.org/10.1126/SCIENCE.1204592>
- 1222 Skowrya, M. L., Schlesinger, P. H., Naismith, T. V., & Hanson, P. I. (2018). Triggered recruitment of ESCRT  
1223 machinery promotes endolysosomal repair. *Science (New York, N.Y.)*, 360(6384).  
1224 <https://doi.org/10.1126/SCIENCE.AAR5078>
- 1225 Spampanato, C., Feeney, E., Li, L., Cardone, M., Lim, J. A., Annunziata, F., Zare, H., Polishchuk, R.,  
1226 Puertollano, R., Parenti, G., Ballabio, A., & Raben, N. (2013). Transcription factor EB (TFEB) is a new  
1227 therapeutic target for Pompe disease. *EMBO Molecular Medicine*, 5(5), 691–706.  
1228 <https://doi.org/10.1002/EMMM.201202176>
- 1229 Srivastava, N. K., Yadav, R., Mukherjee, S., Pal, L., & Sinha, N. (2017). Abnormal lipid metabolism in skeletal  
1230 muscle tissue of patients with muscular dystrophy: In vitro, high-resolution NMR spectroscopy based  
1231 observation in early phase of the disease. *Magnetic Resonance Imaging*, 38, 163–173.  
1232 <https://doi.org/10.1016/j.mri.2017.01.001>
- 1233 Stringer, C., Wang, T., Michaelos, M., & Pachitariu, M. (2021). Cellpose: a generalist algorithm for cellular  
1234 segmentation. *Nature Methods*, 18(1), 100–106. <https://doi.org/10.1038/S41592-020-01018-X>
- 1235 Sun, Z., Wang, X., White, Z., Dormuth, C., Morales, F., & Bernatchez, P. (2023). Dyslipidemia in Muscular  
1236 Dystrophy: A Systematic Review and Meta-Analysis. *Journal of Neuromuscular Diseases*, 10(4), 505–  
1237 516. <https://doi.org/10.3233/JND-230064>
- 1238 Surma, M. A., Gerl, M. J., Herzog, R., Helppi, J., Simons, K., & Klose, C. (2021). Mouse lipidomics reveals  
1239 inherent flexibility of a mammalian lipidome. *Scientific Reports*, 11(1).  
1240 <https://doi.org/10.1038/S41598-021-98702-5>
- 1241 Timpani, C. A., Hayes, A., & Rybalka, E. (2015). Revisiting the dystrophin-ATP connection: How half a  
1242 century of research still implicates mitochondrial dysfunction in Duchenne Muscular Dystrophy  
1243 aetiology. *Medical Hypotheses*, 85(6), 1021–1033. <https://doi.org/10.1016/j.mehy.2015.08.015>
- 1244 Tjondrokoesoemo, A., Schips, T. G., Sargent, M. A., Vanhoutte, D., Kanisicak, O., Prasad, V., Lin, S. C. J.,  
1245 Maillet, M., & Molkentin, J. D. (2016). Cathepsin S contributes to the pathogenesis of muscular  
1246 dystrophy in mice. *Journal of Biological Chemistry*, 291(19), 9920–9928.  
1247 <https://doi.org/10.1074/jbc.M116.719054>
- 1248 Uchimoto, T., Nohara, H., Kamehara, R., Iwamura, M., Watanabe, N., & Kobayashi, Y. (1999). Mechanism  
1249 of apoptosis induced by a lysosomotropic agent, L-Leucyl-L-Leucine methyl ester. *Apoptosis: An  
1250 International Journal on Programmed Cell Death*, 4(5), 357–362.  
1251 <https://doi.org/10.1023/A:1009695221038>
- 1252 Udayar, V., Chen, Y., Sidransky, E., & Jagasia, R. (2022). Lysosomal dysfunction in neurodegeneration:  
1253 emerging concepts and methods. *Trends in Neurosciences*, 45(3), 184–199.  
1254 <https://doi.org/10.1016/J.TINS.2021.12.004>

- 1255 van Putten, M., Hulsker, M., Nadarajah, V. D., van Heiningen, S. H., van Huizen, E., van Iterson, M.,  
1256 Admiraal, P., Messemaker, T., den Dunnen, J. T., 't Hoen, P. a C., & Aartsma-Rus, A. (2012). The effects  
1257 of low levels of dystrophin on mouse muscle function and pathology. *PLoS One*, 7(2), e31937.  
1258 <https://doi.org/10.1371/journal.pone.0031937>
- 1259 Vu Hong, A. (2023). *An integrin-targeting AAV developed using a novel computational rational design  
1260 methodology presents improved targeting of the skeletal muscle and reduced liver tropism.*  
1261 <https://doi.org/10.21203/RS.3.RS-3466229/V1>
- 1262 Vu Hong, A., Bourg, N., Sanatine, P., Poupiot, J., Charton, K., Gicquel, E., Massourides, E., Spinazzi, M.,  
1263 Richard, I., & Israeli, D. (2022). Dlk1-Dio3 cluster miRNAs regulate mitochondrial functions in the  
1264 dystrophic muscle in Duchenne muscular dystrophy. *Life Science Alliance*, 6(1), e202201506.  
1265 <https://doi.org/10.26508/LSA.202201506>
- 1266 Waisman, A., Norris, A. M., Elías Costa, M., & Kopinke, D. (2021). Automatic and unbiased segmentation  
1267 and quantification of myofibers in skeletal muscle. *Scientific Reports*, 11(1).  
1268 <https://doi.org/10.1038/S41598-021-91191-6>
- 1269 Whitaker, J. N., Bertorini, T. E., & Mendell, J. R. (1983). Immunocytochemical studies of cathepsin D in  
1270 human skeletal muscle. *Annals of Neurology*, 13(2), 133–142.  
1271 <https://doi.org/10.1002/ana.410130205>
- 1272 White, Z., Hakim, C. H., Theret, M., Yang, N. N., Rossi, F., Cox, D., Francis, G. A., Straub, V., Selby, K.,  
1273 Panagiotopoulos, C., Duan, D., & Bernatchez, P. (2020). High prevalence of plasma lipid abnormalities  
1274 in human and canine Duchenne and Becker muscular dystrophies depicts a new type of primary  
1275 genetic dyslipidemia. *Journal of Clinical Lipidology*, 14(4), 459-469.e0.  
1276 <https://doi.org/10.1016/j.jacl.2020.05.098>
- 1277 White, Z., Theret, M., Milad, N., Tung, L. W., Chen, W. W., Sirois, M. G., Rossi, F., & Bernatchez, P. (2021).  
1278 Cholesterol absorption blocker ezetimibe prevents muscle wasting in severe dysferlin-deficient and  
1279 mdx mice. *Journal of Cachexia, Sarcopenia and Muscle*. <https://doi.org/10.1002/JCSM.12879>
- 1280 Whyte, L. S., Lau, A. A., Hemsley, K. M., Hopwood, J. J., & Sargeant, T. J. (2017). Endo-lysosomal and  
1281 autophagic dysfunction: a driving factor in Alzheimer's disease? *Journal of Neurochemistry*, 140(5),  
1282 703–717. <https://doi.org/10.1111/JNC.13935>
- 1283 Xie, Z., Zhao, M., Yan, C., Kong, W., Lan, F., Narengaowa, Zhao, S., Yang, Q., Bai, Z., Qing, H., & Ni, J. (2023).  
1284 Cathepsin B in programmed cell death machinery: mechanisms of execution and regulatory  
1285 pathways. *Cell Death & Disease*, 14(4). <https://doi.org/10.1038/S41419-023-05786-0>
- 1286 Yang, H., & Tan, J. X. (2023). Lysosomal quality control: molecular mechanisms and therapeutic  
1287 implications. *Trends in Cell Biology*, 33(9), 749–764. <https://doi.org/10.1016/J.TCB.2023.01.001>
- 1288 Yim, W. W. Y., & Mizushima, N. (2020). Lysosome biology in autophagy. *Cell Discovery*, 6(1).  
1289 <https://doi.org/10.1038/S41421-020-0141-7>

1290 You, J.-S., Karaman, K., Reyes-Ordoñez, A., Lee, S., Kim, Y., Bashir, R., & Chen, J. (2024). Leucyl-tRNA  
1291 Synthetase Contributes to Muscle Weakness through Mammalian Target of Rapamycin Complex 1  
1292 Activation and Autophagy Suppression in a Mouse Model of Duchenne Muscular Dystrophy. *The*  
1293 *American Journal of Pathology*. <https://doi.org/10.1016/J.AJPATH.2024.04.006>

1294 Zhang, T., & Kong, X. (2021). Recent advances of glucocorticoids in the treatment of Duchenne muscular  
1295 dystrophy (Review). *Experimental and Therapeutic Medicine*, 21(5).  
1296 <https://doi.org/10.3892/ETM.2021.9875>

1297

1298

1299

1300

1301

1302

1303

1304

1305

1306

1307

1308

1309

1310

1311

1312

1313 **ACKNOWLEDGEMENTS**

1314 This work was supported by the “Association Française contre les Myopathies” (AFM), and  
1315 “Institut National de la Santé Et de la Recherche Médicale” (INSERM, FranceRelance). The authors  
1316 are Genopole's members, first French biocluster dedicated to genetic, biotechnologies and  
1317 biotherapies. We are grateful to the “Imaging and Cytometry Core Facility” and to the *in vivo*  
1318 evaluation, services of Genethon for technical support, to Ile-de-France Region, to Conseil  
1319 Départemental de l’Essonne (ASTRE), INSERM and GIP Genopole, Evry for the purchase of the  
1320 equipment.

1321 For I.B and S.B, the work was funded by the Association Française contre les myopathies  
1322 (Translamuscle II (22946)).

1323 **AUTHOR CONTRIBUTIONS**

1324 The project was conceptualized by A.J and D.I. A.J conducted experiments and performed data analysis.  
1325 R.B, L.P, E.L, N.B, J.P conducted experiments. L.V.B, A.M and N.D conducted and supervised animal  
1326 experiments. I.B, S.B, M.T.B and T.E provided muscle biopsies and performed histological experiments.  
1327 A.V.H and D.S performed computational analyses. The manuscript was written by A.J, I.R and D.I. All  
1328 authors reviewed the manuscript.

1329

1330 **COMPETING INTERESTS**

1331 The authors declare no competing interests

1

## Supplementary Materials for

2

## Targeting lysosomal damage is a new therapeutic perspective for Duchenne Muscular

3

## Dystrophy

4

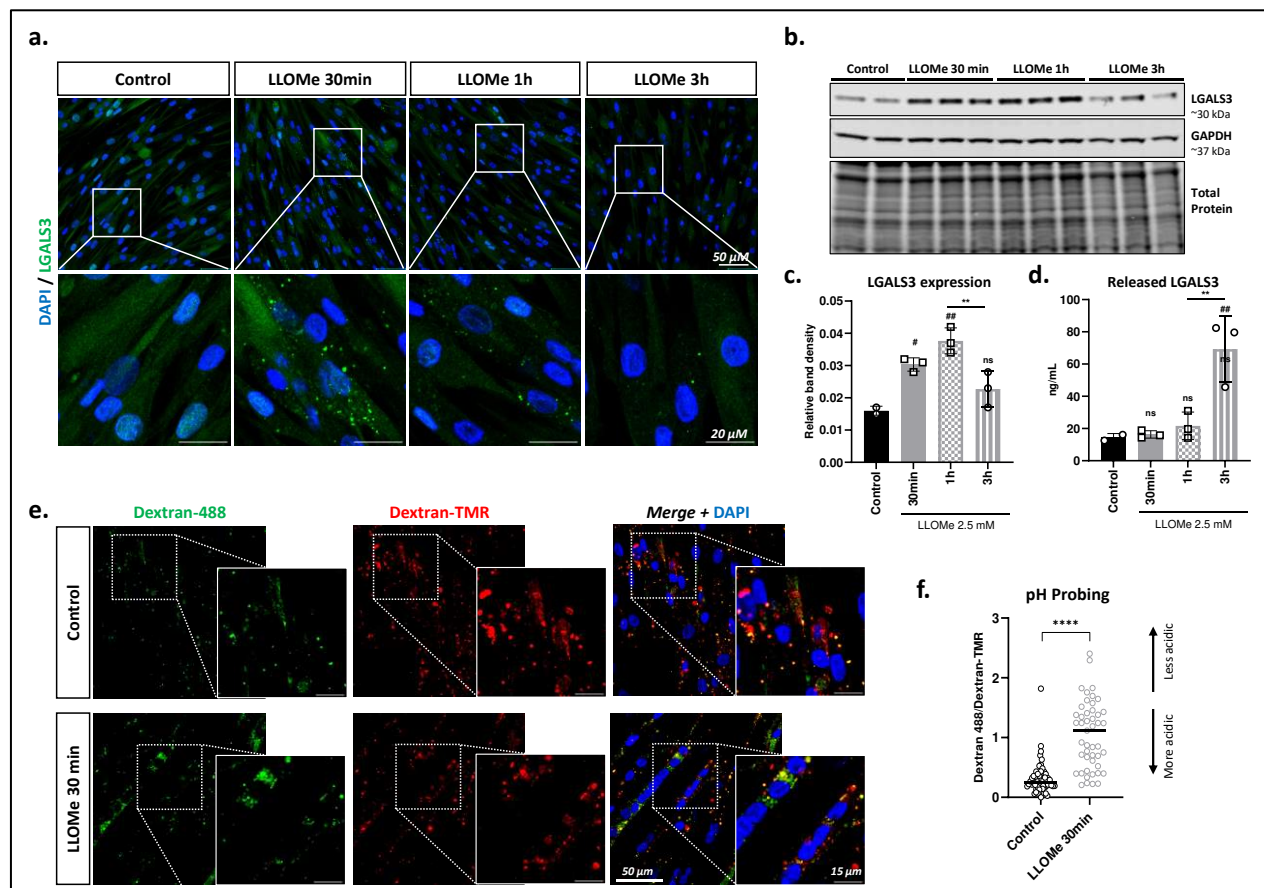
Abbass Jaber et al.

5

Corresponding author: David Israeli, [israeli@genethon.fr](mailto:israeli@genethon.fr)

6

### 7 Supplementary Figures:



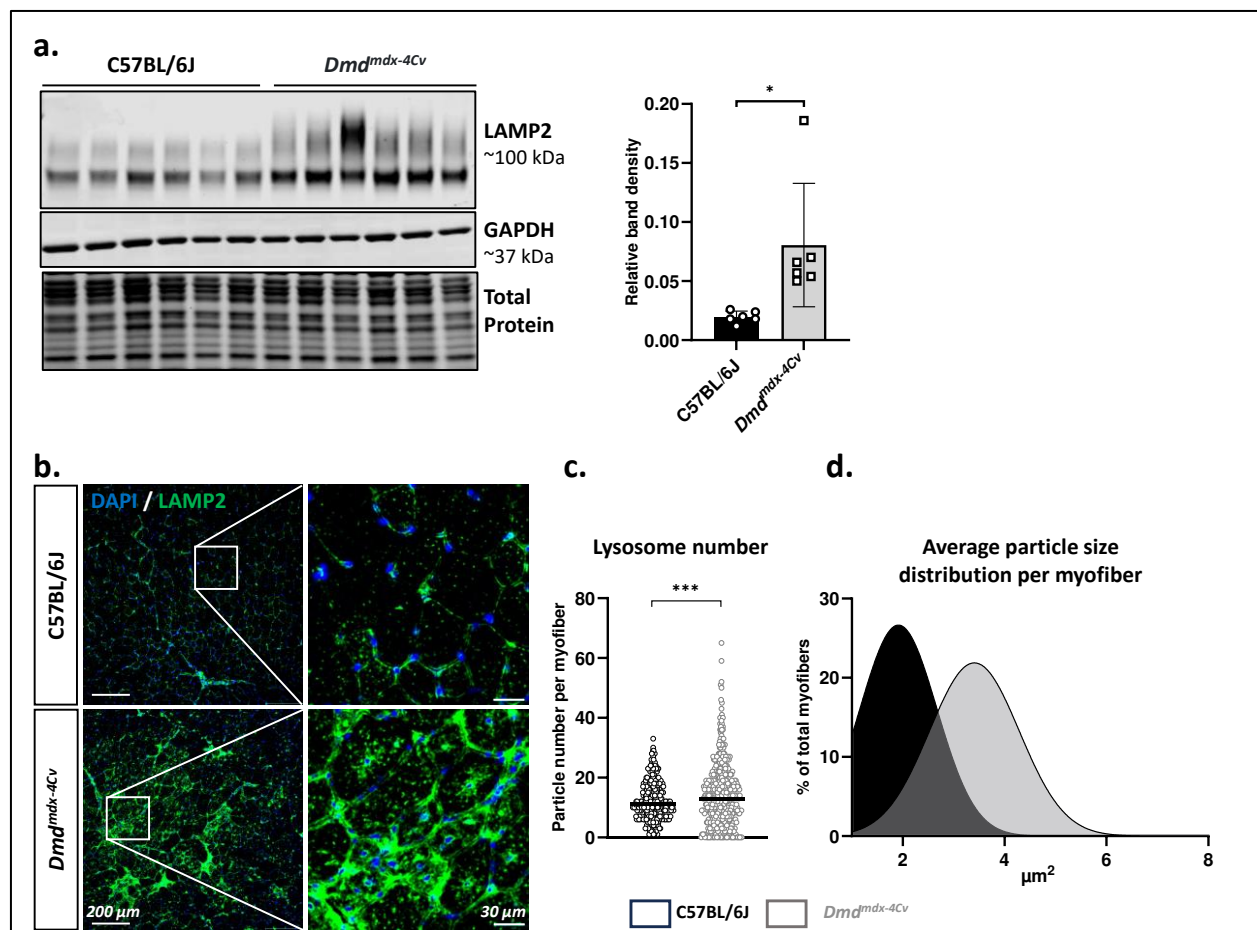
8

9 **Figure S1. Lysosome membrane permeabilization impairs lysosome function in muscle cells and is**

10 **detected with LGALS3 puncta assay. a) Representative plane confocal images of differentiated human**

11 *immortalized myoblasts immunostained for Galectin-3 (green). Cells were treated with LLOMe for 30*  
12 *minutes, 1h or 3h. b) Western blot analysis of human myotubes for LGALS3, using GAPDH as loading control.*  
13 *c) Column plot shows average  $\pm$  SD of LGALS3 band intensity normalized to GAPDH. d) ELISA analysis of*  
14 *released LGALS3 in the media of cultured myotubes. e) Representative plane confocal images of human*  
15 *myotubes stained with dextran-Oregon Green and dextran-TMR. Dextran Green is quenched under acidic*  
16 *pH, so increased green:red ratio denotes impaired lysosomal acidification. f) Scatter plot of Dextran*  
17 *488/Dextran-TMR ratio for at least 45 myotubes. An ANOVA test with Tukey multiple comparison was used*  
18 *for statistical comparisons of multiple groups. ANOVA p-value # $p < 0.05$ , ## $p < 0.001$ , ns=non-significant*  
19 *(compared to Control). An unpaired two tailed t.test was used for 2 groups comparison. T.test p-value*  
20 *\*\*\*\* $p < 0.0001$ .*

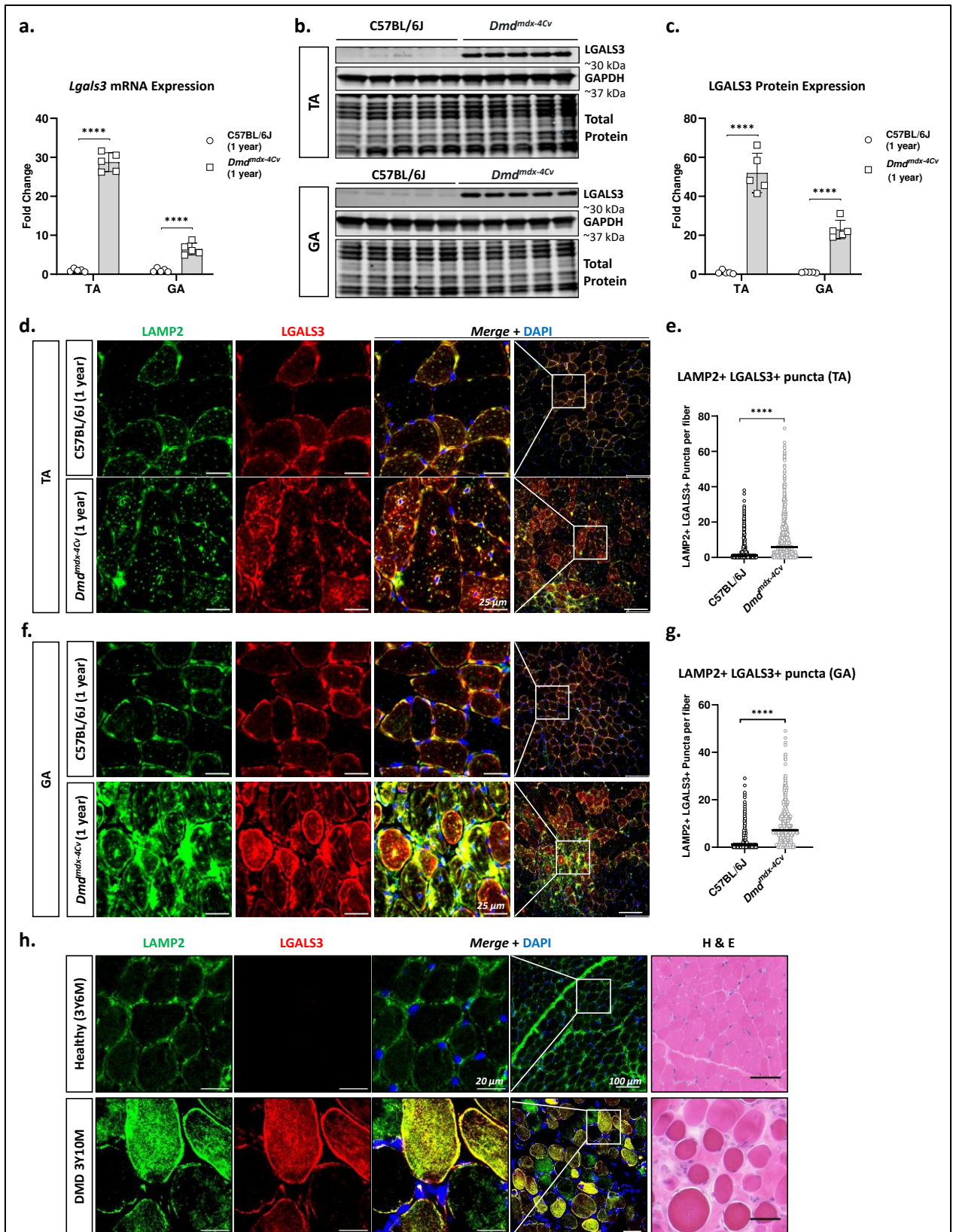
21



22

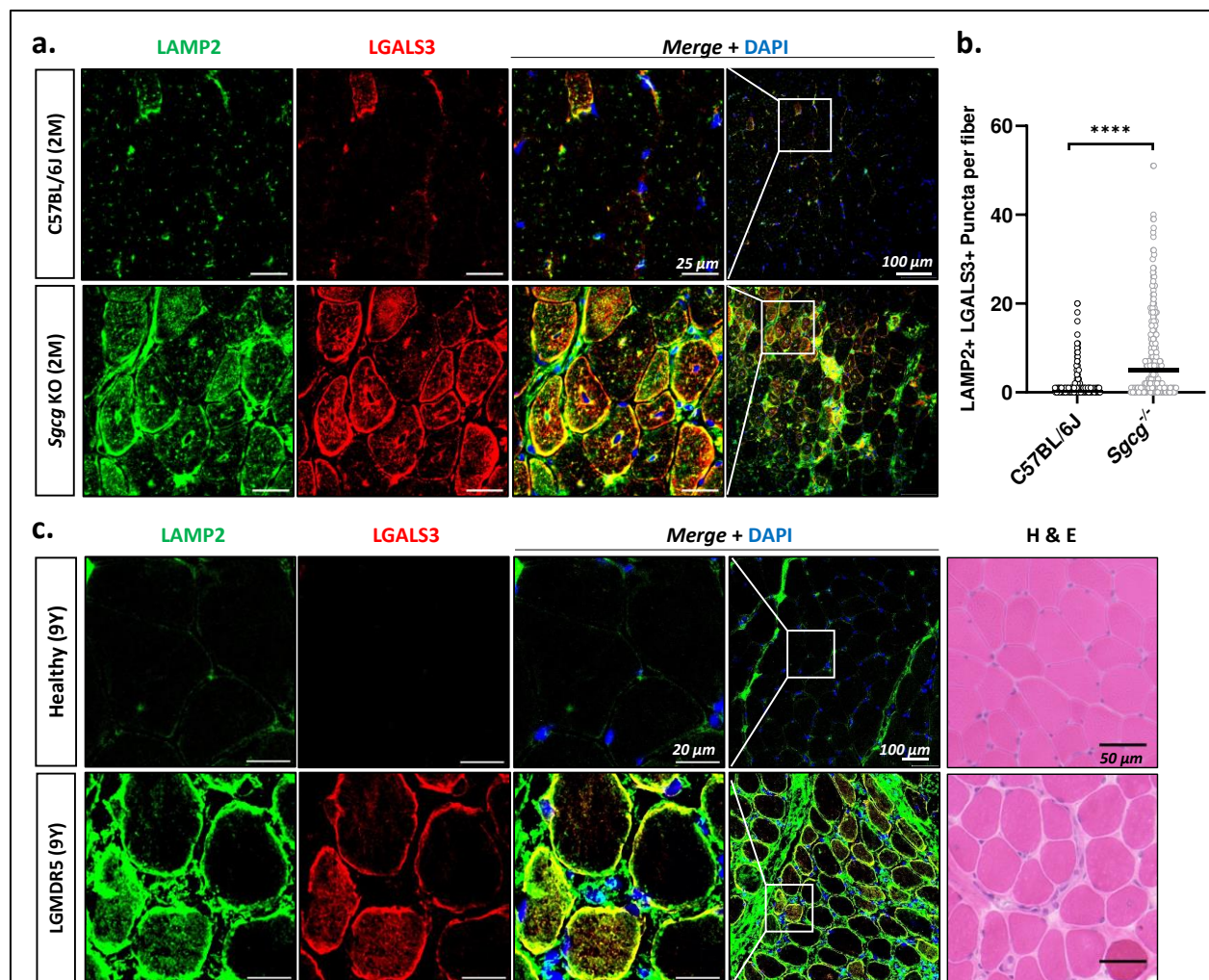
23 **Figure S2. Lysosomal stress in *Dmd<sup>mdx-4Cv</sup>* muscle.** **a)** Western blot analysis of TA muscle for LAMP2 and  
 24 band density quantification of LAMP2, normalized to GAPDH (average  $\pm$  SD) (n=6). **b)** Representative  
 25 confocal images of transversal sections of TA muscle immunostained for LAMP2. **c)** Scatter plot showing  
 26 average number of lysosomes per myofiber, detected by LAMP2 immunostaining on transversal sections  
 27 (>379 myofibers analyzed from n=6). **d)** Density plot with non-linear fit gaussian curve applied, showing  
 28 distribution of average spot size per myofiber (>379 myofibers analyzed from n=6).

29



31 **Figure S3. LGALS3 overexpression indicates LMP in old  $Dmd^{mdx-4Cv}$  mice and a DMD patient. a)** Relative  
32 *Lgals3* mRNA expression in the TA, GA, normalized to *Rplp0*. Data are presented as scatter plots with  
33 average  $\pm$  SD of Fold change relative to WT mice. **b)** Western blot analysis of TA and GA muscles of 1-year  
34 old WT and  $Dmd^{mdx-4Cv}$  mice (n=5). **c)** Band intensity quantification of LGALS3 relative to total protein  
35 staining in TA and GA muscles. Scatter plots show average  $\pm$  SD of Fold change relative to WT mice. **d-f)**  
36 Representative confocal images of transversal sections of TA and GA muscles of 1-year old WT and  $Dmd^{mdx-}$   
37  $^{4Cv}$  mice immunostained for LAMP2 (green) and LGALS3 (red). **e-g)** Quantification of double positive puncta  
38 (LAMP2+LGALS3+) in the myofibers of TA (**e**) and GA (**f**) muscles. Data are represented as scatter plots with  
39 median (n>838 and >464 for GA). **h)** Representative confocal images of transversal sections from muscles  
40 of a DMD patient and a healthy control immunostained for LAMP2 and LGALS3. Left panels show H&E  
41 labeling from the same muscle biopsies. An unpaired two-tailed t.test was used for statistical comparisons  
42 of WT and  $Dmd^{mdx-4Cv}$  groups. T.test p-value \*\*\*\*p<0.0001.

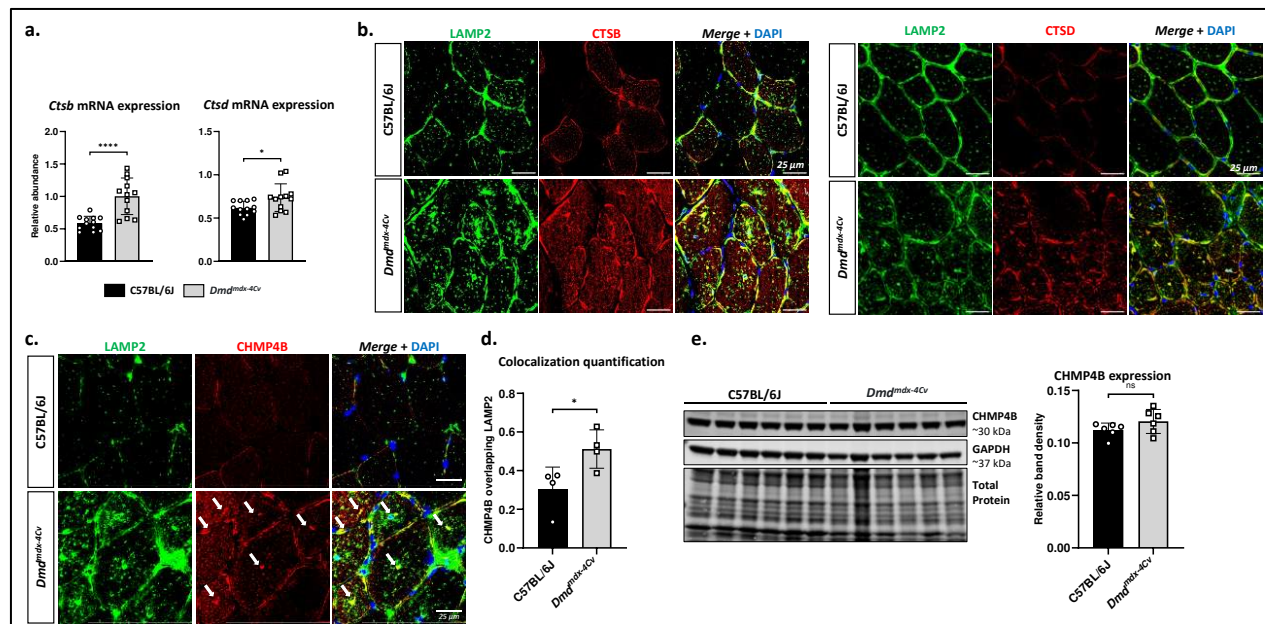
43



44

45 **Figure S4. Detection of LMP in LGMDR5 ( $\gamma$ -Sarcoglycanopathy).** **a)** Representative confocal images of  
 46 transversal sections of GA muscles from 2-months old WT and Sgcg KO mice, immunostained for LAMP2  
 47 (green) and LGALS3 (red). **b)** Quantification of LAMP2+ LGALS3+ puncta per myofiber in the GA muscle.  
 48 Data are presented as scatter plot with median ( $n > 338$ ). **c)** Representative confocal images of transversal  
 49 sections from muscles of a LGMDR5 patient and a healthy control immunostained for LAMP2 and LGALS3.  
 50 Left panels show H&E labeling from the same muscle biopsies.

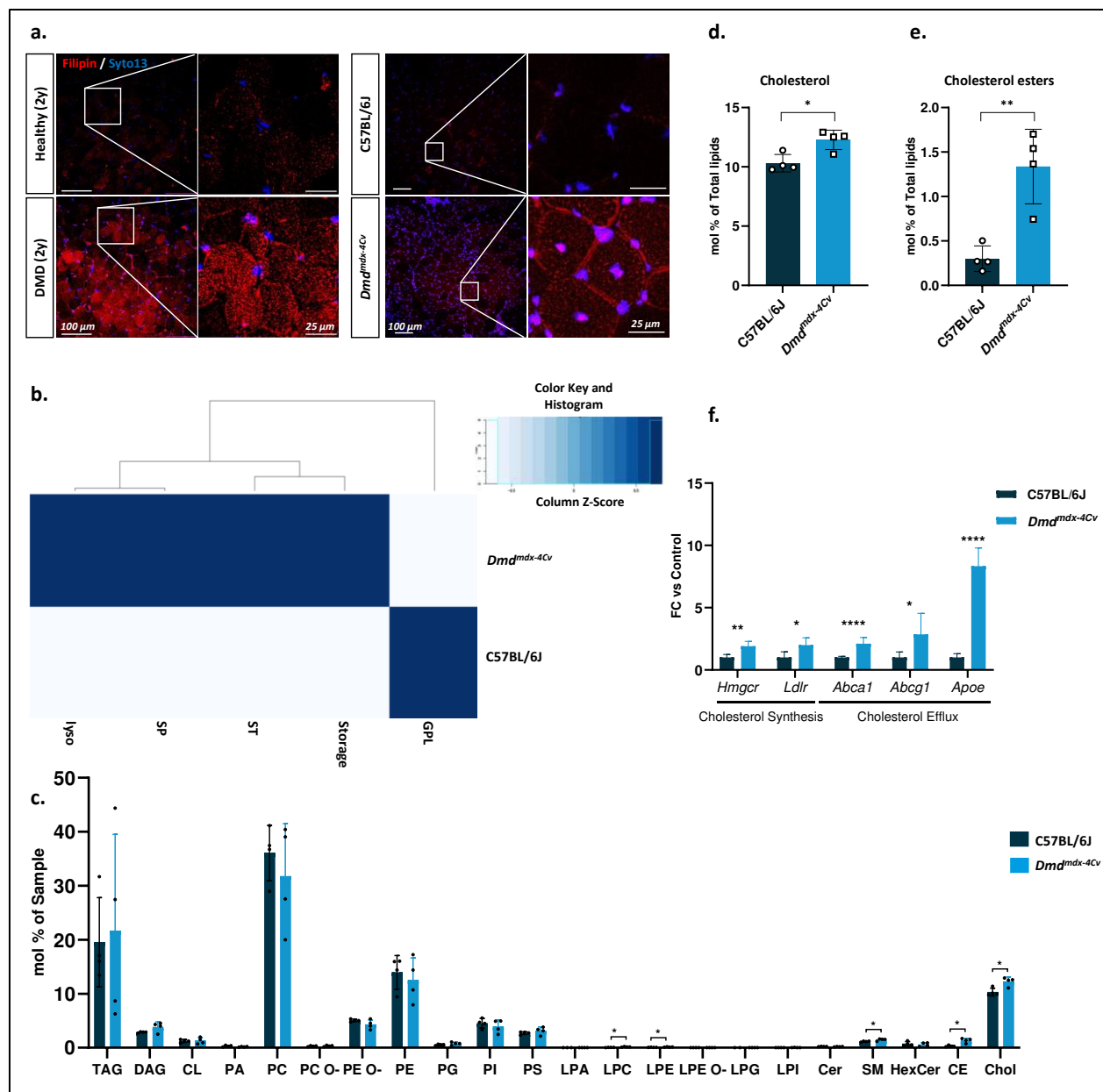
51



52

53 **Figure S5. Activation of lysosomal repair pathway in *Dmd*<sup>mdx-4Cv</sup> muscle. a)** Relative mRNA expression of  
 54 *Ctsb* and *Ctsd* in the TA, normalized to *Rplp0*. Scatter plots represent average ± SD (n=12). **b)** Representative  
 55 confocal images of TA transversal sections immunostained for Cathepsin B (CTSB) or Cathepsin D (CTSD)  
 56 and LAMP2. **c)** Representative confocal images of TA transversal sections immunostained for CHMP4B and  
 57 LAMP2. **d)** Quantification of CHMP4B signal overlapping LAMP2 from images of (c) (n=4). **e)** Western blot  
 58 analysis of TA muscle for CHMP4B, and band density quantification of CHMP4B, normalized to GAPDH  
 59 (average ± SD) (n=6). An unpaired two-tailed t.test was used for statistical comparisons of WT and *Dmd*<sup>mdx-</sup>  
 60 <sup>4Cv</sup> groups. T.test p-value \*p < 0.05, \*\*\*p < 0.001 \*\*\*\*p < 0.0001.

61

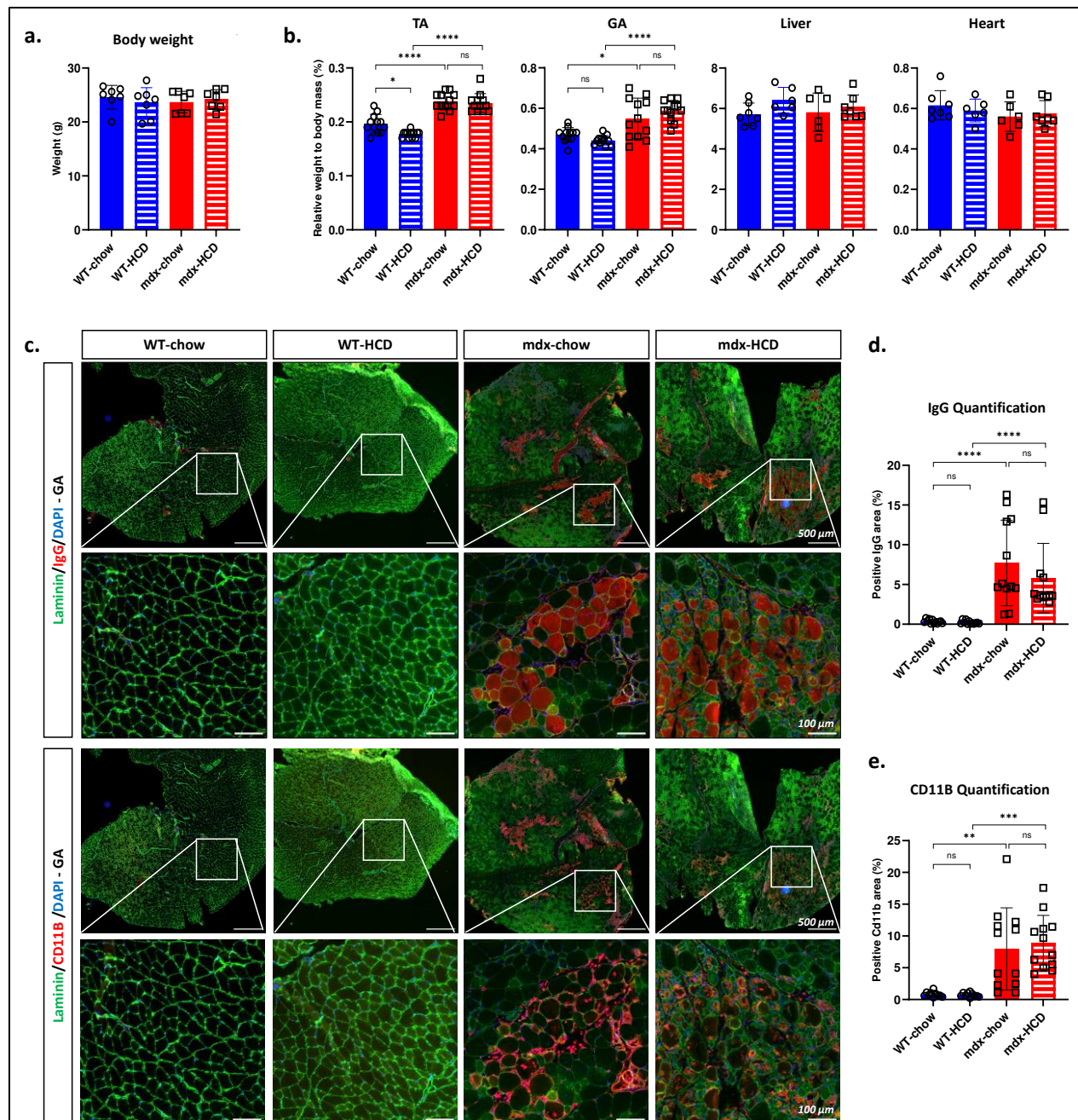


62

63 **Figure S6. Lipid Perturbations in DMD.** **a)** Representative confocal images showing filipin labeling of  
 64 transversal muscle cross sections from a DMD patient and healthy control, and a *Dmd<sup>mdx-4Cv</sup>* mice and a WT  
 65 control (GA muscle). **b)** Heat-Map displaying functional clustering of lipids in GA muscle from 7-week-old  
 66 *Dmd<sup>mdx-4Cv</sup>* mice versus control WT (GPL= glycerophospholipids, ST= sterols, SP= sphingolipids, lyso=  
 67 lysophospholipids) (n=4). **c)** Scatter plots showing different classes of lipids (average  $\pm$  SD). T-Test p-value  
 68 \*p < 0.05 \*\*<0.01. Chol = Cholesterol; CE = Cholesterol Esters; HexCer = hexosylceramide; SM =

69 *Sphingomyelin; Cer = Ceramide; LPI = lyso-Phosphatidylinositol; LPG = lyso-Phosphatidylglycerol; LPE O- =*  
70 *lyso-Phosphatidylethanolamine (-ether); LPE = lyso-Phosphatidylethanolamine; LPC = lyso-*  
71 *Phosphatidylcholine; LPA = lyso-phosphatidate; PS = Phosphatidylserine; PI = Phosphatidylinositol; PG =*  
72 *Phosphatidylglycerol; PE O- = Phosphatidylethanolamine (-ether); PE = Phosphatidylethanolamine; PC O- =*  
73 *Phosphatidylcholine (-ether); PC = Phosphatidylcholine; PA = Phosphatidate; CL = Cardioplin; DAG =*  
74 *Diacylglycerol; TAG = Triacylglycerol. **d-e)** Scatter plots (average  $\pm$  SD) showing increase of cholesterol and*  
75 *cholesterol esters in GA muscle of *Dmd<sup>mdx-4Cv</sup>* mice compared to WT controls. T-test p-value \*p < 0.05*  
76 *\*\*<0.01. **f)** Relative mRNA expression of different genes involved in cholesterol homeostasis, normalized to*  
77 **Rplp0*. Scatter plots represent average  $\pm$  SD of Fold change compared to WT mice. T-test p-value \*p < 0.05*  
78 *\*\*<0.01 \*\*\*\*<0.0001 (n=5-6).*

79

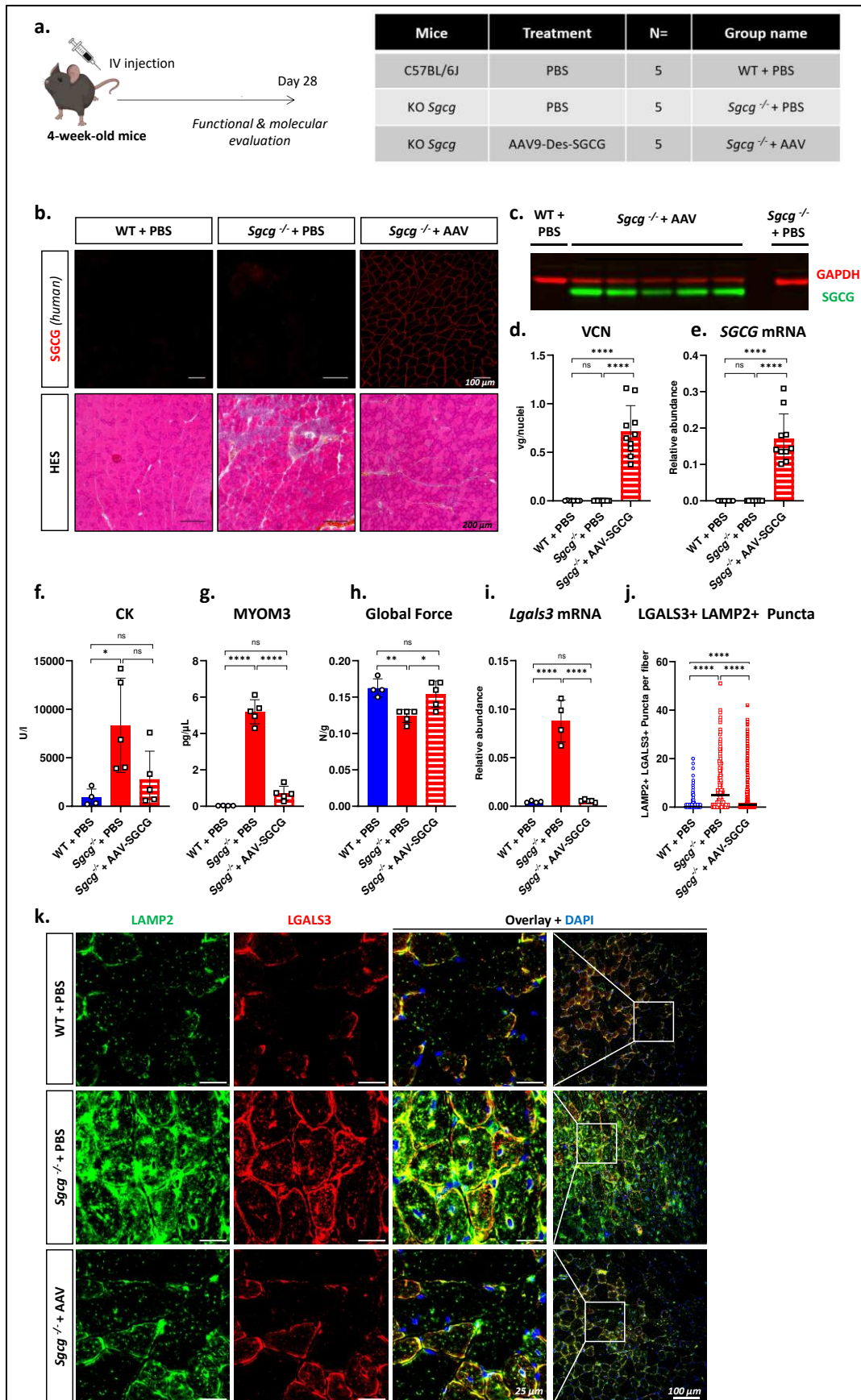


80

81 **Figure S7. High Cholesterol diet does not affect body and muscle weights in mice and does not increase**  
 82 **inflammation or sarcolemma fragility in dystrophic mice. a) Body weigh measurement of mice after 4**  
 83 **weeks of standard or high cholesterol diet (n=7). Data are presented as scatter plot with average  $\pm$  SD.**  
 84 **ANOVA test yield no significant differences across all groups. b) Muscle and tissue weight upon sacrifice,**  
 85 **normalized to mice body weight. Data are presented as scatter plot with average  $\pm$  SD (n=12 for GA and TA,**

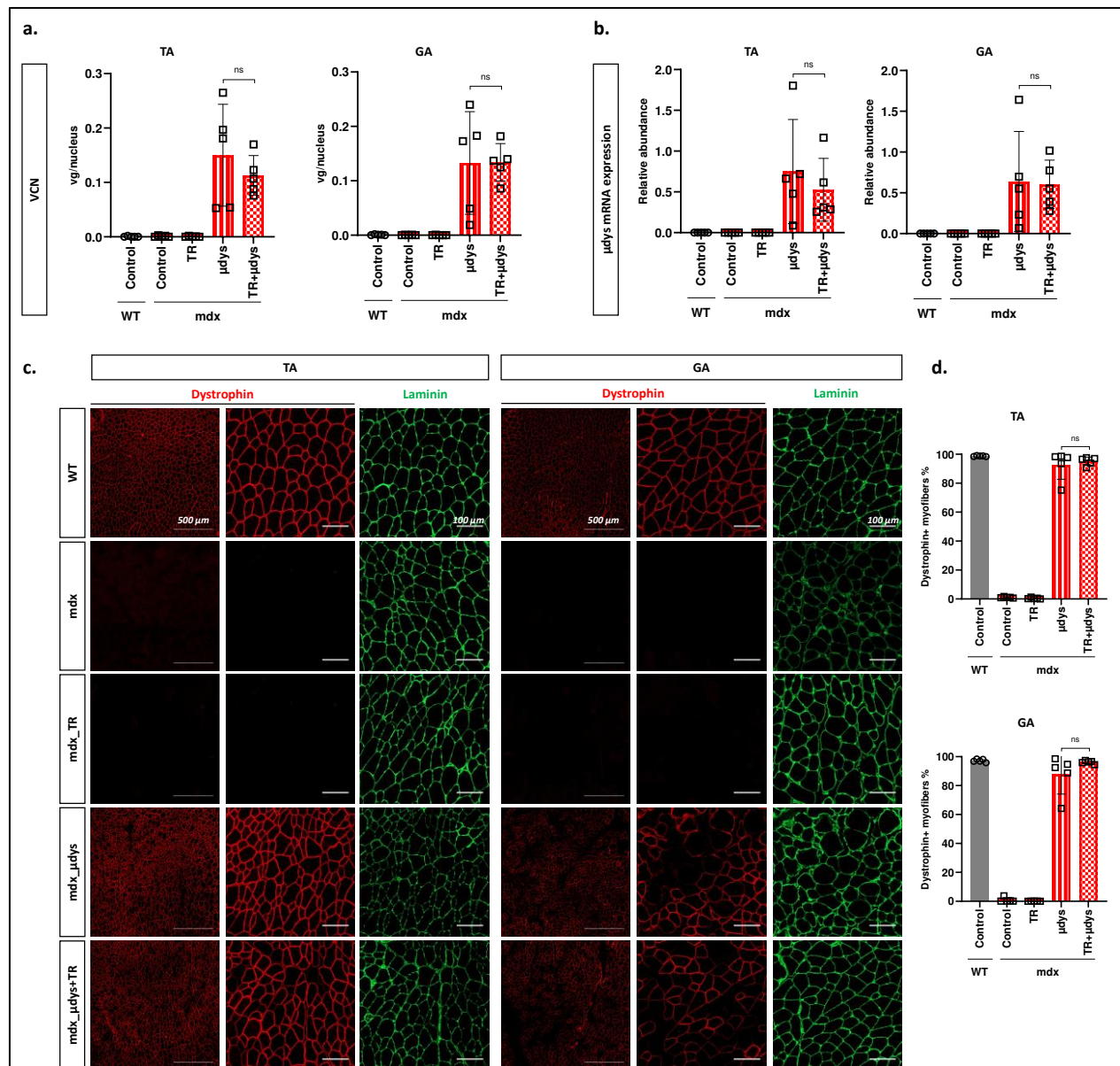
86 *left and right muscles were weighted, n=6 for other tissues). ANOVA p-value \*p < 0.05 \*\*\*\*<0.0001. c)*  
87 *Representative images of GA muscle serial cross-sections labeled with Laminin, mouse IgG and CD11b. d-*  
88 *e) Quantification of IgG and CD11b positive areas on whole muscle cross-sections (n=12, 2 cross-sections*  
89 *per mouse were quantified). ANOVA p-value \*\*p < 0.01 \*\*\*<0.001 \*\*\*\*<0.0001 ns=non-significant.*

90



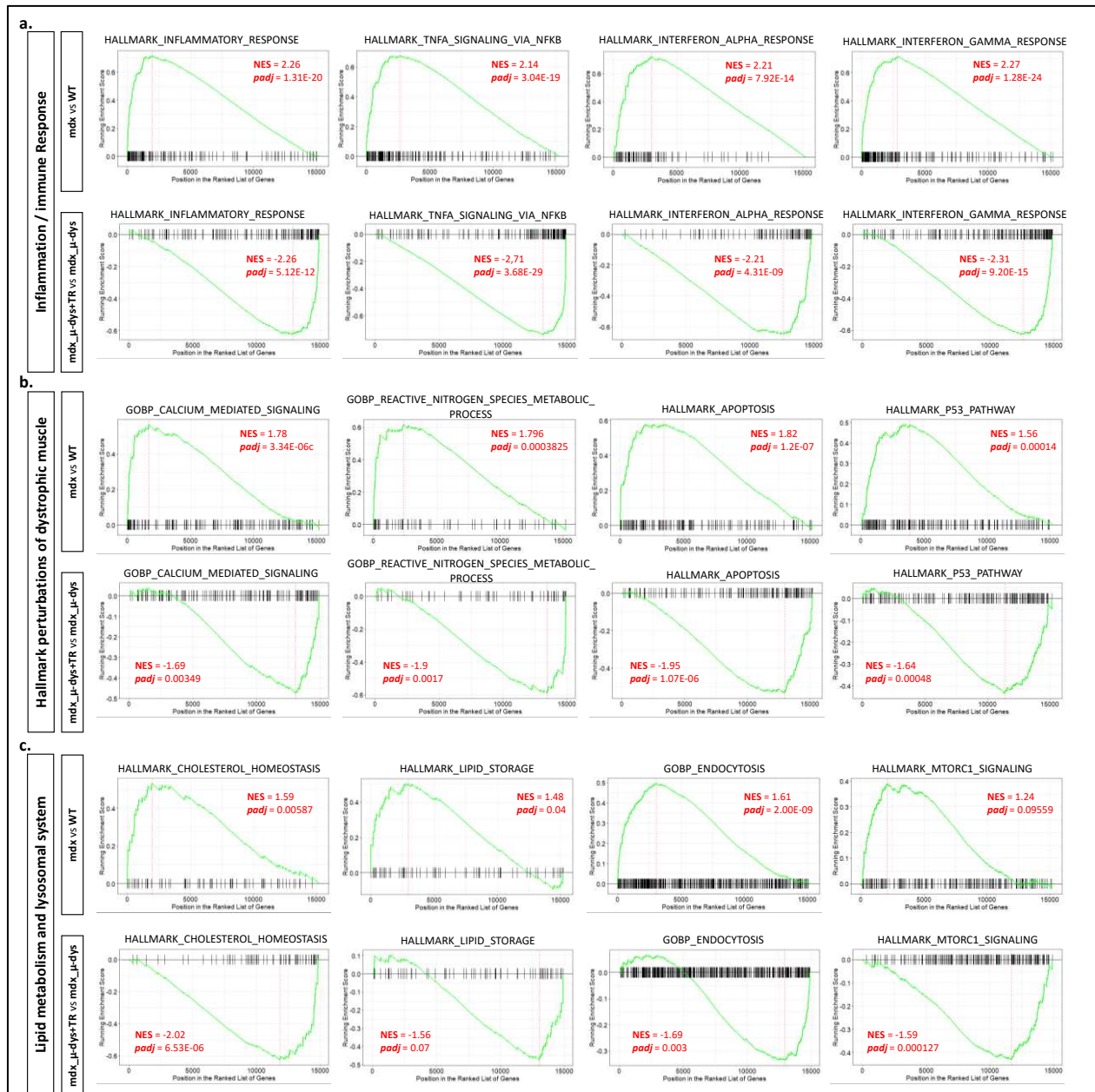
92 **Figure S8. Lysosomal damage is partially corrected by gene therapy in *Sgcg*<sup>-/-</sup> mouse model. a)** Schematic  
93 representation of study set-up. 4-week-old *Sgcg*<sup>-/-</sup> mice were injected intravenously with a rAAV9  
94 encapsulating the human sequence of SGCG, under the control of a desmin promoter, at a dose of 2e13  
95 vg/kg. **b)** Histological characterization of GA muscle. Top panel: representative images of GA cross-sections  
96 immunostained with antibody specific for the human SGCG. Bottom panel: representative images of GA  
97 cross-sections labeled with HES. **c)** Western blot analysis of GA muscles for the expression of human SGCG.  
98 GAPDH is used as loading control. **d)** Viral copy number (VCN) quantification in the GA muscle. Data are  
99 presented as scatter plot (average  $\pm$  SD) ( $n=10$ , right and left GA muscles are analyzed). **e)** Relative SGCG  
100 mRNA expression in the GA normalized to *Rplp0*. Scatter plots represent average  $\pm$  SD. **f)** Dosage of CK in  
101 serum of mice 4-weeks post-injection. Data are presented as scatter plot (average  $\pm$  SD). **g)** ELISA  
102 quantification of MYOM3 in the serum of the mice 4-weeks post injection. Data are presented scatter plot  
103 (average  $\pm$  SD). **h)** Global force evaluation by an escape test before sacrifice of mice. Data are presented as  
104 scatter plot (average  $\pm$  SD) of global force normalized to mice body weight. **i)** Relative *Lgals3* mRNA  
105 expression in the GA normalized to *Rplp0*. Scatter plots represent average  $\pm$  SD. **j)** Quantification of double  
106 positive puncta (LAMP2+LGALS3+) in the myofibers of GA muscles. Data are represented as scatter plots  
107 with median ( $n>338$ ). **k)** Representative confocal images of transversal sections of GA muscle  
108 immunostained for LAMP2 (green) and LGALS3 (red). An ANOVA test with Tukey multiple comparison was  
109 used for all statistical comparisons. ANOVA *p*-value \* $p<0.05$ , \*\* $p<0.05$ , \*\*\* $p<0.001$ , \*\*\*\* $p<0.0001$ ,  
110 *ns*=non-significant.

111



112

113 **Figure S9. Trehalose does not affect rAAV infectivity or transgene expression. a)** Viral copy number (VCN)  
 114 **quantification in the TA and GA muscles. Data are presented as scatter plot (average ± SD). b)** Relative μdys  
 115 **mRNA expression in the TA and GA muscles, normalized to Rplp0. Scatter plots represent average ± SD. c)**  
 116 **Representative fluorescence images of transversal sections of TA and GA muscles immunostained for**  
 117 **Dystrophin (N-terminal) and Laminin. d)** Quantification of Dystrophin positive fibers in the TA and GA  
 118 **muscles. Data are presented as scatter plots (average ± SD). An ANOVA test with Tukey multiple comparison**  
 119 **was used for all statistical comparisons. ANOVA p-value ns=non-significant.**



121

122 **Figure S10. Gene set enrichment analysis (GSEA) of various dysregulated pathways. a) Pathways related**  
 123 **to inflammation and immune response. b) Hallmark dysregulated pathways in the dystrophic muscle,**  
 124 **including calcium signaling, reactive nitrogen species stress and apoptosis. c) Dysregulated pathways**  
 125 **related to lipid metabolism (cholesterol homeostasis, lipid storage) and lysosomal system (endocytosis).**  
 126 **MTORC1 signaling is known to act on both lipid metabolism and trafficking, and on the lysosomal system.**

127 Upper panels represent a comparison between mdx and WT. Lower panels represent a comparison between  
128  $\mu$ dys only and  $\mu$ dys+trehalose treated groups. NES: Normalized enrichment score, padj: BH-adjusted p-  
129 value.

130

131 **Supplementary Table 1: Patients' biopsies details**

Case number	Disease	Mutation	Age
Patient 1	Dystrophinopathy	DMD del<13-36>	2 years
Patient 2	Control	-	2 years
Patient 3	Dystrophinopathy	DMD deletion <53-55>	3 years 10 months
Patient 4	Control	-	3.5 years
Patient 5	Sarcoglycanopathy	gSARC mutation homo del525T	9 years
Patient 6	Control	-	9 years

132

**Supplementary Table 2:** Table of primers used for qPCR and ddPCR analysis.

Application	Primer	Forward (5'-3')	Reverse (5'-3')	Probe (for taqman assays)
<b>Taqman</b>	ITR-GNT	CTCCATCACTAGGGTTCCTTG	GTAGATAAGTAGCATGGC	TAGTTAATGATTAACCC
	ITR-2	GGAACCCCTAGTGATGGAGTT	CGGCCTCAGTGAGCGA	CACTCCCTCTCTGCGCGCTCG
	<i>Rplp0</i>	CTCCAAGCAGATGCAGCAGA	ATAGCCTTGCGCATCATGGT	CCGTGGTGCTGATGGGCAAGAA
	<i>μdys</i>	GCACCACCAGATGCACTAT	GTGTAGGCGTAGCTCTTGAAT	CAGGGCTATGAGAGAACCAGCAGC
<b>SYBR</b>	<i>Rplp0</i>	AGATTCGGGATATGCTGTTGGC	TCGGGTCCTAGACCAGTGTTTC	
	<i>μdys</i>	GATTGAGAAGCTGCTGGACC	TCTGGTGGTGTAGCTGGAAG	
	<i>Lgals3</i>	AGACAGCTTTTCGCTTAACGA	GGGTAGGCACTAGGAGGAGC	
	<i>Ctsb</i>	TCCTTGATCCTTCTTTCTTGCC	ACAGTGCCACACAGCTTCTTC	
	<i>Ctsd</i>	GCTTCCGGTCTTTGACAACCT	CACCAAGCATTAGTTCTCCTCC	
	<i>Hmgcr</i>	TTGACGCTCTTGGAATGC	AGTTGGCCAACACTGACATG	
	<i>Ldlr</i>	ACTCAGACGAACAAGGCTGTC	GTCTCCATCACACACAAACTGC	
	<i>ApoE</i>	TGCTGTTGGTCACATTGCTG	TAATCCCAGAAGCGGTTTCAGG	
	<i>Abca1</i>	TGGTGATGCGGAAGTTTCTG	TTGTCACAACCTGGCTTCAGG	
	<i>Abcg1</i>	CTTCCTACTCTGTACCCGAGG	CGGGGCATTCCATTGATAAGG	

**Supplementary Table 3:** Antibodies details for western blotting

Antibody	Supplier / Reference	Species	Dilution
Anti-CHMP4B	ProteinTech group, 13683-1-1P	Rabbit Polyclonal	1:500
Anti-GAPDH	Sigma, G9545	Rabbit Polyclonal	1:1000
Anti-GAPDH	Sigma, PLA03023	Goat Polyclonal	1:1000

Anti-LAMP2	Abcam, Ab13524	Rat monoclonal	1:1000
Anti-LC3B	Sigma, L7543	Rabbit Monoclonal	1:1000
Anti-LGALS3	R&D, AF1197	Goat Polyclonal	1:1000
Anti-SGCG	Abcam, ab203112	Rabbit Monoclonal	1:2000
Anti-SQSTM1	Sigma, P0067	Rabbit Polyclonal	1:1000
Anti-ALIX	ProteinTech group, 12422-1-AP	Rabbit Polyclonal	1:2000

**Supplementary Table 4:** Primary antibodies used for immunofluorescence.

<b>Antibody</b>	<b>Supplier / Reference</b>	<b>Species</b>	<b>Dilution</b>
Anti-ALIX	Santacruz, sc-53540	Mouse monoclonal IgG1	1:50
Anti-CTSB	Cell Signaling, 31718	Rabbit monoclonal	1:400
Anti-CTSD	Abcam, ab75852	Rabbit monoclonal	1:100
Anti-CD11B	BD Pharmingen, 550282	Rat monoclonal	1:40
Anti-CHMP4B	ProteinTech group, 13683-1-AP	Rabbit polyclonal	1:200
Anti-Dystrophin	Leica, DYSB	Mouse monoclonal IgG1	1:50
Anti-LAMP2	Abcam, Ab13524	Rat monoclonal	1:200
Anti-LAMININ	Abcam, ab11576	Rat monoclonal	1:200
Anti-LAMININ	Invitrogen, PA1-1673	Rabbit polyclonal	1:500
Anti-LC3B	Sigma, L7543	Rabbit polyclonal	1:100
Anti-LGALS3	Santacruz, Sc-32790	Mouse monoclonal IgG1	1:50
Anti-SQSTM1	Sigma, P0067	Rabbit polyclonal	1:100
Anti-TFEB	ThermoFisher Scientific, A303-673A	Rabbit polyclonal	1:100

**Supplementary Table 5: Secondary Antibodies**

Application	Antibody
<b>Western Blot</b>	Licor, 926-68024, Donkey Anti-Goat 680
	Licor, 926-32214, Donkey Anti-Goat 800
	Licor, 926-68073, Donkey Anti-Rabbit 680
	Licor, 926-32213, Donkey Anti-Rabbit 800
	Licor, 926-32219, Donkey Anti-Rat 800
<b>Immunofluorescence</b>	Invitrogen, A11006, Goat-anti Rat 488
	Invitrogen, A21094, Goat-anti Rat 633
	Invitrogen, A11005, Goat-anti Mouse A594
	Invitrogen, A21125, Goat anti-Mouse IgG1 A594
	Invitrogen, A11008, Goat-anti Rabbit A488
	Invitrogen, A11037, Goat-anti Rabbit A594

## II- Detection of Lysosomal Membrane Permeabilization in Various Muscle Disorders

Following the identification of LMP in both DMD and LGMDR5, we aimed to evaluate if LMP also occurs in other LGMDs and muscle disorders. To achieve this, we immunostained muscle cross-sections from various animal models and patient samples for LAMP2 and LGALS3.

In our mouse models for LGMDR3 (alpha-sarcoglycanopathy) and LGMDR9 (FKRP deficiency), positive LGALS3 staining was detected within the myofibers of tibialis anterior (TA) muscle, colocalizing with LAMP2 (**Figure 27**). The staining was more pronounced in the alpha-sarcoglycanopathy model. Additionally, a muscle biopsy from a dysferlinopathy patient (LGMDR2) exhibited a positive pattern of LAMP2 and LGALS3 within some myofibers (**Figure 27**).

We also analyzed a muscle biopsy from an infantile Pompe disease (GSDII) patient (**Figure 27**). Pompe disease, a lysosomal storage disorder affecting multiple tissues including skeletal muscle, is characterized by glycogen accumulation in lysosomes, leading to deregulation of lysosome metabolism and structure. Thus, it serves as a positive control for lysosomal damage in muscle. Immunostaining for LAMP2 and LGALS3 confirmed a high degree of LMP, affecting all muscle fibers.

Additionally, we examined a muscle biopsy from a dog model of Dynamin-2 related Autosomal Dominant Centronuclear Myopathy (ADCNM) <sup>[466]</sup> (**Figure 27**). Strong LGALS3 staining colocalizing with LAMP2 was detected within the myofibers. However, the staining pattern differed from that observed in DMD, LGMDs, or Pompe disease, showing strong expression localized at the center of the myofiber, likely related to organelle aggregation in centronuclear myopathies <sup>[467]</sup>.

These supplementary data are part of an ongoing study to evaluate Gal-3 expression and localization in various hereditary and acquired muscle disorders. Interestingly, we detected LMP in muscular dystrophies (DMD, multiple LGMDs), a metabolic myopathy (Pompe disease), and a congenital myopathy (ADCNM). Remarkably, each class of myopathy exhibited positive staining, though with distinct patterns.

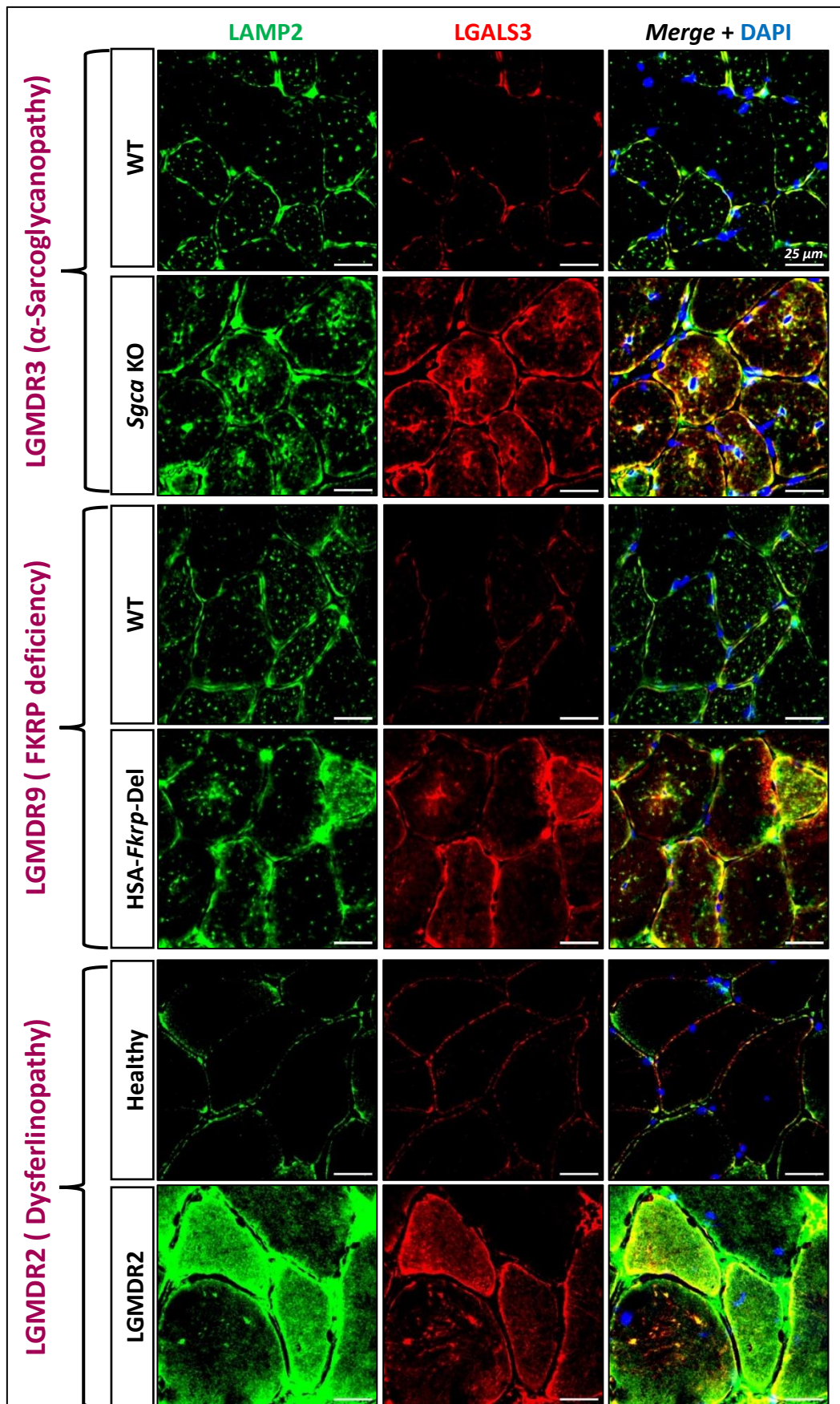


**Figure 27. Detection of lysosome damage in different forms of LGMD.** Representative confocal images of muscle cross-sections immunostained for LAMP2 (green) and LGALS3 (red). First panel is from TA muscles of *Sgca* KO mouse and WT control mice. Second panel shows TA muscles from muscle-specific *Fkrp* KO mouse model and WT controls. Third panel shows muscle biopsies from a dysferlinopathy (LGMDR2) patient and healthy control.

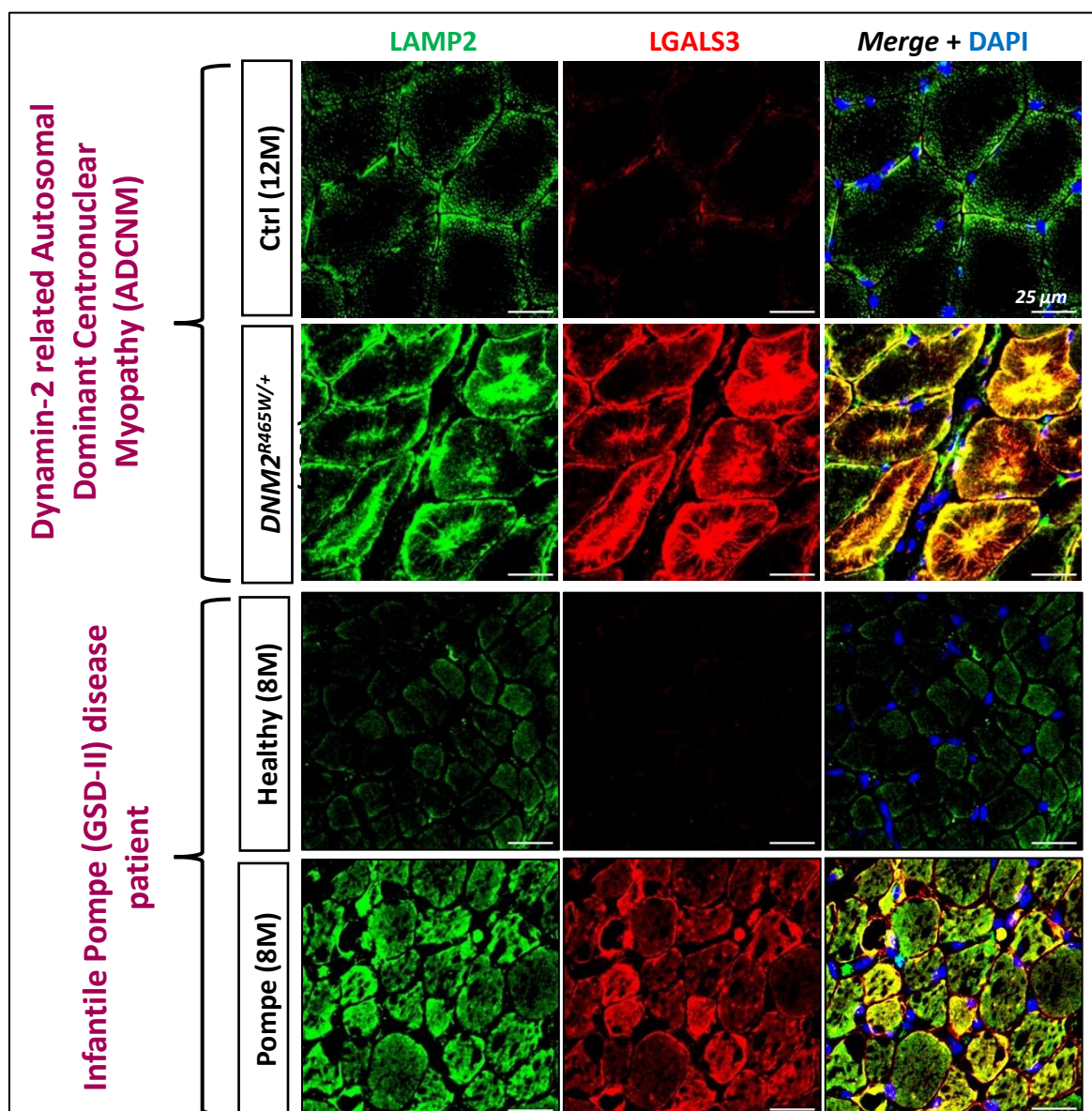


**Figure 28. Detection of lysosome damage in congenital myopathy and Pompe disease.** Representative confocal Images of muscle cross-sections immunostained for LAMP2 (green) and LGALS3 (red). First panel represent muscle cross sections from a dog model for dynamin-2

*related autosomal dominant centronuclear myopathy (ADCNM and WT control. Second panel shows muscle cross sections from an 8-month-old Pompe disease patient and healthy control.*

# DISCUSSION

## I- Summary

Ever since the identification of *DMD* and dystrophin as the causative gene and protein for DMD [43,52], the prevailing view of DMD pathophysiology has emphasized mechanical stress on the sarcolemma, leading to destabilization of myofibers and subsequent degeneration [53]. Recently, however, interest has grown in metabolic disturbances in DMD [107], particularly mitochondrial dysfunction [107,143,144,468]. Additionally, recent studies, including ours, have highlighted lipid perturbations in DMD, especially concerning cholesterol metabolism [142,164,469]. Such disruptions of cholesterol metabolism are often linked with lysosomal damage in both neurodegenerative diseases and LSDs [470,471]. For instance, in Niemann-Pick Disease Type C, the accumulation of undegraded lipids in the lysosome impairs its function [372], leading to cellular dysfunction and the onset of diverse neurological manifestations [372,472]. This led us to hypothesis that, similar to LSDs, excess cholesterol might accumulate in the endolysosomal system in dystrophic muscle, causing lysosomal dysfunction. This hypothesis is supported by previous studies reporting alterations of lysosome structure [446], function [449], autophagy perturbation [153,155] and overexpression of cathepsins in DMD [448,450,451].

To assess the lysosomal function in DMD, we started by evaluating Gal-3, a validated marker of LMP, in various animal models of DMD and patient muscle samples. Although Gal-3 overexpression had been previously reported in DMD [458,459], it was attributed to Gal-3 positive infiltrating macrophages [461]. Our study confirmed Gal-3 overexpression inside the myofibers of dystrophic muscle, and its localization to enlarged lysosomes, indicating LMP. Beyond DMD, we detected LMP in other muscle disorders, including LGMDs (LGMDR5, LGMDR3, LGMDR2, LGMDR9), centronuclear

myopathy related to Dynamin-2 and Pompe disease, suggesting that LMP might be a common pathological hallmark for various muscle disorders. Further validation and characterization of lysosomal perturbations in DMD revealed an increased number and size of lysosomes, cathepsin leakage, activation of the endolysosomal damage response, and defects in autophagy.

Notably, we demonstrated that previously reported autophagy defects <sup>[153,155,156]</sup> might be due to impaired autophagosome-lysosome fusion, secondary to a perturbations in lysosomal function and structure.

To better understand the correlation between cholesterol accumulation and LMP, WT and *Dmd*<sup>mdx-4Cv</sup> mice were fed a cholesterol-rich high-fat diet. While both WT and dystrophic mice showed increased cholesterol load in skeletal muscle, lysosomal cholesterol accumulation, lysosome damage, and fibrosis were significantly more pronounced in the muscle of HCD-fed dystrophic mice compared to those on a standard diet and HCD-fed healthy controls. This indicates a direct causative relationship in this model between elevated cholesterol, lysosomal damage, and the exacerbation of dystrophic parameters.

Following these discoveries, we evaluated the effect of two gene therapies on correcting lysosomal damage. The first therapy involved delivering microdystrophin in the *Dmd*<sup>mdx</sup> mouse model, while the second involved delivering the full-length gamma-sarcoglycan gene in an LGMDR5 mouse model. We observed a dose-relationship, with LMP decreasing as the injected dose of AAV- $\mu$ dys increased. However, significant residual lysosomal damage persisted even in mice treated with a high dose of AAV- $\mu$ dys, which transduces nearly 100% of the myofibers. Interestingly, gene therapy in the LGMDR5 model showed a more effective correction of LMP and overall better recovery of dystrophic features.

Given the insufficiency of microdystrophin gene therapy in fully correcting lysosomal damage, we explored the potential of combining it with a complementary treatment targeting these damages. Trehalose was selected due to its good safety profile as an FDA-approved excipient and dietary supplement <sup>[473]</sup>, and recent studies showing its beneficial effect on restoring lysosomal function in neurodegenerative diseases <sup>[406,407]</sup>. We compared mice treated with either trehalose alone, a suboptimal dose of AAV- $\mu$ dys, or a combination of both treatments. Trehalose alone showed beneficial effects, particularly in correcting LMP and myofiber permeabilization. Importantly, the best therapeutic outcomes were observed in mice receiving the combined therapy, with improvements in overall muscle force, muscle histology, circulating biomarkers, and transcriptomic signature.

In summary, our investigation underscores a previously overlooked and critical role of lysosomal damage in the pathophysiology of DMD. In the *Dmd*<sup>mdx</sup> model, this damage is only partially corrected by  $\mu$ -dystrophin-based gene therapy. We demonstrate that trehalose can significantly alleviate this damage, especially when used in combination with gene therapy to restore functional dystrophin expression. This dual approach, addressing both lysosomal damage and restoring functional dystrophin expression, may offer a promising new therapeutic perspective for DMD.

In the following sections, we will discuss in detail the various results and questions arising from this work.

## **II- Lysosomal Damage Contributes to the Pathogenesis of Muscular Dystrophies**

### **II.1 Galectin-3 overexpression in dystrophic muscle correlates with lysosomal membrane permeabilization and lysosomal stress**

In order to study lysosomal function, we needed a reliable biomarker of lysosomal damage. Gal-3 has been reported to be recruited to damaged lysosomes, making it a sensitive indicator of LMP [386]. However, its assessment in muscle tissue within this context has been limited. To address this, we began by examining Gal-3 expression in WT muscle cells. We found that Gal-3 is expressed in myotubes, and its expression increases when cells are treated with lysomotropic compound (LLOMe), forming puncta that indicate damaged lysosomes. Interestingly, Gal-3 expression and puncta decreased after 3 hours, suggesting effective repair and elimination of damaged lysosomes [412]. The appearance of Gal-3 puncta, indicating LMP, was associated with lysosomal de-acidification, leading to impaired lysosomal function. Gal-3 puncta and expression inversely correlated with secreted Gal-3 in the media detected 3 hours later, suggesting that circulating Gal-3 might be originating from damaged myofibers.

We further demonstrated that Gal-3 is significantly overexpressed in the myofibers of dystrophic muscle, evident in various muscles of the *Dmd<sup>mdx</sup>* mouse model at a young age, as well as in the muscles of GRMD dog model and patient muscle biopsies. Immunostaining showed a colocalization of Gal-3 with lysosomal marker (LAMP2) inside the dystrophic myofibers, indicating LMP. By isolating myofibers from *Dmd<sup>mdx</sup>* mice, we confirmed that Gal-3 overexpression originates at least partially from the myofibers themselves, not solely from infiltrating immune cells as reported previously [461]. Gal-3 was also significantly upregulated in the serum of *Dmd<sup>mdx</sup>* mice, though this upregulation was less pronounced than other circulating biomarkers for muscular dystrophy like CK or MYOM3. Additionally, since Gal-3 increases in the serum of various pathologies, such as heart, kidney and autoimmune diseases [474,475], it may not be as specific as biomarker for muscle damage.

Further analysis of isolated myofibers revealed an increase in lysosome number and the presence of damaged, enlarged lysosomes, indicating an accumulation of undegraded materials <sup>[296]</sup>. Interestingly, different populations of lysosomes were detected in the same myofibers: enlarged lysosomes which normally are accumulating undegraded materials <sup>[296]</sup>, average-sized lysosomes similar to WT myofibers, and smaller lysosomes. These smaller lysosomes could be fragments of lysosomal membranes generated during autophagic lysosomal reformation, a process crucial in muscle <sup>[334]</sup>. This presence of different lysosome populations suggests ongoing cycles of lysosomal damage and repair, with an intact population not positive for LGALS3, representing potentially recycled lysosomes after lysophagy or newly generated ones by the TFEB lysosome biogenesis pathway.

To determine if LMP is an early process in dystrophic pathogenesis or persists with disease evolution, we studied muscles of 1-year-old mice. These mice displayed significant amounts of LAMP2+/LGALS3+ puncta, showing that LMP is not resolved with disease progression. Interestingly, noticeable LMP was also detected in old WT mice compared to younger ones, suggesting a degradation of lysosomal function over time. Given that mitochondrial function and mitophagy degrade with age in muscle <sup>[137]</sup>, and mitophagy relies on healthy lysosomes, the interplay between these organelles merits further investigation in muscle biology.

To evaluate if lysosomal degradation was specific to DMD or common across muscular dystrophies, we studied mouse models of LGMDs, including LGMDR3, LGMDR5, and LGMDR9. Significant amounts of LAMP2+/LGALS3+ puncta were detected in these models, particularly in sarcoglycanopathies, which are closely related to DMD pathophysiology. LGMDR2 and LGMDR5 patients also displayed some LGALS3+/LAMP2+ puncta, although less than DMD patients' muscles, suggesting a correlation between phenotype severity and LMP occurrence. A muscle

biopsy from an infantile Pompe disease patient served as a positive control for lysosomal damage, displaying the most noticeable amount of LGALS3 expression in the myofibers.

Our identification of Gal-3 as an indicator of lysosomal damage in muscular dystrophies provides a new biomarker and indicates a new mechanism contributing to muscular dystrophy pathogenesis. However, protein or mRNA quantification may not accurately represent lysosomal damage, given that overexpression would also indicate the degree of inflammation. Therefore, specific quantification of LAMP2+/LGALS3+ spots within muscle fibers is required.

## **II.2 Activation of the endo-lysosomal damage response and interpretation of autophagy defects:**

The study of lysosomal damage in DMD muscle has revealed important insights into the mechanisms of lysosome replacement, removal, and repair, providing a broader understanding of the disease pathology. Lysosome damage activates the endolysosomal damage response, coordinated by proteins such as Gal-3 [387,412]. This response includes several pathways aimed at mitigating the damage, each playing a distinct role in the pathology of the muscle in DMD.

### **- ESCRT pathway:**

The ESCRT pathway plays a role in lysosomal membrane repair. Recruitment of ESCRT components like ALIX and CHMP4B at lysosomes in *Dmd*<sup>mdx-4Cv</sup> muscles indicates activation of this repair mechanism. However, the ESCRT pathway mainly repairs small-scale lysosomal damage [387,415,419], and given the extent of lysosomal damage in DMD muscle, replacement and elimination pathways might be more crucial.

- **Autophagy and Lysophagy:**

Autophagy defects in DMD muscle are well-documented [153,154], primarily attributed to mTOR hyperactivation suppressing autophagy initiation [155,156]. Our study confirmed autophagy defects in *Dmd*<sup>mdx-4Cv</sup> muscles, with overexpression of SQSTM1 and LC3-I. Additionally, we highlighted for the first time a decrease in the autolysosome ratio in dystrophic muscle, suggesting a defect in autophagosome-lysosome fusion. This fusion depends on the availability of acidic lysosomes, and LMP lowers lysosomal pH [453]. De-acidification of lysosomes is a known cause of autophagy defects in diseases unrelated to autophagy proteins [476,477]. Therefore, autophagy defects in DMD could be attributed to defective autophagosome-lysosome fusion, secondary to lysosomal damage.

Further analysis showed the activation of lysophagy in dystrophic muscle, observed through the colocalization of damaged lysosomes (LAMP2+/LGALS3+) and the autophagosome marker LC3B, indicating enlarged lysosomes sequestered by autophagosome double membranes. Additionally, our results showed a significant increase in the lysophagy ratio in dystrophic muscle. This shift of the autophagic machinery to eliminate damaged lysosomes could saturate the available autophagy machinery, leading to a decrease in other specific autophagy pathways [312].

Comparing DMD with lysosomal storage diseases like Pompe disease reveals similar pathogenic mechanisms. In Pompe disease, glycogen accumulation activates lysophagy, leading to autophagic overload and fusion defects [478,479], despite the downregulation of mTOR signaling which would typically activate autophagy [478]. This comparison underscores the shared processes contributing to disease pathology in both conditions.

The resulting oxidative stress and inflammatory response in Pompe disease parallels also observations in DMD, suggesting that lysosomal defects might be central to autophagic blockade and disease pathology [479].

- **Lysosomal biogenesis pathway:**

The lysosomal biogenesis pathway, regulated by the transcription factor TFEB, is crucial for replacing damaged lysosomes [433]. In dystrophic muscle, the nuclear localization of TFEB indicates the activation of this pathway. This activation is further supported by the upregulation of TFEB target genes related to lysosome structure and function, suggesting an ongoing replacement process for damaged lysosomes. Notably, TFEB activation is particularly prominent in centronucleated fibers (regenerative fibers) in *Dmd*<sup>mdx-4Cv</sup> muscles, pointing to a potential difference in lysosomal biogenesis between regenerative and damaged fibers, which warrants further investigation.

- **Other mechanisms to investigate:**

Recently, additional mechanisms of the endolysosomal damage response have been identified. These include lipid transfer-mediated repair via the phosphoinositide-initiated membrane tethering and lipid transport (PITT) pathway, and stress granule plug-mediated membrane stabilization. Additionally, lysosomal exocytosis has been reported as a mechanism for the elimination of damaged lysosomes. Evaluating these mechanisms in the context of DMD would be of significant interest.

### **II.3 Cathepsin overexpression and implications**

Cathepsins, a family of lysosomal proteases regulated by TFEB, are highly upregulated in DMD muscle. Although their overexpression in DMD was previously reported [448,450,451], the underlying mechanisms were unclear. Our study suggests that cathepsin upregulation may result from lysosomal damage and subsequent TFEB

activation. Immunostaining reveals a diffuse pattern of cathepsin B and D, indicating LMP and leakage into the cytosol. This leakage is associated with cell death in various tissues and may contribute to myofiber degeneration in DMD [385]. The deleterious effects of cathepsins on muscular dystrophy pathogenesis are further highlighted by a study showing that deleting cathepsin S in *Dmd*<sup>mdx</sup> mice alleviates dystrophic symptoms [450]. Additionally, a recent study link cathepsin K overexpression to muscle injury or necrosis in DMD patients [480]. This case report described an asymptomatic dystrophinopathy patient with no muscle dystrophin expression, but reduced cathepsin K expression compared to symptomatic DMD patients, emphasizing cathepsin K overexpression as a direct contributor to DMD pathogenesis. Further research is warranted to fully characterize the expression and localization of different cathepsins in the dystrophic muscle, and their potential effect on myofiber degeneration, which would offer crucial insights towards potential novel therapeutic strategies.

## **II.4 Interplay between lysosomal damage and lipid perturbations**

Our previous study have highlighted lipid perturbation in DMD muscle [142], notably cholesterol accumulation in the muscle of DMD patients and *Dmd*<sup>mdx</sup> mice, along with the activation of the SREBP pathway responsible for cholesterol biosynthesis and uptake. This raised the critical question of whether and how excess cholesterol in dystrophic muscle contributes to the progression of DMD pathology. It has been suggested that DMD may be a primary dyslipidemia [163], and that excess cholesterol and circulating lipids can exacerbate the disease [163,164], presenting a potential therapeutic target [481]. However, few studies have focused on the effects of cholesterol in muscle, apart from its role in fiber structure and its consequent impact on muscle excitation/contraction [435].

### **II.4.1 Cholesterol and DMD phenotype**

The effect of cholesterol on the DMD phenotype was partly addressed by studies from the Bernatchez lab, which showed that increased cholesterol and lipids exacerbate the dystrophic phenotype in models of DMD and limb-girdle muscular dystrophy (LGMDR2). These studies used dystrophic mice crossed with *ApoE* knockout mice, which lack a gene involved in cholesterol efflux from peripheral tissues [163,469,482,483]. However, the *ApoE* gene is upregulated in the muscle of *Dmd*<sup>mdx</sup> mice, as we've shown, likely as a compensatory mechanism to eliminate excess cholesterol. Thus, silencing this gene in dystrophic mice, while exacerbating the phenotype, generates a biased model that does not accurately represent the deregulations of cholesterol metabolism in DMD.

#### **II.4.2 Cholesterol accumulation in the lysosome**

Building on our previous studies showing cholesterol overload in muscle and recent data indicating lysosomal damage, we hypothesized that cholesterol might accumulate in damaged lysosomes. To investigate the effect of cholesterol on muscle in both physiological and pathological contexts, WT and *Dmd*<sup>mdx-4Cv</sup> mice were placed on a cholesterol-rich diet. An increase in muscle fibrosis was observed only in dystrophic mice on this diet, indicating an exacerbation of the dystrophic phenotype. Our investigation confirmed that dystrophic muscle has a higher cholesterol load, which increases further in mice on a cholesterol-rich diet. Importantly, this cholesterol accumulation was localized in the lysosomes of dystrophic mice but not in WT mice. We also assessed the effect of the cholesterol-rich diet on lysosomal damage, finding a significant increase in lysosomal damage in *Dmd*<sup>mdx-4Cv</sup> mice on the diet, as evidenced by galectin puncta assay and increased Gal-3 protein and mRNA expression. Some puncta were also detected in WT mice on a high-fat diet, indicating that cholesterol accumulates in damaged lysosomes in the muscle and contributes to increased lysosomal damage.

### **II.4.3 Implications of cholesterol accumulation**

Although the accumulation of cholesterol and lipids in dystrophic muscle has been previously described <sup>[158,159]</sup>, the origin and consequences of these deregulations remain unclear. Our findings show that cholesterol primarily accumulates in the lysosomal lumen of dystrophic muscle, likely due to dysregulated intracellular cholesterol trafficking. This dysregulation can influence several metabolic pathways, including those mediated by SREBP transcription factors. These factors localize in the ER, and their activation and translocation to the nucleus depend on ER cholesterol levels. Thus, cholesterol accumulation in lysosomes and trafficking deregulation could be the origin of SREBP activation detected in *Dmd<sup>mdx</sup>* mice muscle <sup>[142]</sup>, leading to increased endogenous cholesterol biosynthesis and uptake. Moreover, cholesterol accumulation in lysosomes could impair autophagic flux <sup>[484,485]</sup>.

### **II.4.4 Cholesterol and lysosomal membrane permeabilization:**

Our study also showed that cholesterol accumulation correlates with LMP. Cholesterol and other lipid accumulation in lysosomes could indicate impaired lipid degradation and transport, following endolysosomal system defects, as seen in several LSDs <sup>[486]</sup>. Accumulation of cholesterol and other lipids in peripheral tissues could also cause lipotoxicity, affecting numerous cellular mechanisms, including oxidative stress, energy metabolism, immune system activation <sup>[487]</sup>, and lysosomal stress <sup>[371]</sup>.

However, recent studies on the endolysosomal damage response have identified a new repair pathway involving cholesterol transfer to the damaged lysosomal membrane, facilitating its repair <sup>[418,419]</sup> (described in **III.3.1.c**). It is possible that cholesterol accumulation results from LMP and the subsequent transfer of cholesterol to damaged lysosomes to mediate membrane repair. It can be hypothesized that SREBP activation and subsequent cholesterol upregulation in the dystrophic muscle

might be occurring to mitigate lysosomal damage. This hypothesis aligns with our recent combined therapy study involving AAV-microdystrophin and simvastatin <sup>[488]</sup>, a cholesterol-lowering drug inhibiting the SREBP pathway. In this study, simvastatin did not enhance the effect of microdystrophin but instead increased muscle necrosis <sup>[488]</sup>. One possible explanation for these findings is that while SREBP inhibition reduced cholesterol levels in the muscle, it also impaired lysosomal repair, leading to muscle degeneration.

In summary, our findings suggest that cholesterol accumulation in lysosomes plays a significant role in DMD pathology, linking lipid perturbations to lysosomal damage and muscle fibrosis. It remains to be determined whether cholesterol accumulation causes lysosomal damage or occurs as a result of pre-existing damaged lysosomes. Understanding these interactions may lead to new therapeutic strategies targeting cholesterol metabolism and lysosomal function in DMD.

## **II.5 Lysosomal defects in DMD: cause, consequences and therapeutic opportunities**

In our study, we have detected and characterized a range of lysosomal perturbations in DMD and other muscular dystrophies. However, the exact causes of these damages remain incompletely elucidated. One hypothesis we explored is lipid accumulation, which could disrupt lysosomal function, although lipid perturbation might also be a consequence of lysosomal dysfunction <sup>[371,372]</sup>. Another plausible cause is the excessive ROS in the dystrophic muscle, which can directly damage the lysosome <sup>[374,375,489]</sup>. Additionally, disorganization of the microtubule network, found in muscular dystrophies and crucial for lysosomal movement and function, could be a factor <sup>[92,119,490]</sup>. Nevertheless, the direct link between dystrophin absence (or the collapse of the DAGC as seen in many LGMDs) and lysosomal damage remains to be studied.

Lysosomal defects may play a major role in muscular dystrophy pathogenesis and evolution. In fact, lysosomal function is crucial for muscle health, playing a central role in maintaining cellular homeostasis and facilitating the turnover of cellular components through the degradation and recycling of macromolecules and organelles <sup>[491,492]</sup>. This process is essential for autophagy, which supports muscle adaptation and repair, particularly after exercise or injury <sup>[150,151,493]</sup>. Mitophagy, for instance, a specific form of autophagy that targets damaged mitochondria, is vital for maintaining muscle health and depends on lysosomal function <sup>[137,453,494]</sup>. Additionally, lysosomal exocytosis is crucial for sarcolemma repair, a necessary function given the constant mechanical stress exerted on the myofiber from muscle contraction <sup>[340,343,344]</sup>. Exocytosis also participates in the secretion of various factors important for overall body homeostasis and inter-organ crosstalk; for example, mature form of cathepsin B is secreted and play significant roles in maintaining central nervous system function and neurogenesis <sup>[495,496]</sup>. Lysosomes are also crucial for intracellular signaling, notably calcium signaling, essential for muscle contraction, and mTOR signaling, which regulates muscle growth <sup>[365,433,491]</sup>. Therefore, maintaining healthy lysosomes is essential for myofiber integrity, as LMP leads to the leakage of proteases, particularly cathepsins, which would activate LDCD <sup>[385,395]</sup> and may be contributing directly to myofiber degeneration.

In summary, lysosomal dysfunction in DMD might directly contribute to the pathogenesis of the disease and myofiber degeneration. It may lie at the center of metabolic perturbations in dystrophic muscle, affecting lipid metabolism, mitochondrial function, calcium and mTOR signaling, autophagy, and additionally sarcolemma repair, and cell death. We have detected lysosomal damage not only in DMD but also in many forms of LGMD and other muscle disorders. These findings

indicate that lysosomal damage is a previously underestimated but crucial pathological feature and a potential therapeutic target in various muscle diseases.

### **III- Targeting Lysosomal Damage in DMD Improve Microdystrophin Gene Therapy**

#### **III.1 Correction of LMP following gene therapy varies between the modality of gene therapy approaches in dystrophic models**

Following the identification of LMP in DMD, we sought to evaluate the efficacy of microdystrophin gene therapy in correcting lysosomal damage. While microdystrophin gene therapy is promising, with an approved drug already available, clinical functional improvements have not fully met the expectations set by preclinical studies [497]. This shortfall may be due to microdystrophin lacking several important domains of the full-length dystrophin protein, including parts of the central rod domain and C-terminal. Consequently, microdystrophin gene transfer may not correct all the pathological mechanisms present in dystrophic muscle. We also evaluated the effect of gene therapy in a LGMDR5 mouse model. In this model, in contrast with DMD gene therapy, we are able to restore the complete version of the missing gene, gamma-sarcoglycan.

For microdystrophin gene therapy in the *Dmd*<sup>mdx</sup> mouse model, we tested two doses of AAV9 (5E12 vg/kg and 3E13 vg/kg) delivering the microdystrophin coding sequence. As expected, a dose-dependent effect was observed in terms of restoration of muscle function and various biomolecular and histological parameters. Although higher doses resulted in significant overall dystrophic correction, there was still not a full restoration to WT mice level. Regarding lysosomal damage, a dose-response relationship was evident, with LMP, evaluated by the LGALS3+LAMP2+ puncta,

decreasing as the injected dose of AAV microdystrophin increased. However, significant residual lysosomal damage and IgG positive damaged myofibers persisted even in mice treated with the highest dose of AAV microdystrophin, which transduced nearly 100% of the myofibers, showing clearly that microdystrophin expression is not sufficient to restore lysosomal function, and further corroborating a link between LMP and myofiber permeabilization.

In comparison, gene therapy in an LGMDR5 mouse model, using an optimized dose to deliver the full-length gamma-sarcoglycan transgene <sup>[498]</sup>, resulted in nearly complete reversion of LMP, indicating more efficient lysosomal correction. Additionally, the overall reversion of the dystrophic phenotype, including muscle force, circulating biomarkers, and muscle histology, was more effective in this model compared to microdystrophin gene therapy.

This discrepancy in lysosomal correction between the two gene therapy approaches is particularly interesting given the pathophysiological similarities between these closely related muscular dystrophies. A key difference between the two therapies is the restoration of the full-length gamma-sarcoglycan protein in the LGMDR5 model, compared to the expression of a shorter, partially functional form of dystrophin (microdystrophin) in the *Dmd*<sup>mdx</sup> model. This study suggests that the missing portions of microdystrophin may play a crucial role in regulating lysosomal functions in skeletal myofibers, and most importantly, that microdystrophin expression is not sufficient to correct lysosomal membrane damage. It would therefore be important to evaluate a new approach combining gene therapy to a treatment targeting these deregulations of the endolysosomal system.

### **III.2 Trehalose-mediated correction of lysosomal damage improve overall therapeutic effect of microdystrophin gene therapy**

Following the identification of lysosomal damage in the muscles of *Dmd*<sup>mdx-4Cv</sup> mice and the insufficiency of microdystrophin gene therapy to fully correct this damage, our goal was to evaluate a combined therapy approach [488]. This approach aimed to reduce the required dose of AAV-microdystrophin and potentiate its effect with a complementary treatment targeting lysosomal damages. We selected trehalose for this setup because of its good safety profile [499], affordability as a dietary disaccharide [473], and previous clinical testing in neurodegenerative diseases [500] and Oculopharyngeal Muscular Dystrophy (OPMD) [501,502]. Most importantly, trehalose has been recently shown to promote lysosomal biogenesis and autophagy, effectively alleviating lysosomal damage [406,407]. Another key criterion for our selection was that trehalose activates lysosomal biogenesis independently of mTOR, unlike other known autophagy activators such as rapamycin, which inhibit mTOR signaling. mTOR plays a crucial role in muscle by regulating muscle mass [503], maintaining neuromuscular junction stability [504], and most importantly its inhibition in muscle was reported to cause metabolic and dystrophin defects leading to a severe myopathy [505]. Therefore, it is preferable to use drugs that do not act on mTOR.

In our study, we compared the administration of trehalose alone, a suboptimal dose of AAV-microdystrophin alone, and their combination. In the combined treatment group, mice were treated with trehalose for one week before AAV injection. Notably, trehalose alone demonstrated significant benefits, particularly in reversing LMP (LAMP2+LGALS3+ puncta) and reducing myofiber permeabilization and necrosis (IgG staining). This highlights the positive effect of trehalose on lysosomal dysfunction and suggests a direct association between lysosomal damage and myofiber necrosis. Importantly, the combination of microdystrophin gene therapy and trehalose yielded the best therapeutic results. In the gastrocnemius (GA) muscle of treated mice, we observed correction of myofiber size distribution, improvement in the

centronucleation index, regression of fibrosis and inflammation, and significant improvement in global muscle force compared to untreated dystrophic mice.

To assess the molecular correction achieved with different treatments more deeply, we performed RNA sequencing (RNA-seq) analysis of the GA muscle. Transcriptomic analysis further supported the efficacy of the combined therapy, showing enhanced transcriptomic correction when microdystrophin was combined with trehalose compared to microdystrophin treatment alone. This was evident across various signaling pathways and biological processes, such as inflammation, calcium homeostasis, cell death pathways, lipid metabolism, and the mTOR pathway. Interestingly, trehalose treatment alone did not have a significant effect on the transcriptome but appeared to act synergistically with microdystrophin, as demonstrated by the substantial difference in correction between the microdystrophin alone and combined therapy groups.

One interpretation of these results is that trehalose alone alleviates lysosomal damage, as indicated by the reduction of LMP, which directly impacts myofiber degeneration, resulting in some improvement in muscle force, histology, and other dystrophic parameters. The combination of trehalose with microdystrophin gene therapy synergistically reverses pathological mechanisms. Another explanation is that trehalose acts on additional pathological pathways. Trehalose has been shown to reduce oxidative stress <sup>[506,507]</sup>, inflammation <sup>[508,509]</sup> and fibrosis <sup>[510,511]</sup>, all of which are pathological hallmarks of DMD. Therefore, the beneficial effects of trehalose may not be exclusively mediated by lysosomal correction.

These preliminary results suggest that the endolysosomal system is a promising therapeutic target in muscular dystrophies, which, to our knowledge, has not yet been studied as a therapeutic target in DMD. However, it should be noted that this study was carried out in young mice over a short period. It is necessary to validate

these results over a longer treatment period, which is currently ongoing in our studies.

Regarding clinical translatability, there are some limitations to trehalose use. Trehalose has poor bioavailability due to its susceptibility to enzymatic degradation into glucose by trehalase in the small intestine <sup>[473]</sup>. It is also poorly taken up by cells because of its strong hydrophilicity, making it difficult to cross the phospholipid bilayer. Recently, the use of trehalose-bearing carriers, in which trehalose is incorporated either by chemical conjugation or physical entrapment, has been proposed as an alternative to free trehalose and improve its efficacy <sup>[512]</sup>, though this approach is still in preclinical studies.

In summary, we demonstrated that trehalose administration in *Dmd*<sup>mdx-4Cv</sup> mice can alleviate lysosomal damage and certain functional parameters. When combined with a suboptimal dose of microdystrophin gene therapy, trehalose enhances the therapeutic effect, offering promising new treatment strategy for DMD.

#### **IV- Concluding Remarks**

In the first part of this project, we acquired new knowledge with significant diagnostic and therapeutic implications for DMD and other muscle disorders. The identification of LMP in DMD and other muscle disorders is novel. The galectin puncta assay represents an efficient and rapid method for identifying LMP and may serve as a histological biomarker for lysosomal damage in muscle disorders in general.

Our findings have also advanced our understanding of DMD pathology, suggesting that lysosomal defects may play a central role in the pathogenesis and progression of

muscular dystrophy. The relative importance of lysosomal defects compared to other pathological hallmarks of DMD remains to be determined.

Despite significant progress in treating DMD, there are still many gaps and opportunities for improvement. We believe that a combined therapy approach can enhance therapeutic outcomes. The identification of the endolysosomal system as a promising target for combined therapy is novel, and the proof-of-concept with trehalose may pave the way for other drugs to be tested. Further research is needed to determine whether lysosomal defects are the most relevant mechanism to target in a combined therapy approach. This will deepen our understanding of DMD pathology and help bridge the gap between fundamental research and clinical application.

## BIBLIOGRAPHY

1. Janssen, I., Heymsfield, S. B., Wang, Z. & Ross, R. Skeletal muscle mass and distribution in 468 men and women aged 18–88 yr. *Journal of Applied Physiology* **89**, 81–88 (2000).
2. Frontera, W. R. & Ochala, J. Skeletal Muscle: A Brief Review of Structure and Function. *Calcif Tissue Int* **96**, 183–195 (2015).
3. Wolfe, R. R. The underappreciated role of muscle in health and disease<sup>2</sup>. *The American Journal of Clinical Nutrition* **84**, 475–482 (2006).
4. DeFronzo, R. A., Gunnarsson, R., Björkman, O., Olsson, M. & Wahren, J. Effects of insulin on peripheral and splanchnic glucose metabolism in noninsulin-dependent (type II) diabetes mellitus. *J Clin Invest* **76**, 149–155 (1985).
5. DeFronzo, R. A. & Tripathy, D. Skeletal Muscle Insulin Resistance Is the Primary Defect in Type 2 Diabetes. *Diabetes Care* **32**, S157–S163 (2009).
6. Ferrannini, E. *et al.* The disposal of an oral glucose load in patients with non-insulin-dependent diabetes. *Metabolism* **37**, 79–85 (1988).
7. Reaven, G. M. THE INSULIN RESISTANCE SYNDROME: Definition and Dietary Approaches to Treatment. *Annual Review of Nutrition* **25**, 391–406 (2005).
8. DeFronzo, R. A., Bonadonna, R. C. & Ferrannini, E. Pathogenesis of NIDDM: A Balanced Overview. *Diabetes Care* **15**, 318–368 (1992).
9. Merz, K. E. & Thurmond, D. C. Role of Skeletal Muscle in Insulin Resistance and Glucose Uptake. in *Comprehensive Physiology* 785–809 (John Wiley & Sons, Ltd, 2020). doi:10.1002/cphy.c190029.
10. Bonetto, A. & Bonewald, L. F. Chapter 16 - Bone and Muscle. in *Basic and Applied Bone Biology (Second Edition)* (eds. Burr, D. B. & Allen, M. R.) 317–332 (Academic Press, 2019). doi:10.1016/B978-0-12-813259-3.00016-6.
11. Hoppeler, H., Lüthi, P., Claassen, H., Weibel, E. R. & Howald, H. The ultrastructure of the normal human skeletal muscle. *Pflugers Arch.* **344**, 217–232 (1973).
12. Bailey, K. Myosin and adenosinetriphosphatase. *Biochemical Journal* **36**, 121–139 (1942).
13. Jayasinghe, I. D. & Launikonis, B. S. Three-dimensional reconstruction and analysis of the tubular system of vertebrate skeletal muscle. *Journal of Cell Science* **126**, 4048–4058 (2013).
14. Al-Qusairi, L. & Laporte, J. T-tubule biogenesis and triad formation in skeletal muscle and implication in human diseases. *Skeletal Muscle* **1**, 26 (2011).
15. Galpin, A. J. *et al.* Human skeletal muscle fiber type specific protein content. *Analytical Biochemistry* **425**, 175–182 (2012).
16. Rebeck, R. T. *et al.* Skeletal muscle excitation–contraction coupling: Who are the dancing partners? *The International Journal of Biochemistry & Cell Biology* **48**, 28–38 (2014).
17. Goubel, F. & Linsel-Corbeil, G. *Biomécanique: éléments de mécanique musculaire*. (Masson, 2003).
18. Huxley, H. & Hanson, J. Changes in the cross-striations of muscle during contraction and stretch and their structural interpretation. *Nature* **173**, 973–976 (1954).

19. Huxley, A. F. & Niedergerke, R. Structural changes in muscle during contraction; interference microscopy of living muscle fibres. *Nature* **173**, 971–973 (1954).
20. Romijn, J. A. *et al.* Regulation of endogenous fat and carbohydrate metabolism in relation to exercise intensity and duration. *American Journal of Physiology-Endocrinology and Metabolism* **265**, E380–E391 (1993).
21. Chandel, N. S. Amino Acid Metabolism. *Cold Spring Harb Perspect Biol* **13**, a040584 (2021).
22. Mauro, A. SATELLITE CELL OF SKELETAL MUSCLE FIBERS. *The Journal of Biophysical and Biochemical Cytology* **9**, 493–495 (1961).
23. Yablonka-Reuveni, Z. The Skeletal Muscle Satellite Cell: Still Young and Fascinating at 50. *J Histochem Cytochem.* **59**, 1041–1059 (2011).
24. Feige, P., Brun, C. E., Ritso, M. & Rudnicki, M. A. Orienting Muscle Stem Cells for Regeneration in Homeostasis, Aging, and Disease. *Cell Stem Cell* **23**, 653–664 (2018).
25. Rosenberg, I. H. Sarcopenia: Origins and Clinical Relevance<sup>1</sup>. *The Journal of Nutrition* **127**, 990S–991S (1997).
26. Reid, K. F. *et al.* Longitudinal decline of lower extremity muscle power in healthy and mobility-limited older adults: influence of muscle mass, strength, composition, neuromuscular activation and single fiber contractile properties. *Eur J Appl Physiol* **114**, 29–39 (2014).
27. Nishikawa, H., Asai, A., Fukunishi, S., Nishiguchi, S. & Higuchi, K. Metabolic Syndrome and Sarcopenia. *Nutrients* **13**, 3519 (2021).
28. Alway, S. E., Myers, M. J. & Mohamed, J. S. Regulation of Satellite Cell Function in Sarcopenia. *Frontiers in Aging Neuroscience* **6**, (2014).
29. Deschenes, M. R. Effects of Aging on Muscle Fibre Type and Size. *Sports Med* **34**, 809–824 (2004).
30. Chen, M., Wang, Y., Deng, S., Lian, Z. & Yu, K. Skeletal muscle oxidative stress and inflammation in aging: Focus on antioxidant and anti-inflammatory therapy. *Frontiers in Cell and Developmental Biology* **10**, (2022).
31. Broskey, N. T. *et al.* Skeletal Muscle Mitochondria in the Elderly: Effects of Physical Fitness and Exercise Training. *The Journal of Clinical Endocrinology & Metabolism* **99**, 1852–1861 (2014).
32. Steffl, M. *et al.* Relationship between sarcopenia and physical activity in older people: a systematic review and meta-analysis. *CIA* **12**, 835–845 (2017).
33. Alkner, B. A. & Tesch, P. A. Knee extensor and plantar flexor muscle size and function following 90 days of bed rest with or without resistance exercise. *Eur J Appl Physiol* **93**, 294–305 (2004).
34. Parry, S. M. & Puthuchery, Z. A. The impact of extended bed rest on the musculoskeletal system in the critical care environment. *Extreme Physiology & Medicine* **4**, 16 (2015).
35. Trappe, S. *et al.* Human single muscle fibre function with 84 day bed-rest and resistance exercise. *The Journal of Physiology* **557**, 501–513 (2004).
36. Cohen, S., Nathan, J. A. & Goldberg, A. L. Muscle wasting in disease: molecular mechanisms and promising therapies. *Nat Rev Drug Discov* **14**, 58–74 (2015).
37. Graham, Z. A. *et al.* Mechanisms of exercise as a preventative measure to muscle wasting. *American Journal of Physiology-Cell Physiology* **321**, C40–C57 (2021).
38. Claey, K. G. Congenital myopathies: an update. *Developmental Medicine & Child Neurology* **62**, 297–302 (2020).

39. Richard, I. *et al.* Mutations in the proteolytic enzyme calpain 3 cause limb-girdle muscular dystrophy type 2A. *Cell* **81**, 27–40 (1995).
40. Campbell, K. P. Three muscular dystrophies: Loss of cytoskeleton-extracellular matrix linkage. *Cell* **80**, 675–679 (1995).
41. Shin, J., Tajrishi, M. M., Ogura, Y. & Kumar, A. Wasting mechanisms in muscular dystrophy. *The International Journal of Biochemistry & Cell Biology* **45**, 2266–2279 (2013).
42. Iyadurai, S. J. P. & Kissel, J. T. The Limb-Girdle Muscular Dystrophies and the Dystrophinopathies: *CONTINUUM: Lifelong Learning in Neurology* **22**, 1954–1977 (2016).
43. Hoffman, E. P., Brown, R. H. & Kunkel, L. M. Dystrophin: The protein product of the duchenne muscular dystrophy locus. *Cell* **51**, 919–928 (1987).
44. Ervasti, J. M. & Campbell, K. P. Membrane organization of the dystrophin-glycoprotein complex. *Cell* **66**, 1121–1131 (1991).
45. Ozawa, E. Our trails and trials in the subsarcolemmal cytoskeleton network and muscular dystrophy researches in the dystrophin era. *Proc Jpn Acad Ser B Phys Biol Sci* **86**, 798–821 (2010).
46. Straub, V. *et al.* 229th ENMC international workshop: Limb girdle muscular dystrophies – Nomenclature and reformed classification Naarden, the Netherlands, 17–19 March 2017. *Neuromuscular Disorders* **28**, 702–710 (2018).
47. Fanin, M., Pegoraro, E., Matsuda-Asada, C., Brown, R. H. & Angelini, C. Calpain-3 and dysferlin protein screening in patients with limb-girdle dystrophy and myopathy. *Neurology* **56**, 660–665 (2001).
48. Vainzof, M. *et al.* Sarcoglycanopathies are responsible for 68% of severe autosomal recessive limb-girdle muscular dystrophy in the Brazilian population. *Journal of the Neurological Sciences* **164**, 44–49 (1999).
49. Mendell, J. R. *et al.* Evidence-based path to newborn screening for duchenne muscular dystrophy. *Annals of Neurology* **71**, 304–313 (2012).
50. Moat, S. J., Bradley, D. M., Salmon, R., Clarke, A. & Hartley, L. Newborn bloodspot screening for Duchenne muscular dystrophy: 21 years experience in Wales (UK). *Eur J Hum Genet* **21**, 1049–1053 (2013).
51. Angelini, C. Chapter 31 Muscular dystrophy. in *Handbook of Clinical Neurology* (eds. Aminoff, M. J., Boller, F. & Swaab, D. F.) vol. 95 477–488 (Elsevier, 2009).
52. Koenig, M. *et al.* Complete cloning of the duchenne muscular dystrophy (DMD) cDNA and preliminary genomic organization of the DMD gene in normal and affected individuals. *Cell* **50**, 509–517 (1987).
53. Duan, D., Goemans, N., Takeda, S., Mercuri, E. & Aartsma-Rus, A. Duchenne muscular dystrophy. (2021).
54. Mercuri, E., Bönnemann, C. G. & Muntoni, F. Muscular dystrophies. *The Lancet* **394**, 2025–2038 (2019).
55. Ferrier, P., Bamatter, F. & Klein, D. Muscular Dystrophy (Duchenne) in a Girl with Turner's Syndrome. *Journal of Medical Genetics* **2**, 38–46 (1965).
56. Chelly, J. *et al.* De novo DNA microdeletion in a girl with Turner syndrome and Duchenne muscular dystrophy. *Hum Genet* **74**, 193–196 (1986).

57. Satre, V., Monnier, N., Devillard, F., Amblard, F. & Lunardi, P. J. Prenatal diagnosis of DMD in a female foetus affected by Turner syndrome. *Prenatal Diagnosis* **24**, 913–917 (2004).
58. Chen, J.-J. *et al.* A Chinese girl with Turner syndrome and Duchenne muscular dystrophy: diagnosis and management of this “dual diagnosis”. *Chinese Medical Journal* **134**, 743 (2021).
59. Viggiano, E., Picillo, E., Cirillo, A. & Politano, L. Comparison of X-chromosome inactivation in Duchenne muscle/myocardium-manifesting carriers, non-manifesting carriers and related daughters. *Clinical Genetics* **84**, 265–270 (2013).
60. Sun, M.-X. *et al.* A female patient carrying a novel DMD mutation with non-random X-chromosome inactivation from a DMD family. *BMC Medical Genomics* **17**, 46 (2024).
61. Takeshita, E. *et al.* Duchenne muscular dystrophy in a female with compound heterozygous contiguous exon deletions. *Neuromuscular Disorders* **27**, 569–573 (2017).
62. Battini, R. *et al.* Cognitive profile in Duchenne muscular dystrophy boys without intellectual disability: The role of executive functions. *Neuromuscular Disorders* **28**, 122–128 (2018).
63. Toussaint, M., Chatwin, M. & Soudon, P. Review Article: Mechanical ventilation in Duchenne patients with chronic respiratory insufficiency: clinical implications of 20 years published experience. *Chron Respir Dis* **4**, 167–177 (2007).
64. Ryder, S. *et al.* The burden, epidemiology, costs and treatment for Duchenne muscular dystrophy: an evidence review. *Orphanet Journal of Rare Diseases* **12**, 79 (2017).
65. Kieny, P. *et al.* Evolution of life expectancy of patients with Duchenne muscular dystrophy at AFM Yolaine de Kepper centre between 1981 and 2011. *Annals of Physical and Rehabilitation Medicine* **56**, 443–454 (2013).
66. Quak, Z. X. *et al.* A manifesting female carrier of Duchenne muscular dystrophy: importance of genetics for the dystrophinopathies. *Singapore Medical Journal* **64**, 81 (2023).
67. Song, T.-J., Lee, K.-A., Kang, S.-W., Cho, H. & Choi, Y.-C. Three Cases of Manifesting Female Carriers in Patients with Duchenne Muscular Dystrophy. *Yonsei Medical Journal* **52**, 192–195 (2011).
68. Ishizaki, M., Kobayashi, M., Adachi, K., Matsumura, T. & Kimura, E. Female dystrophinopathy: Review of current literature. *Neuromuscular Disorders* **28**, 572–581 (2018).
69. Asher, D. R. *et al.* Clinical development on the frontier: gene therapy for duchenne muscular dystrophy. *Expert Opinion on Biological Therapy* **20**, 263–274 (2020).
70. Cheeran, D. *et al.* Predictors of Death in Adults With Duchenne Muscular Dystrophy–Associated Cardiomyopathy. *Journal of the American Heart Association* **6**, e006340.
71. Van Ruiten, H. J. A. *et al.* Why are some patients with Duchenne muscular dystrophy dying young: An analysis of causes of death in North East England. *European Journal of Paediatric Neurology* **20**, 904–909 (2016).
72. Sanyal, S. K., Johnson, W. W., Thapar, M. K. & Pitner, S. E. An ultrastructural basis for electrocardiographic alterations associated with Duchenne’s progressive muscular dystrophy. *Circulation* **57**, 1122–1129 (1978).
73. Schultz, T. I., Raucci, F. J. & Salloum, F. N. Cardiovascular Disease in Duchenne Muscular Dystrophy. *JACC: Basic to Translational Science* **7**, 608–625 (2022).
74. Bladen, C. L. *et al.* The TREAT-NMD DMD Global Database: Analysis of More than 7,000 Duchenne Muscular Dystrophy Mutations. *Human Mutation* **36**, 395–402 (2015).

75. Aartsma-Rus, A., Van Deutekom, J. C. T., Fokkema, I. F., Van Ommen, G.-J. B. & Den Dunnen, J. T. Entries in the Leiden Duchenne muscular dystrophy mutation database: An overview of mutation types and paradoxical cases that confirm the reading-frame rule. *Muscle & Nerve* **34**, 135–144 (2006).
76. Magri, F. *et al.* Genotype and phenotype characterization in a large dystrophinopathic cohort with extended follow-up. *J Neurol* **258**, 1610–1623 (2011).
77. Garcia, S. *et al.* Identification of *de novo* Mutations of Duchennè/Becker Muscular Dystrophies in Southern Spain. *International Journal of Medical Sciences* **11**, 988–993 (2014).
78. Kesari, A. *et al.* Integrated DNA, cDNA, and protein studies in Becker muscular dystrophy show high exception to the reading frame rule. *Human Mutation* **29**, 728–737 (2008).
79. Nakamura, A. *et al.* Comparison of the phenotypes of patients harboring in-frame deletions starting at exon 45 in the Duchenne muscular dystrophy gene indicates potential for the development of exon skipping therapy. *J Hum Genet* **62**, 459–463 (2017).
80. Nakamura, A. *et al.* Deletion of exons 3–9 encompassing a mutational hot spot in the DMD gene presents an asymptomatic phenotype, indicating a target region for multiexon skipping therapy. *J Hum Genet* **61**, 663–667 (2016).
81. Chelly, J. *et al.* Dystrophin gene transcribed from different promoters in neuronal and glial cells. *Nature* **344**, 64–65 (1990).
82. Górecki, D. C. *et al.* Expression of four alternative dystrophin transcripts in brain regions regulated by different promoters. *Human Molecular Genetics* **1**, 505–510 (1992).
83. Doorenweerd, N. *et al.* Timing and localization of human dystrophin isoform expression provide insights into the cognitive phenotype of Duchenne muscular dystrophy. *Sci Rep* **7**, 12575 (2017).
84. D'Souza, V. N. *et al.* A novel dystrophin isoform is required for normal retinal electrophysiology. *Human Molecular Genetics* **4**, 837–842 (1995).
85. Lidov, H. G. W., Selig, S. & Kunkel, L. M. Dp140: a novel 140 kDa CNS transcript from the dystrophin locus. *Human Molecular Genetics* **4**, 329–335 (1995).
86. Byers, T. J., Lidov, H. G. W. & Kunkel, L. M. An alternative dystrophin transcript specific to peripheral nerve. *Nat Genet* **4**, 77–81 (1993).
87. Hugnot, J. P. *et al.* Distal transcript of the dystrophin gene initiated from an alternative first exon and encoding a 75-kDa protein widely distributed in nonmuscle tissues. *Proceedings of the National Academy of Sciences* **89**, 7506–7510 (1992).
88. García-Pelagio, K. P., Bloch, R. J., Ortega, A. & González-Serratos, H. Biomechanics of the sarcolemma and costameres in single skeletal muscle fibers from normal and dystrophin-null mice. *J Muscle Res Cell Motil* **31**, 323–336 (2011).
89. Blaauw, B. *et al.* Eccentric contractions lead to myofibrillar dysfunction in muscular dystrophy. *Journal of Applied Physiology* **108**, 105–111 (2010).
90. Petrof, B. J., Shrager, J. B., Stedman, H. H., Kelly, A. M. & Sweeney, H. L. Dystrophin protects the sarcolemma from stresses developed during muscle contraction. *Proceedings of the National Academy of Sciences* **90**, 3710–3714 (1993).
91. Amann, K. J., Renley, B. A. & Ervasti, J. M. A Cluster of Basic Repeats in the Dystrophin Rod Domain Binds F-actin through an Electrostatic Interaction \*. *Journal of Biological Chemistry* **273**, 28419–28423 (1998).

92. Prins, K. W. *et al.* Dystrophin is a microtubule-associated protein. *Journal of Cell Biology* **186**, 363–369 (2009).
93. Nelson, D. M. *et al.* Rapid, redox-mediated mechanical susceptibility of the cortical microtubule lattice in skeletal muscle. *Redox Biology* **37**, 101730 (2020).
94. Lai, Y. *et al.* Dystrophins carrying spectrin-like repeats 16 and 17 anchor nNOS to the sarcolemma and enhance exercise performance in a mouse model of muscular dystrophy. *J Clin Invest* **119**, 624–635 (2009).
95. Lai, Y., Zhao, J., Yue, Y. & Duan, D.  $\alpha 2$  and  $\alpha 3$  helices of dystrophin R16 and R17 frame a microdomain in the  $\alpha 1$  helix of dystrophin R17 for neuronal NOS binding. *Proceedings of the National Academy of Sciences* **110**, 525–530 (2013).
96. Thomas, G. Functional muscle ischemia in Duchenne and Becker muscular dystrophy. *Frontiers in Physiology* **4**, (2013).
97. Duan, D. Systemic AAV Micro-dystrophin Gene Therapy for Duchenne Muscular Dystrophy. *Molecular Therapy* **26**, 2337–2356 (2018).
98. Li, D., Yue, Y., Lai, Y., Hakim, C. H. & Duan, D. Nitrosative stress elicited by nNOS $\mu$  delocalization inhibits muscle force in dystrophin-null mice. *The Journal of Pathology* **223**, 88–98 (2011).
99. Duan, D. Micro-Dystrophin Gene Therapy Goes Systemic in Duchenne Muscular Dystrophy Patients. *Human Gene Therapy* **29**, 733–736 (2018).
100. Huang, X. *et al.* Structure of a WW domain containing fragment of dystrophin in complex with  $\beta$ -dystroglycan. *Nat Struct Mol Biol* **7**, 634–638 (2000).
101. Anderson, J. T., Rogers, R. P. & Jarrett, H. W.  $\text{Ca}^{2+}$ -Calmodulin Binds to the Carboxyl-terminal Domain of Dystrophin (\*). *Journal of Biological Chemistry* **271**, 6605–6610 (1996).
102. Moradi, F. *et al.* Calmodulin-Binding Proteins in Muscle: A Minireview on Nuclear Receptor Interacting Protein, Neurogranin, and Growth-Associated Protein 43. *Int J Mol Sci* **21**, 1016 (2020).
103. Zhao, J. *et al.* Dystrophin contains multiple independent membrane-binding domains. *Human Molecular Genetics* **25**, 3647–3653 (2016).
104. Constantin, B. Dystrophin complex functions as a scaffold for signalling proteins. *Biochimica et Biophysica Acta (BBA) - Biomembranes* **1838**, 635–642 (2014).
105. Dreyfus, J.-C., Schapira, G. & Schapira, F. Serum Enzymes in the Physiopathology of Muscle. *Annals of the New York Academy of Sciences* **75**, 235–249 (1958).
106. Moser, H. Duchenne muscular dystrophy: Pathogenetic aspects and genetic prevention. *Hum Genet* **66**, 17–40 (1984).
107. Timpani, C. A., Hayes, A. & Rybalka, E. Revisiting the dystrophin-ATP connection: How half a century of research still implicates mitochondrial dysfunction in Duchenne Muscular Dystrophy aetiology. *Medical Hypotheses* **85**, 1021–1033 (2015).
108. Yogev, Y. *et al.* Limb girdle muscular disease caused by HMGCR mutation and statin myopathy treatable with mevalonolactone. *Proceedings of the National Academy of Sciences* **120**, e2217831120 (2023).
109. Morales-Rosado, J. A. *et al.* Bi-allelic variants in HMGCR cause an autosomal-recessive progressive limb-girdle muscular dystrophy. *The American Journal of Human Genetics* **110**, 989–997 (2023).

110. Rybakova, I. N., Amann, K. J. & Ervasti, J. M. A new model for the interaction of dystrophin with F-actin. *Journal of Cell Biology* **135**, 661–672 (1996).
111. Rybakova, I. N., Patel, J. R. & Ervasti, J. M. The Dystrophin Complex Forms a Mechanically Strong Link between the Sarcolemma and Costameric Actin. *Journal of Cell Biology* **150**, 1209–1214 (2000).
112. Ayalon, G., Davis, J. Q., Scotland, P. B. & Bennett, V. An Ankyrin-Based Mechanism for Functional Organization of Dystrophin and Dystroglycan. *Cell* **135**, 1189–1200 (2008).
113. Mokri, B. & Engel, A. G. Duchenne dystrophy: Electron microscopic findings pointing to a basic or early abnormality in the plasma membrane of the muscle fiber. *Neurology* **25**, 1111–1111 (1975).
114. Haycock, J. W., Neil, S. M., Jones, P., Harris, J. B. & Mantle, D. Oxidative damage to muscle protein in Duchenne muscular dystrophy. *NeuroReport* **8**, 357 (1996).
115. Terrill, J. R. *et al.* Oxidative stress and pathology in muscular dystrophies: focus on protein thiol oxidation and dysferlinopathies. *The FEBS Journal* **280**, 4149–4164 (2013).
116. Kim, J.-H., Kwak, H.-B., Thompson, L. V. & Lawler, J. M. Contribution of oxidative stress to pathology in diaphragm and limb muscles with Duchenne muscular dystrophy. *J Muscle Res Cell Motil* **34**, 1–13 (2013).
117. Grounds, M. D. *et al.* Biomarkers for Duchenne muscular dystrophy: myonecrosis, inflammation and oxidative stress. *Disease Models & Mechanisms* **13**, dmm043638 (2020).
118. Whitehead, N. P., Yeung, E. W., Froehner, S. C. & Allen, D. G. Skeletal Muscle NADPH Oxidase Is Increased and Triggers Stretch-Induced Damage in the mdx Mouse. *PLOS ONE* **5**, e15354 (2010).
119. Khairallah, R. J. *et al.* Microtubules Underlie Dysfunction in Duchenne Muscular Dystrophy. *Science Signaling* **5**, ra56–ra56 (2012).
120. Prosser, B. L., Ward, C. W. & Lederer, W. J. X-ROS Signaling: Rapid Mechano-Chemo Transduction in Heart. *Science* **333**, 1440–1445 (2011).
121. Williams, I. A. & Allen, D. G. The role of reactive oxygen species in the hearts of dystrophin-deficient mdx mice. *American Journal of Physiology-Heart and Circulatory Physiology* **293**, H1969–H1977 (2007).
122. Hammers, D. W. NOX4 inhibition promotes the remodeling of dystrophic muscle. *JCI Insight* **7**, (2022).
123. Wells, K. E. *et al.* Relocalization of neuronal nitric oxide synthase (nNOS) as a marker for complete restoration of the dystrophin associated protein complex in skeletal muscle. *Neuromuscular Disorders* **13**, 21–31 (2003).
124. Rando, T. A., Disatnik, M.-H., Yu, Y. & Franco, A. Muscle cells from mdx mice have an increased susceptibility to oxidative stress. *Neuromuscular Disorders* **8**, 14–21 (1998).
125. Turner, P. R., Westwood, T., Regen, C. M. & Steinhardt, R. A. Increased protein degradation results from elevated free calcium levels found in muscle from mdx mice. *Nature* **335**, 735–738 (1988).
126. Culligan, K. & Ohlendieck, K. Abnormal Calcium Handling in Muscular Dystrophy. in (2002).
127. Mallouk, N., Jacquemond, V. & Allard, B. Elevated subsarcolemmal Ca<sup>2+</sup> in mdx mouse skeletal muscle fibers detected with Ca<sup>2+</sup>-activated K<sup>+</sup> channels. *Proceedings of the National Academy of Sciences* **97**, 4950–4955 (2000).

128. Altamirano, F. *et al.* Increased Resting Intracellular Calcium Modulates NF- $\kappa$ B-dependent Inducible Nitric-oxide Synthase Gene Expression in Dystrophic mdx Skeletal Myotubes\*. *Journal of Biological Chemistry* **287**, 20876–20887 (2012).
129. Allen, D. G., Whitehead, N. P. & Froehner, S. C. Absence of Dystrophin Disrupts Skeletal Muscle Signaling: Roles of Ca<sup>2+</sup>, Reactive Oxygen Species, and Nitric Oxide in the Development of Muscular Dystrophy. *Physiol Rev* **96**, 253–305 (2016).
130. Murphy, S. *et al.* Proteomic analysis of the sarcolemma-enriched fraction from dystrophic mdx-4cv skeletal muscle. *Journal of Proteomics* **191**, 212–227 (2019).
131. Zabłocka, B., Górecki, D. C. & Zabłocki, K. Disrupted Calcium Homeostasis in Duchenne Muscular Dystrophy: A Common Mechanism behind Diverse Consequences. *International Journal of Molecular Sciences* **22**, 11040 (2021).
132. Bellinger, A. M. *et al.* Hypernitrosylated ryanodine receptor calcium release channels are leaky in dystrophic muscle. *Nat Med* **15**, 325–330 (2009).
133. Kushnir, A., Wajsberg, B. & Marks, A. R. Ryanodine receptor dysfunction in human disorders. *Biochimica et Biophysica Acta (BBA) - Molecular Cell Research* **1865**, 1687–1697 (2018).
134. Hyatt, H. W. & Powers, S. K. The Role of Calpains in Skeletal Muscle Remodeling with Exercise and Inactivity-induced Atrophy. *Int J Sports Med* **41**, 994–1008 (2020).
135. Phillips, M. F. & Quinlivan, R. Calcium antagonists for Duchenne muscular dystrophy. *Cochrane Database of Systematic Reviews* (2008) doi:10.1002/14651858.CD004571.pub2.
136. Sander, M. *et al.* Functional muscle ischemia in neuronal nitric oxide synthase-deficient skeletal muscle of children with Duchenne muscular dystrophy. *Proceedings of the National Academy of Sciences* **97**, 13818–13823 (2000).
137. Hood, D. A., Memme, J. M., Oliveira, A. N. & Triolo, M. Maintenance of Skeletal Muscle Mitochondria in Health, Exercise, and Aging. *Annu Rev Physiol* **81**, 19–41 (2019).
138. Budzinska, M., Zimna, A. & Kurpisz, M. The role of mitochondria in Duchenne muscular dystrophy. *J Physiol Pharmacol* **72**, (2021).
139. Kuznetsov, A. V. *et al.* Impaired mitochondrial oxidative phosphorylation in skeletal muscle of the dystrophin-deficient mdx mouse. *Mol Cell Biochem* **183**, 87–96 (1998).
140. Schuh, R. A., Jackson, K. C., Khairallah, R. J., Ward, C. W. & Spangenburg, E. E. Measuring mitochondrial respiration in intact single muscle fibers. *American Journal of Physiology-Regulatory, Integrative and Comparative Physiology* **302**, R712–R719 (2012).
141. Rybalka, E., Timpani, C. A., Cooke, M. B., Williams, A. D. & Hayes, A. Defects in Mitochondrial ATP Synthesis in Dystrophin-Deficient Mdx Skeletal Muscles May Be Caused by Complex I Insufficiency. *PLOS ONE* **9**, e115763 (2014).
142. Amor, F. *et al.* Cholesterol metabolism is a potential therapeutic target in Duchenne muscular dystrophy. *Journal of Cachexia, Sarcopenia and Muscle* **12**, 677–693 (2021).
143. Vu Hong, A. *et al.* Dlk1-Dio3 cluster miRNAs regulate mitochondrial functions in the dystrophic muscle in Duchenne muscular dystrophy. *Life Sci. Alliance* **6**, e202201506 (2023).
144. Sanson, M. *et al.* miR-379 links glucocorticoid treatment with mitochondrial response in Duchenne muscular dystrophy. *Scientific Reports* **10**, 9139 (2020).
145. Turrens, J. F. Mitochondrial formation of reactive oxygen species. *J Physiol* **552**, 335–344 (2003).

146. Babu, D. *et al.* Mitochondria and NADPH oxidases are the major sources of TNF- $\alpha$ /cycloheximide-induced oxidative stress in murine intestinal epithelial MODE-K cells. *Cellular Signalling* **27**, 1141–1158 (2015).
147. Hughes, M. C. *et al.* Early myopathy in Duchenne muscular dystrophy is associated with elevated mitochondrial H<sub>2</sub>O<sub>2</sub> emission during impaired oxidative phosphorylation. *Journal of Cachexia, Sarcopenia and Muscle* **10**, 643–661 (2019).
148. Pauly, M. *et al.* ER stress disturbs SR/ER-mitochondria Ca<sup>2+</sup> transfer: Implications in Duchenne muscular dystrophy. *Biochimica et Biophysica Acta (BBA) - Molecular Basis of Disease* **1863**, 2229–2239 (2017).
149. Moorwood, C. & Barton, E. R. Caspase-12 ablation preserves muscle function in the mdx mouse. *Human Molecular Genetics* **23**, 5325–5341 (2014).
150. Sandri, M. Autophagy in skeletal muscle. *FEBS Letters* **584**, 1411–1416 (2010).
151. Sandri, M., Coletto, L., Grumati, P. & Bonaldo, P. Misregulation of autophagy and protein degradation systems in myopathies and muscular dystrophies. *Journal of Cell Science* **126**, 5325–5333 (2013).
152. Malicdan, M. C. V. & Nishino, I. Autophagy in Lysosomal Myopathies. *Brain Pathology* **22**, 82–88 (2012).
153. De Palma, C. *et al.* Autophagy as a new therapeutic target in Duchenne muscular dystrophy. *Cell Death Dis* **3**, e418–e418 (2012).
154. De Palma, C., Perrotta, C., Pellegrino, P., Clementi, E. & Cervia, D. Skeletal Muscle Homeostasis in Duchenne Muscular Dystrophy: Modulating Autophagy as a Promising Therapeutic Strategy. *Front. Aging Neurosci.* **6**, (2014).
155. Pal, R. *et al.* Src-dependent impairment of autophagy by oxidative stress in a mouse model of Duchenne muscular dystrophy. *Nat Commun* **5**, 4425 (2014).
156. You, J.-S. *et al.* Leucyl-tRNA synthetase contributes to muscle weakness through mTORC1 activation and autophagy suppression in a mouse model of Duchenne Muscular Dystrophy. *The American Journal of Pathology* (2024) doi:10.1016/j.ajpath.2024.04.006.
157. Pauly, M. *et al.* AMPK Activation Stimulates Autophagy and Ameliorates Muscular Dystrophy in the mdx Mouse Diaphragm. *The American Journal of Pathology* **181**, 583–592 (2012).
158. Saini-Chohan, H. K., Mitchell, R. W., Vaz, F. M., Zelinski, T. & Hatch, G. M. Delineating the role of alterations in lipid metabolism to the pathogenesis of inherited skeletal and cardiac muscle disorders. *Journal of Lipid Research* **53**, 4–27 (2012).
159. Tahallah, N., Brunelle, A., De La Porte, S. & Laprévotte, O. Lipid mapping in human dystrophic muscle by cluster-time-of-flight secondary ion mass spectrometry imaging. *Journal of Lipid Research* **49**, 438–454 (2008).
160. Srivastava, N. K., Yadav, R., Mukherjee, S., Pal, L. & Sinha, N. Abnormal lipid metabolism in skeletal muscle tissue of patients with muscular dystrophy: In vitro, high-resolution NMR spectroscopy based observation in early phase of the disease. *Magnetic Resonance Imaging* **38**, 163–173 (2017).
161. Srivastava, N. K., Pradhan, S., Mittal, B. & Gowda, G. A. N. High resolution NMR based analysis of serum lipids in Duchenne muscular dystrophy patients and its possible diagnostic significance. *NMR in Biomedicine* **23**, 13–22 (2010).

162. Srivastava, N. K., Mukherjee, S. & Sinha, N. Alteration of phospholipids in the blood of patients with Duchenne muscular dystrophy (DMD): in vitro, high resolution <sup>31</sup>P NMR-based study. *Acta Neurol Belg* **116**, 573–581 (2016).
163. White, Z. *et al.* High prevalence of plasma lipid abnormalities in human and canine Duchenne and Becker muscular dystrophies depicts a new type of primary genetic dyslipidemia. *Journal of Clinical Lipidology* **14**, 459-469.e0 (2020).
164. Sun, Z. *et al.* Dyslipidemia in Muscular Dystrophy: A Systematic Review and Meta-Analysis. *Journal of Neuromuscular Diseases* **10**, 505–516 (2023).
165. Tsonaka, R., Seyer, A., Aartsma-Rus, A. & Spitali, P. Plasma lipidomic analysis shows a disease progression signature in mdx mice. *Sci Rep* **11**, 12993 (2021).
166. Whitehead, N. P., Kim, M. J., Bible, K. L., Adams, M. E. & Froehner, S. C. A new therapeutic effect of simvastatin revealed by functional improvement in muscular dystrophy. *Proceedings of the National Academy of Sciences* **112**, 12864–12869 (2015).
167. Kim, M. J. *et al.* Simvastatin provides long-term improvement of left ventricular function and prevents cardiac fibrosis in muscular dystrophy. *Physiological Reports* **7**, e14018 (2019).
168. Evans, N. P., Misyak, S. A., Robertson, J. L., Bassaganya-Riera, J. & Grange, R. W. Immune-Mediated Mechanisms Potentially Regulate the Disease Time-Course of Duchenne Muscular Dystrophy and Provide Targets for Therapeutic Intervention. *PM&R* **1**, 755–768 (2009).
169. Langen, R. C. J., Schols, A. M. W. J., Kelders, M. C. J. M., Wouters, E. F. M. & Janssen-Heininger, Y. M. W. Inflammatory cytokines inhibit myogenic differentiation through activation of nuclear factor- $\kappa$ B. *The FASEB Journal* **15**, 1169–1180 (2001).
170. Villalta, S. A., Deng, B., Rinaldi, C., Wehling-Henricks, M. & Tidball, J. G. IFN- $\gamma$  Promotes Muscle Damage in the mdx Mouse Model of Duchenne Muscular Dystrophy by Suppressing M2 Macrophage Activation and Inhibiting Muscle Cell Proliferation. *The Journal of Immunology* **187**, 5419–5428 (2011).
171. Theret, M., Saclier, M., Messina, G. & Rossi, F. M. V. Macrophages in Skeletal Muscle Dystrophies, An Entangled Partner. *Journal of Neuromuscular Diseases* **9**, 1–23 (2022).
172. Spencer, M. J., Montecino-Rodriguez, E., Dorshkind, K. & Tidball, J. G. Helper (CD4+) and Cytotoxic (CD8+) T Cells Promote the Pathology of Dystrophin-Deficient Muscle. *Clinical Immunology* **98**, 235–243 (2001).
173. Spencer, M. J., Walsh, C. M., Dorshkind, K. A., Rodriguez, E. M. & Tidball, J. G. Myonuclear apoptosis in dystrophic mdx muscle occurs by perforin-mediated cytotoxicity. *J Clin Invest* **99**, 2745–2751 (1997).
174. Tidball, J. G., Welc, S. S. & Wehling-Henricks, M. Immunobiology of Inherited Muscular Dystrophies. in *Comprehensive Physiology* 1313–1356 (John Wiley & Sons, Ltd, 2018). doi:10.1002/cphy.c170052.
175. Tidball, J. G. Inflammatory processes in muscle injury and repair. *American Journal of Physiology-Regulatory, Integrative and Comparative Physiology* **288**, R345–R353 (2005).
176. Gorospe, J. R. M., Tharp, M., Demitsu, T. & Hoffman, E. P. Dystrophin-deficient myofibers are vulnerable to mast cell granule-induced necrosis. *Neuromuscular Disorders* **4**, 325–333 (1994).

177. Gorospe, J. R. M., Tharp, M. D., Hinckley, J., Kornegay, J. N. & Hoffman, E. P. A role for mast cells in the progression of Duchenne muscular dystrophy?: Correlations in dystrophin-deficient humans, dogs, and mice. *Journal of the Neurological Sciences* **122**, 44–56 (1994).
178. Kirschner, J. *et al.* Treatment of Duchenne muscular dystrophy with ciclosporin A: a randomised, double-blind, placebo-controlled multicentre trial. *The Lancet Neurology* **9**, 1053–1059 (2010).
179. Iannitti, T., Capone, S., Feder, D. & Palmieri, B. Clinical Use of Immunosuppressants in Duchenne Muscular Dystrophy. *Journal of Clinical Neuromuscular Disease* **12**, 1 (2010).
180. Sacco, A. *et al.* Short Telomeres and Stem Cell Exhaustion Model Duchenne Muscular Dystrophy in mdx/mTR Mice. *Cell* **143**, 1059–1071 (2010).
181. Souza, G. T. de *et al.* Satellite Cells: Regenerative Mechanisms and Applicability in Muscular Dystrophy. *Stem Cells International* **2015**, e487467 (2015).
182. Chang, N. C. *et al.* The Dystrophin Glycoprotein Complex Regulates the Epigenetic Activation of Muscle Stem Cell Commitment. *Cell Stem Cell* **22**, 755–768.e6 (2018).
183. Lumeng, C. *et al.* Interactions between  $\beta$ 2-syntrophin and a family of microtubule-associated serine/threonine kinases. *Nat Neurosci* **2**, 611–617 (1999).
184. Dumont, N. A. *et al.* Dystrophin expression in muscle stem cells regulates their polarity and asymmetric division. *Nat Med* **21**, 1455–1463 (2015).
185. Dumont, N. A. & Rudnicki, M. A. Targeting muscle stem cell intrinsic defects to treat Duchenne muscular dystrophy. *npj Regen Med* **1**, 1–7 (2016).
186. Kodippili, K. & Rudnicki, M. A. Satellite cell contribution to disease pathology in Duchenne muscular dystrophy. *Front. Physiol.* **14**, 1180980 (2023).
187. Wynn, T. A. & Ramalingam, T. R. Mechanisms of fibrosis: therapeutic translation for fibrotic disease. *Nat Med* **18**, 1028–1040 (2012).
188. Zhou, L. & Lu, H. Targeting Fibrosis in Duchenne Muscular Dystrophy. *Journal of Neuropathology & Experimental Neurology* **69**, 771–776 (2010).
189. Serrano, A. L. *et al.* Chapter seven - Cellular and Molecular Mechanisms Regulating Fibrosis in Skeletal Muscle Repair and Disease. in *Current Topics in Developmental Biology* (ed. Pavlath, G. k.) vol. 96 167–201 (Academic Press, 2011).
190. Molina, T., Fabre, P. & Dumont, N. A. Fibro-adipogenic progenitors in skeletal muscle homeostasis, regeneration and diseases. *Open Biol* **11**, 210110 (2021).
191. Contreras, O., Rebolledo, D. L., Oyarzún, J. E., Olguín, H. C. & Brandan, E. Connective tissue cells expressing fibro/adipogenic progenitor markers increase under chronic damage: relevance in fibroblast-myofibroblast differentiation and skeletal muscle fibrosis. *Cell Tissue Res* **364**, 647–660 (2016).
192. Lemos, D. R. *et al.* Nilotinib reduces muscle fibrosis in chronic muscle injury by promoting TNF-mediated apoptosis of fibro/adipogenic progenitors. *Nat Med* **21**, 786–794 (2015).
193. Chen, W., You, W., Valencak, T. G. & Shan, T. Bidirectional roles of skeletal muscle fibro-adipogenic progenitors in homeostasis and disease. *Ageing Research Reviews* **80**, 101682 (2022).
194. Ceco, E. & McNally, E. M. Modifying muscular dystrophy through transforming growth factor- $\beta$ . *The FEBS Journal* **280**, 4198–4209 (2013).

195. Wynn, T. Cellular and molecular mechanisms of fibrosis. *The Journal of Pathology* **214**, 199–210 (2008).
196. Bernasconi, P. *et al.* Expression of transforming growth factor-beta 1 in dystrophic patient muscles correlates with fibrosis. Pathogenetic role of a fibrogenic cytokine. *J Clin Invest* **96**, 1137–1144 (1995).
197. Heydemann, A. *et al.* Latent TGF- $\beta$ -binding protein 4 modifies muscular dystrophy in mice. *J Clin Invest* **119**, 3703–3712 (2009).
198. Zhou, L. *et al.* Temporal and spatial mRNA expression patterns of TGF- $\beta$ 1, 2, 3 and T $\beta$ RI, II, III in skeletal muscles of mdx mice. *Neuromuscular Disorders* **16**, 32–38 (2006).
199. Shi, Y. & Massagué, J. Mechanisms of TGF- $\beta$  Signaling from Cell Membrane to the Nucleus. *Cell* **113**, 685–700 (2003).
200. Leask, A. & Abraham, D. J. TGF- $\beta$  signaling and the fibrotic response. *The FASEB Journal* **18**, 816–827 (2004).
201. Runyan, C. E., Schnaper, H. W. & Poncelet, A.-C. Smad3 and PKC $\delta$  mediate TGF- $\beta$ 1-induced collagen I expression in human mesangial cells. *American Journal of Physiology-Renal Physiology* **285**, F413–F422 (2003).
202. Border, W. A. & Noble, N. A. Transforming Growth Factor  $\beta$  in Tissue Fibrosis. *New England Journal of Medicine* **331**, 1286–1292 (1994).
203. Sun, G. *et al.* Connective tissue growth factor is overexpressed in muscles of human muscular dystrophy. *Journal of the Neurological Sciences* **267**, 48–56 (2008).
204. Hinz, B. Tissue stiffness, latent TGF- $\beta$ 1 Activation, and mechanical signal transduction: Implications for the pathogenesis and treatment of fibrosis. *Curr Rheumatol Rep* **11**, 120–126 (2009).
205. Smith, L., Cho, S. & Discher, D. E. Mechanosensing of matrix by stem cells: From matrix heterogeneity, contractility, and the nucleus in pore-migration to cardiogenesis and muscle stem cells in vivo. *Seminars in Cell & Developmental Biology* **71**, 84–98 (2017).
206. Fischer, M., Rikeit, P., Knaus, P. & Coirault, C. YAP-Mediated Mechanotransduction in Skeletal Muscle. *Frontiers in Physiology* **7**, (2016).
207. Desguerre, I. *et al.* Endomysial Fibrosis in Duchenne Muscular Dystrophy: A Marker of Poor Outcome Associated With Macrophage Alternative Activation. *Journal of Neuropathology & Experimental Neurology* **68**, 762–773 (2009).
208. Birnkrant, D. J. *et al.* Diagnosis and management of Duchenne muscular dystrophy, part 1: diagnosis, and neuromuscular, rehabilitation, endocrine, and gastrointestinal and nutritional management. *The Lancet Neurology* **17**, 251–267 (2018).
209. Birnkrant, D. J. *et al.* Diagnosis and management of Duchenne muscular dystrophy, part 2: respiratory, cardiac, bone health, and orthopaedic management. *The Lancet Neurology* **17**, 347–361 (2018).
210. Birnkrant, D. J. *et al.* Diagnosis and management of Duchenne muscular dystrophy, part 3: primary care, emergency management, psychosocial care, and transitions of care across the lifespan. *The Lancet Neurology* **17**, 445–455 (2018).
211. Zhang, T. & Kong, X. Recent advances of glucocorticoids in the treatment of Duchenne muscular dystrophy (Review). *Experimental and Therapeutic Medicine* **21**, 1–7 (2021).

212. Dichiaro, M., McMahon, M., Horn, P., Petersen, A. & Wong, B. L. P4.2 Duchenne Muscular Dystrophy and corticosteroids: Timed motor performance predictive of time to loss of ambulation. *Neuromuscular Disorders* **21**, 704–705 (2011).
213. Schreiber, A. *et al.* Corticosteroids in Duchenne muscular dystrophy: impact on the motor function measure sensitivity to change and implications for clinical trials. *Developmental Medicine & Child Neurology* **60**, 185–191 (2018).
214. McDonald, C. M. *et al.* Longitudinal pulmonary function testing outcome measures in Duchenne muscular dystrophy: Long-term natural history with and without glucocorticoids. *Neuromuscular Disorders* **28**, 897–909 (2018).
215. Sanchez, M. J., Scott, W., Pessana, F., Castro, D. & Ramaciotti, C. Comparison of the effect of three steroid regimens on cardiac function in Duchenne muscular dystrophy. *Progress in Pediatric Cardiology* **67**, 101557 (2022).
216. Kinali, M. *et al.* Predictive factors for the development of scoliosis in Duchenne muscular dystrophy. *European Journal of Paediatric Neurology* **11**, 160–166 (2007).
217. Matthews, E., Brassington, R., Kuntzer, T., Jichi, F. & Manzur, A. Y. Corticosteroids for the treatment of Duchenne muscular dystrophy. *Cochrane Database of Systematic Reviews* (2016) doi:10.1002/14651858.CD003725.pub4.
218. Smith, E. C. *et al.* Efficacy and safety of vamorolone in Duchenne muscular dystrophy: An 18-month interim analysis of a non-randomized open-label extension study. *PLOS Medicine* **17**, e1003222 (2020).
219. Mah, J. K. *et al.* Efficacy and Safety of Vamorolone in Duchenne Muscular Dystrophy: A 30-Month Nonrandomized Controlled Open-Label Extension Trial. *JAMA Network Open* **5**, e2144178 (2022).
220. Guglieri, M. *et al.* Efficacy and Safety of Vamorolone vs Placebo and Prednisone Among Boys With Duchenne Muscular Dystrophy: A Randomized Clinical Trial. *JAMA Neurology* **79**, 1005–1014 (2022).
221. Dang, U. J. *et al.* Efficacy and Safety of Vamorolone Over 48 Weeks in Boys With Duchenne Muscular Dystrophy. *Neurology* **102**, e208112 (2024).
222. Mozzetta, C., Sartorelli, V. & Puri, P. L. HDAC inhibitors as pharmacological treatment for Duchenne muscular dystrophy: a discovery journey from bench to patients. *Trends in Molecular Medicine* **30**, 278–294 (2024).
223. Minetti, G. C. *et al.* Functional and morphological recovery of dystrophic muscles in mice treated with deacetylase inhibitors. *Nat Med* **12**, 1147–1150 (2006).
224. Consalvi, S. *et al.* Preclinical Studies in the mdx Mouse Model of Duchenne Muscular Dystrophy with the Histone Deacetylase Inhibitor Givinostat. *Mol Med* **19**, 79–87 (2013).
225. Bettica, P. *et al.* Histological effects of givinostat in boys with Duchenne muscular dystrophy. *Neuromuscular Disorders* **26**, 643–649 (2016).
226. Mercuri, E. *et al.* Safety and efficacy of givinostat in boys with Duchenne muscular dystrophy (EPIDYS): a multicentre, randomised, double-blind, placebo-controlled, phase 3 trial. *The Lancet Neurology* **23**, 393–403 (2024).
227. Zambon, A. A. *et al.* Respiratory Function and Sleep Disordered Breathing in Pediatric Duchenne Muscular Dystrophy. *Neurology* **99**, e1216–e1226 (2022).

228. Duboc, D. *et al.* Effect of perindopril on the onset and progression of left ventricular dysfunction in Duchenne muscular dystrophy. *Journal of the American College of Cardiology* **45**, 855–857 (2005).
229. Duboc, D. *et al.* Perindopril preventive treatment on mortality in Duchenne muscular dystrophy: 10 years' follow-up. *American Heart Journal* **154**, 596–602 (2007).
230. McNally, E. M. *et al.* Contemporary Cardiac Issues in Duchenne Muscular Dystrophy. *Circulation* **131**, 1590–1598 (2015).
231. Atchison, R. W., Casto, B. C. & Hammon, W. McD. Adenovirus-Associated Defective Virus Particles. *Science* **149**, 754–756 (1965).
232. Blacklow, N. R., Hoggan, M. D. & Rowe, W. P. Isolation of adenovirus-associated viruses from man. *Proceedings of the National Academy of Sciences* **58**, 1410–1415 (1967).
233. Hermonat, P. L. & Muzyczka, N. Use of adeno-associated virus as a mammalian DNA cloning vector: transduction of neomycin resistance into mammalian tissue culture cells. *Proceedings of the National Academy of Sciences* **81**, 6466–6470 (1984).
234. Ylä-Herttua, S. Endgame: Glybera Finally Recommended for Approval as the First Gene Therapy Drug in the European Union. *Molecular Therapy* **20**, 1831–1832 (2012).
235. Miraldi Utz, V., Coussa, R. G., Antaki, F. & Traboulsi, E. I. Gene therapy for RPE65-related retinal disease. *Ophthalmic Genetics* **39**, 671–677 (2018).
236. Hoy, S. M. Onasemnogene Apeparvovec: First Global Approval. *Drugs* **79**, 1255–1262 (2019).
237. Srivastava, A., Lusby, E. W. & Berns, K. I. Nucleotide sequence and organization of the adeno-associated virus 2 genome. *Journal of Virology* **45**, 555–564 (1983).
238. McLaughlin, S. K., Collis, P., Hermonat, P. L. & Muzyczka, N. Adeno-associated virus general transduction vectors: analysis of proviral structures. *Journal of Virology* **62**, 1963–1973 (1988).
239. Yan, Z., Zak, R., Zhang, Y. & Engelhardt, J. F. Inverted Terminal Repeat Sequences Are Important for Intermolecular Recombination and Circularization of Adeno-Associated Virus Genomes. *Journal of Virology* **79**, 364–379 (2005).
240. Gao, G. *et al.* Clades of Adeno-Associated Viruses Are Widely Disseminated in Human Tissues. *Journal of Virology* **78**, 6381–6388 (2004).
241. Li, C. & Samulski, R. J. Engineering adeno-associated virus vectors for gene therapy. *Nat Rev Genet* **21**, 255–272 (2020).
242. Calcedo, R., Vandenberghe, L. H., Gao, G., Lin, J. & Wilson, J. M. Worldwide Epidemiology of Neutralizing Antibodies to Adeno-Associated Viruses. *The Journal of Infectious Diseases* **199**, 381–390 (2009).
243. Flotte, T. R. Gene Therapy Progress and Prospects: Recombinant adeno-associated virus (rAAV) vectors. *Gene Ther* **11**, 805–810 (2004).
244. Kotterman, M. A. & Schaffer, D. V. Engineering adeno-associated viruses for clinical gene therapy. *Nat Rev Genet* **15**, 445–451 (2014).
245. Wang, D., Tai, P. W. L. & Gao, G. Adeno-associated virus vector as a platform for gene therapy delivery. *Nat Rev Drug Discov* **18**, 358–378 (2019).
246. Belova, L., Kochergin-Nikitsky, K., Erofeeva, A., Lavrov, A. & Smirnikhina, S. Approaches to purification and concentration of rAAV vectors for gene therapy. *BioEssays* **44**, 2200019 (2022).

247. Scott, J. M. *et al.* Viral vectors for gene transfer of micro-, mini-, or full-length dystrophin. *Neuromuscular Disorders* **12**, S23–S29 (2002).
248. Le Guiner, C. *et al.* Long-term microdystrophin gene therapy is effective in a canine model of Duchenne muscular dystrophy. *Nat Commun* **8**, 16105 (2017).
249. Muntoni, F., Torelli, S. & Ferlini, A. Dystrophin and mutations: one gene, several proteins, multiple phenotypes. *The Lancet Neurology* **2**, 731–740 (2003).
250. Davies, K. E. & Vogt, J. Long-term clinical follow-up of a family with Becker muscular dystrophy associated with a large deletion in the *DMD* gene. *Neuromuscular Disorders* **39**, 5–9 (2024).
251. England, S. B. *et al.* Very mild muscular dystrophy associated with the deletion of 46% of dystrophin. *Nature* **343**, 180–182 (1990).
252. Mullard, A. FDA approves first gene therapy for Duchenne muscular dystrophy, despite internal objections. *Nature Reviews Drug Discovery* **22**, 610–610 (2023).
253. Rind, D. M. The FDA and Gene Therapy for Duchenne Muscular Dystrophy. *JAMA* (2024) doi:10.1001/jama.2024.5613.
254. Chamberlain, J. S. *et al.* Microdystrophin Expression as a Surrogate Endpoint for Duchenne Muscular Dystrophy Clinical Trials. *Human Gene Therapy* **34**, 404–415 (2023).
255. Mendell, J. R. *et al.* Assessment of Systemic Delivery of rAAVrh74.MHCK7.micro-dystrophin in Children With Duchenne Muscular Dystrophy: A Nonrandomized Controlled Trial. *JAMA Neurology* **77**, 1122–1131 (2020).
256. Mendell, J. R. *et al.* Expression of SRP-9001 dystrophin and stabilization of motor function up to 2 years post-treatment with delandistrogene moxeparovec gene therapy in individuals with Duchenne muscular dystrophy. *Frontiers in Cell and Developmental Biology* **11**, (2023).
257. Greg. Summary of Pfizer Phase 1 Microdystrophin Gene Therapy Trial. *CureDuchenne* <https://cureduchenne.org/blog/summary-of-pfizer-phase-1-microdystrophin-gene-therapy-trial/> (2019).
258. Birch, S. M. *et al.* Assessment of systemic AAV-microdystrophin gene therapy in the GRMD model of Duchenne muscular dystrophy. *Science Translational Medicine* **15**, eabo1815 (2023).
259. Phelps, S. F. *et al.* Expression of full-length and truncated dystrophin mini-genes in transgenic mdx mice. *Human Molecular Genetics* **4**, 1251–1258 (1995).
260. Wells, D. J. *et al.* Expression of human full-length and minidystrophin in transgenic mdx mice: implications for gene therapy of Duchenne muscular dystrophy. *Human Molecular Genetics* **4**, 1245–1250 (1995).
261. Ronzitti, G., Gross, D.-A. & Mingozi, F. Human Immune Responses to Adeno-Associated Virus (AAV) Vectors. *Front. Immunol.* **11**, (2020).
262. Bönnemann, C. G. *et al.* Dystrophin Immunity after Gene Therapy for Duchenne’s Muscular Dystrophy. *New England Journal of Medicine* (2023) doi:10.1056/NEJMc2212912.
263. Howard, Z. M. *et al.* Micro-dystrophin gene therapy prevents heart failure in an improved Duchenne muscular dystrophy cardiomyopathy mouse model. *JCI Insight* **6**, (2021).
264. Wang, H. *et al.* Proteomic analysis identifies key differences in the cardiac interactomes of dystrophin and micro-dystrophin. *Human Molecular Genetics* **30**, 1321–1336 (2021).

265. Piepho, A. B. *et al.* Micro-dystrophin gene therapy demonstrates long-term cardiac efficacy in a severe Duchenne muscular dystrophy model. *Molecular Therapy Methods & Clinical Development* **28**, 344–354 (2023).
266. Hart, C. C. *et al.* Potential limitations of micro-dystrophin gene therapy for Duchenne muscular dystrophy. <https://insight-jci-org.proxy.insermbiblio.inist.fr/articles/view/165869/pdf> (2024) doi:10.1172/jci.insight.165869.
267. Philippidis, A. Boy Dosed with Pfizer's Duchenne Muscular Dystrophy Gene Therapy Dies a Year After Phase II Trial. *Human Gene Therapy* (2024) doi:10.1089/hum.2024.53426.bfs.
268. Tabebordbar, M. *et al.* Directed evolution of a family of AAV capsid variants enabling potent muscle-directed gene delivery across species. *Cell* **184**, 4919–4938.e22 (2021).
269. Weinmann, J. *et al.* Identification of a myotropic AAV by massively parallel in vivo evaluation of barcoded capsid variants. *Nat Commun* **11**, 5432 (2020).
270. El Andari, J. *et al.* Semirational bioengineering of AAV vectors with increased potency and specificity for systemic gene therapy of muscle disorders. *Science Advances* **8**, eabn4704 (2022).
271. Hong, A. V., Suel, L., Poupiot, J. & Richard, I. An integrin-targeting AAV developed using a novel computational rational design methodology presents improved targeting of the skeletal muscle and reduced liver tropism. (2023) doi:10.21203/rs.3.rs-3466229/v1.
272. Lai, Y. *et al.* Efficient in vivo gene expression by trans-splicing adeno-associated viral vectors. *Nat Biotechnol* **23**, 1435–1439 (2005).
273. Koo, T., Popplewell, L., Athanasopoulos, T. & Dickson, G. Triple Trans-Splicing Adeno-Associated Virus Vectors Capable of Transferring the Coding Sequence for Full-Length Dystrophin Protein into Dystrophic Mice. *Human Gene Therapy* **25**, 98–108 (2014).
274. Kodippili, K. *et al.* Dual AAV Gene Therapy for Duchenne Muscular Dystrophy with a 7-kb Mini-Dystrophin Gene in the Canine Model. *Human Gene Therapy* **29**, 299–311 (2018).
275. Albin, S. *et al.* Assessment of Therapeutic Potential of a Dual AAV Approach for Duchenne Muscular Dystrophy. *International Journal of Molecular Sciences* **24**, 11421 (2023).
276. Tasfaout, H. *et al.* Split intein-mediated protein trans-splicing to express large dystrophins. *Nature* 1–9 (2024) doi:10.1038/s41586-024-07710-8.
277. Zhou, Y., Zhang, C., Xiao, W., Herzog, R. W. & Han, R. Systemic delivery of full-length dystrophin in Duchenne muscular dystrophy mice. *Nat Commun* **15**, 6141 (2024).
278. Aartsma-Rus, A. *et al.* Theoretic applicability of antisense-mediated exon skipping for Duchenne muscular dystrophy mutations. *Human Mutation* **30**, 293–299 (2009).
279. Alfano, L. N. *et al.* Long-term treatment with eteplirsen in nonambulatory patients with Duchenne muscular dystrophy. *Medicine* **98**, e15858 (2019).
280. Mendell, J. R. *et al.* Longitudinal effect of eteplirsen versus historical control on ambulation in Duchenne muscular dystrophy. *Annals of Neurology* **79**, 257–271 (2016).
281. Frank, D. E. *et al.* Increased dystrophin production with golodirsen in patients with Duchenne muscular dystrophy. *Neurology* **94**, e2270–e2282 (2020).
282. Roshmi, R. R. & Yokota, T. Viltolarsen for the treatment of Duchenne muscular dystrophy. *Drugs Today (Barc)* **55**, 627–639 (2019).

283. Wagner, K. R. *et al.* Safety, tolerability, and pharmacokinetics of casimersen in patients with Duchenne muscular dystrophy amenable to exon 45 skipping: A randomized, double-blind, placebo-controlled, dose-titration trial. *Muscle & Nerve* **64**, 285–292 (2021).
284. Heo, Y.-A. Golodirsen: First Approval. *Drugs* **80**, 329–333 (2020).
285. Komaki, H. *et al.* Viltolarsen in Japanese Duchenne muscular dystrophy patients: A phase 1/2 study. *Annals of Clinical and Translational Neurology* **7**, 2393–2408 (2020).
286. Iannaccone, S. *et al.* P.132 Casimersen in patients with Duchenne muscular dystrophy amenable to exon 45 skipping: Interim results from the Phase 3 ESSENCE trial. *Neuromuscular Disorders* **32**, S102 (2022).
287. Doudna, J. A. & Charpentier, E. The new frontier of genome engineering with CRISPR-Cas9. *Science* **346**, 1258096 (2014).
288. Adli, M. The CRISPR tool kit for genome editing and beyond. *Nat Commun* **9**, 1911 (2018).
289. Chemello, F., Bassel-Duby, R. & Olson, E. N. Correction of muscular dystrophies by CRISPR gene editing. *J Clin Invest* **130**, 2766–2776 (2020).
290. Min, Y.-L. *et al.* CRISPR-Cas9 corrects Duchenne muscular dystrophy exon 44 deletion mutations in mice and human cells. *Science Advances* **5**, eaav4324 (2019).
291. Zhang, Y., Bassel-Duby, R. & Olson, E. N. CRISPR-Cas9 Correction of Duchenne Muscular Dystrophy in Mice by a Self-Complementary AAV Delivery System. in *Muscular Dystrophy Therapeutics: Methods and Protocols* (eds. Maruyama, R. & Yokota, T.) 411–425 (Springer US, New York, NY, 2023). doi:10.1007/978-1-0716-2772-3\_21.
292. Ousterout, D. G. *et al.* Multiplex CRISPR/Cas9-based genome editing for correction of dystrophin mutations that cause Duchenne muscular dystrophy. *Nat Commun* **6**, 6244 (2015).
293. Duchêne, B. L. *et al.* CRISPR-Induced Deletion with SaCas9 Restores Dystrophin Expression in Dystrophic Models In Vitro and In Vivo. *Molecular Therapy* **26**, 2604–2616 (2018).
294. Sengupta, K. *et al.* Genome Editing-Mediated Utrophin Upregulation in Duchenne Muscular Dystrophy Stem Cells. *Molecular Therapy - Nucleic Acids* **22**, 500–509 (2020).
295. Lek, A. *et al.* Unexpected Death of a Duchenne Muscular Dystrophy Patient in an N-of-1 Trial of rAAV9-delivered CRISPR-transactivator. 2023.05.16.23289881 Preprint at <https://doi.org/10.1101/2023.05.16.23289881> (2023).
296. Barral, D. C. *et al.* Current methods to analyze lysosome morphology, positioning, motility and function. *Traffic* **23**, 238–269 (2022).
297. Settembre, C. & Perera, R. M. Lysosomes as coordinators of cellular catabolism, metabolic signalling and organ physiology. *Nat Rev Mol Cell Biol* **25**, 223–245 (2024).
298. Ouimet, M. *et al.* Autophagy Regulates Cholesterol Efflux from Macrophage Foam Cells via Lysosomal Acid Lipase. *Cell Metabolism* **13**, 655–667 (2011).
299. Dubland, J. A. & Francis, G. A. Lysosomal acid lipase: at the crossroads of normal and atherogenic cholesterol metabolism. *Front. Cell Dev. Biol.* **3**, (2015).
300. Forgac, M. Vacuolar ATPases: rotary proton pumps in physiology and pathophysiology. *Nat Rev Mol Cell Biol* **8**, 917–929 (2007).
301. Mindell, J. A. Lysosomal Acidification Mechanisms\*. *Annual Review of Physiology* **74**, 69–86 (2012).

302. Shin, H. R. *et al.* Lysosomal GPCR-like protein LYCHOS signals cholesterol sufficiency to mTORC1. *Science* **377**, 1290–1298 (2022).
303. Cabukusta, B. & Neefjes, J. Mechanisms of lysosomal positioning and movement. *Traffic* **19**, 761–769 (2018).
304. Pu, J., Guardia, C. M., Keren-Kaplan, T. & Bonifacino, J. S. Mechanisms and functions of lysosome positioning. *Journal of Cell Science* **129**, 4329–4339 (2016).
305. Kaushik, S. & Cuervo, A. M. Chaperone-mediated autophagy: a unique way to enter the lysosome world. *Trends in Cell Biology* **22**, 407–417 (2012).
306. Dubouloz, F., Deloche, O., Wanke, V., Camerini, E. & Virgilio, C. D. The TOR and EGO Protein Complexes Orchestrate Microautophagy in Yeast. *Molecular Cell* **19**, 15–26 (2005).
307. Papadopoulos, C., Kravic, B. & Meyer, H. Repair or Lysophagy: Dealing with Damaged Lysosomes. *Journal of Molecular Biology* **432**, 231–239 (2020).
308. Nakatogawa, H. & Mochida, K. Reticulophagy and nucleophagy: New findings and unsolved issues. *Autophagy* **11**, 2377–2378 (2015).
309. Jin, S. M. & Youle, R. J. PINK1- and Parkin-mediated mitophagy at a glance. *Journal of Cell Science* **125**, 795–799 (2012).
310. Fujiwara, Y., Wada, K. & Kabuta, T. Lysosomal degradation of intracellular nucleic acids-multiple autophagic pathways. *J Biochem* **161**, 145–154 (2017).
311. Zhang, S. *et al.* The regulation, function, and role of lipophagy, a form of selective autophagy, in metabolic disorders. *Cell Death Dis* **13**, 1–11 (2022).
312. Germain, K. *et al.* Upregulated pexophagy limits the capacity of selective autophagy. *Nat Commun* **15**, 375 (2024).
313. Mizushima, N. & Komatsu, M. Autophagy: Renovation of Cells and Tissues. *Cell* **147**, 728–741 (2011).
314. Perera, R. M. & Zoncu, R. The Lysosome as a Regulatory Hub. *Annu Rev Cell Dev Biol* **32**, 223–253 (2016).
315. Kim, J., Kundu, M., Viollet, B. & Guan, K.-L. AMPK and mTOR regulate autophagy through direct phosphorylation of Ulk1. *Nat Cell Biol* **13**, 132–141 (2011).
316. Egan, D. F. *et al.* Phosphorylation of ULK1 (hATG1) by AMP-Activated Protein Kinase Connects Energy Sensing to Mitophagy. *Science* **331**, 456–461 (2011).
317. Yin, Z., Pascual, C. & Klionsky, D. J. Autophagy: machinery and regulation. *Microbial Cell* **3**, 588–596 (2016).
318. Ohsumi, Y. Molecular dissection of autophagy: two ubiquitin-like systems. *Nat Rev Mol Cell Biol* **2**, 211–216 (2001).
319. Mizushima, N. The ATG conjugation systems in autophagy. *Current Opinion in Cell Biology* **63**, 1–10 (2020).
320. Tanida, I., Ueno, T. & Kominami, E. LC3 conjugation system in mammalian autophagy. *The International Journal of Biochemistry & Cell Biology* **36**, 2503–2518 (2004).
321. Han, J., Pluhackova, K. & Böckmann, R. A. The Multifaceted Role of SNARE Proteins in Membrane Fusion. *Front. Physiol.* **8**, (2017).
322. Kümmel, D. & Ungermann, C. Principles of membrane tethering and fusion in endosome and lysosome biogenesis. *Current Opinion in Cell Biology* **29**, 61–66 (2014).

323. Jiang, P. *et al.* The HOPS complex mediates autophagosome–lysosome fusion through interaction with syntaxin 17. *MBoC* **25**, 1327–1337 (2014).
324. Hosokawa, N. *et al.* Nutrient-dependent mTORC1 Association with the ULK1–Atg13–FIP200 Complex Required for Autophagy. *MBoC* **20**, 1981–1991 (2009).
325. Park, J.-M. *et al.* The ULK1 complex mediates MTORC1 signaling to the autophagy initiation machinery via binding and phosphorylating ATG14. *Autophagy* **12**, 547–564 (2016).
326. Shang, L. *et al.* Nutrient starvation elicits an acute autophagic response mediated by Ulk1 dephosphorylation and its subsequent dissociation from AMPK. *Proceedings of the National Academy of Sciences* **108**, 4788–4793 (2011).
327. Lawrence, R. E. & Zoncu, R. The lysosome as a cellular centre for signalling, metabolism and quality control. *Nat Cell Biol* **21**, 133–142 (2019).
328. Sancak, Y. *et al.* The Rag GTPases Bind Raptor and Mediate Amino Acid Signaling to mTORC1. *Science* **320**, 1496–1501 (2008).
329. Sancak, Y. *et al.* Regulator-Rag Complex Targets mTORC1 to the Lysosomal Surface and Is Necessary for Its Activation by Amino Acids. *Cell* **141**, 290–303 (2010).
330. Sardiello, M. *et al.* A Gene Network Regulating Lysosomal Biogenesis and Function. *Science* **325**, 473–477 (2009).
331. Settembre, C. *et al.* TFEB Links Autophagy to Lysosomal Biogenesis. *Science* **332**, 1429–1433 (2011).
332. Yu, L. *et al.* Termination of autophagy and reformation of lysosomes regulated by mTOR. *Nature* **465**, 942–946 (2010).
333. Chen, Y. & Yu, L. Recent progress in autophagic lysosome reformation. *Traffic* **18**, 358–361 (2017).
334. McGrath, M. J. *et al.* Defective lysosome reformation during autophagy causes skeletal muscle disease. *Journal of Clinical Investigation* **131**, e135124 (2021).
335. McNeil, P. L. & Khakee, R. Disruptions of muscle fiber plasma membranes. Role in exercise-induced damage. *Am J Pathol* **140**, 1097–1109 (1992).
336. Rodríguez, A., Webster, P., Ortego, J. & Andrews, N. W. Lysosomes Behave as Ca<sup>2+</sup>-regulated Exocytic Vesicles in Fibroblasts and Epithelial Cells. *J Cell Biol* **137**, 93–104 (1997).
337. Reddy, A., Caler, E. V. & Andrews, N. W. Plasma Membrane Repair Is Mediated by Ca<sup>2+</sup>-Regulated Exocytosis of Lysosomes. *Cell* **106**, 157–169 (2001).
338. Tam, C. *et al.* Exocytosis of acid sphingomyelinase by wounded cells promotes endocytosis and plasma membrane repair. *Journal of Cell Biology* **189**, 1027–1038 (2010).
339. Holopainen, J. M., Angelova, M. I. & Kinnunen, P. K. J. Vectorial Budding of Vesicles by Asymmetrical Enzymatic Formation of Ceramide in Giant Liposomes. *Biophysical Journal* **78**, 830–838 (2000).
340. Castro-Gomes, T., Corrotte, M., Tam, C. & Andrews, N. W. Plasma Membrane Repair Is Regulated Extracellularly by Proteases Released from Lysosomes. *PLOS ONE* **11**, e0152583 (2016).
341. Idone, V. *et al.* Repair of injured plasma membrane by rapid Ca<sup>2+</sup>-dependent endocytosis. *Journal of Cell Biology* **180**, 905–914 (2008).
342. Lariccia, V. *et al.* Massive calcium-activated endocytosis without involvement of classical endocytic proteins. *Journal of General Physiology* **137**, 111–132 (2010).

343. Corrotte, M. *et al.* Caveolae internalization repairs wounded cells and muscle fibers. *eLife* **2**, e00926 (2013).
344. Michailowsky, V. *et al.* Defects in sarcolemma repair and skeletal muscle function after injury in a mouse model of Niemann–Pick type A/B disease. *Skeletal Muscle* **9**, 1 (2019).
345. Zoncu, R. *et al.* mTORC1 Senses Lysosomal Amino Acids Through an Inside-Out Mechanism That Requires the Vacuolar H<sup>+</sup>-ATPase. *Science* **334**, 678–683 (2011).
346. Yue, S., Li, G., He, S. & Li, T. The Central Role of mTORC1 in Amino Acid Sensing. *Cancer Research* **82**, 2964–2974 (2022).
347. Leprivier, G. & Rotblat, B. How does mTOR sense glucose starvation? AMPK is the usual suspect. *Cell Death Discov.* **6**, 1–5 (2020).
348. Davis, O. B. *et al.* NPC1-mTORC1 Signaling Couples Cholesterol Sensing to Organelle Homeostasis and Is a Targetable Pathway in Niemann-Pick Type C. *Developmental Cell* **56**, 260–276.e7 (2021).
349. Lama-Sherpa, T. D., Jeong, M.-H. & Jewell, J. L. Regulation of mTORC1 by the Rag GTPases. *Biochemical Society Transactions* **51**, 655–664 (2023).
350. Zoncu, R., Efeyan, A. & Sabatini, D. M. mTOR: from growth signal integration to cancer, diabetes and ageing. *Nat Rev Mol Cell Biol* **12**, 21–35 (2011).
351. Kim, E., Goraksha-Hicks, P., Li, L., Neufeld, T. P. & Guan, K.-L. Regulation of TORC1 by Rag GTPases in nutrient response. *Nat Cell Biol* **10**, 935–945 (2008).
352. Magnuson, B., Ekim, B. &ingar, D. C. Regulation and function of ribosomal protein S6 kinase (S6K) within mTOR signalling networks. *Biochemical Journal* **441**, 1–21 (2011).
353. Gingras, A.-C. *et al.* Regulation of 4E-BP1 phosphorylation: a novel two-step mechanism. *Genes Dev.* **13**, 1422–1437 (1999).
354. Martina, J. A., Chen, Y., Gucek, M. & Puertollano, R. mTORC1 functions as a transcriptional regulator of autophagy by preventing nuclear transport of TFEB. *Autophagy* **8**, 903–914 (2012).
355. Settembre, C. & Ballabio, A. Lysosome: regulator of lipid degradation pathways. *Trends in Cell Biology* **24**, 743–750 (2014).
356. Morales, P. E., Bucarey, J. L. & Espinosa, A. Muscle Lipid Metabolism: Role of Lipid Droplets and Perilipins. *Journal of Diabetes Research* **2017**, 1789395 (2017).
357. Pfisterer, S. G., Peränen, J. & Ikonen, E. LDL-cholesterol transport to the endoplasmic reticulum: current concepts. *Current Opinion in Lipidology* **27**, 282 (2016).
358. Juhl, A. D. & Wüstner, D. Pathways and Mechanisms of Cellular Cholesterol Efflux—Insight From Imaging. *Front. Cell Dev. Biol.* **10**, 834408 (2022).
359. Lloyd-Evans, E. & Waller-Evans, H. Lysosomal Ca<sup>2+</sup> Homeostasis and Signaling in Health and Disease. *Cold Spring Harb Perspect Biol* **12**, a035311 (2020).
360. Hu, M. *et al.* The ion channels of endomembranes. *Physiological Reviews* **104**, 1335–1385 (2024).
361. Cao, Q. *et al.* Calcium release through P2X4 activates calmodulin to promote endolysosomal membrane fusion. *Journal of Cell Biology* **209**, 879–894 (2015).
362. Rosato, A. S., Tang, R. & Grimm, C. Two-pore and TRPML cation channels: Regulators of phagocytosis, autophagy and lysosomal exocytosis. *Pharmacology & Therapeutics* **220**, 107713 (2021).

363. LaPlante, J. M. *et al.* Lysosomal exocytosis is impaired in mucopolipidosis type IV. *Molecular Genetics and Metabolism* **89**, 339–348 (2006).
364. Medina, D. L. *et al.* Transcriptional Activation of Lysosomal Exocytosis Promotes Cellular Clearance. *Developmental Cell* **21**, 421–430 (2011).
365. Medina, D. L. *et al.* Lysosomal calcium signalling regulates autophagy through calcineurin and TFEB. *Nat Cell Biol* **17**, 288–299 (2015).
366. Zhang, X. *et al.* MCOLN1 is a ROS sensor in lysosomes that regulates autophagy. *Nat Commun* **7**, 12109 (2016).
367. Nakamura, S. *et al.* LC3 lipidation is essential for TFEB activation during the lysosomal damage response to kidney injury. *Nat Cell Biol* **22**, 1252–1263 (2020).
368. Ballabio, A. & Gieselmann, V. Lysosomal disorders: From storage to cellular damage. *Biochimica et Biophysica Acta (BBA) - Molecular Cell Research* **1793**, 684–696 (2009).
369. Cheng, X. *et al.* The intracellular Ca<sup>2+</sup> channel MCOLN1 is required for sarcolemma repair to prevent muscular dystrophy. *Nat Med* **20**, 1187–1192 (2014).
370. Yu, L. *et al.* Small-molecule activation of lysosomal TRP channels ameliorates Duchenne muscular dystrophy in mouse models. *Science Advances* **6**, eaaz2736.
371. Lakpa, K. L., Khan, N., Afghah, Z., Chen, X. & Geiger, J. D. Lysosomal Stress Response (LSR): Physiological Importance and Pathological Relevance. *J Neuroimmune Pharmacol* **16**, 219–237 (2021).
372. Wheeler, S. & Sillence, D. J. Niemann–Pick type C disease: cellular pathology and pharmacotherapy. *Journal of Neurochemistry* **153**, 674–692 (2020).
373. Liao, G. *et al.* Cholesterol Accumulation Is Associated with Lysosomal Dysfunction and Autophagic Stress in Npc1<sup>-/-</sup> Mouse Brain. *The American Journal of Pathology* **171**, 962–975 (2007).
374. Terman, A., Kurz, T., Gustafsson, B. & Brunk, U. T. Lysosomal labilization. *IUBMB Life* **58**, 531–539 (2006).
375. Krenn, M. A. *et al.* Ferritin-stimulated lipid peroxidation, lysosomal leak, and macroautophagy promote lysosomal “metastability” in primary hepatocytes determining *in vitro* cell survival. *Free Radical Biology and Medicine* **80**, 48–58 (2015).
376. Eaton, J. W. & Qian, M. Molecular bases of cellular iron toxicity<sup>12</sup>. *Free Radical Biology and Medicine* **32**, 833–840 (2002).
377. Zhitomirsky, B. & Assaraf, Y. G. Lysosomal sequestration of hydrophobic weak base chemotherapeutics triggers lysosomal biogenesis and lysosome-dependent cancer multidrug resistance. *Oncotarget* **6**, 1143–1156 (2014).
378. Fedele, A. O. & Proud, C. G. Chloroquine and bafilomycin A mimic lysosomal storage disorders and impair mTORC1 signalling. *Bioscience Reports* **40**, BSR20200905 (2020).
379. Mauthe, M. *et al.* Chloroquine inhibits autophagic flux by decreasing autophagosome-lysosome fusion. *Autophagy* **14**, 1435–1455 (2018).
380. Nara, A., Aki, T., Funakoshi, T., Unuma, K. & Uemura, K. Hyperstimulation of macropinocytosis leads to lysosomal dysfunction during exposure to methamphetamine in SH-SY5Y cells. *Brain Research* **1466**, 1–14 (2012).

381. Funakoshi-Hirose, I. *et al.* Distinct effects of methamphetamine on autophagy–lysosome and ubiquitin–proteasome systems in HL-1 cultured mouse atrial cardiomyocytes. *Toxicology* **312**, 74–82 (2013).
382. Nash, B. *et al.* Morphine-Induced Modulation of Endolysosomal Iron Mediates Upregulation of Ferritin Heavy Chain in Cortical Neurons. *eNeuro* **6**, (2019).
383. Johnson, D. E., Ostrowski, P., Jaumouillé, V. & Grinstein, S. The position of lysosomes within the cell determines their luminal pH. *Journal of Cell Biology* **212**, 677–692 (2016).
384. Boya, P. & Kroemer, G. Lysosomal membrane permeabilization in cell death. *Oncogene* **27**, 6434–6451 (2008).
385. Wang, F., Gómez-Sintes, R. & Boya, P. Lysosomal membrane permeabilization and cell death. *Traffic* **19**, 918–931 (2018).
386. Aits, S. *et al.* Sensitive detection of lysosomal membrane permeabilization by lysosomal galectin puncta assay. *Autophagy* **11**, 1408–1424 (2015).
387. Jia, J. *et al.* Galectin-3 Coordinates a Cellular System for Lysosomal Repair and Removal. *Developmental Cell* **52**, 69-87.e8 (2020).
388. Freeman, D. *et al.* Alpha-Synuclein Induces Lysosomal Rupture and Cathepsin Dependent Reactive Oxygen Species Following Endocytosis. *PLOS ONE* **8**, e62143 (2013).
389. Ditaranto, K., Tekirian, T. L. & Yang, A. J. Lysosomal Membrane Damage in Soluble A $\beta$ -Mediated Cell Death in Alzheimer’s Disease. *Neurobiology of Disease* **8**, 19–31 (2001).
390. Uchimoto, T. *et al.* Mechanism of apoptosis induced by a lysosomotropic agent, L-Leucyl-L-Leucine methyl ester. *Apoptosis* **4**, 357–362 (1999).
391. Kurz, T., Eaton, J. W. & Brunk, U. T. The role of lysosomes in iron metabolism and recycling. *The International Journal of Biochemistry & Cell Biology* **43**, 1686–1697 (2011).
392. Uchiyama, A. *et al.* Translocation of iron from lysosomes into mitochondria is a key event during oxidative stress-induced hepatocellular injury. *Hepatology* **48**, 1644–1654 (2008).
393. Yambire, K. F. *et al.* Impaired lysosomal acidification triggers iron deficiency and inflammation in vivo. *eLife* **8**, e51031 (2019).
394. Redmann, M. *et al.* Inhibition of autophagy with bafilomycin and chloroquine decreases mitochondrial quality and bioenergetic function in primary neurons. *Redox Biology* **11**, 73–81 (2017).
395. Boya, P. & Kroemer, G. Lysosomal membrane permeabilization in cell death. *Oncogene* **27**, 6434–6451 (2008).
396. Galluzzi, L. *et al.* Molecular mechanisms of cell death: recommendations of the Nomenclature Committee on Cell Death 2018. *Cell Death Differ* **25**, 486–541 (2018).
397. de Castro, M. a. G., Bunt, G. & Wouters, F. S. Cathepsin B launches an apoptotic exit effort upon cell death-associated disruption of lysosomes. *Cell Death Discovery* **2**, 1–8 (2016).
398. Laforge, M. *et al.* DRAM Triggers Lysosomal Membrane Permeabilization and Cell Death in CD4+ T Cells Infected with HIV. *PLOS Pathogens* **9**, e1003328 (2013).
399. Gómez-Sintes, R., Ledesma, M. D. & Boya, P. Lysosomal cell death mechanisms in aging. *Ageing Research Reviews* **32**, 150–168 (2016).
400. Zhang, L., Sheng, R. & Qin, Z. The lysosome and neurodegenerative diseases. *Acta Biochimica et Biophysica Sinica* **41**, 437–445 (2009).

401. Nixon, R. A. The aging lysosome: An essential catalyst for late-onset neurodegenerative diseases. *Biochimica et Biophysica Acta (BBA) - Proteins and Proteomics* **1868**, 140443 (2020).
402. Chen, G., Kroemer, G. & Kepp, O. Mitophagy: An Emerging Role in Aging and Age-Associated Diseases. *Front. Cell Dev. Biol.* **8**, (2020).
403. Marques, A. R. A. & Saftig, P. Lysosomal storage disorders – challenges, concepts and avenues for therapy: beyond rare diseases. *Journal of Cell Science* **132**, jcs221739 (2019).
404. Parenti, G., Andria, G. & Ballabio, A. Lysosomal Storage Diseases: From Pathophysiology to Therapy. *Annual Review of Medicine* **66**, 471–486 (2015).
405. Nixon, R. A. The role of autophagy in neurodegenerative disease. *Nat Med* **19**, 983–997 (2013).
406. Palmieri, M. *et al.* mTORC1-independent TFEB activation via Akt inhibition promotes cellular clearance in neurodegenerative storage diseases. *Nat Commun* **8**, 14338 (2017).
407. Rusmini, P. *et al.* Trehalose induces autophagy via lysosomal-mediated TFEB activation in models of motoneuron degeneration. *Autophagy* **15**, 631–651 (2019).
408. Bartlett, J. J., Trivedi, P. C., Yeung, P., Kienesberger, P. C. & Pulinilkunnil, T. Doxorubicin impairs cardiomyocyte viability by suppressing transcription factor EB expression and disrupting autophagy. *Biochemical Journal* **473**, 3769–3789 (2016).
409. Santin, Y. *et al.* Inhalation of acidic nanoparticles prevents doxorubicin cardiotoxicity through improvement of lysosomal function. *Theranostics* **13**, 5435–5451 (2023).
410. Arhzaouy, K. *et al.* VCP maintains lysosomal homeostasis and TFEB activity in differentiated skeletal muscle. *Autophagy* **15**, 1082–1099 (2019).
411. Steen, M. S., Adams, M. E., Tesch, Y. & Froehner, S. C. Amelioration of Muscular Dystrophy by Transgenic Expression of Niemann-Pick C1. *MBoC* **20**, 146–152 (2009).
412. Meyer, H. & Kravic, B. The Endo-Lysosomal Damage Response. *Annual Review of Biochemistry* (2024) doi:10.1146/annurev-biochem-030222-102505.
413. Yang, H. & Tan, J. X. Lysosomal quality control: molecular mechanisms and therapeutic implications. *Trends in Cell Biology* **33**, 749–764 (2023).
414. Radulovic, M. *et al.* ESCRT -mediated lysosome repair precedes lysophagy and promotes cell survival. *The EMBO Journal* **37**, e99753 (2018).
415. Skowyra, M. L., Schlesinger, P. H., Naismith, T. V. & Hanson, P. I. Triggered recruitment of ESCRT machinery promotes endolysosomal repair. *Science* **360**, eaar5078 (2018).
416. Henne, W. M., Stenmark, H. & Emr, S. D. Molecular Mechanisms of the Membrane Sculpting ESCRT Pathway. *Cold Spring Harb Perspect Biol* **5**, a016766 (2013).
417. Niekamp, P. *et al.* Ca<sup>2+</sup>-activated sphingomyelin scrambling and turnover mediate ESCRT-independent lysosomal repair. *Nat Commun* **13**, 1875 (2022).
418. Tan, J. X. & Finkel, T. A phosphoinositide signalling pathway mediates rapid lysosomal repair. *Nature* **609**, 815–821 (2022).
419. Radulovic, M. *et al.* Cholesterol transfer via endoplasmic reticulum contacts mediates lysosome damage repair. *The EMBO Journal* **41**, e112677 (2022).
420. Yim, W. W.-Y., Yamamoto, H. & Mizushima, N. Annexins A1 and A2 are recruited to larger lysosomal injuries independently of ESCRTs to promote repair. *FEBS Letters* **596**, 991–1003 (2022).
421. Bussi, C. *et al.* Stress granules plug and stabilize damaged endolysosomal membranes. *Nature* **623**, 1062–1069 (2023).

422. Jia, J. *et al.* Stress granules and mTOR are regulated by membrane atg8ylation during lysosomal damage. *Journal of Cell Biology* **221**, e202207091 (2022).
423. Markmiller, S. *et al.* Context-Dependent and Disease-Specific Diversity in Protein Interactions within Stress Granules. *Cell* **172**, 590-604.e13 (2018).
424. Raben, N. *et al.* Deconstructing Pompe Disease by Analyzing Single Muscle Fibers: "To See a World in a Grain of Sand...". *Autophagy* **3**, 546-552 (2007).
425. Hung, Y.-H., Chen, L. M.-W., Yang, J.-Y. & Yuan Yang, W. Spatiotemporally controlled induction of autophagy-mediated lysosome turnover. *Nat Commun* **4**, 2111 (2013).
426. Maejima, I. *et al.* Autophagy sequesters damaged lysosomes to control lysosomal biogenesis and kidney injury. *The EMBO Journal* **32**, 2336-2347 (2013).
427. Chauhan, S. *et al.* TRIMs and Galectins Globally Cooperate and TRIM16 and Galectin-3 Co-direct Autophagy in Endomembrane Damage Homeostasis. *Developmental Cell* **39**, 13-27 (2016).
428. Jia, J. *et al.* AMPK, a Regulator of Metabolism and Autophagy, Is Activated by Lysosomal Damage via a Novel Galectin-Directed Ubiquitin Signal Transduction System. *Molecular Cell* **77**, 951-969.e9 (2020).
429. Eapen, V. V., Swarup, S., Hoyer, M. J., Paulo, J. A. & Harper, J. W. Quantitative proteomics reveals the selectivity of ubiquitin-binding autophagy receptors in the turnover of damaged lysosomes by lysophagy. *eLife* **10**, e72328 (2021).
430. Burbidge, K. *et al.* LGALS3 (galectin 3) mediates an unconventional secretion of SNCA/ $\alpha$ -synuclein in response to lysosomal membrane damage by the autophagic-lysosomal pathway in human midbrain dopamine neurons. *Autophagy* **18**, 1020-1048 (2022).
431. Xu, Y. *et al.* TFEB regulates lysosomal exocytosis of tau and its loss of function exacerbates tau pathology and spreading. *Mol Psychiatry* **26**, 5925-5939 (2021).
432. Domingues, N. *et al.* Connexin43 promotes exocytosis of damaged lysosomes through actin remodelling. *The EMBO Journal* 1-23 (2024) doi:10.1038/s44318-024-00177-3.
433. Napolitano, G. & Ballabio, A. TFEB at a glance. *Journal of Cell Science* **129**, 2475-2481 (2016).
434. Rocznik-Ferguson, A. *et al.* The Transcription Factor TFEB Links mTORC1 Signaling to Transcriptional Control of Lysosome Homeostasis. *Science Signaling* **5**, ra42-ra42 (2012).
435. Barrientos, G., Sánchez-Aguilera, P., Jaimovich, E., Hidalgo, C. & Llanos, P. Membrane Cholesterol in Skeletal Muscle: A Novel Player in Excitation-Contraction Coupling and Insulin Resistance. *Journal of Diabetes Research* **2017**, e3941898 (2017).
436. Cox, B. E., Griffin, E. E., Ullery, J. C. & W. Gray, J. Effects of cellular cholesterol loading on macrophage foam cell lysosome acidification. *Journal of Lipid Research* **48**, 1012-1021 (2007).
437. Folts, C. J., Scott-Hewitt, N., Pröschel, C., Mayer-Pröschel, M. & Noble, M. Lysosomal Re-acidification Prevents Lysosphingolipid-Induced Lysosomal Impairment and Cellular Toxicity. *PLoS Biol* **14**, e1002583 (2016).
438. Shen, D. *et al.* Lipid storage disorders block lysosomal trafficking by inhibiting a TRP channel and lysosomal calcium release. *Nat Commun* **3**, 731 (2012).
439. Rocha, N. *et al.* Cholesterol sensor ORP1L contacts the ER protein VAP to control Rab7-RILP-p150Glued and late endosome positioning. *Journal of Cell Biology* **185**, 1209-1225 (2009).
440. Sobo, K. *et al.* Late Endosomal Cholesterol Accumulation Leads to Impaired Intra-Endosomal Trafficking. *PLOS ONE* **2**, e851 (2007).

441. Fraldi, A. *et al.* Lysosomal fusion and SNARE function are impaired by cholesterol accumulation in lysosomal storage disorders. *The EMBO Journal* **29**, 3607–3620 (2010).
442. Strauss, K. *et al.* Exosome Secretion Ameliorates Lysosomal Storage of Cholesterol in Niemann-Pick Type C Disease\*. *Journal of Biological Chemistry* **285**, 26279–26288 (2010).
443. Rodriguez-Navarro, J. A. & Cuervo, A. M. Dietary lipids and aging compromise chaperone-mediated autophagy by similar mechanisms. *Autophagy* **8**, 1152–1154 (2012).
444. Xie, Y., Li, J., Kang, R. & Tang, D. Interplay Between Lipid Metabolism and Autophagy. *Frontiers in Cell and Developmental Biology* **8**, (2020).
445. Cheng, C., Deng, X. & Xu, K. Increased expression of sterol regulatory element binding protein-2 alleviates autophagic dysfunction in NAFLD. *International Journal of Molecular Medicine* **41**, 1877–1886 (2018).
446. Gelman, B. B., Davis, M. H., Morris, R. E. & Gruenstein, E. Structural changes in lysosomes from cultured human fibroblasts in Duchenne's muscular dystrophy. *Journal of Cell Biology* **88**, 329–337 (1981).
447. Kominami, E., Kunio, I. & Katunuma, N. Activation of the intramyofibrillar autophagic-lysosomal system in muscular dystrophy. *Am J Pathol* **127**, 461–466 (1987).
448. Whitaker, J. N., Bertorini, T. E. & Mendell, J. R. Immunocytochemical studies of cathepsin D in human skeletal muscle. *Annals of Neurology* **13**, 133–142 (1983).
449. Duguez, S. *et al.* Dystrophin deficiency leads to disturbance of LAMP1-vesicle-associated protein secretion. *Cell. Mol. Life Sci.* **70**, 2159–2174 (2013).
450. Tjondrokoesoemo, A. *et al.* Cathepsin S Contributes to the Pathogenesis of Muscular Dystrophy in Mice\*. *Journal of Biological Chemistry* **291**, 9920–9928 (2016).
451. Sano, M. *et al.* Immunolocalization of cathepsins B, H and L in skeletal muscle of X-linked muscular dystrophy (mdx) mouse. *Acta Neuropathol* **75**, 217–225 (1988).
452. Spitali, P. *et al.* Autophagy is Impaired in the Tibialis Anterior of Dystrophin Null Mice. *PLoS Curr* **5**, ecurrents.md.e1226cefa851a2f079bbc406c0a21e80 (2013).
453. Yim, W. W.-Y. & Mizushima, N. Lysosome biology in autophagy. *Cell Discov* **6**, 1–12 (2020).
454. Myerowitz, R., Puertollano, R. & Raben, N. Impaired autophagy: The collateral damage of lysosomal storage disorders. *EBioMedicine* **63**, 103166 (2021).
455. Call, J. A. & Nichenko, A. S. Autophagy: an essential but limited cellular process for timely skeletal muscle recovery from injury. *Autophagy* **16**, 1344–1347 (2020).
456. Ikeda, S. *et al.* YAP plays a crucial role in the development of cardiomyopathy in lysosomal storage diseases. *J Clin Invest* **131**, (2021).
457. Barondes, S. H. *et al.* Galectins: A family of animal  $\beta$ -galactoside-binding lectins. *Cell* **76**, 597–598 (1994).
458. Marotta, M. *et al.* Muscle genome-wide expression profiling during disease evolution in mdx mice. *Physiological Genomics* **37**, 119–132 (2009).
459. Van Putten, M. *et al.* The Effects of Low Levels of Dystrophin on Mouse Muscle Function and Pathology. *PLoS ONE* **7**, e31937 (2012).
460. Henderson, N. C. & Sethi, T. The regulation of inflammation by galectin-3. *Immunological Reviews* **230**, 160–171 (2009).

461. Coulis, G. *et al.* Single-cell and spatial transcriptomics identify a macrophage population associated with skeletal muscle fibrosis. *Science Advances* **9**, eadd9984 (2023).
462. Cerri, D. G. *et al.* Endogenous galectin-3 is required for skeletal muscle repair. *Glycobiology* **31**, 1295–1307 (2021).
463. Rancourt, A. *et al.* Galectin-3 and N-acetylglucosamine promote myogenesis and improve skeletal muscle function in the mdx model of Duchenne muscular dystrophy. *The FASEB Journal* **32**, 6445–6455 (2018).
464. Abmayr, S., Gregorevic, P., Allen, J. M. & Chamberlain, J. S. Phenotypic Improvement of Dystrophic Muscles by rAAV/Microdystrophin Vectors Is Augmented by *Igf1* Codelivery. *Molecular Therapy* **12**, 441–450 (2005).
465. Heller, K. N., Mendell, J. T., Mendell, J. R. & Rodino-Klapac, L. R. MicroRNA-29 overexpression by adeno-associated virus suppresses fibrosis and restores muscle function in combination with micro-dystrophin. *JCI Insight* **2**, (2017).
466. Böhm, J. *et al.* A dog model for centronuclear myopathy carrying the most common DNM2 mutation. *Dis Model Mech* **15**, dmm049219 (2022).
467. Gómez-Oca, R., Cowling, B. S. & Laporte, J. Common Pathogenic Mechanisms in Centronuclear and Myotubular Myopathies and Latest Treatment Advances. *International Journal of Molecular Sciences* **22**, 11377 (2021).
468. Casati, S. R. *et al.* Mitochondria and Reactive Oxygen Species: The Therapeutic Balance of Powers for Duchenne Muscular Dystrophy. *Cells* **13**, 574 (2024).
469. Milad, N. *et al.* Increased plasma lipid levels exacerbate muscle pathology in the mdx mouse model of Duchenne muscular dystrophy. *Skeletal Muscle* **7**, 19 (2017).
470. Schulze, H. & Sandhoff, K. Lysosomal Lipid Storage Diseases. *Cold Spring Harb Perspect Biol* **3**, a004804 (2011).
471. Whyte, L. S., Lau, A. A., Hemsley, K. M., Hopwood, J. J. & Sargeant, T. J. Endo-lysosomal and autophagic dysfunction: a driving factor in Alzheimer's disease? *Journal of Neurochemistry* **140**, 703–717 (2017).
472. Las Heras, M. *et al.* Understanding the phenotypic variability in Niemann-Pick disease type C (NPC): a need for precision medicine. *npj Genom. Med.* **8**, 1–13 (2023).
473. Chen, A. & Gibney, P. A. Dietary Trehalose as a Bioactive Nutrient. *Nutrients* **15**, 1393 (2023).
474. Hara, A. *et al.* Galectin-3 as a Next-Generation Biomarker for Detecting Early Stage of Various Diseases. *Biomolecules* **10**, 389 (2020).
475. Nguyen, M.-N. *et al.* Mechanisms responsible for increased circulating levels of galectin-3 in cardiomyopathy and heart failure. *Sci Rep* **8**, 8213 (2018).
476. Inami, Y. *et al.* Hepatic steatosis inhibits autophagic proteolysis via impairment of autophagosomal acidification and cathepsin expression. *Biochemical and Biophysical Research Communications* **412**, 618–625 (2011).
477. Colacurcio, D. J. & Nixon, R. A. Disorders of lysosomal acidification—The emerging role of v-ATPase in aging and neurodegenerative disease. *Ageing Research Reviews* **32**, 75–88 (2016).
478. Do, H., Meena, N. K. & Raben, N. Failure of Autophagy in Pompe Disease. *Biomolecules* **14**, 573 (2024).

479. Kohler, L., Puertollano, R. & Raben, N. Pompe Disease: From Basic Science to Therapy. *Neurotherapeutics* **15**, 928–942 (2018).
480. Kimura, S. *et al.* Increase in cathepsin K gene expression in Duchenne muscular dystrophy skeletal muscle. *Neuropathology* **n/a**.
481. White, Z. *et al.* Cholesterol absorption blocker ezetimibe prevents muscle wasting in severe dysferlin-deficient and *mdx* mice. *J cachexia sarcopenia muscle* **13**, 544–560 (2022).
482. Donen, G. S. *et al.* Thermoneutral Housing and a Western Diet Combination Exacerbates DYSFERLIN-DEFICIENT Muscular Dystrophy. *Muscle and Nerve* **66**, 513–522 (2022).
483. Sellers, S. L. *et al.* Increased nonHDL cholesterol levels cause muscle wasting and ambulatory dysfunction in the mouse model of LGMD2B. *Journal of Lipid Research* **59**, 261–272 (2018).
484. Maharjan, Y. *et al.* Intracellular cholesterol transport inhibition Impairs autophagy flux by decreasing autophagosome–lysosome fusion. *Cell Communication and Signaling* **20**, 189 (2022).
485. Elrick, M. J., Yu, T., Chung, C. & Lieberman, A. P. Impaired proteolysis underlies autophagic dysfunction in Niemann-Pick type C disease. *Hum Mol Genet* **21**, 4876–4887 (2012).
486. Platt, F. M., d’Azzo, A., Davidson, B. L., Neufeld, E. F. & Tiffet, C. J. Lysosomal storage diseases. *Nat Rev Dis Primers* **4**, 27 (2018).
487. Nishi, H., Higashihara, T. & Inagi, R. Lipotoxicity in Kidney, Heart, and Skeletal Muscle Dysfunction. *Nutrients* **11**, 1664 (2019).
488. Bourg, N. *et al.* Co-Administration of Simvastatin Does Not Potentiate the Benefit of Gene Therapy in the *mdx* Mouse Model for Duchenne Muscular Dystrophy. *International Journal of Molecular Sciences* **23**, 2016 (2022).
489. Song, S. B. & Hwang, E. S. High Levels of ROS Impair Lysosomal Acidity and Autophagy Flux in Glucose-Deprived Fibroblasts by Activating ATM and Erk Pathways. *Biomolecules* **10**, 761 (2020).
490. Oyarzún, J. E. *et al.* Lysosome motility and distribution: Relevance in health and disease. *Biochimica et Biophysica Acta (BBA) - Molecular Basis of Disease* **1865**, 1076–1087 (2019).
491. Abou Sawan, S., Mazzulla, M., Moore, D. R. & Hodson, N. More than just a garbage can: emerging roles of the lysosome as an anabolic organelle in skeletal muscle. *American Journal of Physiology-Cell Physiology* **319**, C561–C568 (2020).
492. Triolo, M., Oliveira, A. N., Kumari, R. & Hood, D. A. The influence of age, sex, and exercise on autophagy, mitophagy, and lysosome biogenesis in skeletal muscle. *Skeletal Muscle* **12**, 13 (2022).
493. Xia, Q. *et al.* The Role of Autophagy in Skeletal Muscle Diseases. *Front. Physiol.* **12**, (2021).
494. Lei, Y. *et al.* The role of mitochondrial dynamics and mitophagy in skeletal muscle atrophy: from molecular mechanisms to therapeutic insights. *Cellular & Molecular Biology Letters* **29**, 59 (2024).
495. Moon, H. Y. *et al.* Running-Induced Systemic Cathepsin B Secretion Is Associated with Memory Function. *Cell Metabolism* **24**, 332–340 (2016).
496. Matthews, I. *et al.* Skeletal muscle TFEB signaling promotes central nervous system function and reduces neuroinflammation during aging and neurodegenerative disease. *Cell Reports* **42**, 113436 (2023).
497. Mullard, A. Sarepta’s DMD gene therapy falls flat. *Nature Reviews Drug Discovery* **20**, 91–91 (2021).

498. Israeli, D. *et al.* An AAV-SGCG Dose-Response Study in a  $\gamma$ -Sarcoglycanopathy Mouse Model in the Context of Mechanical Stress. *Molecular Therapy - Methods & Clinical Development* **13**, 494–502 (2019).
499. Richards, A. B. *et al.* Trehalose: a review of properties, history of use and human tolerance, and results of multiple safety studies. *Food and Chemical Toxicology* **40**, 871–898 (2002).
500. Pupyshev, A. B., Klyushnik, T. P., Akopyan, A. A., Singh, S. K. & Tikhonova, M. A. Disaccharide trehalose in experimental therapies for neurodegenerative disorders: Molecular targets and translational potential. *Pharmacological Research* **183**, 106373 (2022).
501. Davies, J. E., Sarkar, S. & Rubinsztein, D. C. Trehalose reduces aggregate formation and delays pathology in a transgenic mouse model of oculopharyngeal muscular dystrophy. *Human Molecular Genetics* **15**, 23–31 (2006).
502. Argov, Z., Vornovitsky, H., Blumen, S. & Caraco, Y. First Human Use of High Dose IV Trehalose: Safety, Tolerability and Pharmacokinetic Results from the Oculopharyngeal Muscular Dystrophy (OPMD) Therapy Trial (P7.068). *Neurology* **84**, P7.068 (2015).
503. Bodine, S. C. The role of mTORC1 in the regulation of skeletal muscle mass. *F1000Prime Rep* **11**, (2022).
504. Baraldo, M. *et al.* Skeletal muscle mTORC1 regulates neuromuscular junction stability. *Journal of Cachexia, Sarcopenia and Muscle* **11**, 208–225 (2020).
505. Risson, V. *et al.* Muscle inactivation of mTOR causes metabolic and dystrophin defects leading to severe myopathy. *Journal of Cell Biology* **187**, 859–874 (2009).
506. Tang, Q. *et al.* Trehalose ameliorates oxidative stress-mediated mitochondrial dysfunction and ER stress via selective autophagy stimulation and autophagic flux restoration in osteoarthritis development. *Cell Death Dis* **8**, e3081–e3081 (2017).
507. Mizunoe, Y. *et al.* Trehalose protects against oxidative stress by regulating the Keap1–Nrf2 and autophagy pathways. *Redox Biology* **15**, 115–124 (2018).
508. Liu, Z. *et al.* Trehalose Induces Autophagy Against Inflammation by Activating TFEB Signaling Pathway in Human Corneal Epithelial Cells Exposed to Hyperosmotic Stress. *Investigative Ophthalmology & Visual Science* **61**, 26 (2020).
509. Echigo, R. *et al.* Trehalose treatment suppresses inflammation, oxidative stress, and vasospasm induced by experimental subarachnoid hemorrhage. *J Transl Med* **10**, 80 (2012).
510. Miyake, T. *et al.* Trehalose ameliorates peritoneal fibrosis by promoting Snail degradation and inhibiting mesothelial-to-mesenchymal transition in mesothelial cells. *Sci Rep* **10**, 14292 (2020).
511. Wu, N. *et al.* Trehalose attenuates TGF- $\beta$ 1-induced fibrosis of hSCFs by activating autophagy. *Mol Cell Biochem* **470**, 175–188 (2020).
512. Maruf, A., Milewska, M., Varga, M. & Wandzik, I. Trehalose-Bearing Carriers to Target Impaired Autophagy and Protein Aggregation Diseases. *J. Med. Chem.* **66**, 15613–15628 (2023).

# ANNEX

## Scientific Productions

- **Oral presentations:**

- 2023 Padua Days on Muscle & Mobility Medicine, Padua, Italy, March 29 – April 1<sup>st</sup>  
2023: "Perturbations of cholesterol metabolism in the dystrophic muscle in DMD"  
- [Youtube Recording](#).
- 2023 Journée de l'école doctorale EDSV, Université Paris-Saclay, France, May 16<sup>th</sup>,  
2023: "Cholesterol perturbations in Duchenne Muscular Dystrophy: toward combined approaches".
- Journées de l'Institut des Biothérapies (IDB), Étiolles, France, September 18-19<sup>th</sup>  
2023: short presentation "Perturbations of cholesterol metabolism in the dystrophic muscle in DMD: towards combined approaches"
- 20èmes Journées de la Société Française de Myologie (JSFM) 2023, Palais des Congrès, La Baule, France, November 15-17<sup>th</sup> 2023 : "Targeting lysosome damage in Duchenne muscular dystrophy improves micro-dystrophin gene therapy »  
**→ BEST ORAL PRESENTATION AWARD**
- 8th International congress myology, Palais des Congrès de Paris, France, April 22-25<sup>th</sup> 2024: « Targeting lysosome damage in Duchenne muscular dystrophy improves micro-dystrophin gene therapy" → **BEST ORAL PRESENTATION AWARD**
- Conférence 'Optimiser les thérapies innovantes : criblage thérapeutique et stratégie combinatoires', Génopole/Université d'Evry, July 2<sup>nd</sup> 2024 : « Targeting lysosome damage in Duchenne muscular dystrophy improves micro-dystrophin gene therapy ».

- **Posters (1<sup>st</sup> author):**

- 19èmes Journées de la Société Française de Myologie (JSFM) 2022, Toulouse, 23-25 November 2022 « Novel pathological mechanisms and therapeutic opportunities in Duchenne Muscular Dystrophy ».
- World Muscle Society, Charleston, South Carolina, USA, October 3<sup>rd</sup>-7<sup>th</sup> 2023: "Galectin-3 is a biomarker for lysosomal damage in muscular dystrophy".
- 8th International congress myology, Palais des Congrès de Paris, France, April 22-25<sup>th</sup> 2024: "Occurrence of lysosomal damage in the dystrophic muscle and its evaluation by Galectin-3".
- Lysosome and Endocytosis Gordon Research Conference 2024, June 16-21<sup>st</sup> 2024, Andover, New Hampshire, USA: "The damaged lysosome is a therapeutic target for combined therapy in Duchenne muscular dystrophy".

- **Patents:**

- [GALECTIN-3, A BIOMARKER OF LYSOSOMAL DAMAGE IN MUSCULAR DYSTROPHY] – Filled in Europe on August 31<sup>st</sup>, 2023, under number EP23194414.1.
- [TREHALOSE-BASED COMBINED THERAPY FOR LYSOSOMAL DAMAGE] – Filled in Europe on August 31<sup>st</sup>, 2023, under number EP23194612.0.

- **Papers**

- Bourg N, Vu Hong A, Lostal W, **Jaber A** *et al.* Co-Administration of Simvastatin Does Not Potentiate the Benefit of Gene Therapy in the mdx Mouse Model for Duchenne Muscular Dystrophy. *International Journal of Molecular Sciences* **23**, 2016 (2022)

- Lemoine J, Dubois A, Dorval A, **Jaber A** *et al.* Correction of Exon 2, Exon 2-9 and Exons 8-9 duplications in DMD patient myogenic cells by a Single CRISPR/Cas9 system. **Accepted for publication**
- Palmieri L, Pili L, **Jaber A** *et al.* Disease exacerbation in MYOrganoids derived from Duchenne Muscular Dystrophy iPSC reveals limitations of microdystrophin therapeutic efficacy. **Submitted**
- **Jaber A.\*** *et al.* Advances and Challenges in Microdystrophin gene therapy for Duchenne Muscular Dystrophy: progress and future directions. *Cahiers de Myologie* – **In Press** (\*corresponding author)
- **Jaber A** *et al.* Targeting lysosomal damage in the dystrophic muscle as a new therapeutic perspective for Duchenne Muscular Dystrophy - **Submitted**
- Kauffmann D [...] **Jaber A** *et al.* Light My Cells Challenge Database: Open Source Transmitted Light and Fluorescence Microscopy Image Collection. **In preparation for submission**

## Manuscript Summary in French

La dystrophie musculaire de Duchenne (DMD) est une maladie musculaire récessive liée à l'X, due à l'absence de dystrophine, la protéine encodée par le gène *DMD*. Elle touche environ 1 garçon sur 5000 et constitue la forme la plus courante de dystrophie musculaire infantile. La perte de dystrophine dans la fibre musculaire entraîne une déstabilisation du complexe glycoprotéique associé à la dystrophine, qui relie le cytosquelette à la matrice extracellulaire. Cette perturbation déclenche une cascade d'événements pathologiques, notamment des perturbations de l'homéostasie calcique, un stress oxydatif, un dysfonctionnement mitochondrial, une inflammation chronique, une transformation fibro-adipocytaire et, par conséquent, une perte de la fonction mécanique musculaire.

La prise en charge clinique actuelle de la DMD implique une approche multidisciplinaire pour traiter les manifestations musculaires et extra-musculaires de la maladie. Les traitements approuvés comprennent principalement les glucocorticoïdes, recommandés dès que possible. Bien que les glucocorticoïdes aient montré une amélioration significative de la fonction motrice, ils restent un traitement symptomatique et peuvent au mieux retarder la progression de la maladie. Par ailleurs, plusieurs approches thérapeutiques en développement visent à restaurer une forme fonctionnelle de la dystrophine. L'une des approches les plus avancées et prometteuses est la thérapie génique par microdystrophine ( $\mu$ -dystrophine), qui consiste à délivrer une copie raccourcie mais fonctionnelle du gène de la dystrophine à l'aide d'un vecteur adéno-associé recombinant (AAVr). Cette approche est confrontée à un défi majeur : l'optimisation du dosage thérapeutique. Des doses élevées peuvent déclencher des réponses immunitaires graves et une toxicité tandis que de faibles doses peuvent ne pas avoir l'effet thérapeutique souhaité.

Bien qu'une thérapie génique par  $\mu$ -dystrophine (*delandistrogene moxeparvovec*) ait récemment reçu l'autorisation de commercialisation par la FDA, les améliorations fonctionnelles pour les patients n'ont pas reproduit les résultats précliniques. L'amélioration fonctionnelle limitée observée dans les essais cliniques avec la  $\mu$ -dystrophine pourrait être attribuée à plusieurs facteurs, notamment l'absence de certains domaines fonctionnels présents dans la dystrophine complète. Par conséquent, le transfert de la  $\mu$ -dystrophine ne serait pas en mesure d'inverser tous les mécanismes pathologiques dans le muscle. Il est alors essentiel d'identifier les mécanismes pathologiques spécifiques qui ne sont pas corrigés par la thérapie génique par  $\mu$ -dystrophine et d'explorer des approches combinatoires avec des traitements complémentaires ciblant ces mécanismes.

Depuis le clonage du gène *DMD* et la caractérisation de la dystrophine, la théorie dominante concernant la pathogenèse de la DMD postule qu'un stress mécanique exercé sur le sarcolemme de la fibre musculaire entraîne sa déstabilisation, aboutissant finalement à la dégénérescence de la fibre. Cependant, l'intérêt s'est récemment accru pour les perturbations métaboliques, en particulier le dysfonctionnement mitochondrial. De plus, des études récentes, y compris la nôtre, ont mis en évidence des perturbations lipidiques, notamment en ce qui concerne le métabolisme du cholestérol. Ces perturbations sont souvent associées à des anomalies lysosomales dans les maladies neurodégénératives et les maladies de surcharge lysosomale. Par exemple, dans la maladie de Niemann-Pick de type C, l'accumulation de lipides non dégradés dans le lysosome altère sa fonction, provoquant des dysfonctionnements cellulaires et diverses manifestations neurologiques. Cela nous a conduits à émettre l'hypothèse que, comme dans les maladies lysosomales, l'excès de cholestérol pourrait s'accumuler dans le système endolysosomal des muscles dystrophiques, provoquant un dysfonctionnement

lysosomal. Cette hypothèse est soutenue par des études précédentes montrant des altérations de la structure et de la fonction des lysosomes, des perturbations de l'autophagie et une surexpression des cathepsines dans la DMD.

Le premier objectif de cette thèse était de caractériser le système endolysosomal dans le muscle dystrophique et d'étudier son lien avec le métabolisme perturbé du cholestérol. Le second objectif était de développer une thérapie combinée, associant le transfert de  $\mu$ -dystrophine via des vecteurs AAVr à la correction des troubles métaboliques secondaires.

Pour évaluer la fonction lysosomale dans la DMD, nous avons commencé par examiner la galectine-3 (Gal-3), un marqueur validé de la perméabilité de la membrane lysosomale (PML), dans divers modèles animaux de DMD et des biopsies musculaires de patients. Bien que la surexpression de Gal-3 ait été précédemment montrée dans la DMD, elle était attribuée aux macrophages infiltrants positifs pour Gal-3. Notre étude a confirmé la surexpression de Gal-3 dans les muscles dystrophiques et a démontré sa localisation aux lysosomes élargis dans les fibres musculaires, indiquant une PML. En outre, nous avons détecté ces dommages lysosomaux dans d'autres myopathies, notamment les dystrophies des ceintures (LGMDR5, LGMDR3, LGMDR2, LGMDR9), la myopathie centronucléaire liée à la dynamine-2 et la maladie de Pompe, suggérant que la PML pourrait être une caractéristique pathologique commune à diverses myopathies. Une validation et une caractérisation plus poussées des perturbations lysosomales dans la DMD ont révélé une augmentation du nombre et de la taille des lysosomes, des fuites de cathepsines dans le cytosol, l'activation de la réponse aux dommages lysosomaux et des défauts de l'autophagie. Nous avons notamment démontré que les défauts d'autophagie précédemment observés sont dus à un défaut de fusion entre les lysosomes et les autophagosomes, causé par des perturbations de la fonction et de la structure

lysosomales. De plus, la saturation de la machinerie d'autophagie par l'élimination des lysosomes endommagés (lysophagie) contribue également à ces défauts.

Pour mieux comprendre la corrélation entre l'accumulation de cholestérol et la PML, des souris *wild-type* (WT) et dystrophiques ( $Dmd^{mdx-4Cv}$ ) ont été soumises à un régime riche en graisses et en cholestérol (*high-cholesterol-diet*, HCD). Bien que les souris WT et dystrophiques présentaient toutes une augmentation de la charge en cholestérol dans le muscle squelettique, l'accumulation lysosomale de cholestérol, les dégâts lysosomaux et la fibrose étaient nettement plus prononcés dans les muscles des souris dystrophiques sous diète HCD que dans ceux des souris soumises à un régime standard et des souris WT sous diète HCD. Cela indique une relation causale directe dans ce modèle dystrophique entre l'accumulation du cholestérol, les lésions lysosomales et l'exacerbation des paramètres dystrophiques.

Par suite de ces découvertes, nous avons évalué l'effet de deux thérapies géniques sur la correction des lésions lysosomales. La première thérapie consistait à transférer la  $\mu$ -dystrophine par vecteurs AAVr dans le modèle de souris  $Dmd^{mdx}$ , tandis que la seconde consistait à administrer le gène de la gamma-sarcoglycane complet dans un modèle murin de sarcoglycanopathie (LGMDR5). Nous avons observé une relation dose-réponse, avec une diminution de la PML à mesure que la dose injectée d'AAV- $\mu$ -dystrophine augmentait. Cependant, des lésions lysosomales résiduelles significatives ont persisté même chez les souris traitées avec une dose élevée d'AAV- $\mu$ -dystrophine, qui transduit près de 100 % des fibres musculaires. En contraste, la thérapie génique dans le modèle LGMDR5 a montré une correction plus efficace de la PML et une meilleure amélioration globale des caractéristiques dystrophiques.

Étant donné que la thérapie génique par  $\mu$ -dystrophine ne permet pas de corriger complètement les lésions lysosomales, nous avons exploré la possibilité de la combiner avec un traitement complémentaire ciblant ces lésions. Cette approche

visait à réduire la dose nécessaire d'AAV- $\mu$ -dystrophine tout en potentialisant son effet avec un traitement complémentaire ciblant les dommages lysosomaux. Nous avons choisi la tréhalose pour cette configuration en raison de son bon profil de sécurité, de son prix abordable en tant que disaccharide alimentaire, et des essais cliniques précédents dans les maladies neurodégénératives et la dystrophie musculaire oculopharyngée (OPMD). Plus important encore, il a été récemment démontré que le tréhalose favorise la biogenèse lysosomale et l'autophagie, atténuant ainsi efficacement les dommages lysosomaux.

Nous avons comparé des souris dystrophiques *Dmd*<sup>*mdx-4Cv*</sup> traitées soit avec de la tréhalose seule, soit avec une dose sous-optimale d'AAV- $\mu$ dystrophine, soit avec une combinaison des deux traitements. Dans le groupe de traitement combiné, les souris ont été traitées avec de la tréhalose pendant une semaine avant l'injection d'AAVr. Notamment, la tréhalose seule a montré des effets bénéfiques, notamment en inversant la PML (puncta LAMP2+LGALS3+) et en réduisant la perméabilisation et la nécrose des myofibres. Cela met en évidence l'effet positif de la tréhalose sur le dysfonctionnement lysosomal et suggère une association directe entre les dommages lysosomaux et la nécrose des myofibres. Les meilleurs résultats thérapeutiques ont été observés chez les souris recevant la thérapie combinée. Dans le muscle gastrocnémien (GA) des souris traitées, nous avons observé une correction de la distribution de la taille des myofibres, une amélioration de l'indice de centronucléation, une régression de la fibrose et de l'inflammation, ainsi qu'une amélioration significative de la force musculaire globale par rapport aux souris dystrophiques non traitées.

Pour évaluer davantage la correction moléculaire obtenue avec les différents traitements, nous avons effectué une analyse par séquençage de l'ARN (RNA-seq) du muscle GA. L'analyse transcriptomique a confirmé l'efficacité de la thérapie combinée,

montrant une correction transcriptomique accrue lorsque la  $\mu$ -dystrophine était combinée au tréhalose par rapport au traitement à la  $\mu$ -dystrophine seule. Cette correction était évidente dans diverses voies de signalisation et processus biologiques, tels que l'inflammation, l'homéostasie calcique, les voies de mort cellulaire, le métabolisme des lipides et la voie mTOR.

Il est intéressant de noter que le traitement au tréhalose seule n'a pas eu d'effet significatif sur le transcriptome, mais semble agir en synergie avec la  $\mu$ -dystrophine. Cette synergie est mise en évidence par la différence substantielle de correction entre le groupe traité à la  $\mu$ -dystrophine seule et le groupe traité avec la thérapie combinée.

En résumé, dans la première partie de ce projet, nous avons acquis de nouvelles connaissances ayant des implications diagnostiques et thérapeutiques significatives pour la DMD et d'autres myopathies. L'identification de la PML dans la DMD et d'autres myopathies est une avancée novatrice. L'immunomarquage avec Gal-3 représente une méthode efficace et rapide pour identifier la PML et peut servir de biomarqueur histologique pour détecter les lésions lysosomales dans les myopathies en général.

Nos résultats ont également fait progresser notre compréhension de la pathologie de la DMD, suggérant que les défauts lysosomaux peuvent jouer un rôle central dans la pathogenèse et la progression de la dystrophie musculaire. L'importance relative des anomalies lysosomales par rapport à d'autres caractéristiques pathologiques de la DMD reste à déterminer. Malgré les progrès significatifs réalisés dans le traitement de la DMD, il existe encore de nombreux écarts et possibilités d'amélioration. Une approche thérapeutique combinée pourrait améliorer significativement les résultats thérapeutiques. L'identification du système endolysosomal comme cible prometteuse pour une thérapie combinée est une avancée, et la preuve de concept avec la

tréhalose pourrait ouvrir la voie à l'évaluation d'autres médicaments. Des recherches supplémentaires sont nécessaires pour déterminer si les défauts lysosomaux sont le mécanisme le plus pertinent à cibler dans une approche de thérapie combinée. Cela permettra d'approfondir notre compréhension de la pathogenèse et la progression de la DMD et de combler le fossé entre la recherche fondamentale et l'application clinique.



**Titre :** Anomalies lysosomales dans la myopathie de Duchenne : vers des approches thérapeutiques combinées

**Mots-Clés :** Dystrophie Musculaire de Duchenne, Cholestérol, Lysosome, Thérapie génique, Microdystrophine, Tréhalose

**Résumé :** La dystrophie musculaire de Duchenne (DMD) est une maladie musculaire dégénérative touchant principalement les jeunes garçons, caractérisée par la perte de l'expression fonctionnelle de la dystrophine. Bien que la thérapie génique visant à restaurer une forme tronquée fonctionnelle de la dystrophine, appelée  $\mu$ -dystrophine, ait montré des résultats prometteurs dans les études précliniques, son efficacité thérapeutique chez les patients DMD traités reste limitée, nécessitant des améliorations urgentes. Le travail présenté dans cette thèse vise d'abord à améliorer notre compréhension des perturbations métaboliques et cellulaires dans la DMD, puis à proposer de nouvelles approches thérapeutiques combinées, associant la thérapie génique aux traitements des dérégulations identifiées. Nous avons récemment identifié des dérégulations du métabolisme du cholestérol dans le muscle DMD, un phénomène souvent lié au dysfonctionnement lysosomal dans les troubles neurodégénératifs. Sur cette base, nous avons émis l'hypothèse d'une interaction potentielle entre l'accumulation de cholestérol et les perturbations lysosomales dans la pathogenèse de la DMD. Notre étude a identifié une augmentation de la Galectine-3 (LGALS3), un biomarqueur de la perméabilisation de la membrane des lysosomes (PML), dans les muscles dystrophiques des patients DMD et des modèles animaux, indiquant l'occurrence de la PML dans les myofibres dystrophiques. Ce phénomène a été corrélé à

un stress lysosomal important, mis en évidence par des changements dans le nombre, la morphologie et le positionnement des lysosomes, ainsi que par l'activation des voies de biogenèse, de réparation et d'élimination des lysosomes. La PML a été exacerbée chez les souris nourries avec un régime riche en cholestérol et n'a pas été entièrement corrigée par la thérapie génique par  $\mu$ -dystrophine. Pour remédier à cette limitation, nous avons sélectionné la tréhalose, un composé approuvé par la FDA et connu pour restaurer la fonction lysosomale, pour l'utiliser en combinaison avec une dose sous-optimale de thérapie génique par  $\mu$ -dystrophine. Le traitement combiné a permis de corriger la PML et d'améliorer la correction des paramètres dystrophiques, y compris la fonction motrice, l'histologie musculaire et la signature transcriptomique, par rapport à la thérapie génique suboptimale de la  $\mu$ -dystrophine seule. Les travaux de cette thèse soulignent l'importance des lésions lysosomales dans la physiopathologie de la DMD et suggèrent qu'une approche synergique combinant une supplémentation en tréhalose et une dose sous-optimale d'AAV  $\mu$ -dystrophine est prometteuse pour améliorer les résultats thérapeutiques dans la DMD.

**Title:** Lysosomal Defects in Duchenne Muscular Dystrophy: Advancing Combined Therapeutic Approaches

**Keywords:** Duchenne Muscular Dystrophy, Cholesterol, Lysosome, Gene Therapy, Microdystrophin, Trehalose

**Abstract:** Duchenne Muscular Dystrophy (DMD) is a muscle degenerative disease primarily affecting young boys, characterized by the loss of dystrophin expression. While gene therapy targeting the restoration of a functional truncated form of dystrophin, known as  $\mu$ -dystrophin, has shown promise in preclinical studies, its therapeutic efficacy in treated DMD patients remains limited, necessitating urgent improvements. The aim of the work presented in this thesis is to first improve our understanding of the metabolic and cellular perturbations in DMD, and secondly to propose new combined therapy approaches, associating gene therapy to treatments of identified dysregulations. We have recently identified dysregulations of cholesterol metabolism in DMD muscle, a phenomenon frequently associated with lysosomal dysfunction in neurodegenerative disorders. Building upon this association, we hypothesized a potential interplay between cholesterol accumulation and lysosomal perturbations in DMD pathogenesis. Our study identified an upregulation of Galectin-3 (LGALS3), a known biomarker of lysosome membrane permeabilization (LMP), in the dystrophic muscle of DMD patients and animal models, indicating the

occurrence of LMP within dystrophic myofibers. This correlated with significant lysosomal stress evidenced by changes in lysosome number, morphology, positioning and activation of lysosomal biogenesis, repair and removal pathways. Remarkably, LMP was exacerbated in mice fed a cholesterol-rich diet and was not fully corrected by  $\mu$ -dystrophin gene therapy. Subsequently, we selected trehalose, an FDA-approved compound known to restore lysosomal function, for use in combination with a suboptimal dose of AAV- $\mu$ -dystrophin gene therapy. The combined treatment resulted in correction of lysosomal defects and improved correction of dystrophic parameters, including motor function, muscle histology, and transcriptome signature, compared to  $\mu$ -dystrophin gene therapy alone. This work underscores the significance of lysosomal damage in DMD pathophysiology and suggests that a synergistic approach combining trehalose supplementation with a suboptimal dose of AAV  $\mu$ -dystrophin holds promise for enhancing therapeutic outcomes in DMD.

